NASA-CR-165624
19810002770

KSC TR 32-3
December 1979

NASA Contract Report 165624

Optical Fiber Dispersion Characterization Study

Final Report

National Aeronautics and
Space Administration

John F. Kennedy Space Center

NASA

KSC FORM 16-12 (REV 8/76)

OPTICAL FIBER DISPERSION CHARACTERIZATION STUDY

CONTRACT #NAS10-9455

FINAL REPORT

DECEMBER 1979

ABSTRACT

"Optical Fiber Dispersion Characterization Study"

NAS10-9455 FINAL REPORT

This report presents the theory, design, and results of optical fiber pulse dispersion measurements. Detailed descriptions of both the hardware and software required to perform this type of measurement are presented. Hardware includes a thermoelectrically cooled ILD (Injection Laser Diode) source, an 800 GH_z gain-bandwidth produce APD (Avalanche Photo Diode) and an input mode scrambler. Software for a HP 9825 computer includes fast fouirer transform, inverse fouirer transform, and optimal compensation deconvolution. Test set construction details are also included.

Test results include data collected on a 1 Km fiber, a 4 Km fiber, a fused spliced, eight 600-meter length fibers concatenated to form 4.8 Km, and up to nine optical connectors.

This work was performed at Kennedy Space Center with the aid of University of Central Florida, Orlando, Florida, under contract NAS10-9455.

OPTICAL FIBER DISPERSION CHARACTERIZATION STUDY AT KENNEDY SPACE CENTER, PART II

by

Sedki M. Riad, Michael E. Padgett
Alan Geeslin, Achia AR Riad

An optical fiber dispersion characterization test set was developed at Kennedy Space Center with the aid of the University of Central Florida, Orlando, Florida. This development included the test algorithin development, hardware design and signal processing software implementation for HP 9825 computer. Part I, presented at FOC 79, reported the characterization of fibers up to 24 Km in length. Test set and software modifications include the thermoelectrically cooled ILD source, 800 GH_Z gain bandwidth product APD, addition of a modescrambler and development of a frequency domain optimal compensation deconvolution routine. Test data was collected on 4 Km lengths of fiber, a fused splice, eight 600 meter lengths of fiber concatenated to form 4.8 Km, and up to nine optical connectors. Results showed the 4 Km fiber to have a bandwidth of 290 MH_Z, which relates to a 1.16 GH_Z Km capacity and a dispersion of 1.10 ns full duration at half maximum FDHM or 0.275 ns/Km. The fused splice showed a bandwidth of greater than 2 GH_Z, as did a total of nine connectors.

FOREWORD

The work reported herein was accomplished by Drs. Sedki, M. Riad and Aicha A. R. Riad, formerly Assistant Professors of Electrical Engineering, University of Central Florida, Orlando, Florida, and currently with the Electrical Engineering Department, Virginia Polytechnic Institute and State University.

The following students participated in the work accomplishment:

1 - Alan E. Geeslin, M.S.

2 - Robert B. Stafford, M.S.

3 - Seward T. Salvage

4 - Glenn A. Birket

Mr. Geeslin and Mr. Stafford used their work for their Master's degrees in Electrical Engineering, University of Central Florida, December 1979.

The authors would like to asknowledge the invaluable cooperation of Mr. Michael E. Padgett, Design Engineer, Electro-Optic Laboratory, Kennedy Space Center, throughout the course of this work.

OVERVIEW

Kennedy Space Center's requirements for high data rate and wideband transmission led to the development of an optical fiber communication evaluation program in 1973. This program has involved the development and evaluation of optical fiber components and systems. In June 1977 an optical fiber cable was installed in KSC's harsh, underground ducts for evaluation. This 2Km, fiber cable has been used to test fiber systems up to 16 Km in length. In addition to testing major system components, the optical parameters of the fiber are being closely monitored.

The pulse dispersion characteristics/frequency transfer function of the optical fiber is considered to be one of the key parameters of the cable. KSC required technical assistance in developing a method to measure and analyze this parameter. This was the subject of the first portion of the study performed by the Optical Communications and Signal Processing Group at UCF in cooperation with the Electro-Optic Laboratory at KSC. The basic objective of this study effort is to design an algorithm for optical fiber dispersion analysis to be used by the KSC Electro-Optics Laboratory on a regular basis to detect possible changes in optical fiber transmission links with age. It will also establish a basis for evaluating, specifying, and acceptance testing future fiber cables. Dispersion information about an installed fiber system is

essential to obtain maximum bandwidth capability.

As a result of the first portion of the study, an algorithm for determining the fiber's optical dispersion was developed, an experimental set up for measuring the optical dispersion was built, and the associated signal acquisition and processing software was written and debugged. The following is an outline for the optical dispersion test algorithm:

1. Launch a short duration optical pulse into a reference fiber.
2. Measure and record the detected fiber output. This signal is considered the reference waveform.
3. The response waveform is to be recorded by repeating the above procedure while inserting the fiber under test in the optical path.
4. Apply the Fast Fourier Transform to both the reference and the response waveforms to obtain their frequency domain forms.
5. Apply frequency domain deconvolution to both frequency domain transforms to obtain the fibers transfer function and impulse response.
6. The frequency domain resolution of the resulting transfer function can be increased by using a resolution enhancement procedure developed for this study.
7. Display the magnitude and phase components of the inverse of the transfer function in the form of

attenuation in dB and phase in degrees vs frequency on a logarithmic scale.

8. Fiber bandwidth is the frequency at which the attenuation is 3 dB higher than its low frequency value. And fiber dispersion can be indicated by the full duration at half the maximum (FDHM) of the impulse response.

The short duration optical pulse used in steps 1 and 3 above was generated using an Injection Laser Diode (ILD), and an Avalanche Photo-Diode (APD) was used for the optical detection in steps 2 and 3. Signal acquisition and processing were performed using a Digital Processing Oscilloscope (Tektronix DPO) interfaced with an HP9825 desk-top minicomputer.

Optical dispersion data were collected for 1 and 2.4 km fiber pieces. The results of these measurements indicated that several test set modifications could improve the measurement capability. Such modification would allow the measurement of KSC's 8 km link used for lab work and component and system evaluation.

As an extension to the above mentioned study, KSC requested the design of modifications to the existing pulse dispersion test set to increase its measurement capabilities. The target for the measurement dynamic range was 45 dB, and for the bandwidth was 100 MHz to 3 GHz with 10 MHz resolution. KSC also requested the collection and analysis of dispersion data for various fiber lengths as well as various types of fiber connectors and splices. This information is to be used to

predict the total dispersion properties of a fiber link composed of various fiber lengths, connectors and splices.

As a result of the study extension, the following modifications to the pulse dispersion test set (PDTS) were designed and implemented:

1. The design and construction of a highly stable, long life, ILD impulse generator/trigger source. The impulse generator is operating at a higher repetition rate (~ 15 kHz) and is thermoelectrically cooled.
2. The design and construction of a new APD biasing/coupling circuit which reduces the transient overloading of the DPO's sampling unit (Tek. 7S12/S6).
3. The use of a high gain-bandwidth product APD, (Spec. 800 GHz). The maximum bandwidth of this APD is 2 GHz, at gain values up to 100.
4. The use of reliable, wideband, low attenuation connectors for inserting the fiber under test in the optical path. In this method the reference fiber is to be included in the response measurement and therefore maintaining the same launch and coupling conditions in both reference and response measurements.
5. The development of the optimal compensation frequency domain deconvolution technique which proved to yield good results with very low noise content.

The computer software was modified to accommodate the above mentioned modification. And the modified PDTS was used

for testing a 4 km fiber length. The current dynamic range of the modified PDTs is sufficient for testing fibers up to 8 km in length.

The modified PDTS was used to study dispersion properties of a fuse splice and one type of connectors. The study showed that both the splice and the connector have frequency bandwidths greater than 2 GHz, (the PDTS' current bandwidth measurement limitation). Also, measurements were made to determine the dispersion properties of concatenated fibers. The results of this test displayed some irregularity. However, an average relation for the fiber's bandwidth vs. length is graphed in the report.

In the conclusion of this study, KSC has the capability to evaluate optical dispersion properties of fibers and fiber components, and to determine their useful bandwidths. The test set and software may require future modifications to allow the evaluation of single mode fibers and corresponding components, as well as the operation at longer wavelengths.

The ability to evaluate optical fiber dispersion parameters will play an important role in KSC's specifications, procurement, and operation of future fiber communication systems.

Principle Investigator: Sedki M. Riad Sedki M. Riad

Co-Investigator : Aicha A. R. Riad Aicha A R. Riad

C O N T E N T S

OPTICAL FIBER DISPERSION CHARACTERIZATION STUDY

CONTRACT # NAS 10-9455 FINAL REPORT

DECEMBER 1979

I. INTRODUCTION

Kennedy Space Center's requirements for high data rate and wideband transmission led to the development of an optical fiber communication evaluation program in 1973. This program has involved the development and evaluation of optical fiber components and systems. In June 1977 an optical fiber cable was installed in KSC's harsh, underground ducts for evaluation. This 2Km, fiber cable has been used to test fiber systems up to 16 Km in length. In addition to testing major system components, the optical parameters of the fiber are being closely monitored.

The pulse dispersion characteristics/frequency transfer function of the optical fiber is considered to be one of the key parameters of the cable. KSC required technical assistance in developing a method to measure and analyze this parameter. This was the subject of the first half of the study performed by the Optical Communications and Signal Processing Group at UCF in cooperation with the Electro-Optic Laboratory at KSC. The basic objective of this study effort is to design an algorithm for optical fiber dispersion analysis to be used by the KSC Electro-

Optics Laboratory on a regular basis to detect possible changes in optical fiber transmission links with age. It will also establish a basis for evaluating, specifying, and acceptance testing future fiber cables. Dispersion information about an installed fiber system is essential to obtain maximum bandwidth capability.

As an extension to the above mentioned study, KSC requested the design of modifications to the existing pulse dispersion test set to increase its measurement capabilities. The target for the measurement dynamic range was 45 dB, and for the bandwidth was 100 MHz to 3 GHz with 10 MHz resolution. KSC also requested the collection and analysis of dispersion data for various fiber lengths as well as various types of fiber connectors and splices. This information is to be used to predict the total dispersion properties of a fiber link composed of various fiber lengths, connections, and splices. This final report is a complete overview of the work done in the above mentioned optical dispersion study. The report presents the approach, the experiment, the analysis, as well as the results of the study.

II. APPROACH

To fully characterize a device (a fiber or connector, etc.) in terms of its pulse dispersion, it is needed to define either:

1. The impulse response waveform h(t); which is the device output due to an ideal impulsive input (Dirac delta impulse).

2. The complex transfer function $H(e^{j\omega})$; which is the ratio between the device harmonic output $Y(e^{j\omega})$ and the exciting harmonic input $X(e^{j\omega})$.

Presenting the device response in the time domain form h(t) displays its dispersion properties and therefore the limit on signaling speed (rate) of the transmitted information. However, h(t) will not give a direct measure for frequency or phase-shift distortion at high transmission rates. This information, as well as a direct determination of the useful frequency bandwidth of the fiber, is directly obtainable from the frequency domain presentation $H(e^{j\omega})$.

Since a true Dirac delta time impulse cannot be generated, a duration-limited input impulse x(t) will be used. The output waveform y(t) due to x(t) can be written as

$$y(t) = h(t) * x(t)$$

where (*) denotes the convolution operation, Figure 1. Appendix A* describes in detail the deconvolution procedure to obtain $H(e^{j\omega})$ and h(t). In the following a brief summary of the procedure is presented.

---

*Appendix A is a copy of a paper submitted for publication to the IEEE Trans. on Acoust., Speach & Signal Processing.

First, apply the Fourier transform to the time domain waveforms x(t) and y(t) to obtain $X(e^{j\omega})$ and $Y(e^{j\omega})$, respectively, for which

$$Y(e^{j\omega}) = H(e^{j\omega}) \cdot X(e^{j\omega}).$$

Second, calculate $H(e^{j\omega})$, the complex transfer function as given by

$$H(e^{j\omega}) = Y(e^{j\omega}) \cdot X^*(e^{j\omega})/[|X(e^{j\omega})|^2 + \lambda]$$

where $X^*(e^{j\omega})$ is the complex conjugate of $X(e^{j\omega})$, and λ is an optimization parameter. The optimum value for the parameter λ yields the lowest noise content in the deconvolution result. Finally, apply the inverse Fourier transform on $H(e^{j\omega})$ to obtain h(t). This is the optimal compensation frequency domain approach to deconvolve x(t) from y(t) to yield h(t), Figure 2. In this approach both $H(e^{j\omega})$ and h(t) are available.

III. EXPERIMENT

Figure 3 shows the experimental set-up and devices to be used in the dispersion characterization test. For cost, size, and convenience considerations, an injection laser diode (ILD) is to be used for optical impulse generation, and an avalanche photodiode (APD) for optical detection. To insure uniform mode loading in the fiber/connector under test, a mode scrambler is used at the ILD (launch) side. The faster the temporal (impulse) response of the ILD/mode scrambler/APD combination, the better the accuracy of the

results will be. For picosecond time resolution, a sampling oscilloscope is needed to observe the detected waveforms. Also, to compensate for the signal time delay in various devices, as well as in the fiber length, a variable time delay unit is needed. Delay variations should correspond to various fiber lengths used in the test set. Finally, for signal processing, a digitizing, acquisition and computation system is needed, e.g. a digital processing oscilloscope (DPO) / minicomputer combination.

The dispersion test is designed to be an insertion type measurement. For fiber testing, a typical arrangement is shown in Figure 4, and the corresponding procedure would be as follows: A reference waveform x(t) is recorded as the detected APD output while a short piece of fiber (∿2 m length) is joining the optical path between the mode scrambler and the APD. The short fiber is used to account for the input and output launch conditions such that the resulting transfer function becomes more independent of alignment and interface geometry. The response waveform, y(t), is then recorded by inserting the fiber to be characterized between the mode scrambler and the short fiber and acquiring the output of the APD. The insertion is performed by the help of fiber connectors. The connectors used were tested to show repeatability within ±0.5 dB. The connector's response has to be accounted for in the

signal processing to determine the fiber's response.

However, for the fiber connector dispersion test, long fiber pieces are needed on both sides of the connector(s) to simulate real applications. The arrangement for this test is shown in Figure 5 to consist of the same mode scrambler and short fiber pieces, two 600 m (long) pieces, and a 6 m piece fuse-spliced to the two 600 m fibers. The reference waveform x(t) is recorded and then the 6 m piece is broken at a point where the connector under test is installed and the response waveform y(t) is then acquired.

IV. DEVICES

This section of the report discusses the choice of devices to be used in the test, Figure 3, and the electronic circuitry associated with them.

A. The Optical Source

The SG 2002 semiconductor injection laser diode (ILD) was chosen because it is one of the commercially available pulsed ILD's with low current threshold and capable of generating 2 watts of optical power in the form of approximately 100 ps pulses [1].

This ILD requires a current pulse generator that can deliver 3.5 Amps for time durations less than 1 ns (100 ps to 1 ns). An impulse generator having these specifications,

with repetition rates suitable for sampling oscilloscope monitoring, was designed by Dr. James R. Andrews of the National Bureau of Standards, Boulder Laboratories [1]. The impulse generator schematic is given in Figure 6. This impulse generator requires a triggering pulse of approximately 2 volts amplitude and 2 ns duration. A trigger circuit designed to meet these requirements is given in Figure 7. This circuit also provides two additional features:

a) variable delay control for the trigger output with respect to the pretrigger which triggers the DPO, and,

b) variable repetition rate control.

The repetition rate has to be kept low (∿5 KHz) for long life operation of the impulse generator's avalanche transistor. However, for better signal acquisition, the repetition rate has to be increased. This problem was resolved by increasing the repetition rate while cooling the avalanche transistor.

The impulse generator circuit/ILD were built on a thermoelectrically cooled copper block. Cooling both the avalanche transistor and the ILD help increase their life-times as well as reduce the jitter noise in the generated optical pulse. Both the avalanche transistor and the ILD were thermally in contact with the cooled block. The

construction details of the impulse generator circuit/ILD are given in Figure 8, and the thermoelectric cooling element and regulating circuit are shown in Figure 9.

B. The Mode Scrambler

The mode scrambler used is shown in Figure 10. It consists of joining three 1 m fiber pieces in series, a step-index fiber, a graded-index, and a step-index fiber [2]. The joints are made by fuse splicing the fibers together. This mode scrambler significantly reduced the dispersion measurement variations due to source launch-condition changes.

C. The Optical Detector

The PD 1002 semiconductor avalanche photodiode (APD) was chosen as the optical detector because it is the best commercially available APD. This APD is specified by the manufacturer to have an 800 GHz gain-bandwidth product. Figure 11 shows the circuit used to bias the APD and couple the detected output to the sampling oscilloscope.

D. Sampling Oscilloscope / Signal Processing Systems

The sampling oscilloscope used in this set-up for acquiring the detected waveforms is a Tektronix S6-7S12 sampling unit installed in a digital processing oscilloscope (DPO). This DPO was interfaced and controlled by an HP 9825 computer. Software was written to acquire, process, and display data taken using this equipment configuration.

One important finding to report at this point is that the test set-up as described here displayed about 20 ps of jitter noise in detected waveforms. This jitter noise was reduced considerably by software signal averaging. However, due to the long time involved in this process (approximately 4 minutes for 50 averages), other sources of noise and errors such as thermal fluctuations and drifts are introduced in the averaged waveform.

V. SIGNAL PROCESSING

The dispersion test as described before requires the acquisition of two time domain waveforms. These waveforms will then be transformed to the frequency domain using the fast Fourier transform (FFT). The FFT's frequency domain resolution is related to both the time domain resolution and the number of processed points (samples) by the relation: [3]

$$\Delta T \cdot \Delta f = 1 / N$$

where ΔT is the time duration between two samples in the time domain waveform, and Δf is the frequency spacing between two samples in the frequency domain transform, Figure 12.

To increase the signal processing accuracy and resolution, N must be taken as large as possible. The DPO can give up to 512 time domain samples for a waveform. However, for a duration limited signal, it is possible to increase the number of processed points by adding new points (samples)

of zero magnitude, thereby extending the time window. N can be increased using this "add zeros" technique up to 1024 points, a limit imposed by the KSC's HP 9825 capacity and the amount of signal processing involved in the dispersion test. It is important to realize that the "add zeros" technique can be used only to enhance the frequency domain resolution since ΔT, and hence the time domain resolution, is limited by the 512 samples limit imposed by the DPO, and also by the acquisition time window.

Having these limits in mind, the choice of the acquisition time window is critical and is the only controllable variable in setting the time and frequency domain resolutions. The following example illustrates this point:

Example: Let τ denote the fastest transition duration in the acquired time domain waveform. The corresponding bandwidth in the frequency domain can be estimated as: [4]

$$BW \simeq 0.35/\tau$$

Time and frequency domain resolutions can be expressed in terms of N_t and N_f: the number of samples within τ and BW, respectively, Figure 13.

$$\tau = N_t \cdot \Delta T$$

$$BW = N_f \cdot \Delta f$$

Using these relations, it follows that:

$$N_t \cdot N_f \cdot \Delta T \cdot \Delta f = \tau \cdot BW = 0.35$$

but

$$\Delta T \cdot \Delta f = 1/N = 1/1024$$

therefore,

$$N_t \cdot N_f \simeq 360$$

For equal degrees of resolution in both time and frequency domains, take

$$N_t \simeq N_f \simeq 20 \text{ samples.}$$

Therefore,

$$\Delta T = \tau/N_t \simeq \tau/20$$

and the corresponding DPO acquisition time window is given by

$$512\ \Delta T \simeq 25\tau, \text{ or } \tau \simeq T/25.$$

As will be seen later in this section, it is possible to increase the frequency domain resolution, i.e. increase N_f, with interpolation using the FFT properties. Hence it might be advisable to favor N_t over N_f rather than equating them.

In the dispersion test, both reference and response waveforms must be acquired with the same ΔT in order to have point to point correspondence in both time and frequency domains. In this case it is preferable to choose T based on the impulse response information. A preliminary run can be used to estimate τ for the impulse response waveform, from which T can be chosen.

Once the waveforms are acquired, the FFT is used to obtain the corresponding frequency domain transforms. The complex transfer function $H(e^{j\omega})$ is then obtained as described in Appendix A. The impulse response h(t) can be obtained by applying the inverse fast Fourier transform (IFFT) to the obtained $H(e^{j\omega})$.

As mentioned earlier in this section, the transfer function's frequency domain resolution can be increased with an interpolation technique using the FFT properties. The process is shown in a block diagram form in Figure 14. The idea is to apply IFFT on M sample points out of the total N sample points ($M < N$), provided the transfer function's bandwidth is included in the processed band ($M/2 > N_f$). The obtained time domain transform (impulse response) will contain M sample points equally spaced by

$$\Delta T_M = 1/(M \cdot \Delta f)$$

Using the "add zeros" technique to increase the number of processed points back to N, the resulting frequency domain transfer function will contain N sample points with frequency spacing:

$$\Delta f_M = 1/(N \cdot \Delta T_M)$$

$$= \frac{M}{N} \Delta f$$

which is less than Δf; i.e. the frequency domain resolution was increased by a factor of N/M.

Finally, the complex transfer function $H(e^{j\omega})$ can be presented in magnitude and phase functions of frequency. An alternative is to present the information in the $1/H(e^{j\omega})$ magnitude of phase (attenuation and phase) functions of frequency. The attenuation function expressed in DB is given by:

$$\text{ATTEN} = -10 \log_{10} H(e^{j\omega})$$

and the phase function is given by:

$$\text{PHASE} = - \arg [H(e^{j\omega})]$$

where arg [ ] is the continuous argument function. This argument function is to be formed by reconstructing the computed argument defined between $-\pi$ and $+\pi$, to make it a continuous one by adding (or subtracting) integer multiples of 2π, Figure 15. The continuous argument function will contain a linear phase component, which needs to be removed in order to reveal the details of the phase function. This linear phase component is due to the difference between the fiber-length delay and the compensating delay-unit delay times. Eliminating this linear component does not affect the information content of the phase function regarding the dispersion characteristics, and therefore the amount of linear phase to be eliminated is arbitrary, Figure 16.

VI. SOFTWARE

The required computer software for performing the dispersion characterization test as described earlier was written for the DPO/HP9825 system. This software is given here in three forms: block diagram in Figure 17, flow charts, and HP9825 listings in Appendix B.

VII. DISPERSION MEASUREMENTS AND RESULTS

In this section, four dispersion tests will be presented along with the corresponding results. The four tests were performed to study long fiber length dispersion properties, the effect of concatenating fiber lengths on dispersion, dispersion properties of a fused-splice and finally dispersion properties of a single-connector and multi-connectors in optical fiber links.

A. Dispersion due to long fiber lengths

The optical fiber dispersion characterization test was performed on fiber lengths up to 4 km. The various test waveforms and related processing signals for the 4 km length fiber are demonstrated in Figure 18. As seen from the figure for the computed fiber's impulse response h(t), the 4 km fiber has a 1.10 ns full duration at half the maximum value (FDHM), which corresponds to an FDHM

dispersion of 0.275 ns/km. Also, from the figure for the fiber's attenuation function, the 3 DB bandwidth of the 4 km fiber is 290 MHz, which corresponds to a 1.16 GHz.km fiber bandwidth capacity (bandwidth-length product). These values are in close agreement with the 2.4 km results previously given in Progress report III. The 2.4 km values are 0.28 ns/km for dispersion and 1.34 GHz.km for bandwidth-length product.

b. Concatenation of Fibers and Dispersion

In this experiment, eleven 600 m fiber loops were used to study the effect of concatenation on dispersion. The dispersion test was performed on the individual 600 m. loops, the results are given in Appendix C. A sample result(loop #1) is given in Figures 19 and 20. Ten of the eleven 600 m. loops were then used to form five 1.2 km loops by fuse splicing. The dispersion test was run on the individual 1.2 km loops. The test results are also given in Appendix C, and a sample result is given in Figure 21 and 22. This time, four of the five 1.2 km loops were used to form two 2.4 km loops. Again, the dispersion results on the individual 2.4 km loops are given in Appendix C, and a sample is given in Figure 23. Finally, the two 2.4 km loops were concatenated to form one 4.8 km loop. The dispersion test was performed on the 4.8 km loop and the result is given in Appendix C as well as in Figures 24 and 25.

TABLE 1

600 m		1.2 km		2.4 km		4.8 km	
LOOP #	BW MHz	LOOP #	BW MHz	LOOP #	BW MHz	LOOP #	BW MHz
1	1300						
2	1400	2,3	870	2-5	455	2-9	110
3	1260						
4	1380	4,5	1580				
5	1600						
6	1105	6,7	915	6-9	440		
7	1740						
8	1145	8,9	905				
9	1490						
10	1600	10,11	1420				
11	1405						

The 3 dB frequency bandwidths as computed from the fiber loops transfer functions are listed in Table 1. These data are also plotted in Figure 26 in an attempt to fit them to the power relation

$$\ell (BW)^m = \text{constant}$$

where ℓ is the length of the fiber loop and BW is at 3 dB frequency bandwidth. Taking the log of the above relation, it can be written that,

$$\log(BW) = -\frac{1}{m} \log (\ell) + \text{constant}$$

Plotting log BW vs. log ℓ in Figure 26 did not display the straight line relation suggested by the above equation. However, local fitting of the power relation for various ranges of ℓ yields the following values of m:

$m \simeq 1.63$	$0.6 \text{ km} < \ell < 1.2 \text{ km}$
$m \simeq 1.04$	$1.2 \text{ km} < \ell < 2.4 \text{ km}$
$m \simeq 0.5$	$2.4 \text{ km} < \ell < 4.8 \text{ km}$

c. Optical dispersion of a fuse-splice

The test arrangement for the fuse-splice was described earlier in this report and is shown in Figure 5. The reference waveform was acquired using a 6 m piece fuse-spliced to two 600 m fiber loops. The 6 m piece was then broken then fuse-spliced and the response waveform was acquired. Reference and response waveforms are shown in

Figures 27 and 28a, respectively. Figure 28b shows the fuse-splice attenuation and phase as functions of frequency. As seen from the Figure, the 3 dB frequency bandwidth of the fuse-splice is >2 GHz.

d. Optical dispersion of connectors

The same arrangement and procedure used to test the fuse-splice was used to test a single connector. The reference waveform in this test is the same one aquired in the fuse-splice test, given in Figure 27. The single connector response waveform as well as the attenuation and phase functions are given in Figures 29a and 29b, respectively. Figure 29b shows a 3 dB bandwidth of the single connector to be >2 GHz.

The dispersion test was repeated while inserting more connectors within the 6 m piece. This experiment was performed to study the effect of closely spaced connectors on dispersion. The results for the cases of 3, 6, and 9 connectors are given in Figures 30, 31, and 32, respectively. The 3 dB bandwidth for these 3 cases was also >2 GHz.

VIII. DISCUSSION

Dispersion measurement performed on the 4.8 km concatenated fibers revealed that the current dynamic range of the KSC pulse dispersion test set (PDTS) is approximately 25 dB. With the addition of a 20 dB gain wideband amplifier on the detected signal line, the dynamic range can be increased to the requested 45 dB value. One of such wideband amplifiers has been ordered by KSC and was not available for use until the present time.

On the other hand, dispersion measurements on splices and connectors showed that the PDTS' bandwidth is in the neighbourhood of 2 GHz with 6.25 MHz resolution. Although all the proposed techniques for improving the system's bandwidth was not obtained. The current limiting factors are:

1-Limited number of waveforms acquired for averaging because of the long averaging time.

2-Limited bandwidth of optical detection, although the manufacturer's specifications for the APD used is 800 GHz gain-bandwidth product, the bandwidth of the APD was found to be about 2 GHz.

In the following, the results of the dispersion test presented in the previous section will be discussed, and their implications will be analyzed.

a-The results of the 4 km fiber test were in close agreement with those of the 2.4 km fiber. This shows consistency of the KSC PDTS performance. It also increas-

es the confidence level in the test results.

b-Although the test on an 8 km fiber length was not performed because of time limitations, it is felt that the PDTS is capable of performing such measurement. The reasons are: first, the 8 km fiber requires less bandwidth limitations than the 4 km fiber. And second, the 4 km fiber displayed low frequency attenuation of 10 dB, i.e. the 8 km fiber is expected to have about 20 dB low frequency attenuation, which is within the PDTS current dynamic range.

c-Test results on concatenated fibers showed some tendency to be inconsistent. As seen from Table 1, joining two 600m fiber pieces, loop #4 with 1380 MHz bandwidth, and loop #5 with 1600 MHz bandwidth, resulted in a 1580 MHz bandwidth for the concatenated 1.2 km loop. While joining loops #10 and #11 with bandwidths 1600 MHz and 1405 MHz, respectively, yielded a 1420 MHz bandwidth for the combination. Also, in concatenating 1.2 km fibers to form 2.4 km lengths, bandwidths of 870 MHz and 1580 MHz resulted in a 455 MHz, while 915 MHz and 905 MHz yielded 440 MHz. This inconsistency is due to the differences between the various fiber pieces in their graded-index of refraction profile (dispersion compensation). An overcompensated fiber piece concatenated with an undercompensated one may result in an overall performance close to that of a correctly compensated fiber.

d-The dispersion test was performed on only one type of splices and only one type of connectors because other types were not available for testing in time. The test showed that the fuse splice as well as the connector have faily wide bandwidths (greater than 2 GHz). The test also showed that the PDTS is unable to yield an accurate value for bandwidths greater than 2 GHz.

Finally, two points need to be discussed concerning the current KSC's PDTS limitations mentioned earlier in this section:

1. Limited signal averaging capability can be improved only by high speed hardware signal Averaging.
2. Limited optical detection bandwidth can be improved by using faster optical detectors.

Neither the high speed hardware signal Averager or the faster optical detector are commercially available. But, it is believed that the speed of the currently used APD can be improved by removing it from its commercial packaging and mount it on a high frequency strip line built on a substrate using the Thick-Film technique. The biasing and coupling circuit can be also built on the same substrate.

IX. REFERENCES

[1] J. R. Andrews, "Inexpensive Laser Diode Pulse Generator for Optical Waveguide Studies," Rev. Sci. Instrum., Vol. 45, No. 1, pp. 22-24, January 1974.

[2] W. F. Love, "Novel Mode Scrambler for Use in Optical-Fiber Bandwidth Measurements," Topical Meeting on Optical Fiber Communication Digest, Washington, D.C., pp. 118-120, March 6-8, 1979.

[3] W. D. Stanley, Digital Signal Processing, Reston Publishing Company, Inc., a Prentice-Hall Company, Reston,Virginia, 1975, Ch. 9.

[4] H. Wallman, and G. E. Valley, Vacuum Tube Amplifiers, New York: McGraw-Hill, 1948.

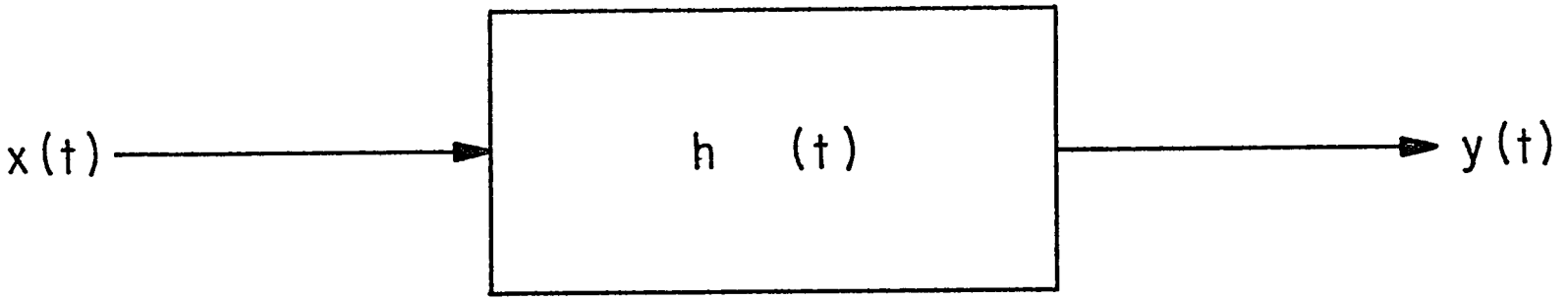

$$y(t) = h(t) * x(t)$$

$$Y(e^{j\omega}) = H(e^{j\omega}) \bullet X(e^{j\omega})$$

FIGURE 1: TIME DOMAIN INPUT-OUTPUT RELATION AND THE CORRESPONDING FREQUENCY DOMAIN TRANSFORMATION.

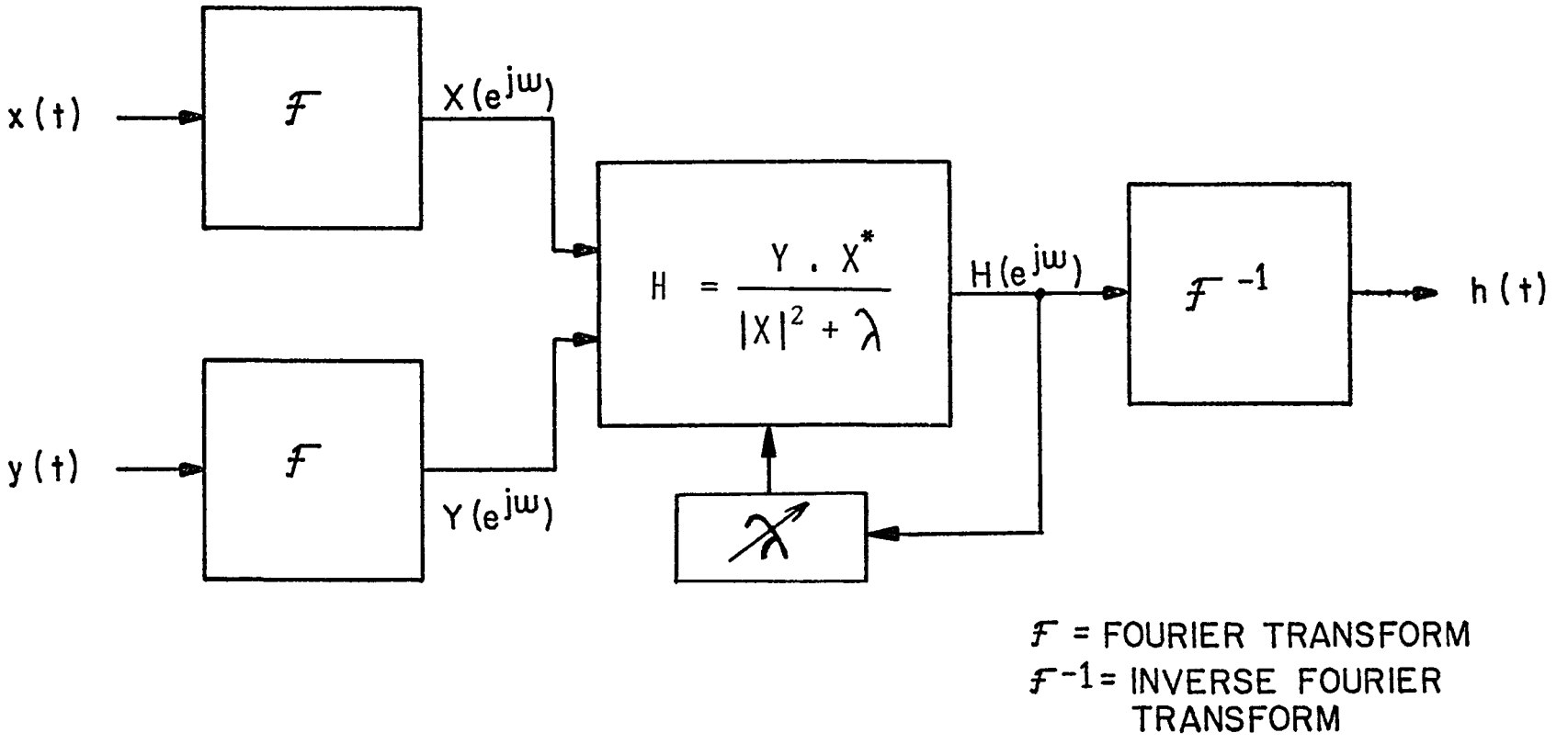

FIGURE 2: THE OPTIMAL COMPENSATION FREQUENCY DOMAIN DECONVOLUTION PROCESS

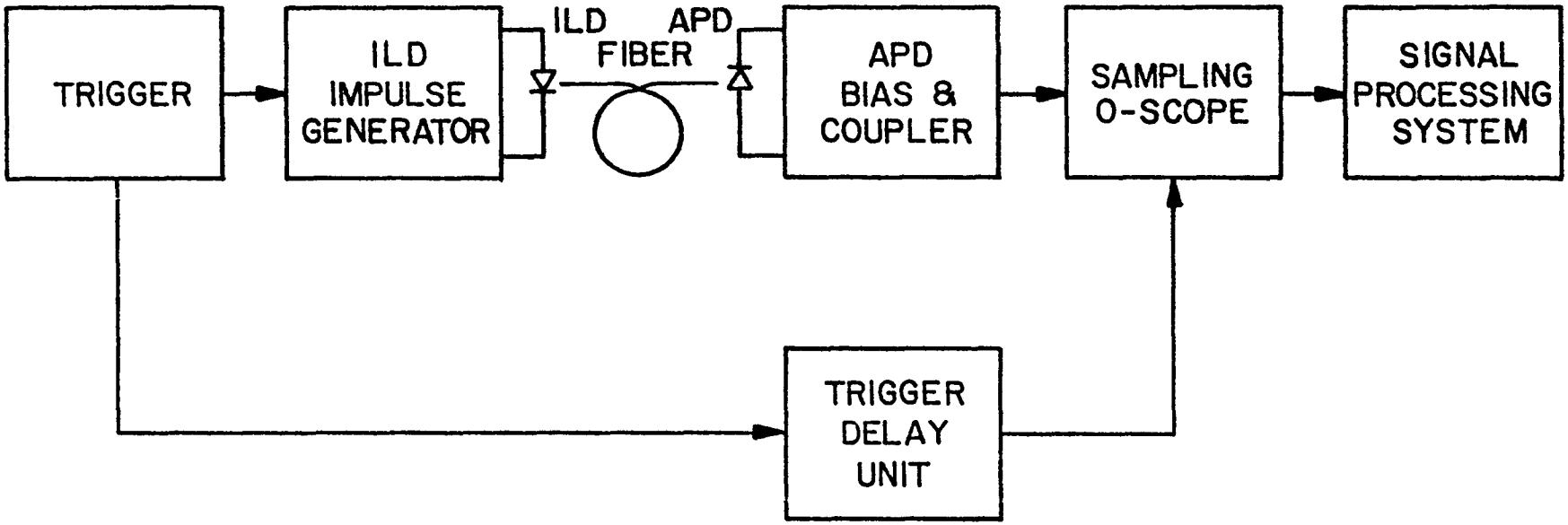

FIGURE 3: THE KSC PULSE DISPERSION TEST SET (PDTS).

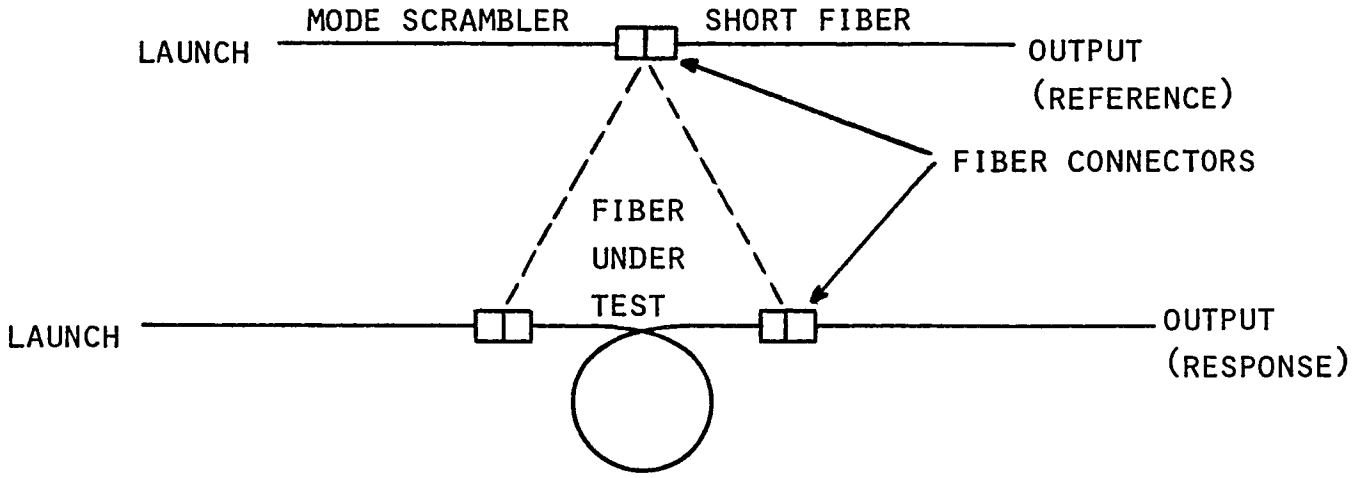

FIGURE 4: FIBER INSERTION MEASUREMENT USING FIBER CONNECTORS.

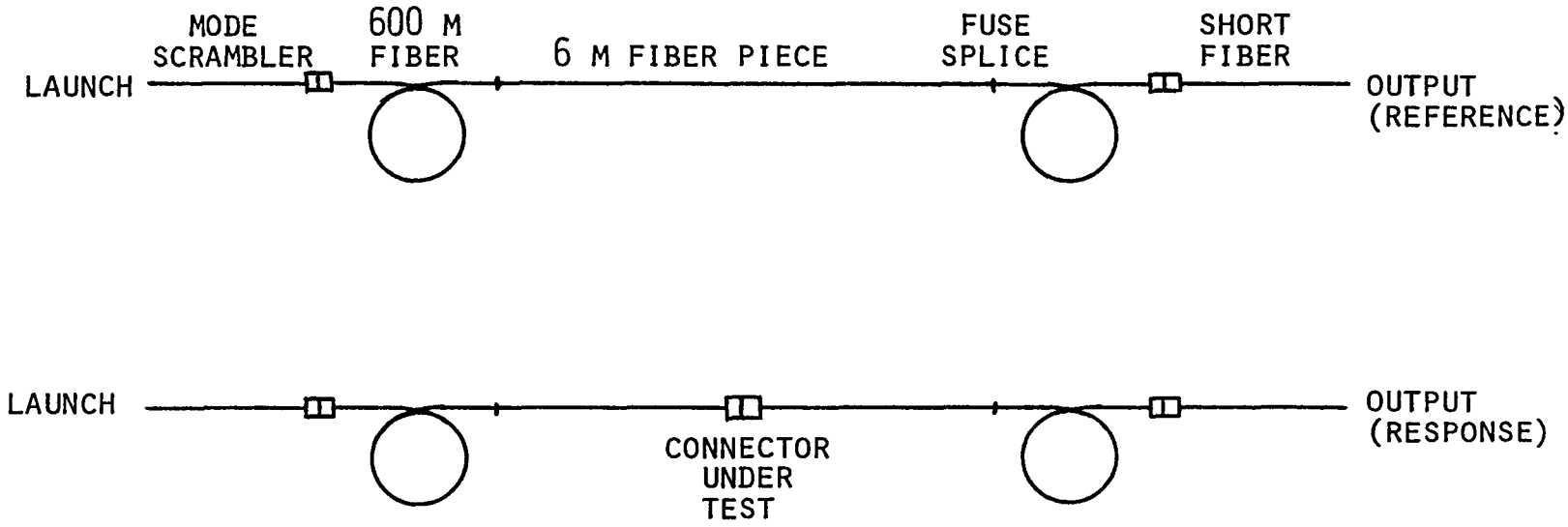

FIGURE 5: CONNECTOR(S) OR SPLICE INSERTION MEASUREMENT

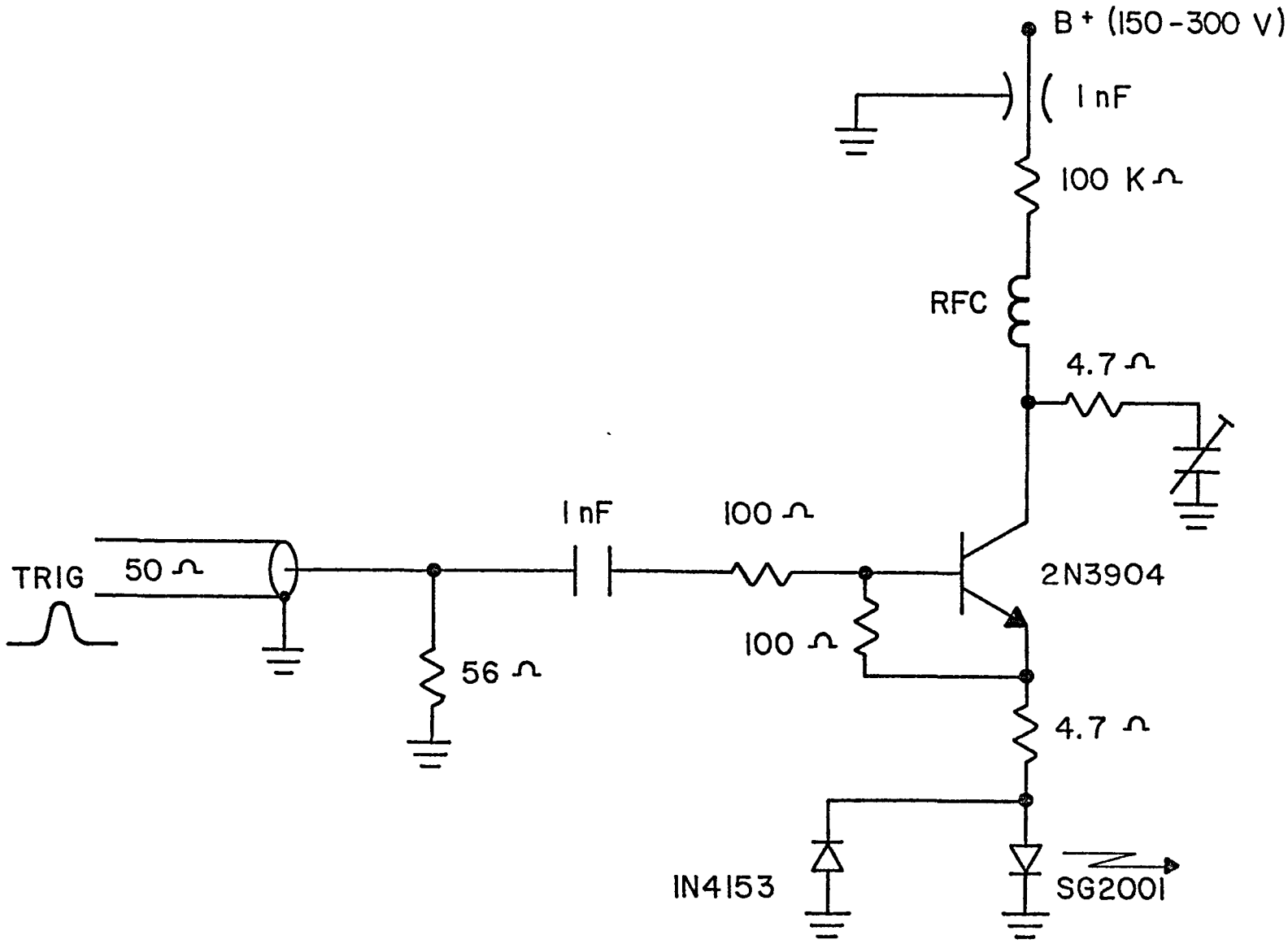

FIGURE 6: ILD IMPULSE GENERATOR SCHEMATIC DIAGRAM.

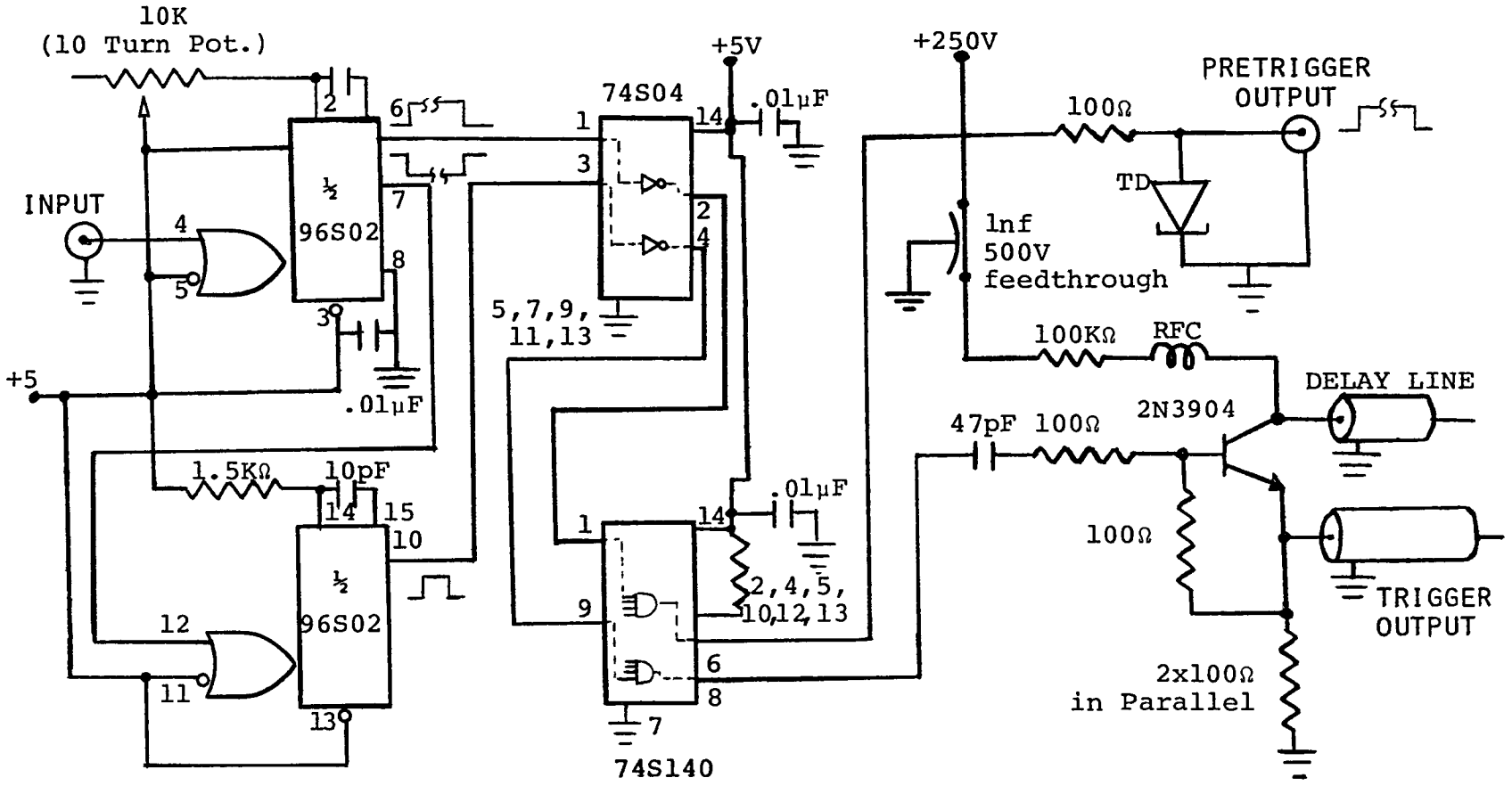

FIGURE 7: TRIGGER CIRCUIT

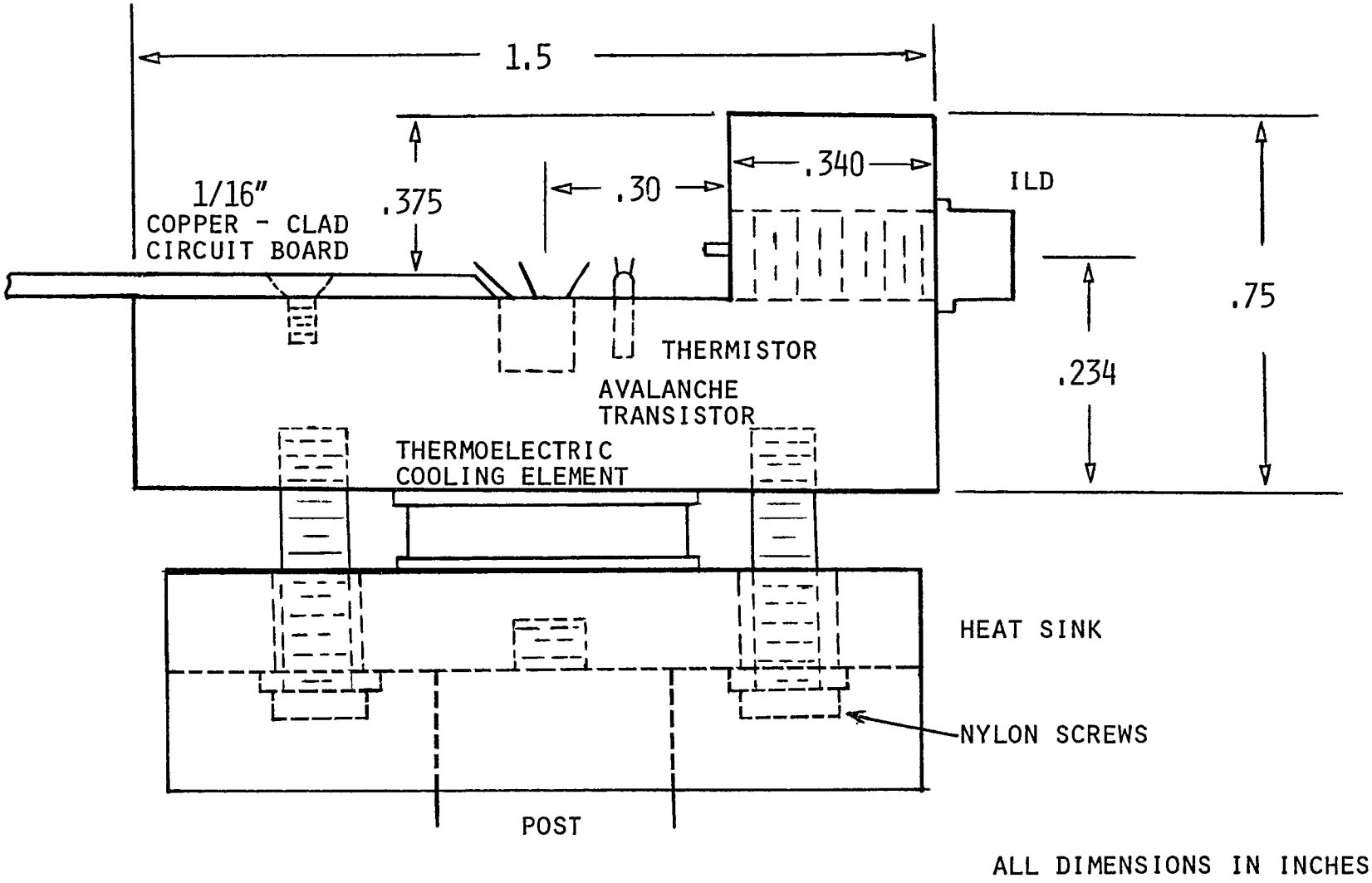

FIGURE 8: IMPULSE GENERATOR/ILD CONSTRUCTION DETAILS

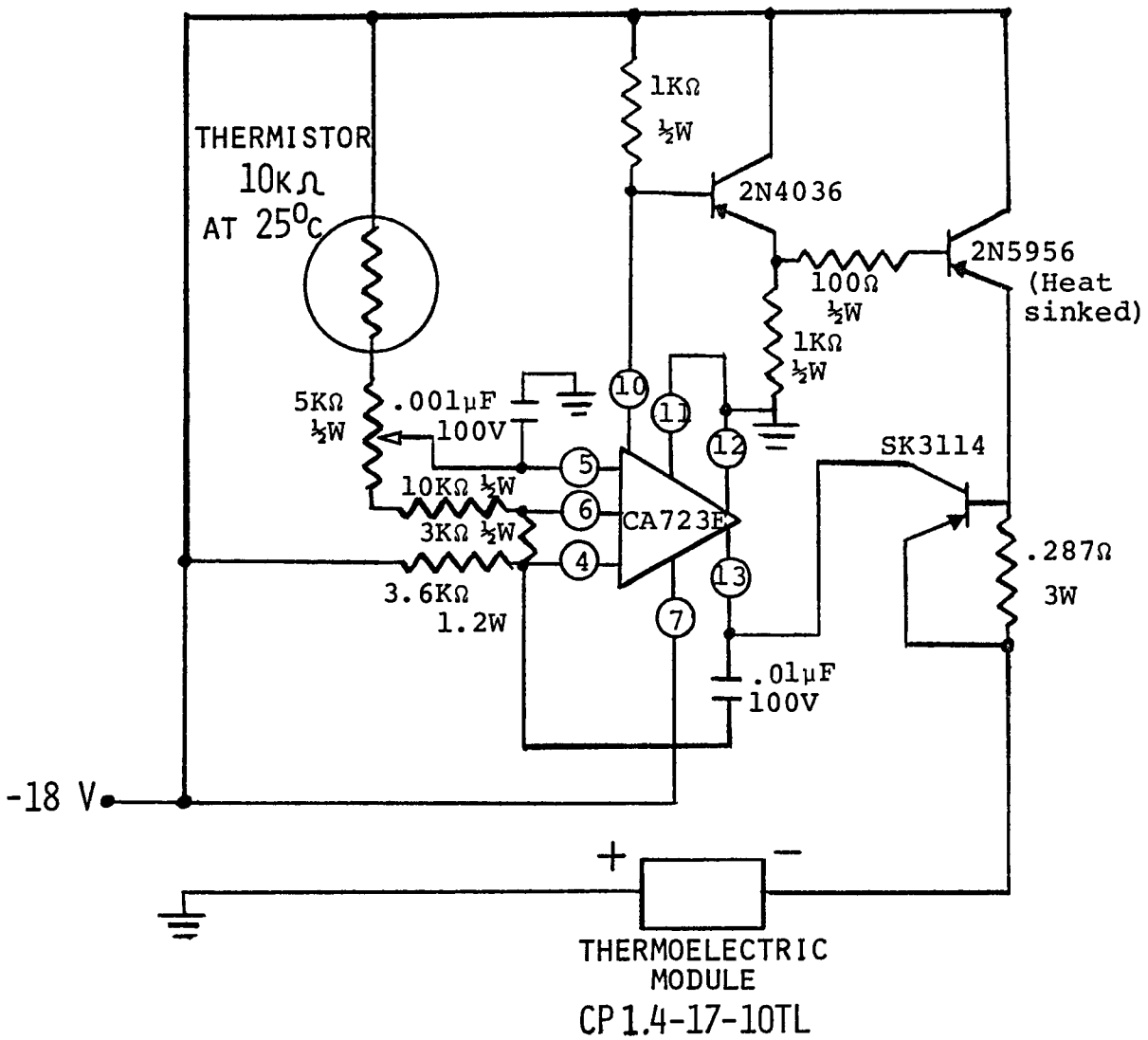

FIGURE 9: THERMOELECTRIC COOLING CIRCUIT

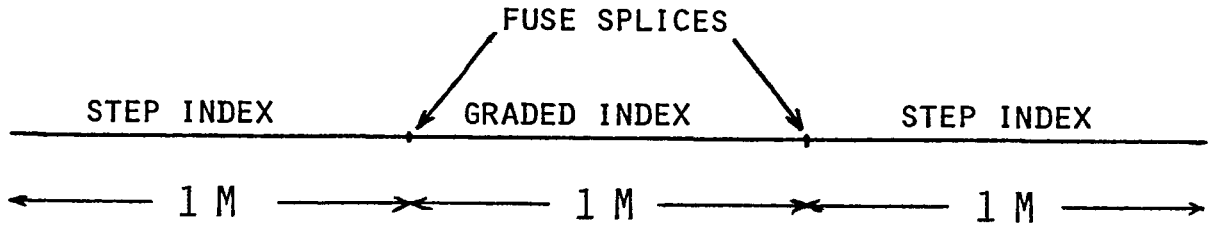

FIGURE 10: MODE SCRAMBLER

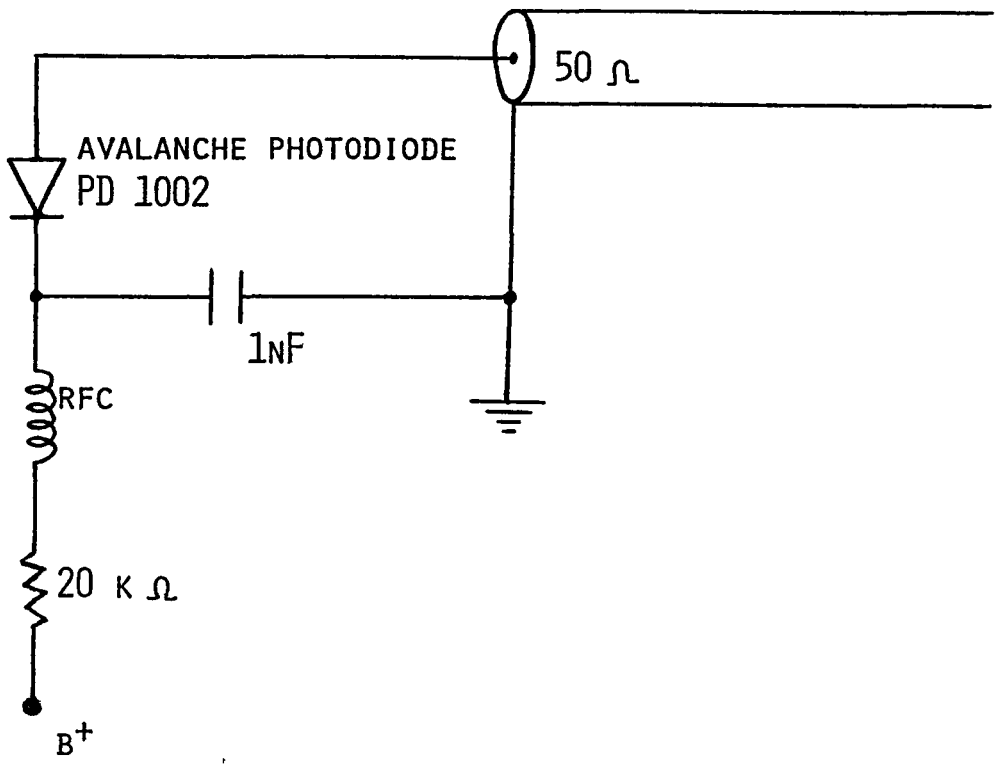

FIGURE 11: APD BIAS AND COUPLING CIRCUIT

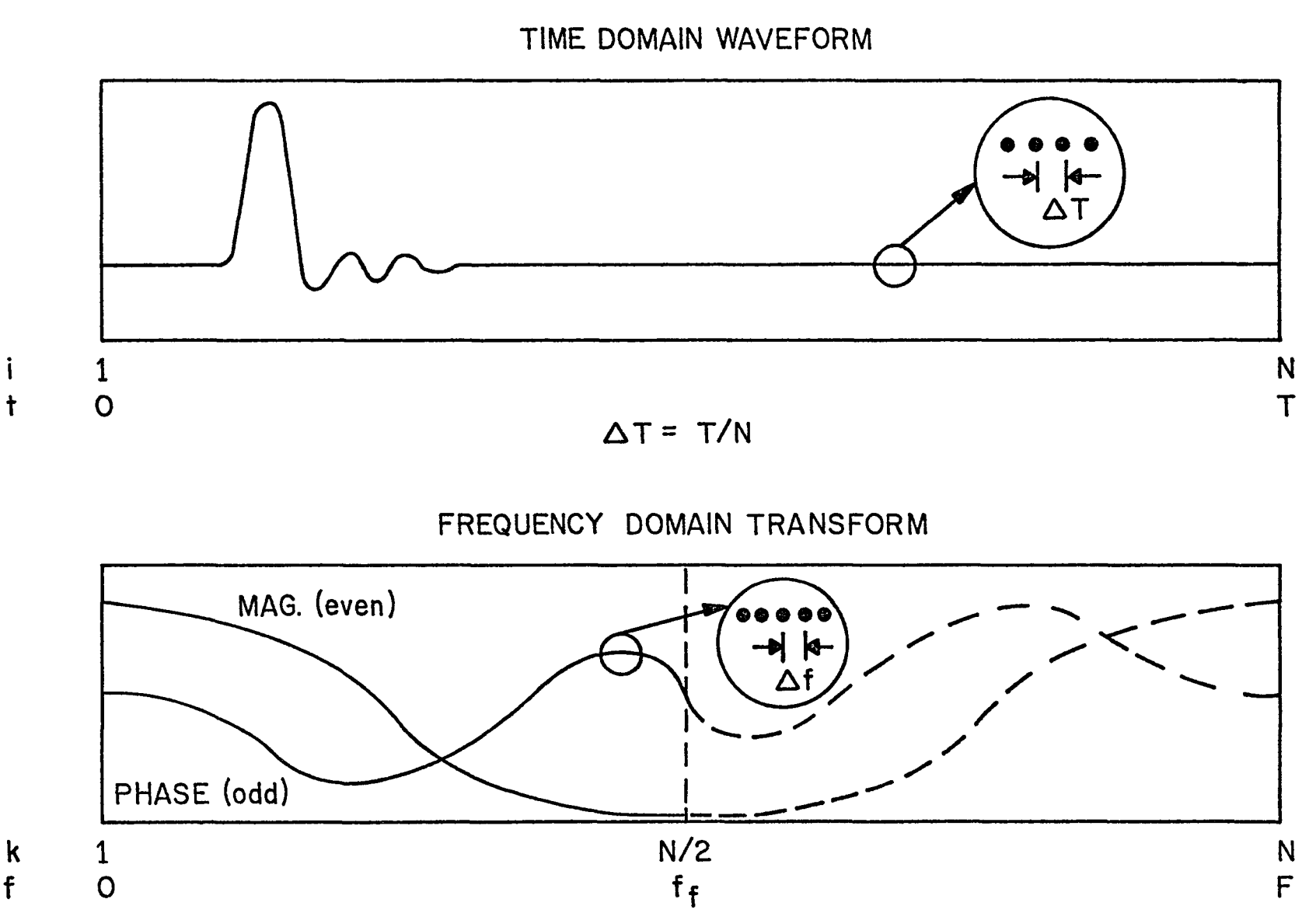

FIGURE 12: THE FAST FOURIER TRANSFORM (FFT).

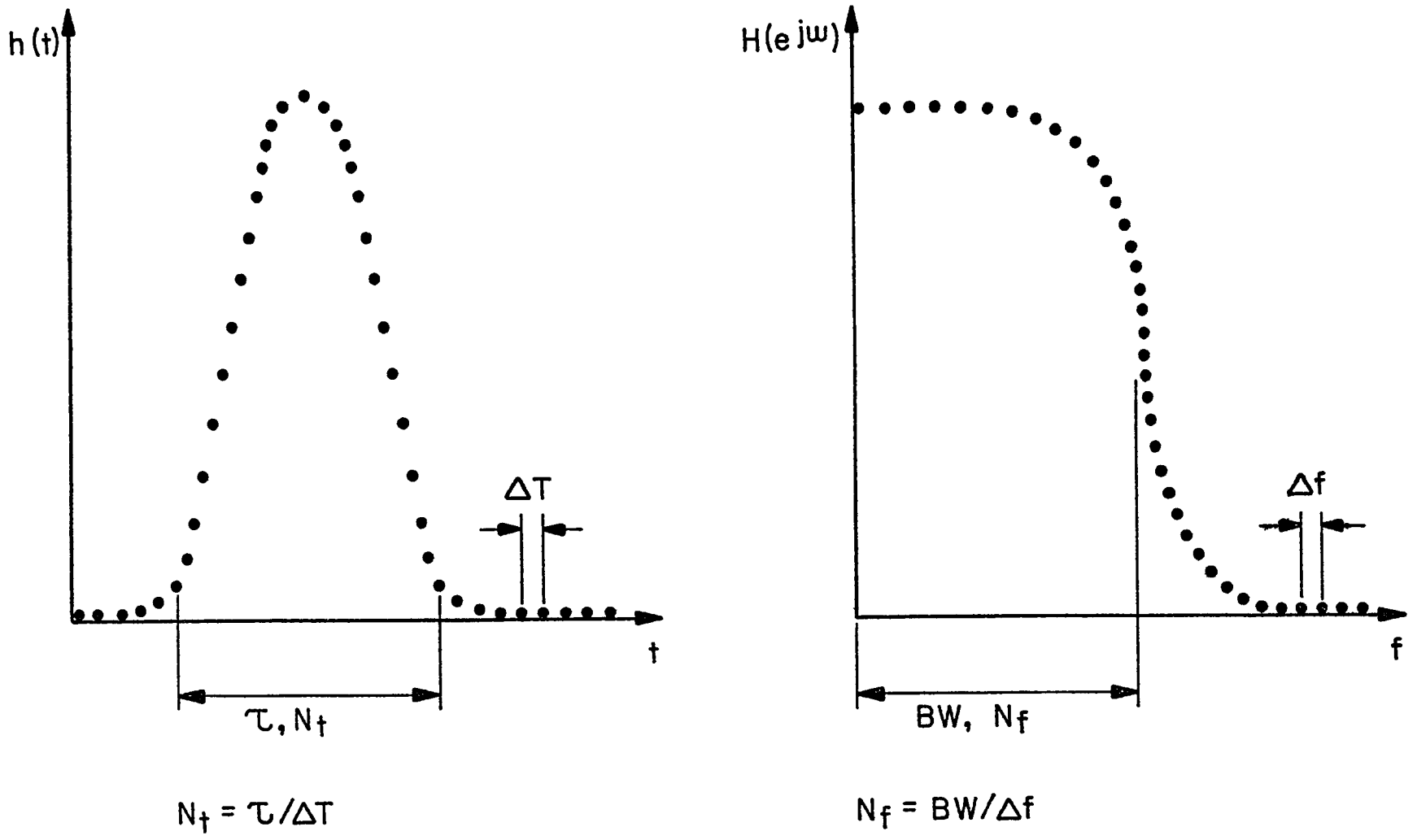

FIGURE 13: TIME AND FREQUENCY DOMAIN RESOLUTIONS.

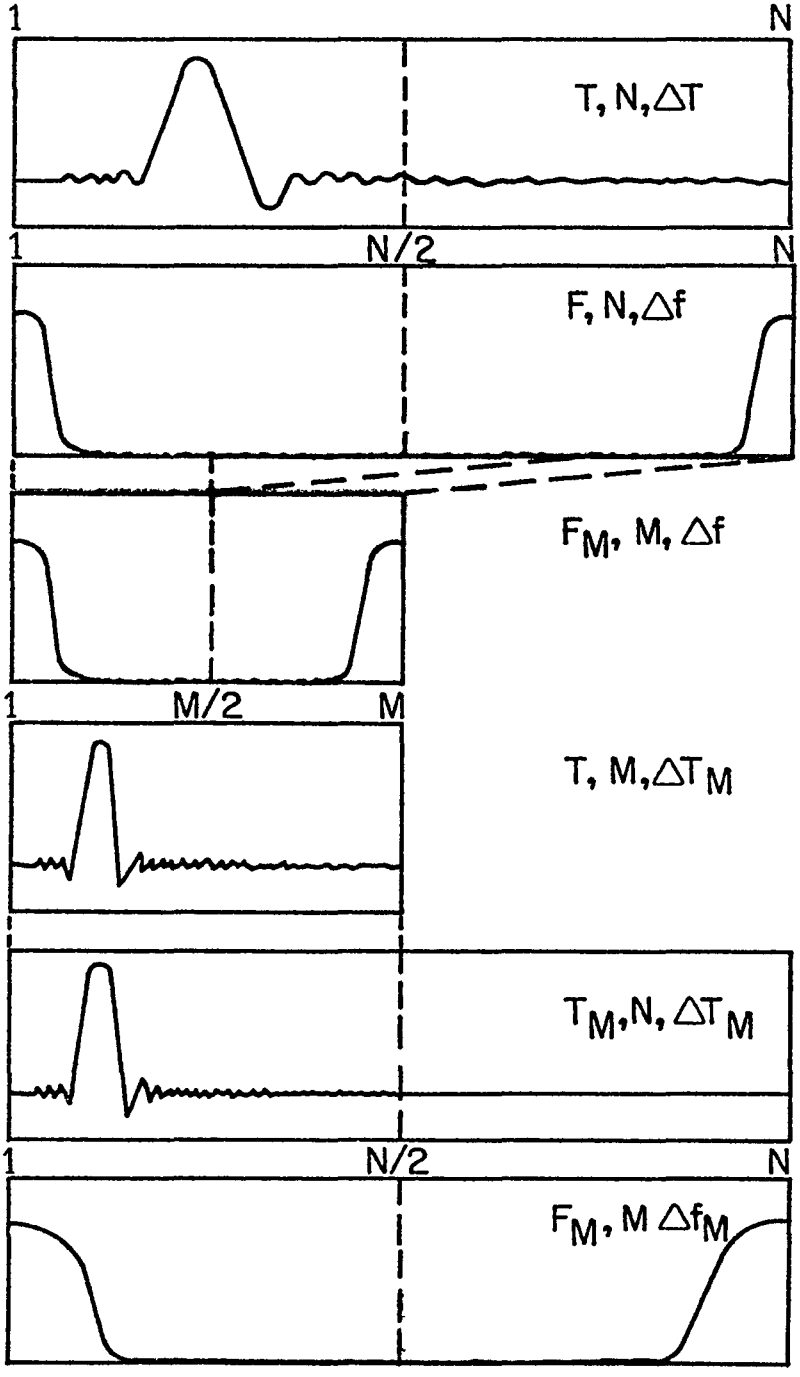

TIME DOMAIN
$\Delta T = T/N$

FREQUENCY DOMAIN
$\Delta f = 1/(N \bullet \Delta T)$
$f_f = \frac{N}{2}\Delta f,\ F = N \bullet \Delta f$

FREQUENCY DOMAIN

$f_{f_M} = \frac{M}{2}\Delta f,\ F_M = M \bullet \Delta f$

TIME DOMAIN
$\Delta T_M = 1/F_M = \frac{N}{M}\Delta T$
$M \bullet \Delta T_M = N \bullet \Delta T = T$

TIME DOMAIN
$T_M = N \bullet \Delta T_M$

FREQUENCY DOMAIN
$\Delta f_M = 1/T_M = F_M/N$
$\Delta f_M = \frac{M}{N}\Delta f$

FIGURE 14: FREQUENCY DOMAIN RESOLUTION ENHANCEMENT WITH INTERPOLATION USING THE FFT PROPERTIES.

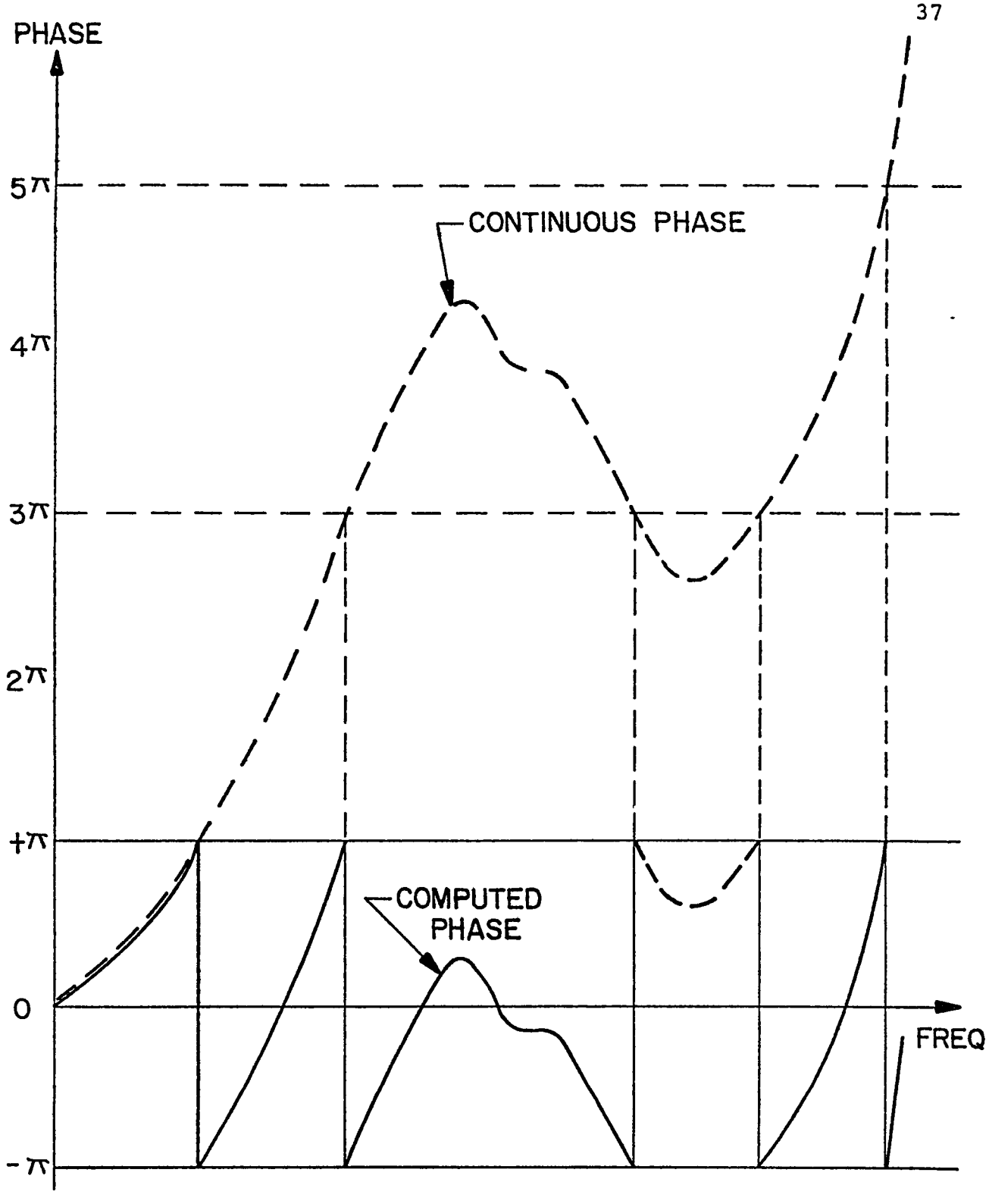

FIGURE 15: COMPUTED AND RECONSTRUCTED CONTINUOUS PHASE FUNCTIONS.

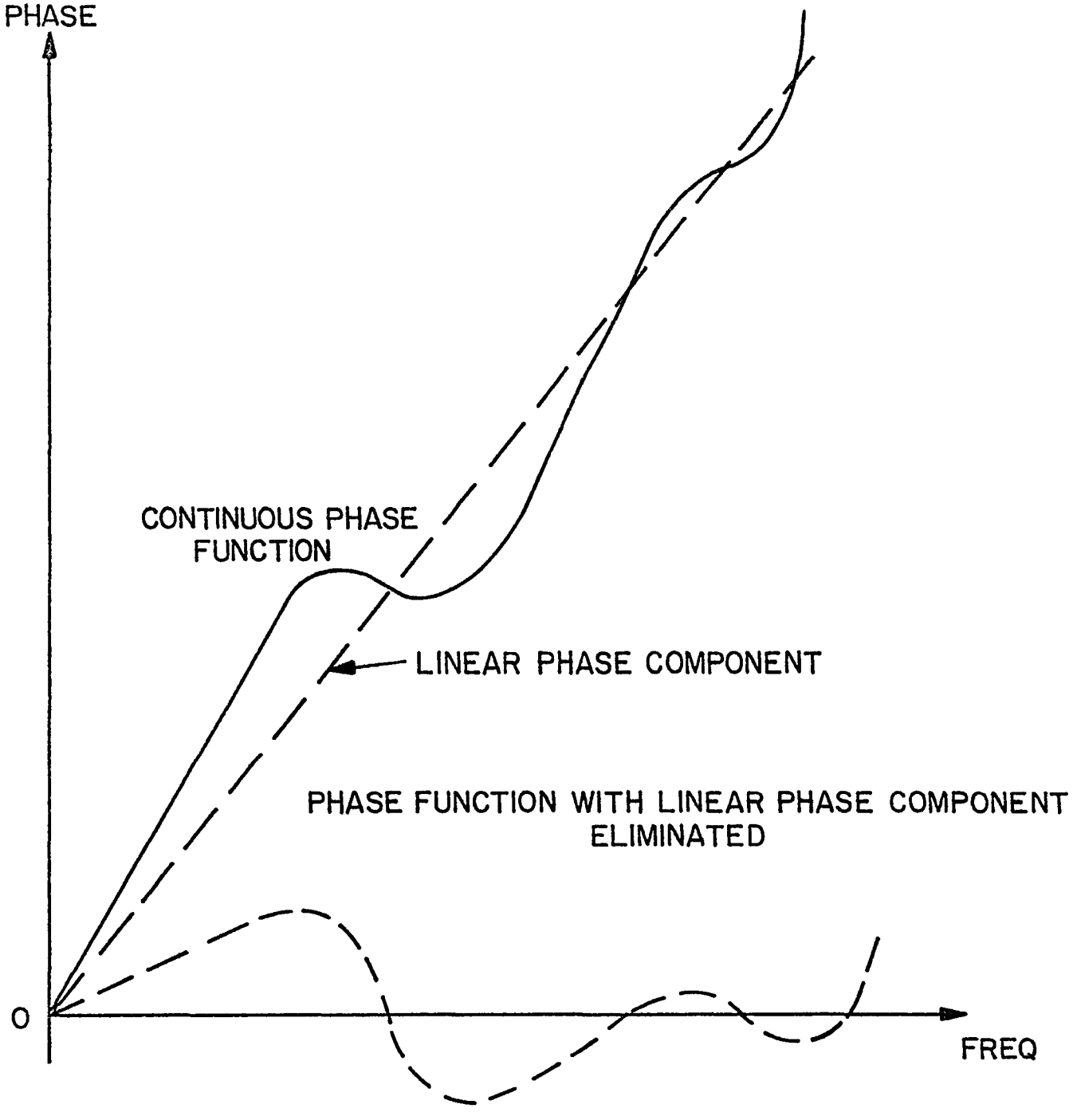

FIGURE 16: ELIMINATING LINEAR PHASE COMPONENT TO REVEAL PHASE DETAILS.

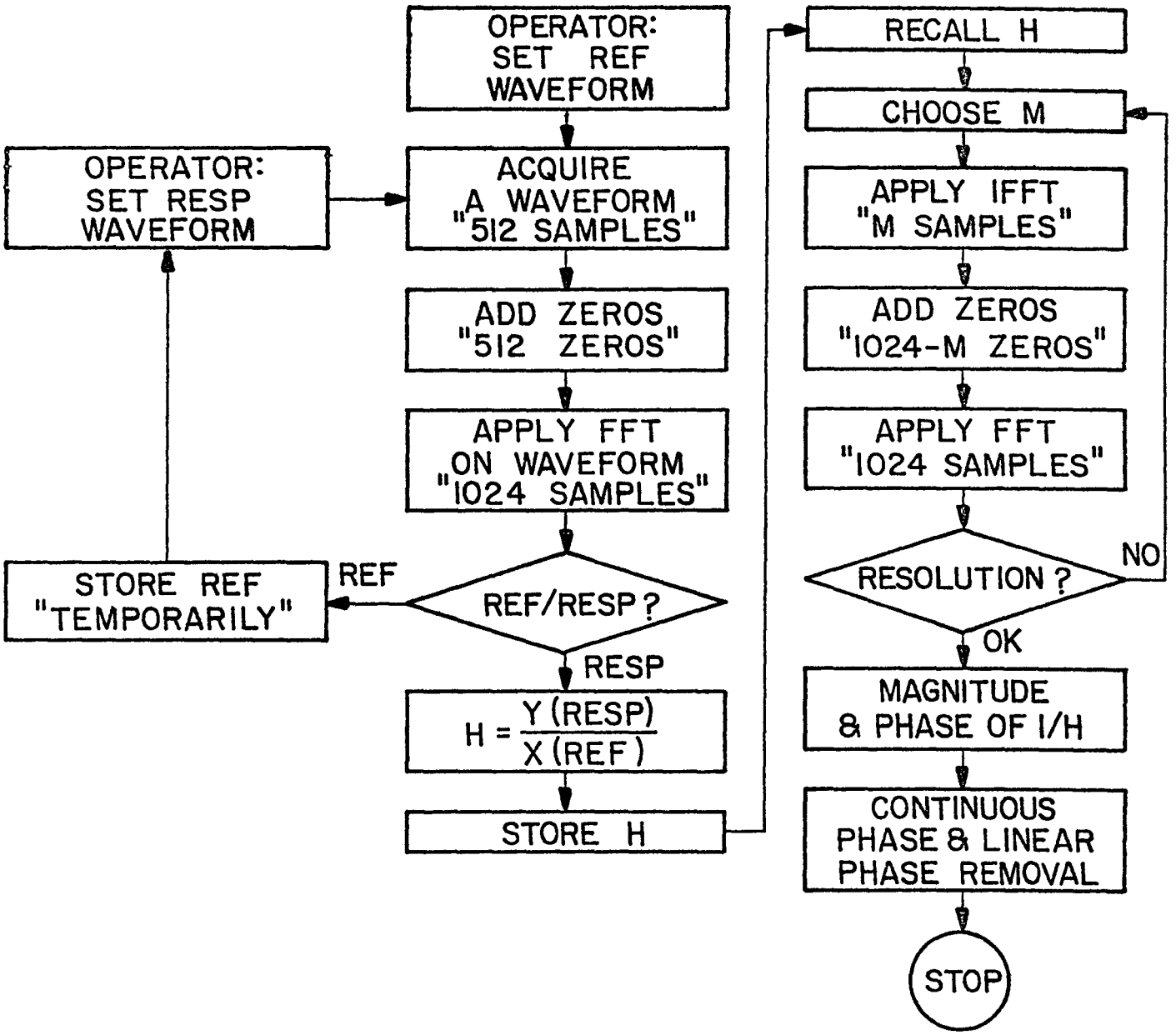

FIGURE 17: DISPERSION TEST SIGNAL PROCESSING FLOW CHART

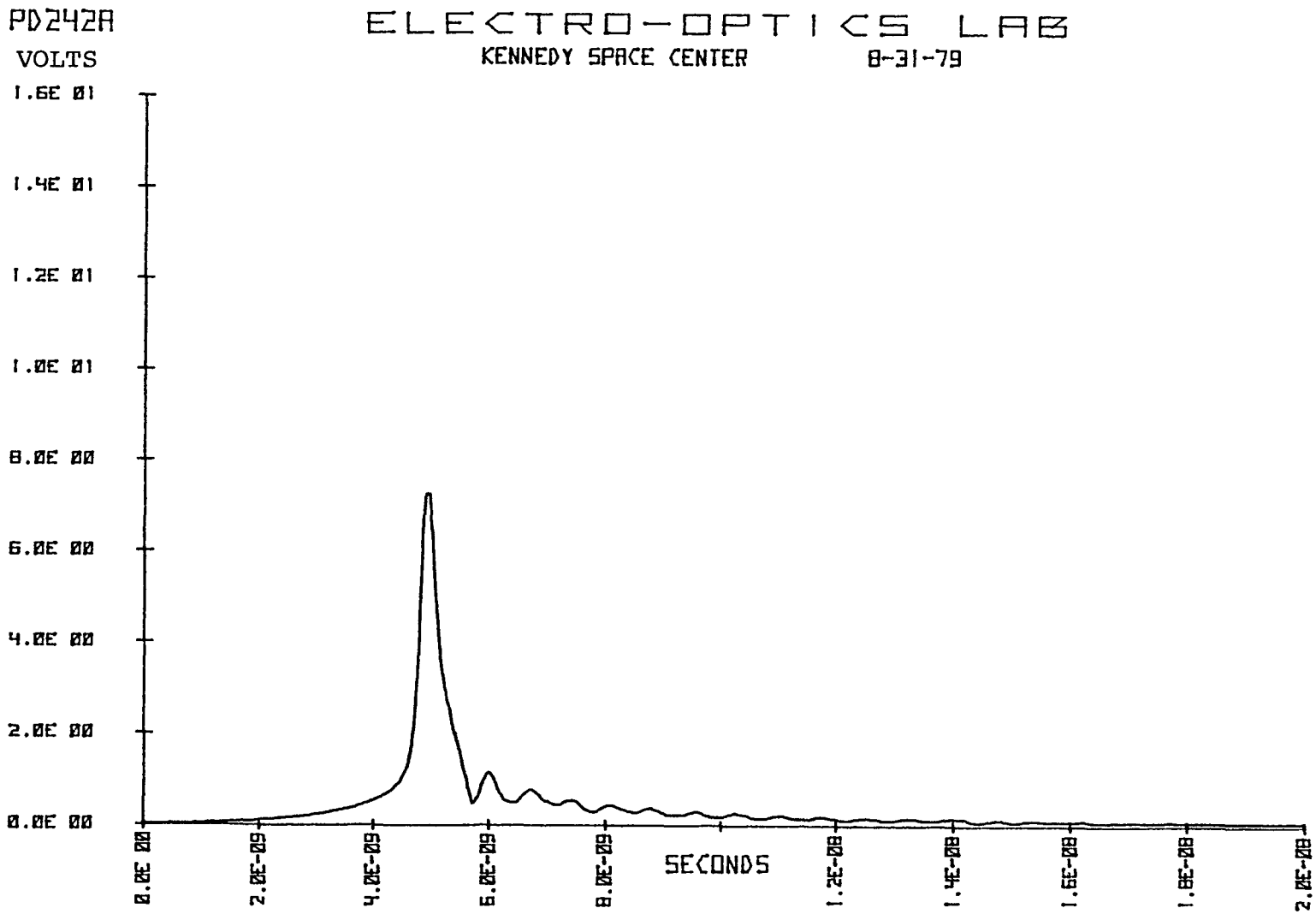

FIGURE 18a: REFERENCE WAVEFORM FOR TESTING 4km FIBER.

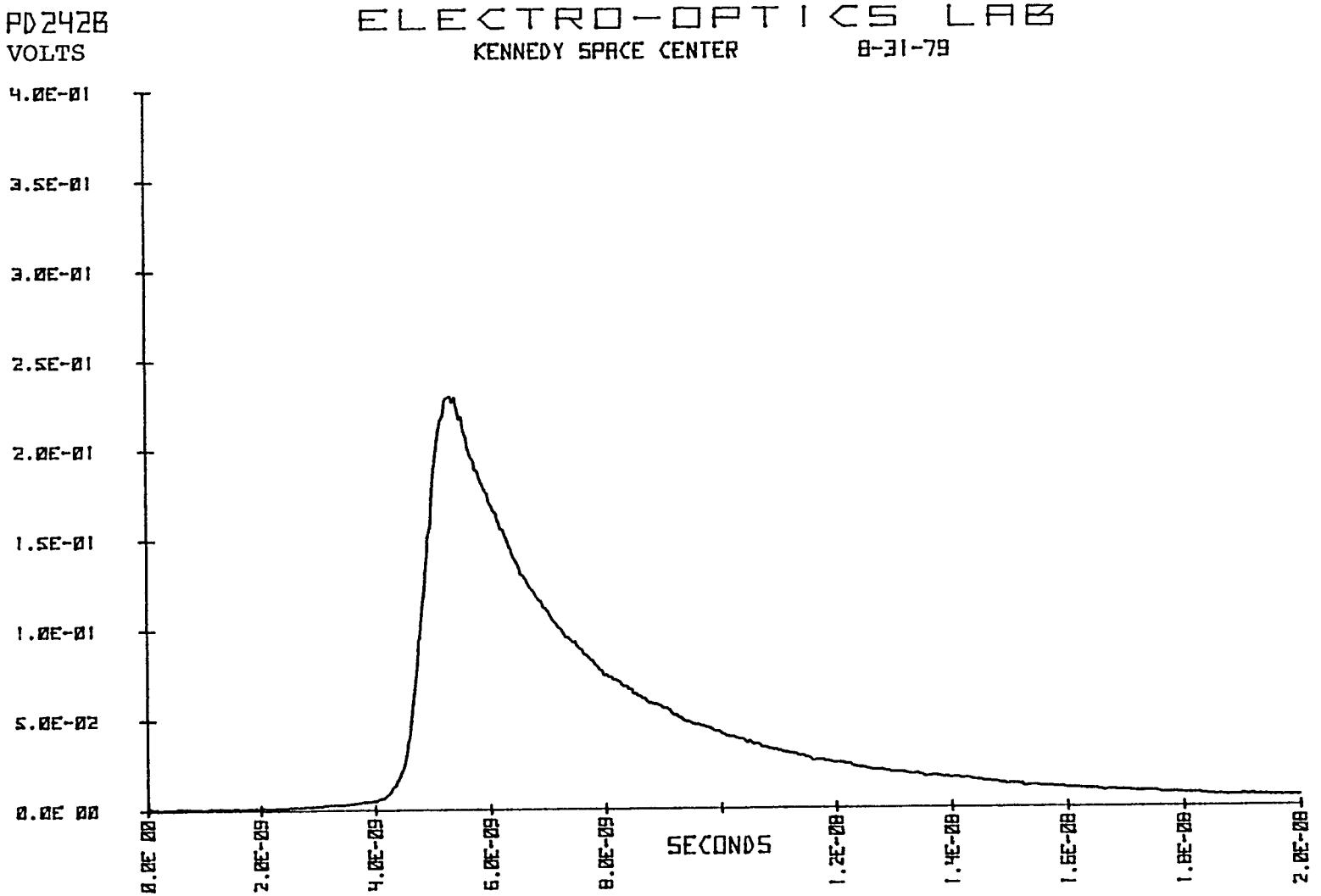

FIGURE 18b: RESPONSE WAVEFORM OF 4 km FIBER.

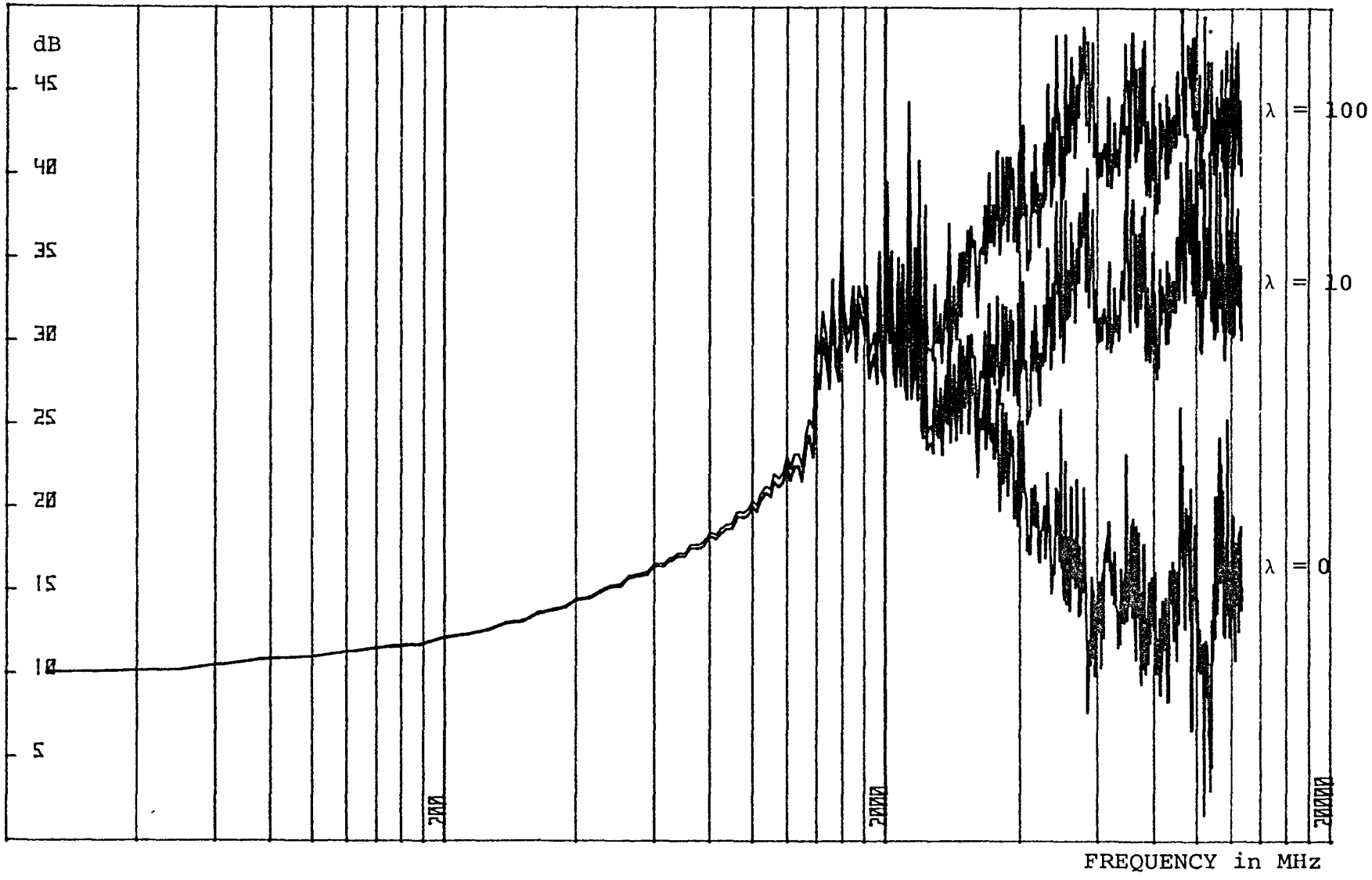

FIGURE 18c: 4 km FIBER ATTENUATION FOR VARIOUS VALUES OF λ.

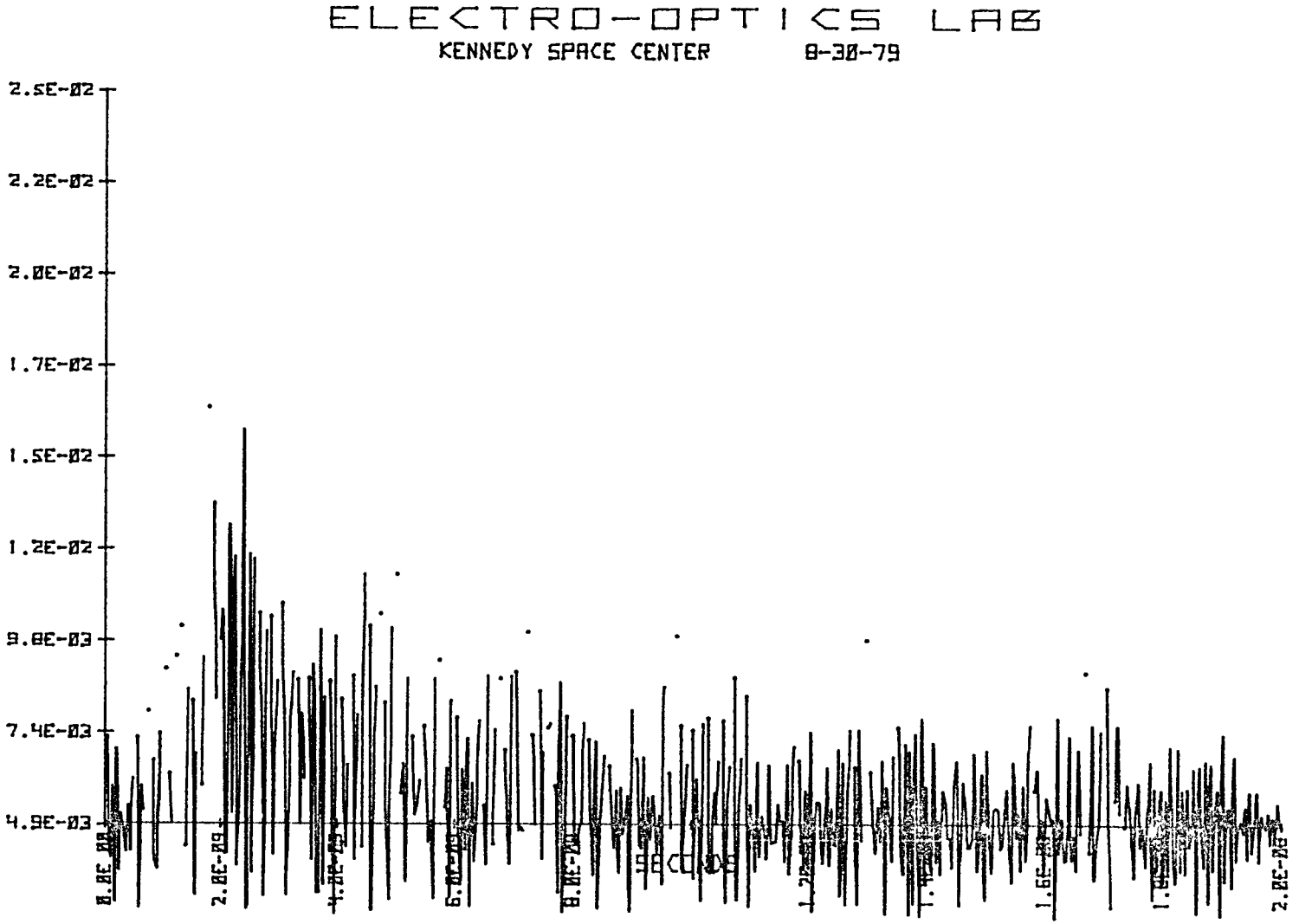

FIGURE 18d: 4km FIBER IMPULSE RESPONSE AS COMPUTED USING $\lambda = 0$.

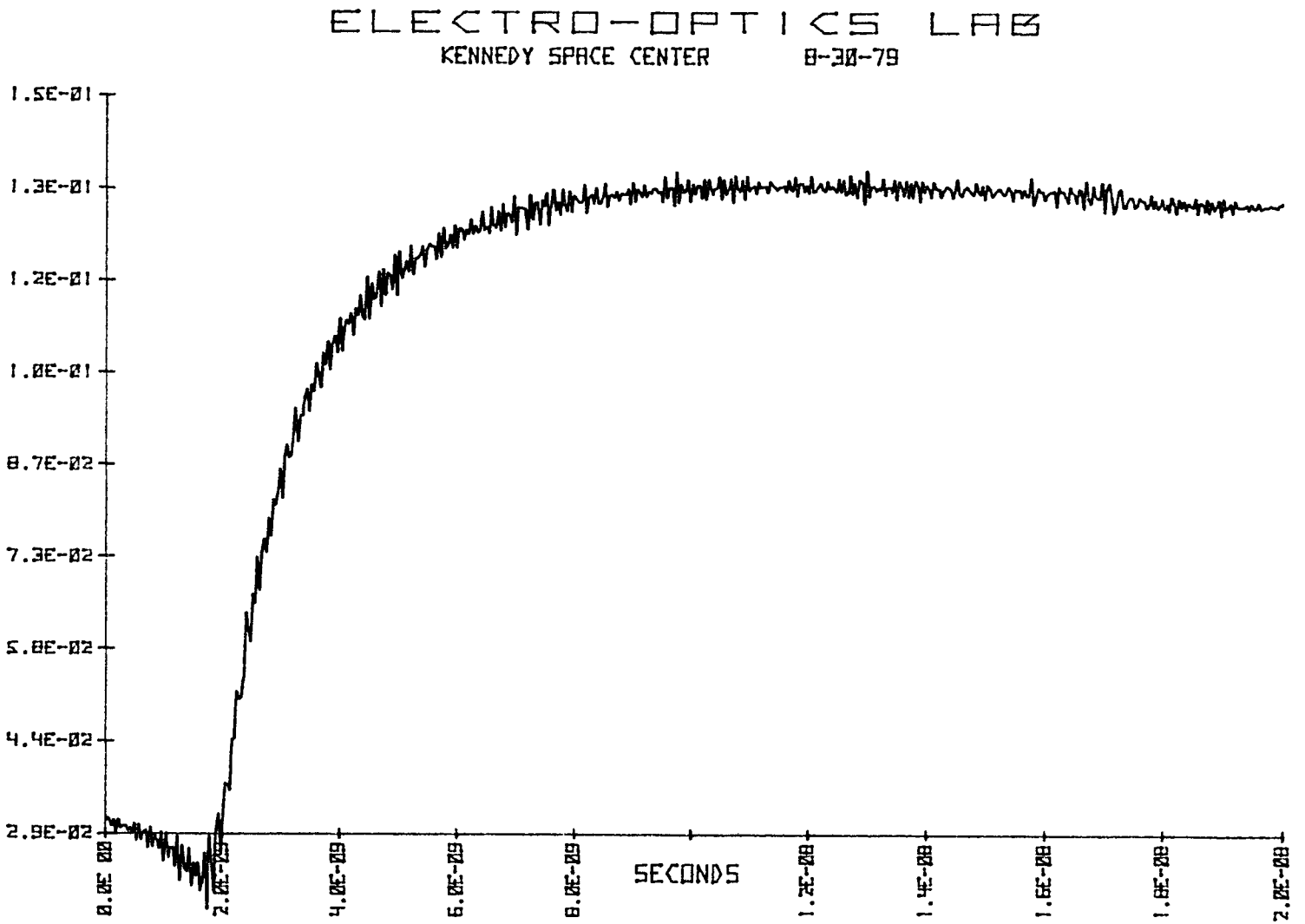

FIGURE 18e: 4km FIBER STEP RESPONSE AS COMPUTED USING $\lambda = 0$.

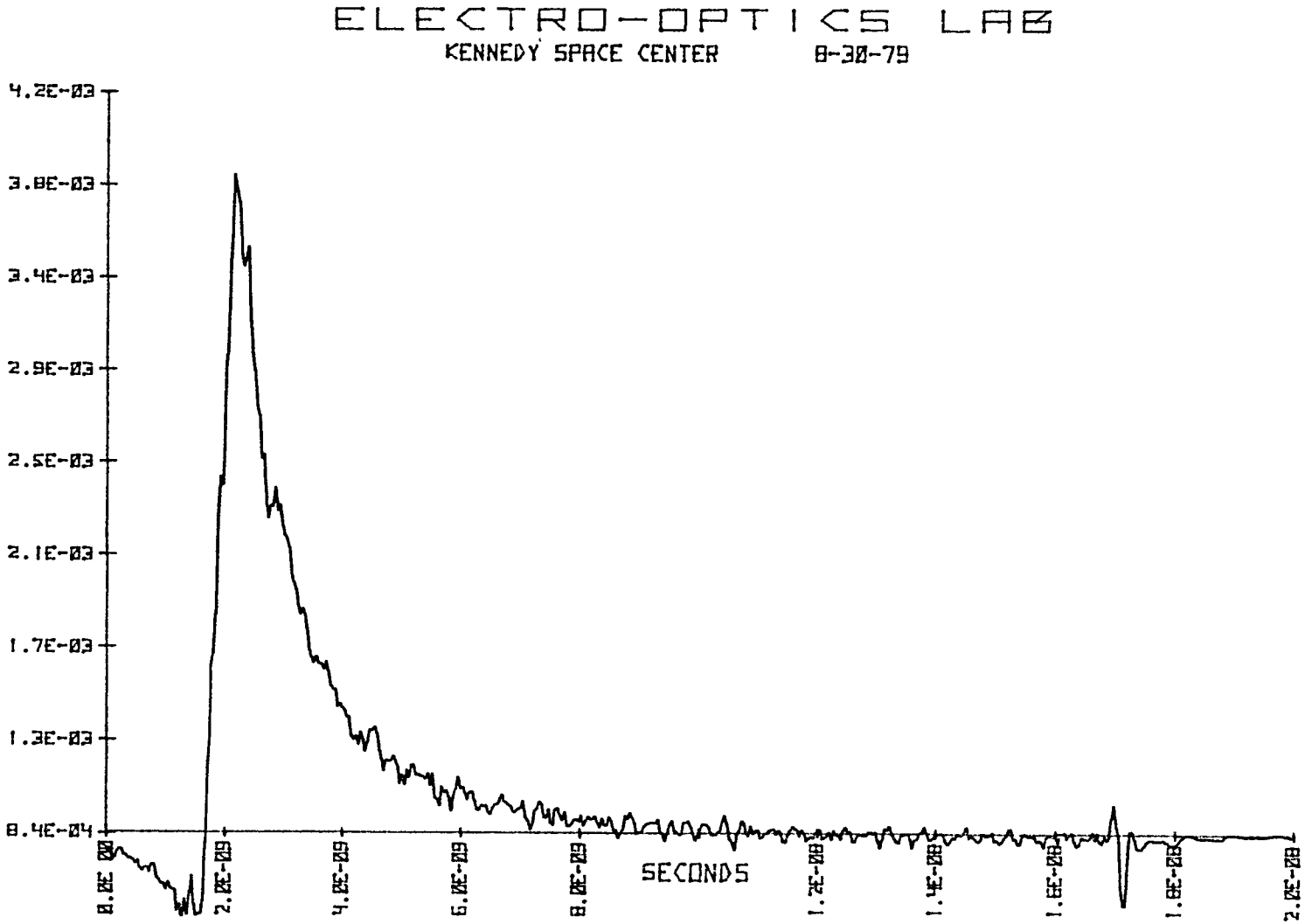

FIGURE 18f: 4km FIBER IMPULSE RESPONSE AS COMPUTED USING λ = 10.

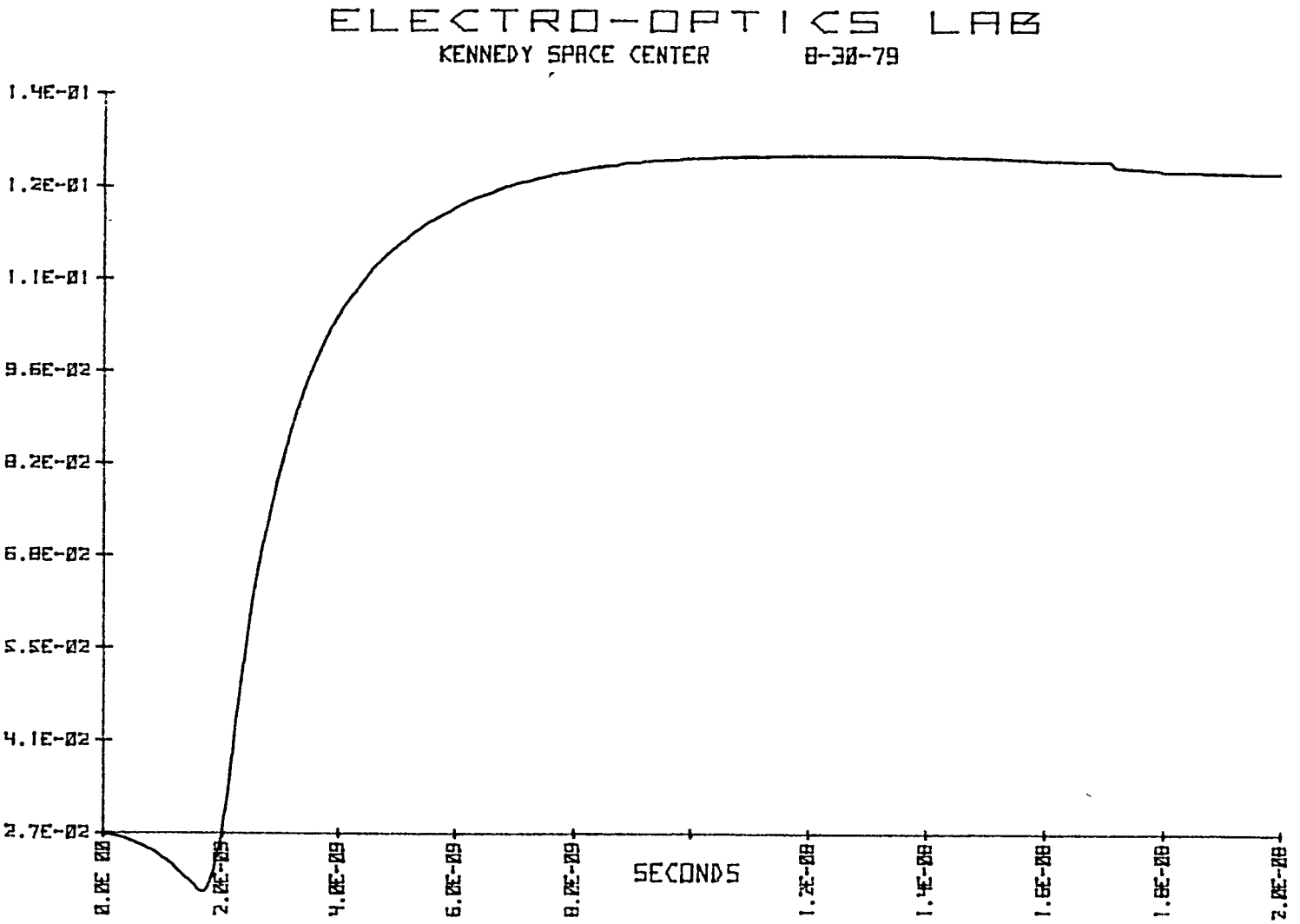

FIGURE 18g: 4km FIBER STEP RESPONSE AS COMPUTED USING $\lambda = 10$

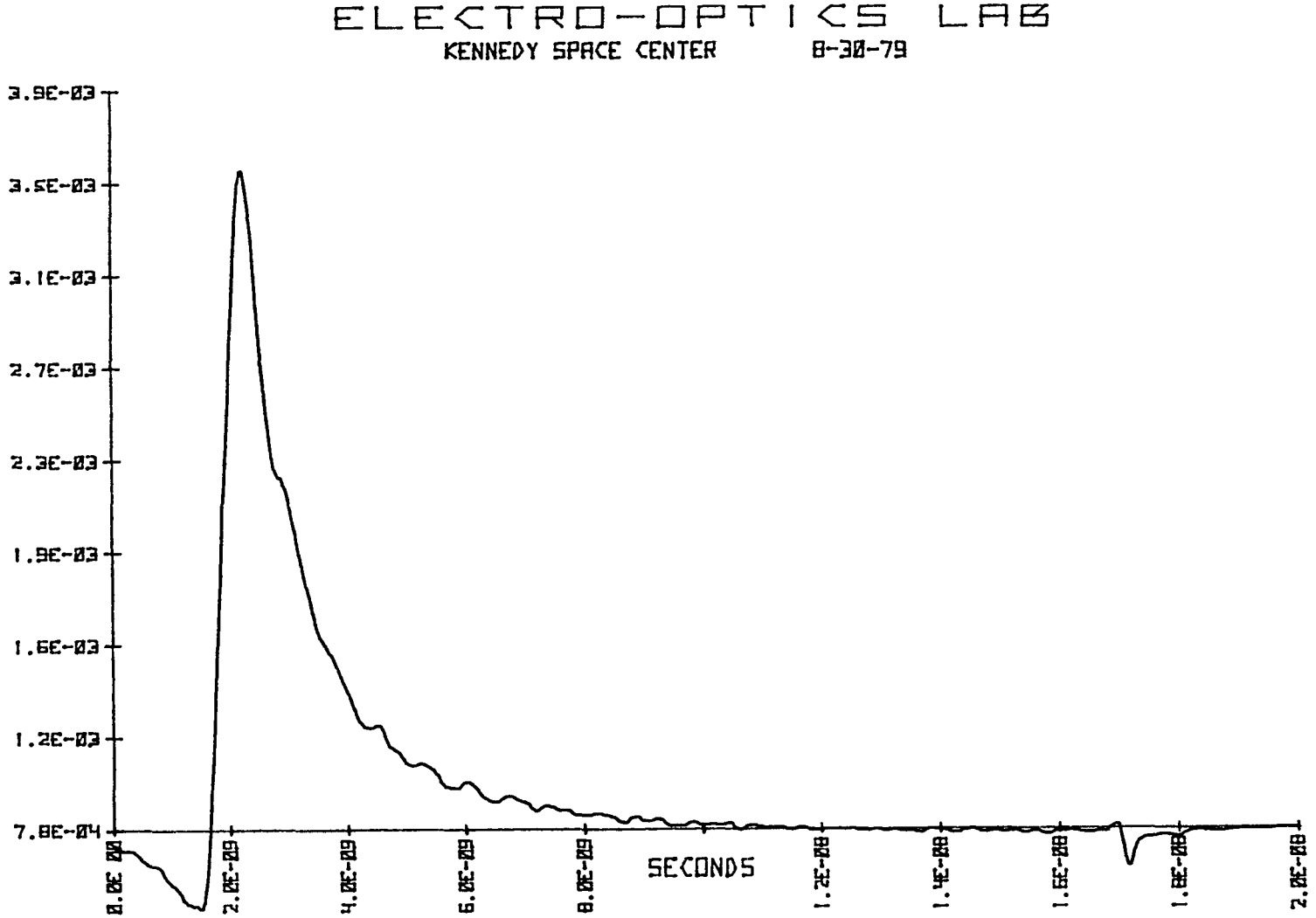

FIGURE 18h: 4km FIBER IMPULSE RESPONSE AS COMPUTED USING λ= 100.

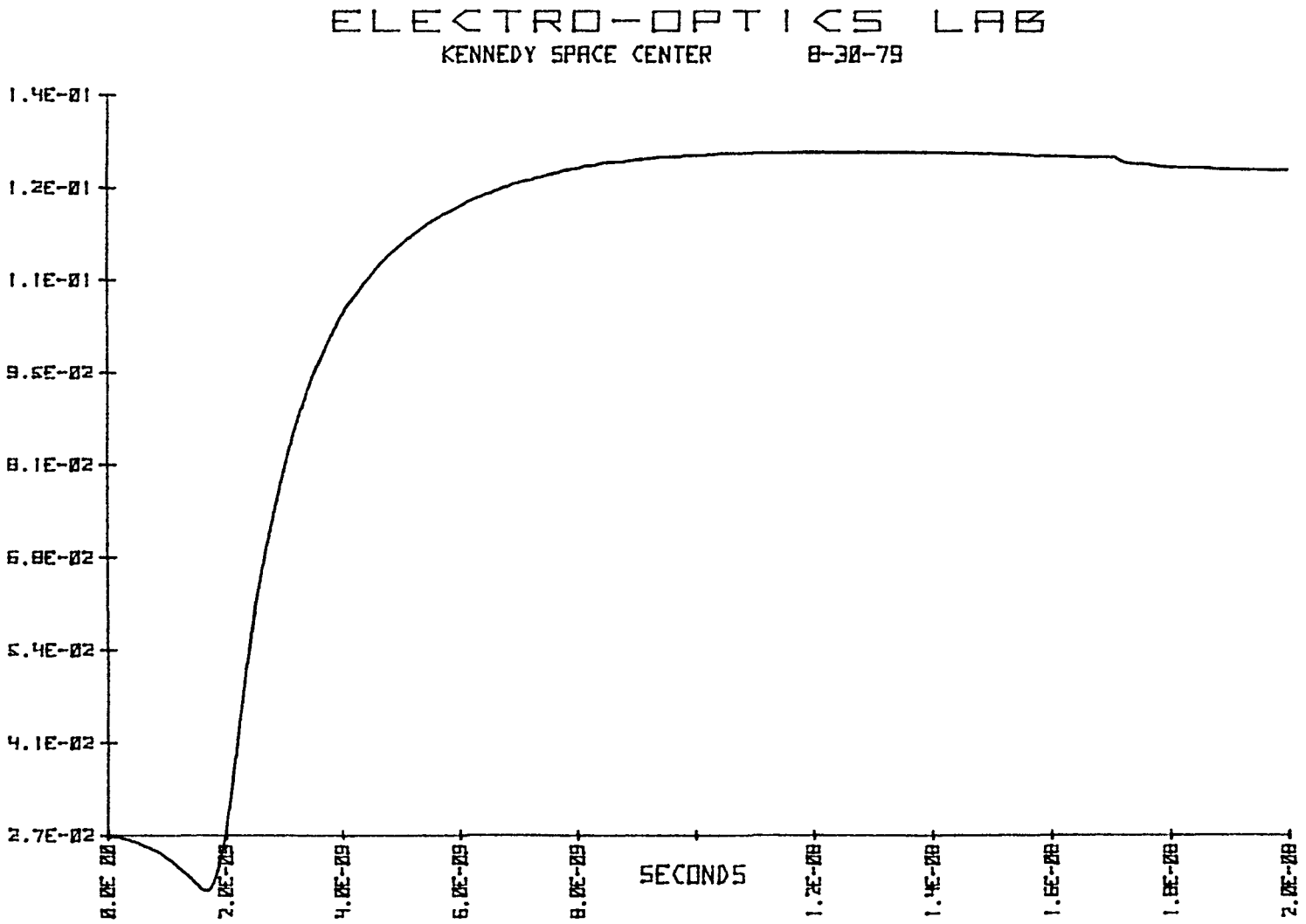

FIGURE 18i: 4km FIBER STEP RESPONSE AS COMPUTED USING λ = 100

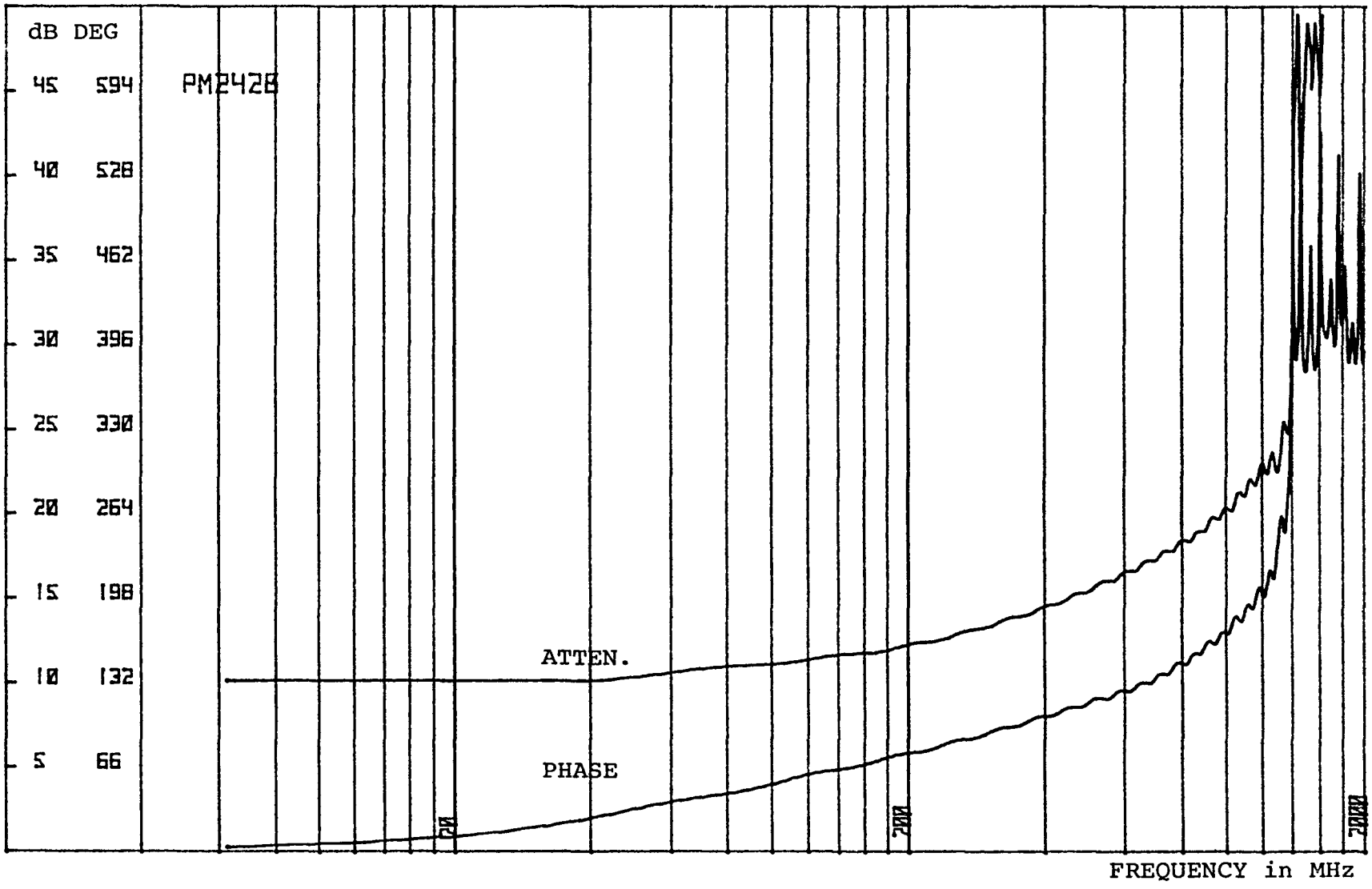

FIGURE 18j: 4km FIBER ATTENUATION AND PHASE FUNCTIONS USING OPTIMUM VALUE OF λ (= 100).

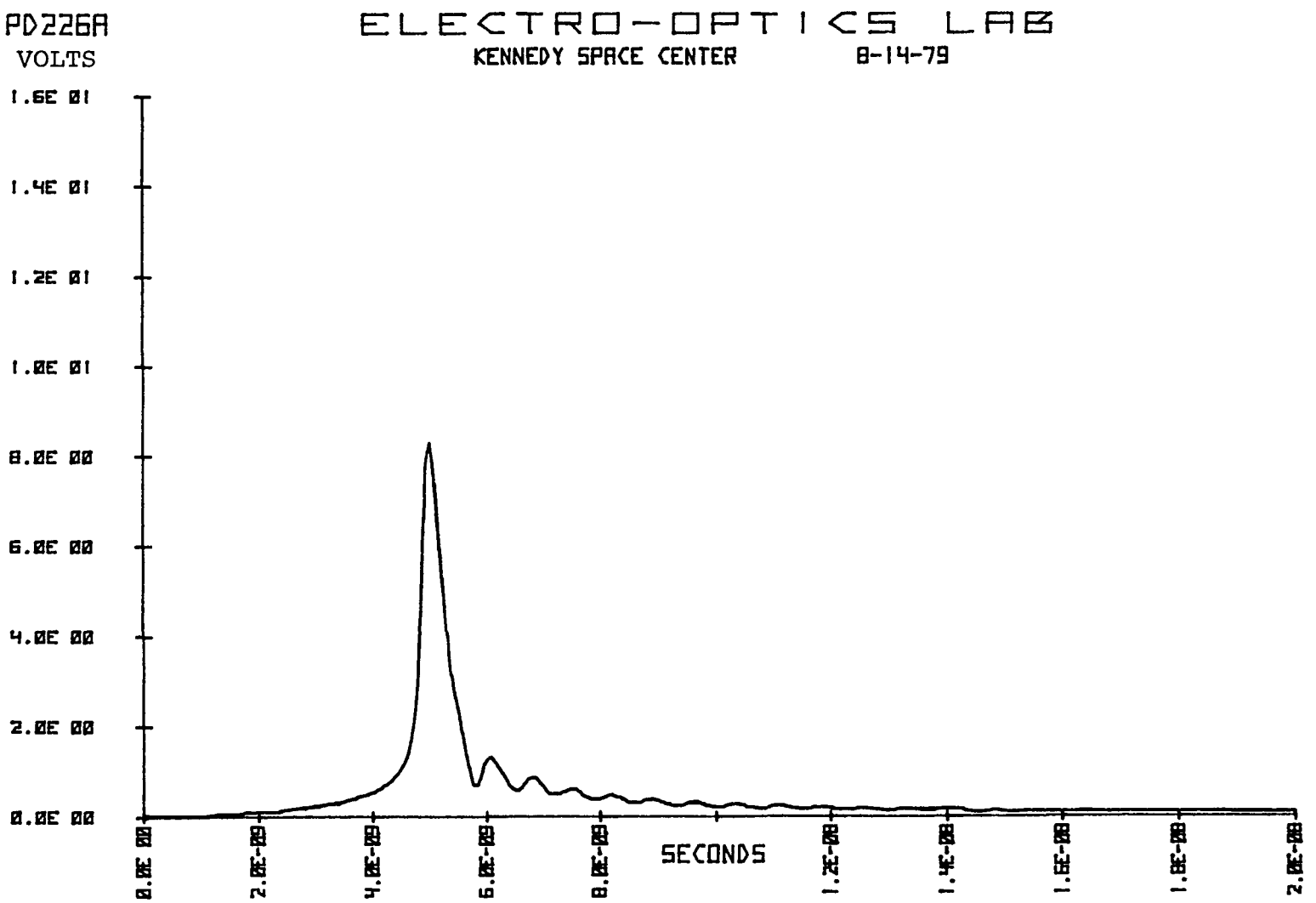

FIGURE 19: REFERENCE WAVEFORM FOR TESTING 600 m FIBER LOOPS.

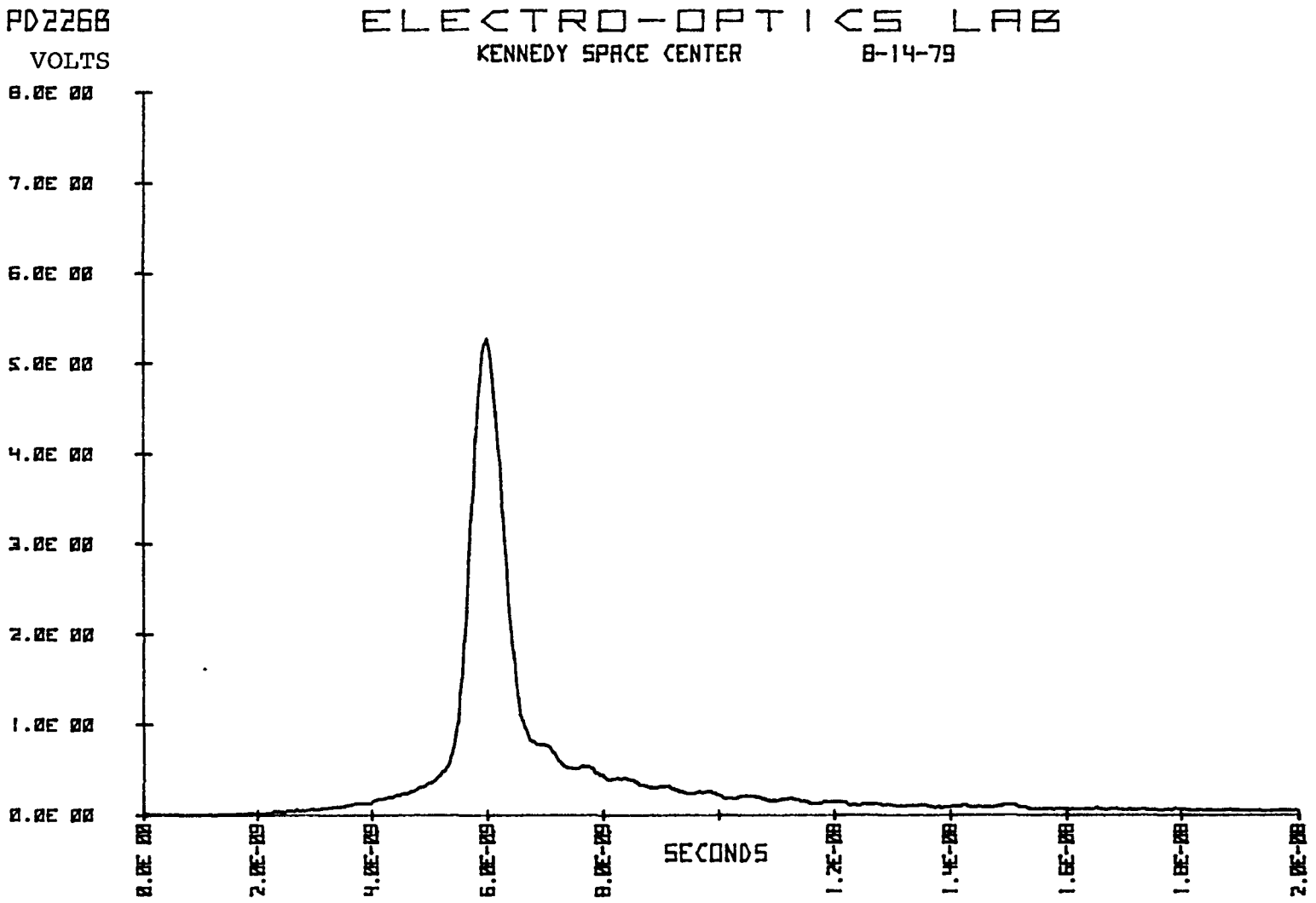

FIGURE 20a: RESPONSE WAVEFORM OF LOOP #1 600 m FIBER.

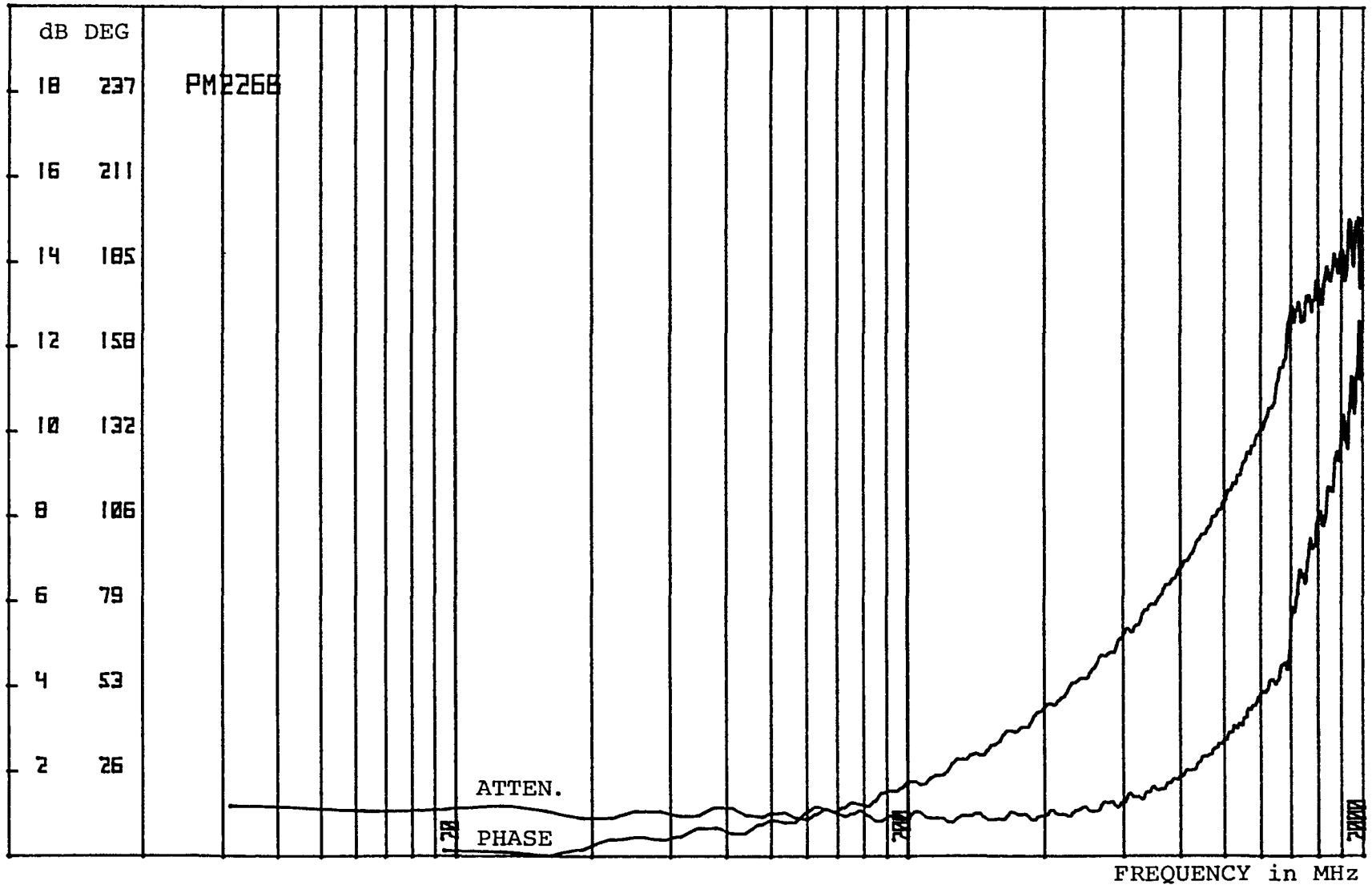

FIGURE 20b: ATTENUATION AND PHASE FUNCTIONS OF LOOP #1 600m FIBER.

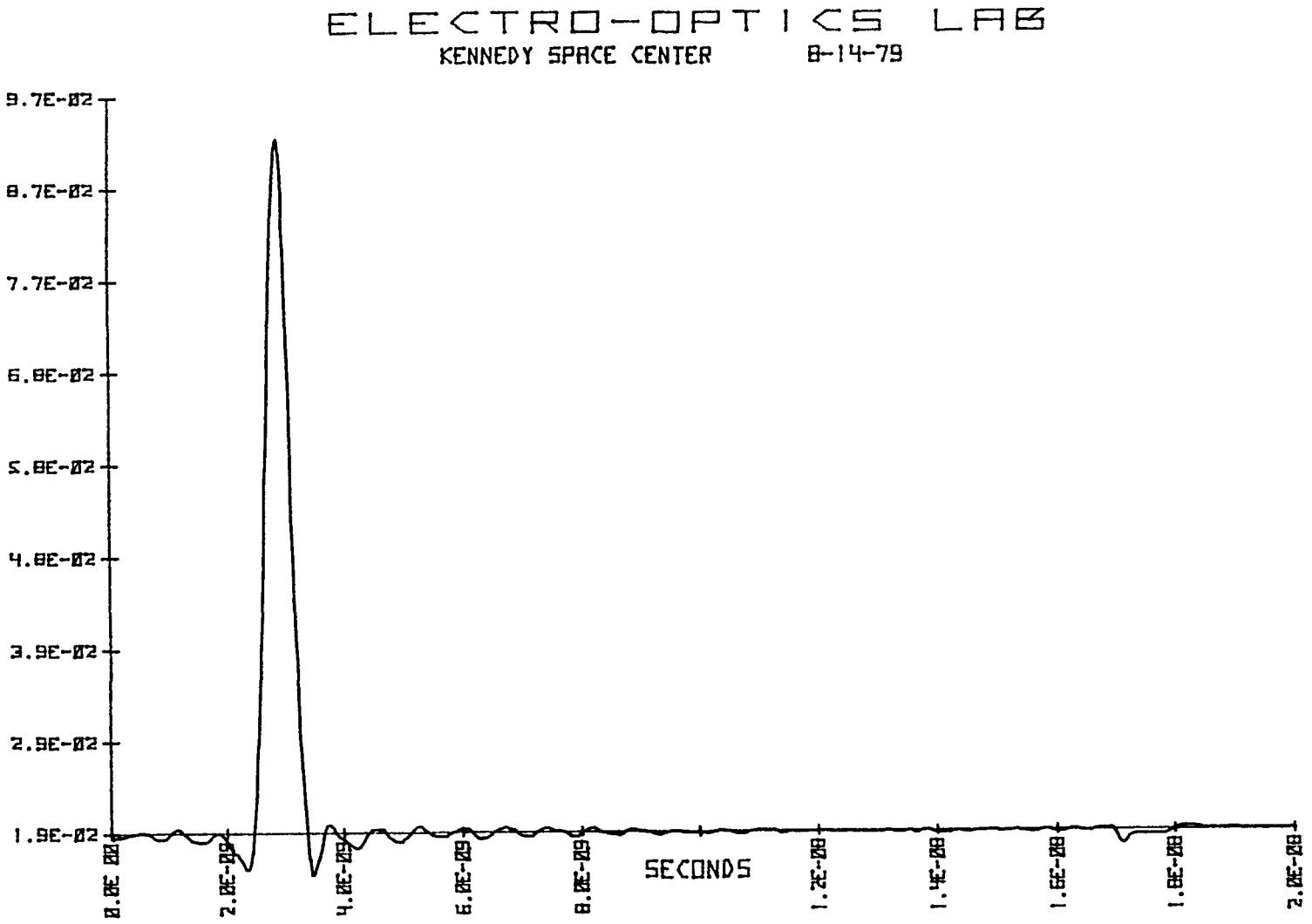

FIGURE 20c: IMPULSE RESPONSE OF LOOP #1 600 m FIBER.

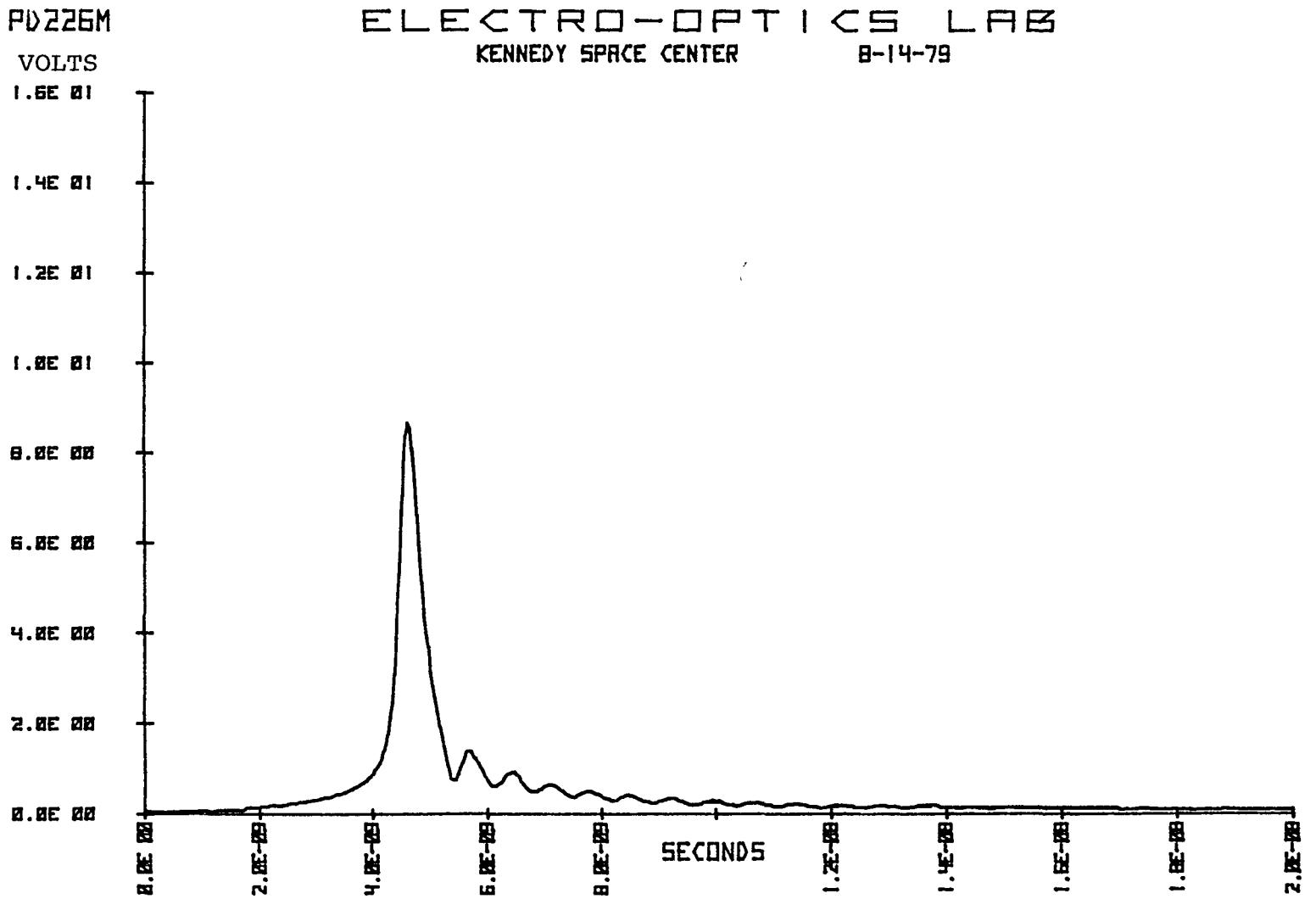

FIGURE 21: REFERENCE WAVEFORM FOR TESTING 1.2 km and 2.4 km LENGTHS.

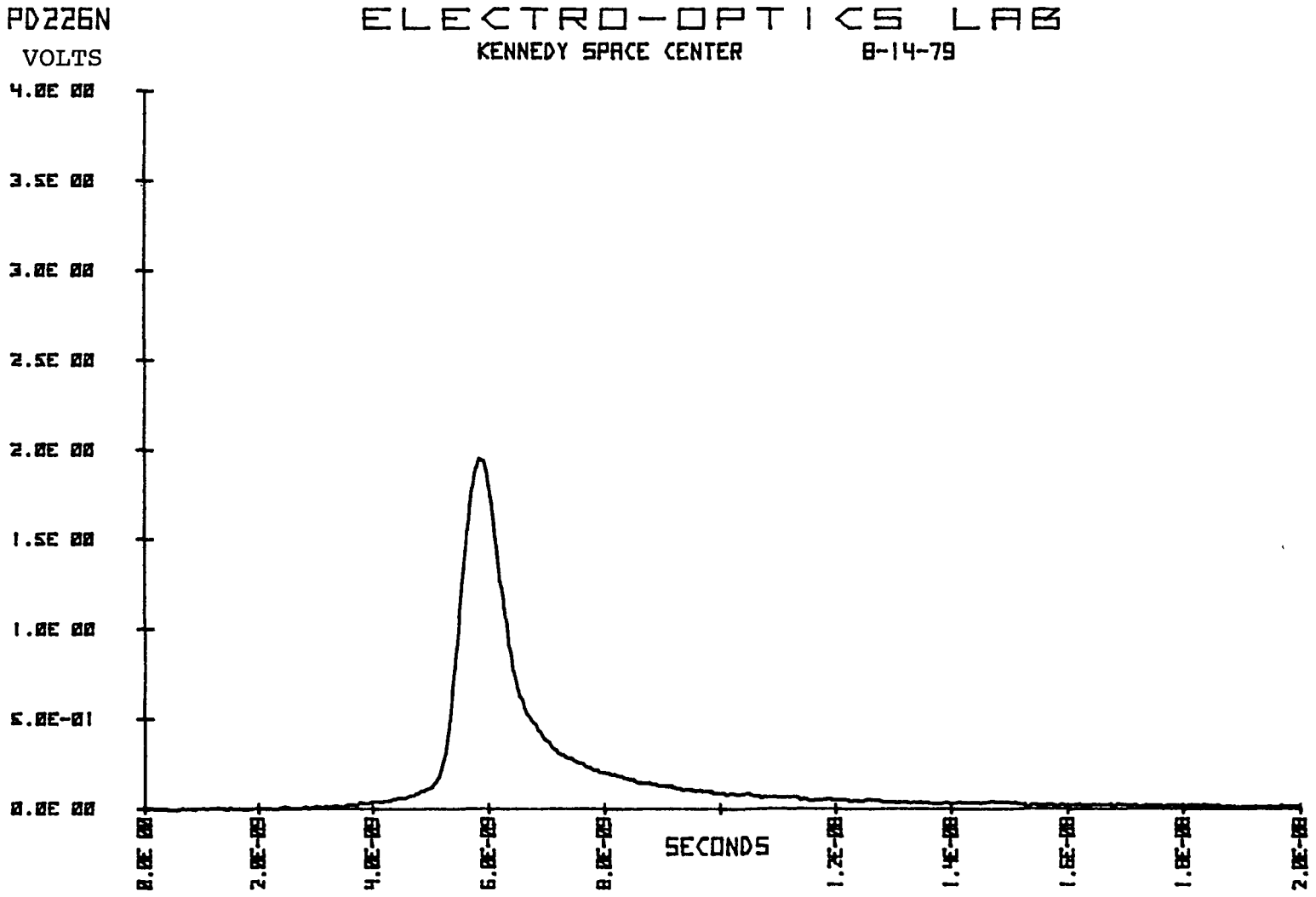

FIGURE 22a: RESPONSE WAVEFORM OF 1.2 km FIBER (LOOPS 2 & 3).

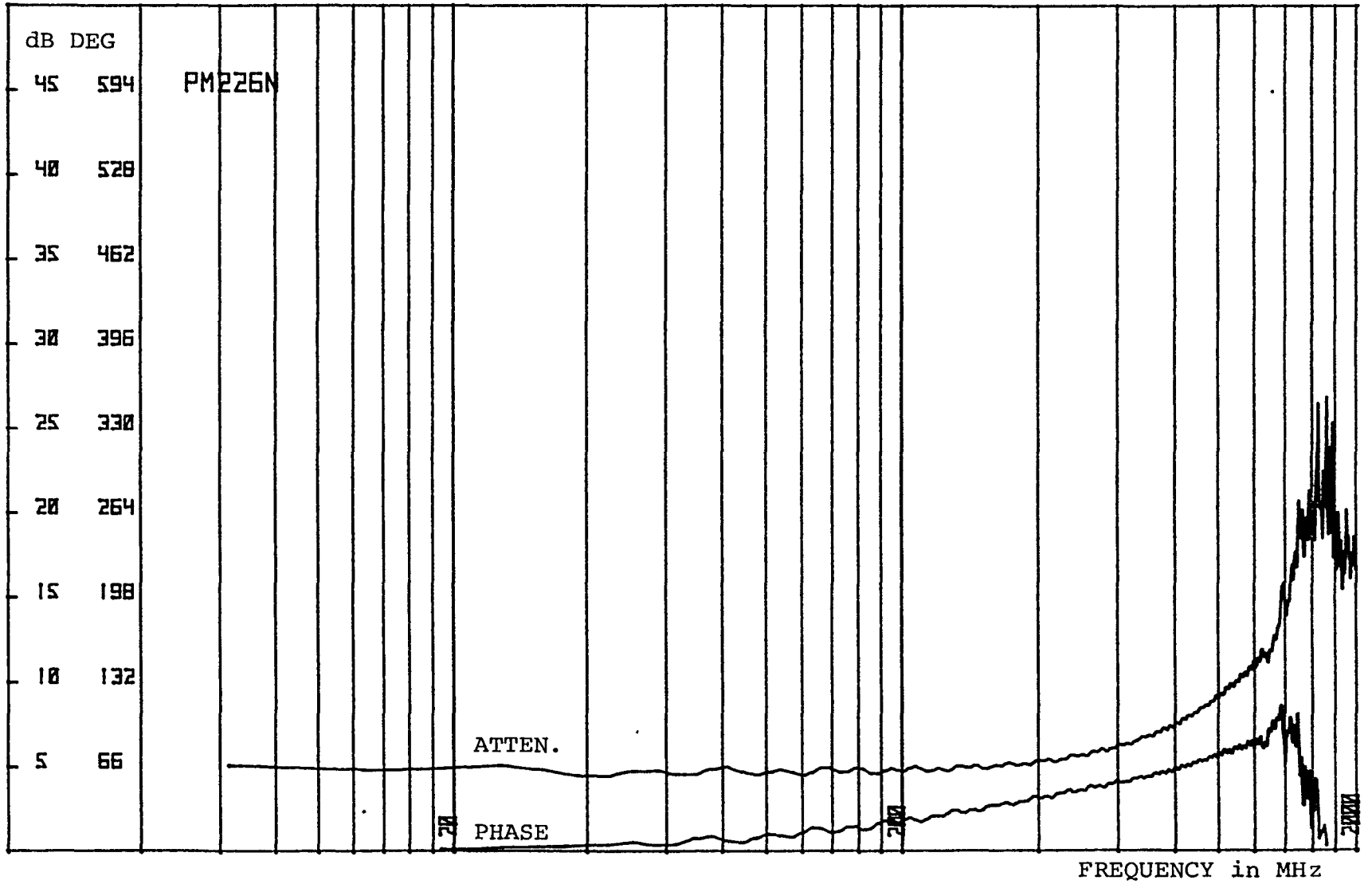

FIGURE 22b: ATTENUATION AND PHASE FUNCTIONS OF 1.2 km FIBER (LOOPS 2 & 3).

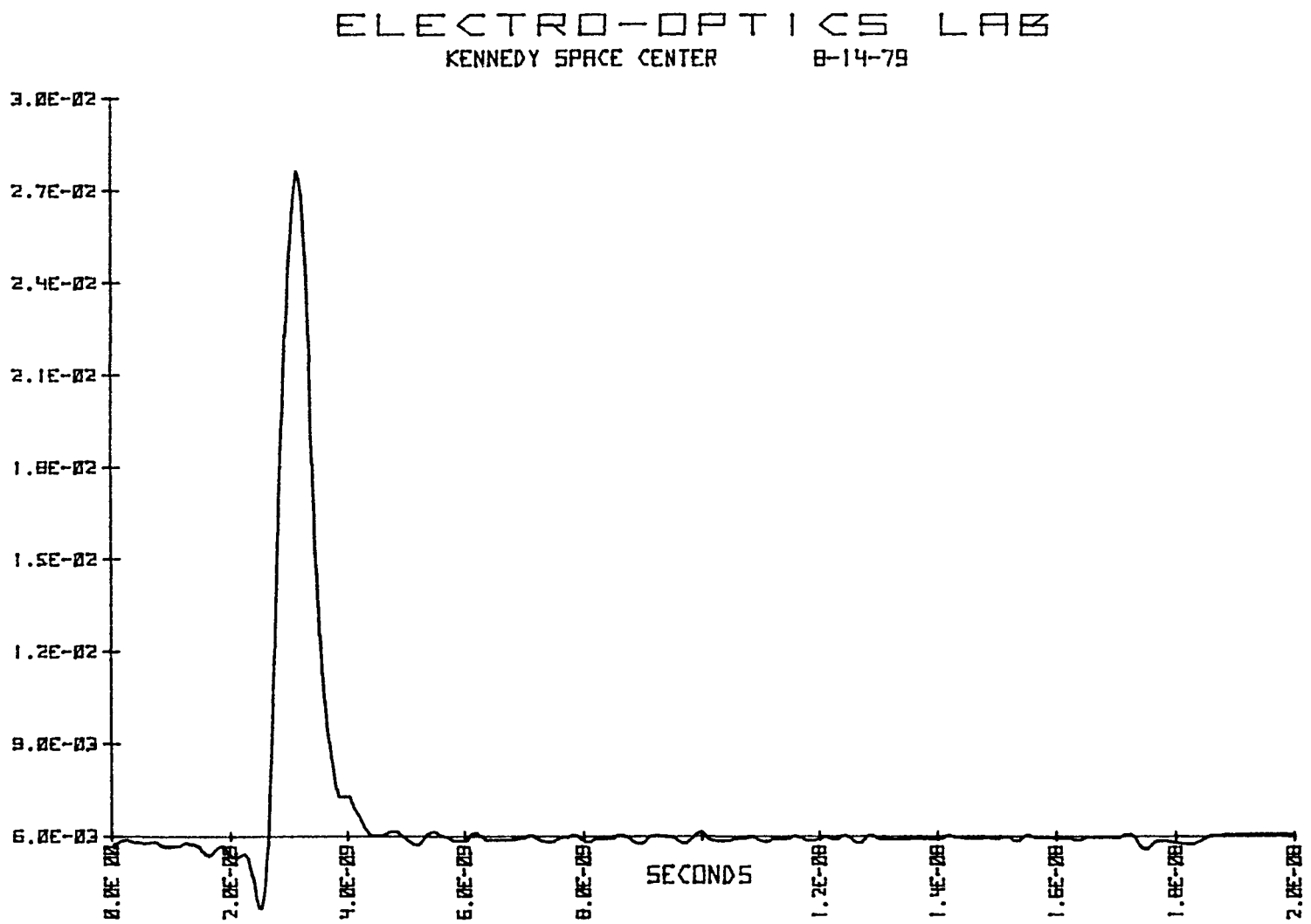

FIGURE 22c: IMPULSE RESPONSE OF 1.2 km FIBER (LOOPS 2 & 3).

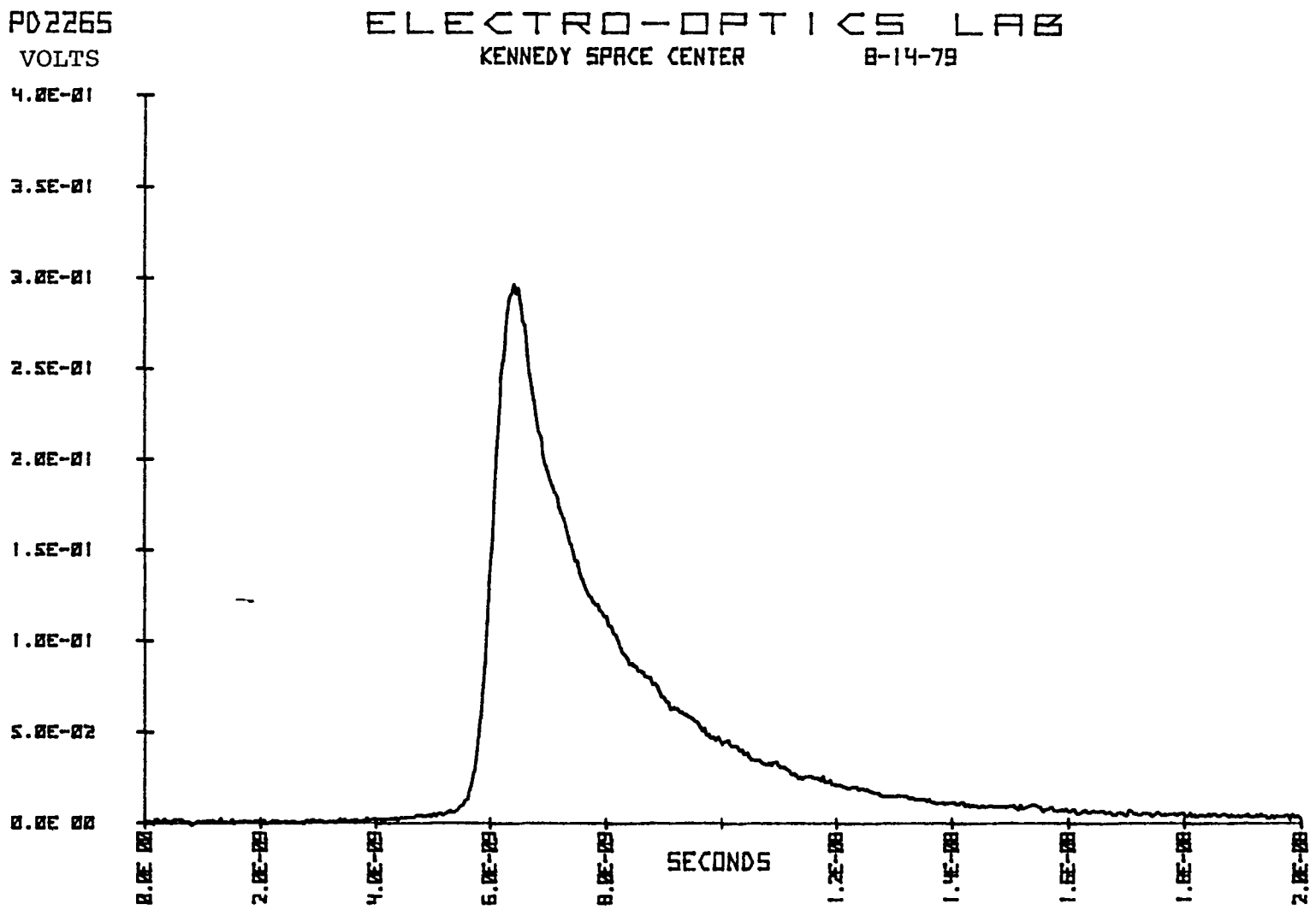

FIGURE 23a: RESPONSE WAVEFORM OF 2.4 km FIBER (LOOPS 2 - 5).

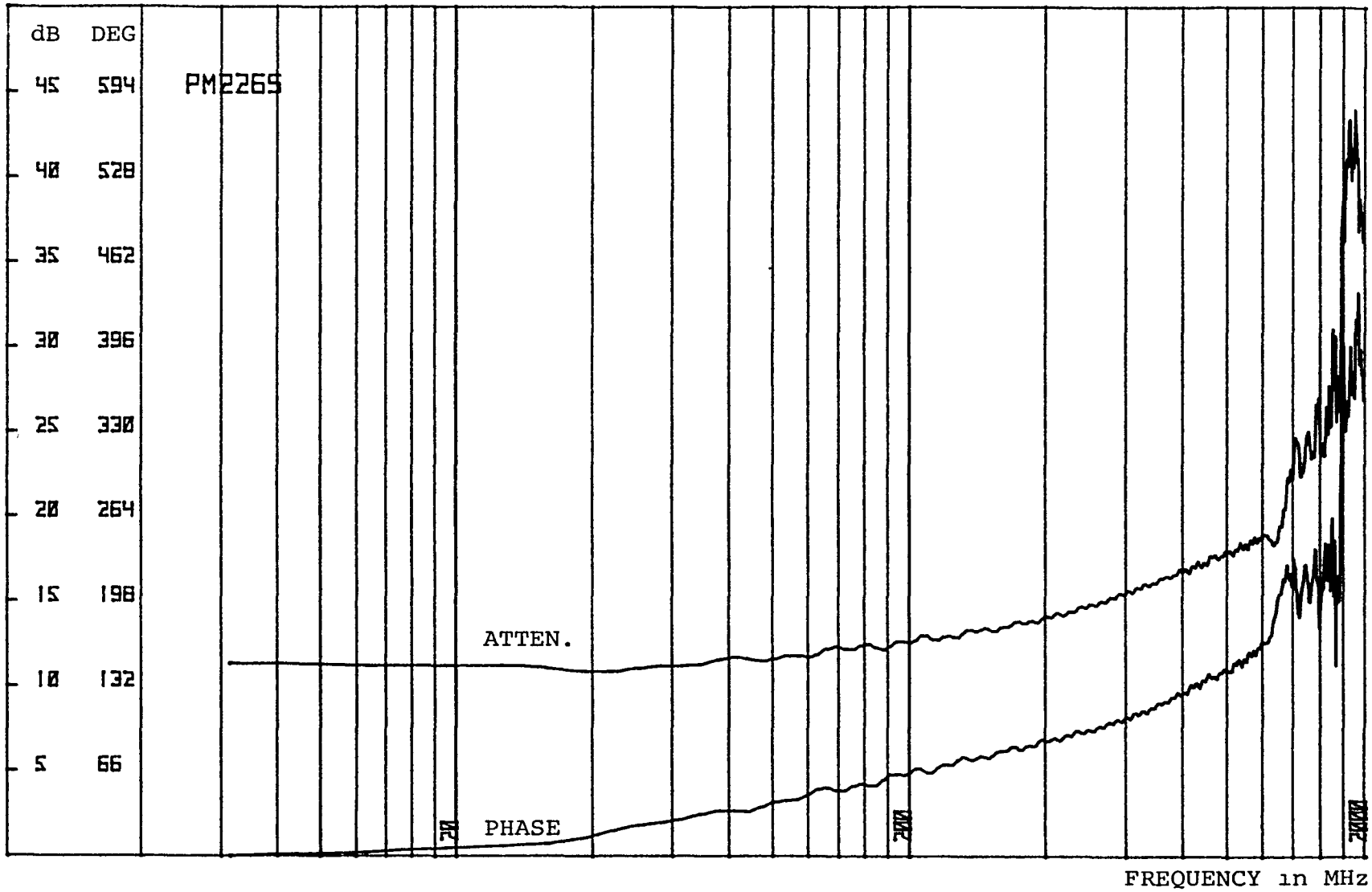

FIGURE 23b: ATTENUATION AND PHASE FUNCTIONS OF 2.4 km FIBER (LOOPS 2 - 5).

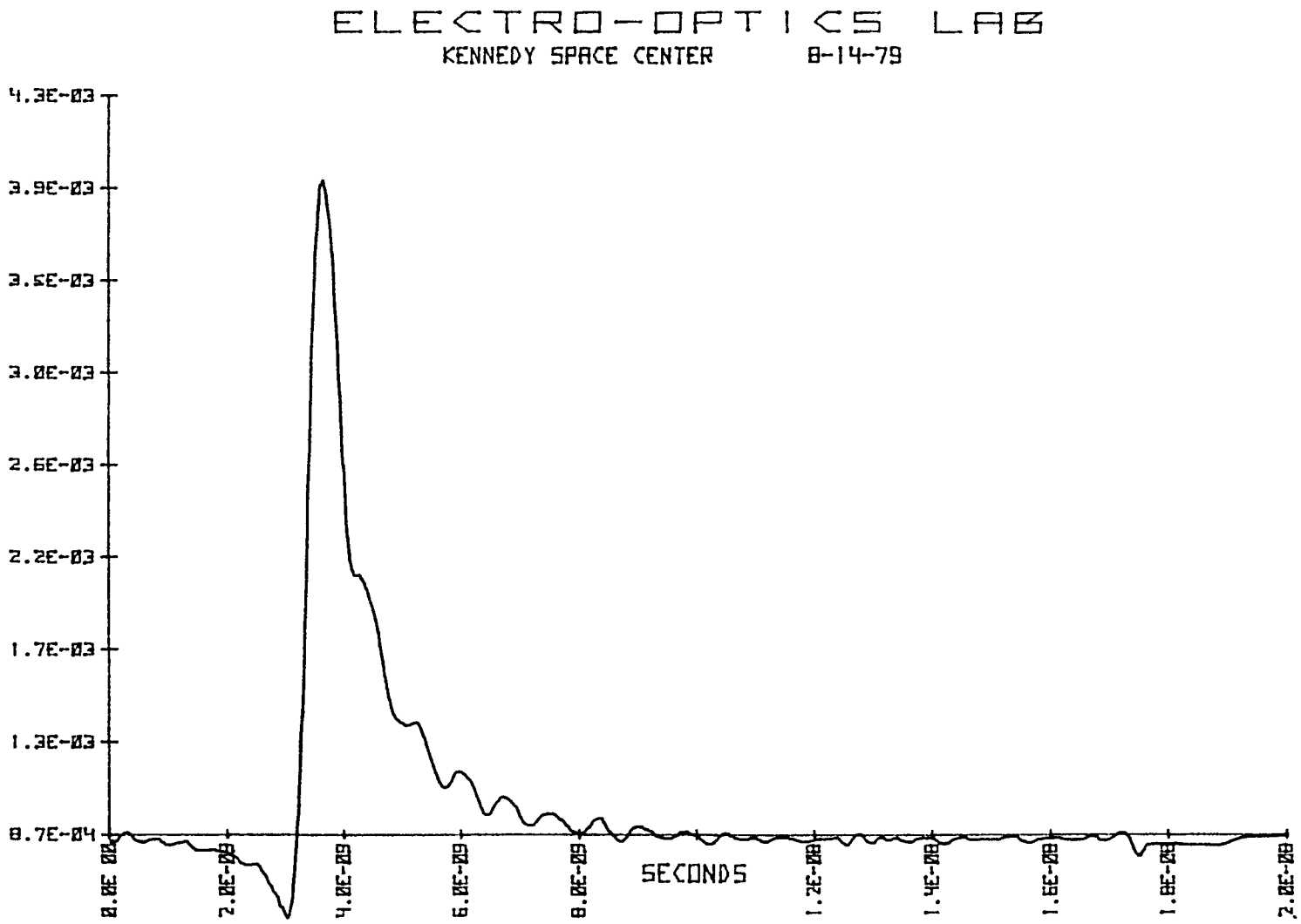

FIGURE 23c: IMPULSE RESPONSE OF 2.4 km FIBER (LOOPS 2 - 5).

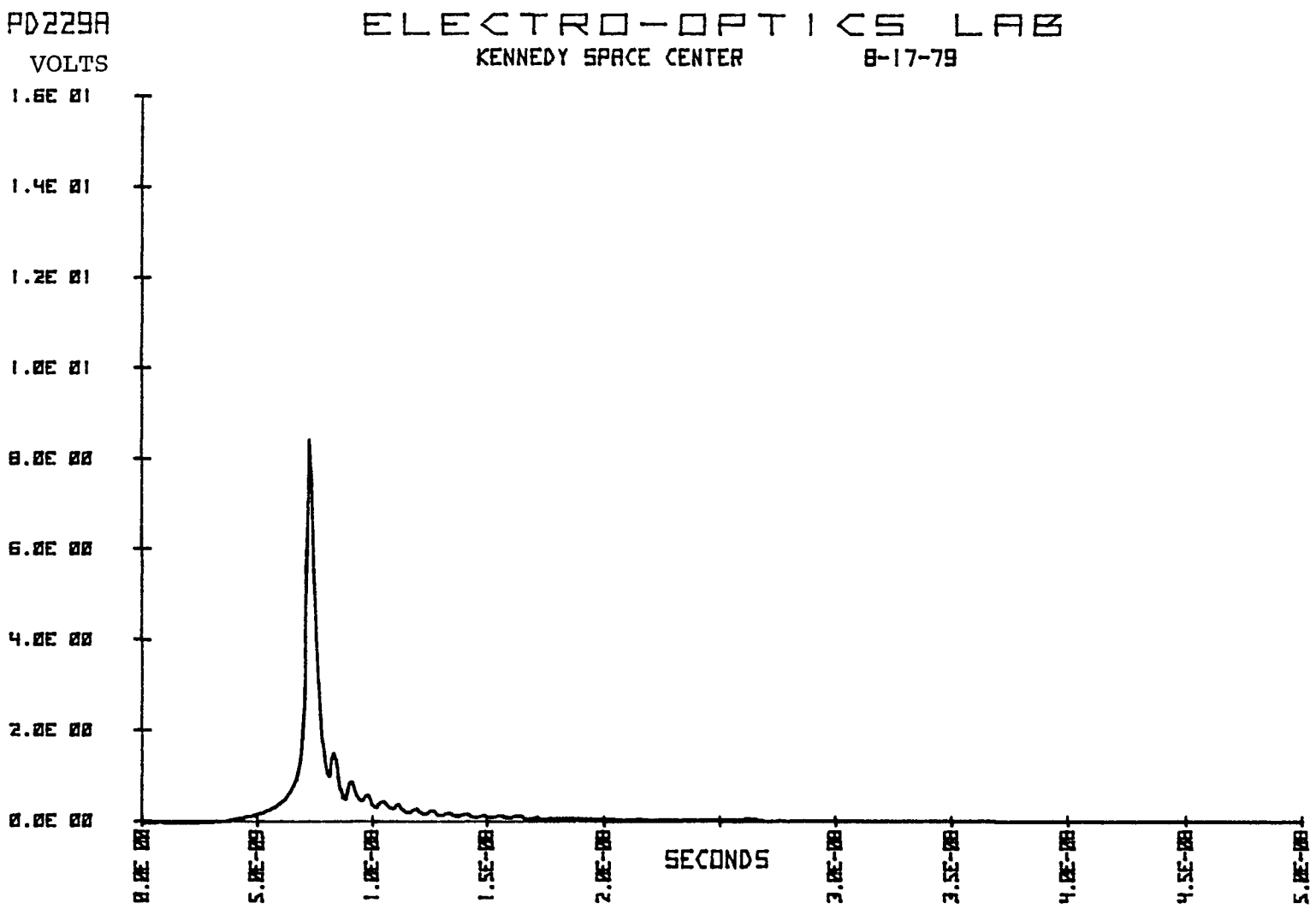

FIGURE 24: REFERENCE WAVEFORM FOR TESTING 4.8 km FIBER.

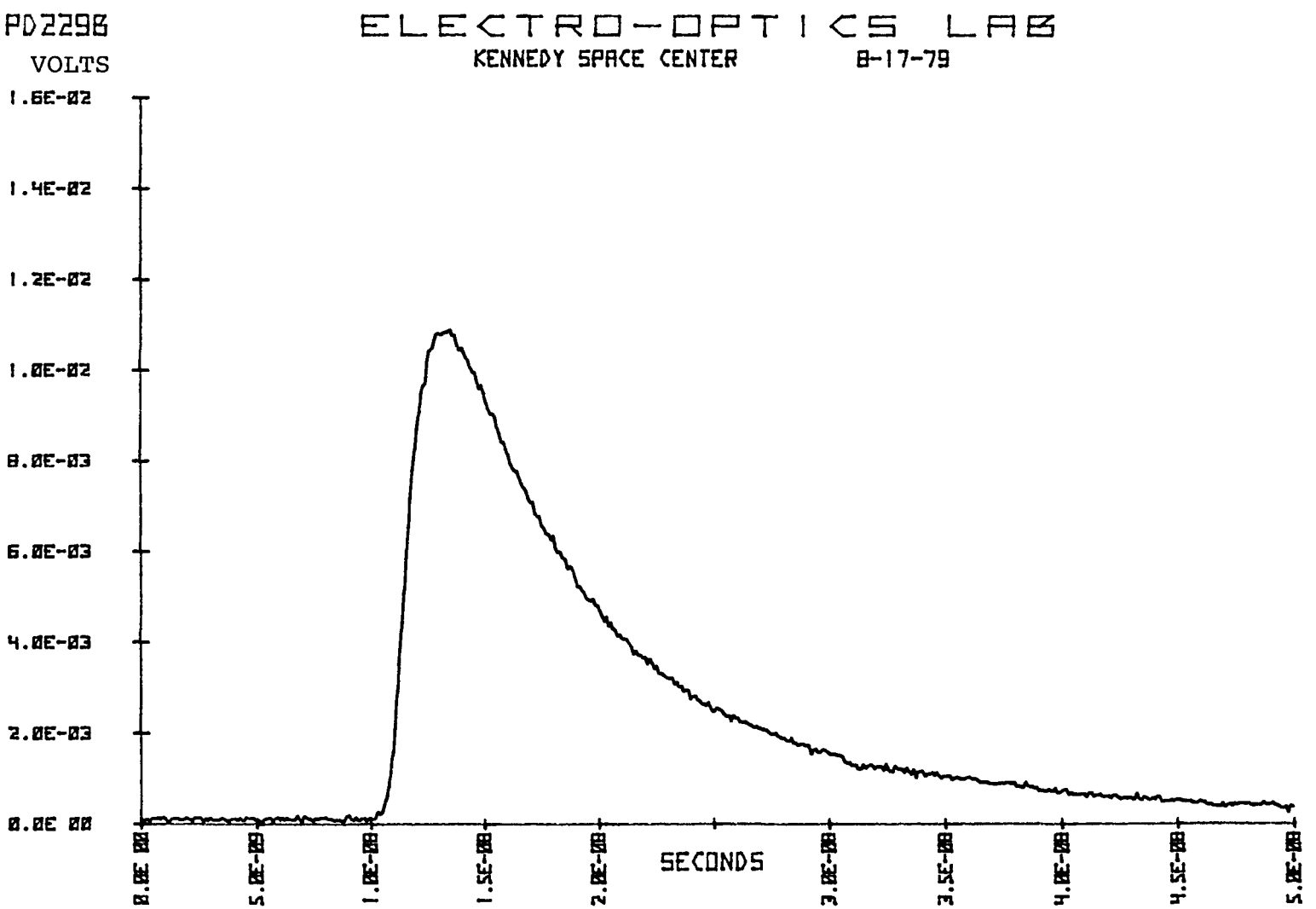

FIGURE 25a: RESPONSE WAVEFORM OF 4.8 km FIBER (LOOPS 2 - 9).

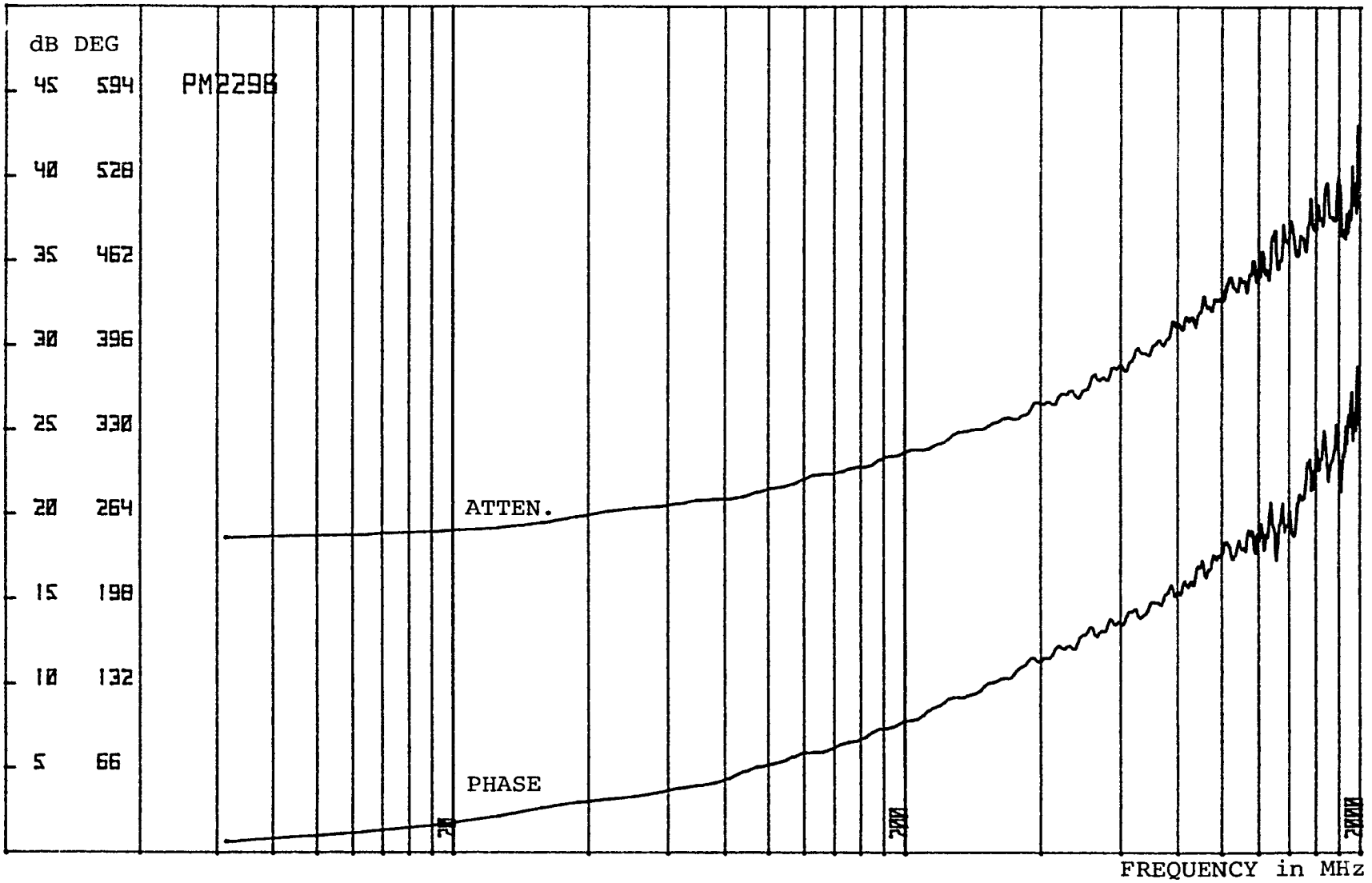

FIGURE 25b: ATTENUATION AND PHASE FUNCTIONS OF 4.8 km FIBER (LOOPS 2 - 9).

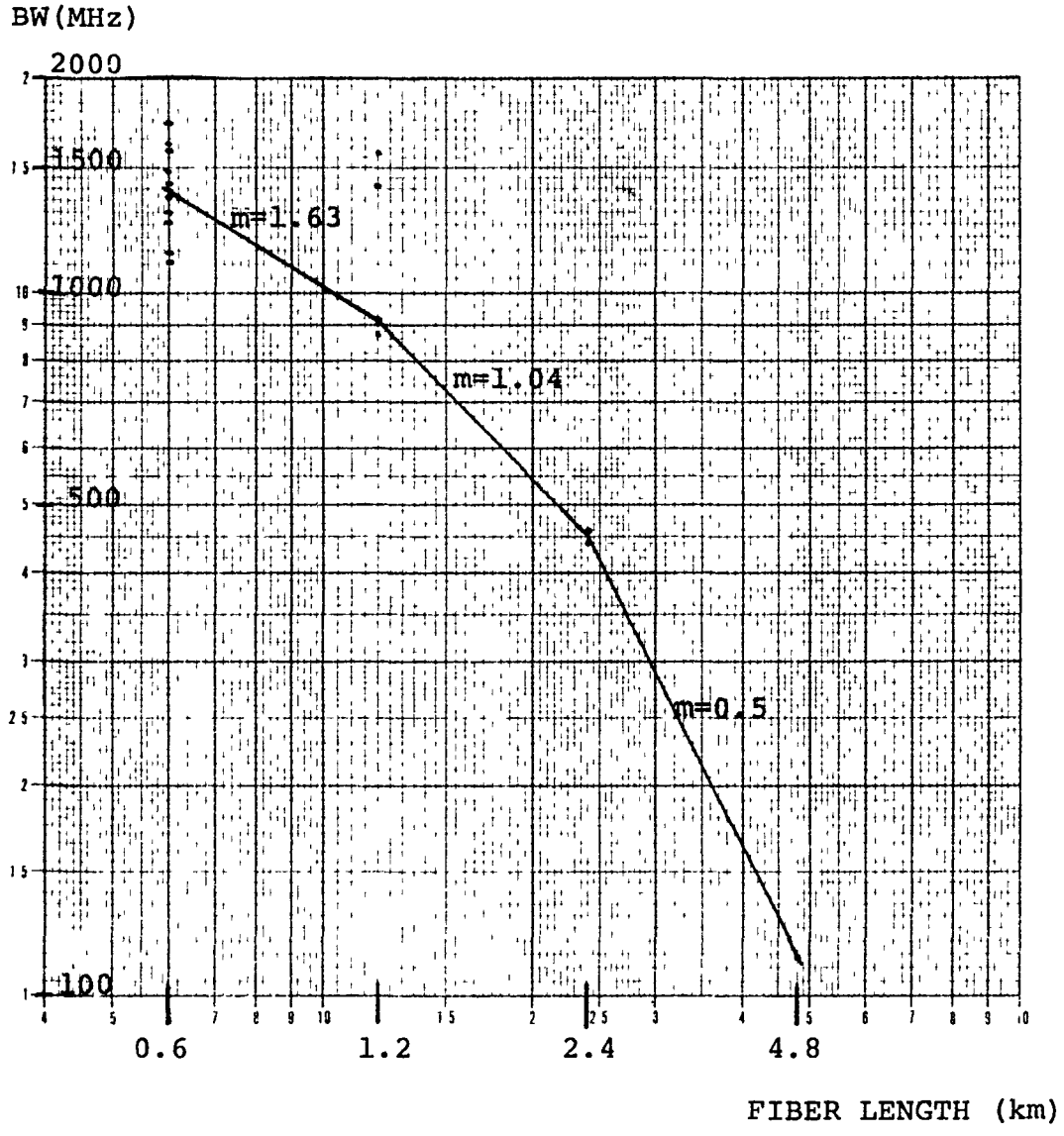

FIGURE 26: CONCATENATED FIBER BANDWIDTH (BW) vs. LENGTH.

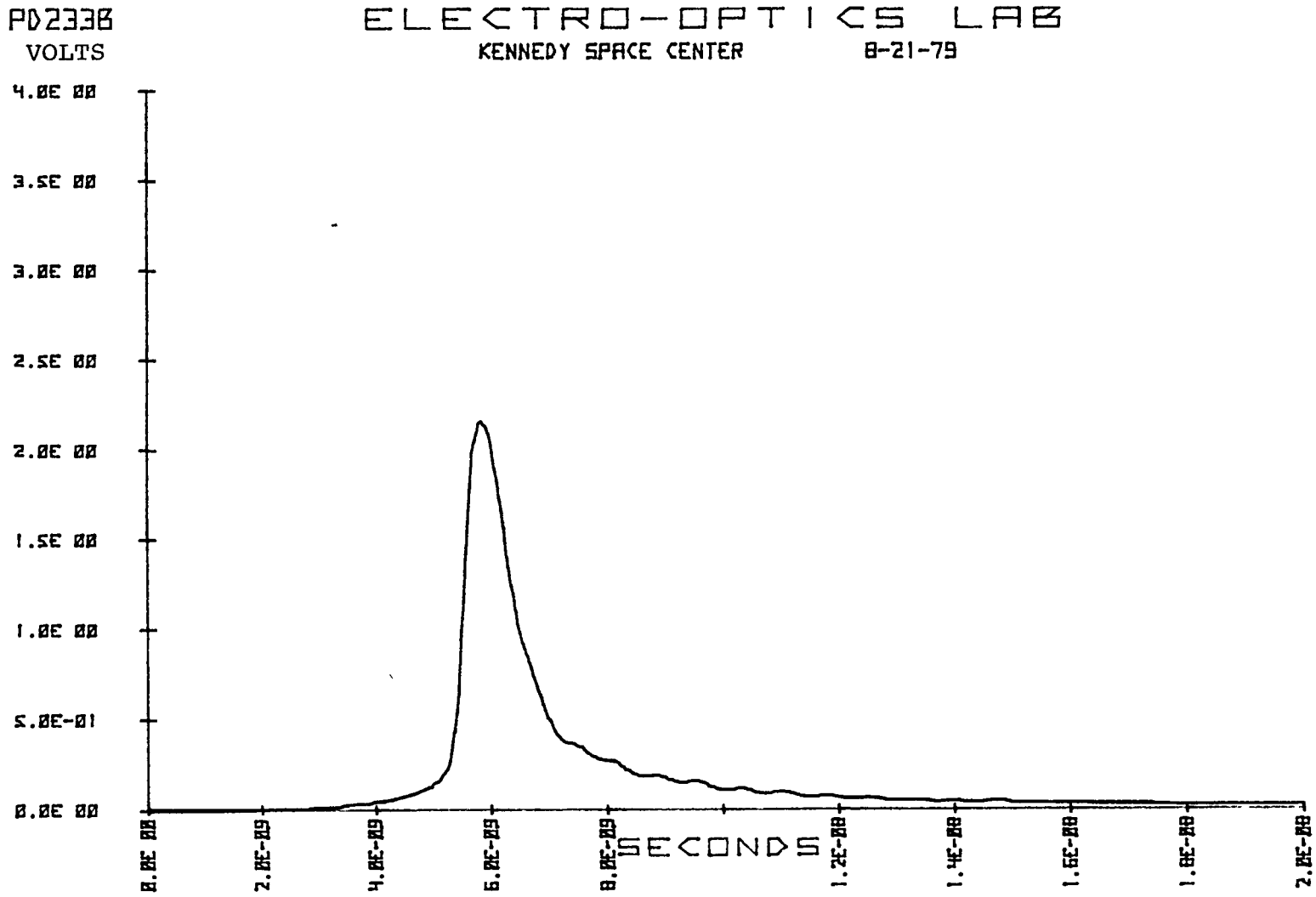

FIGURE 27: REFERENCE WAVEFORM FOR CONNECTOR DISPERSION TEST (Two 600 m loops & a 6m fuse spliced in between).

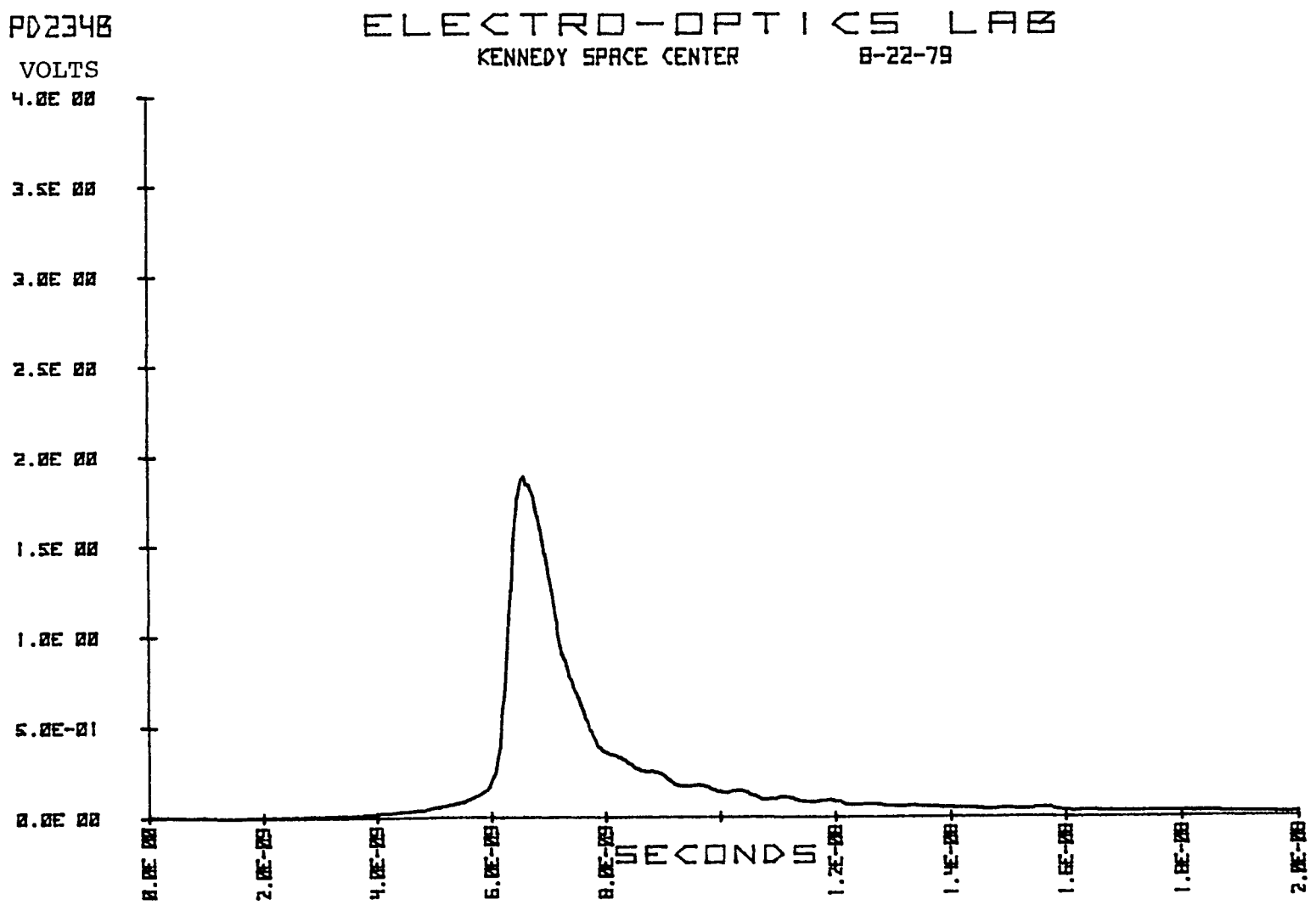

FIGURE 28a. RESPONSE WAVEFORM OF A FUSE SPLICE.

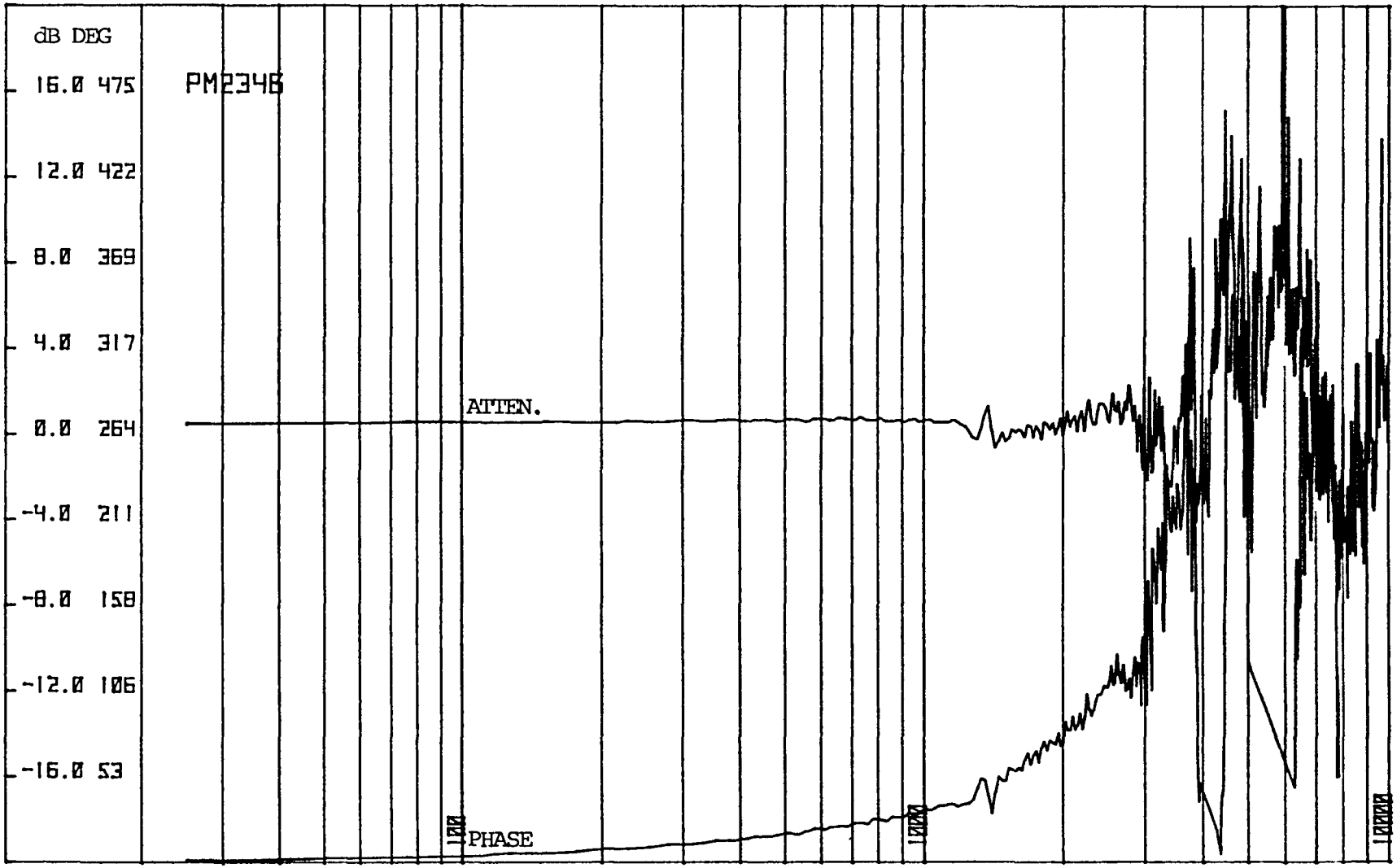

FIGURE 28b: ATTENUATION AND PHASE FUNCTIONS OF A FUSE SPLICE.

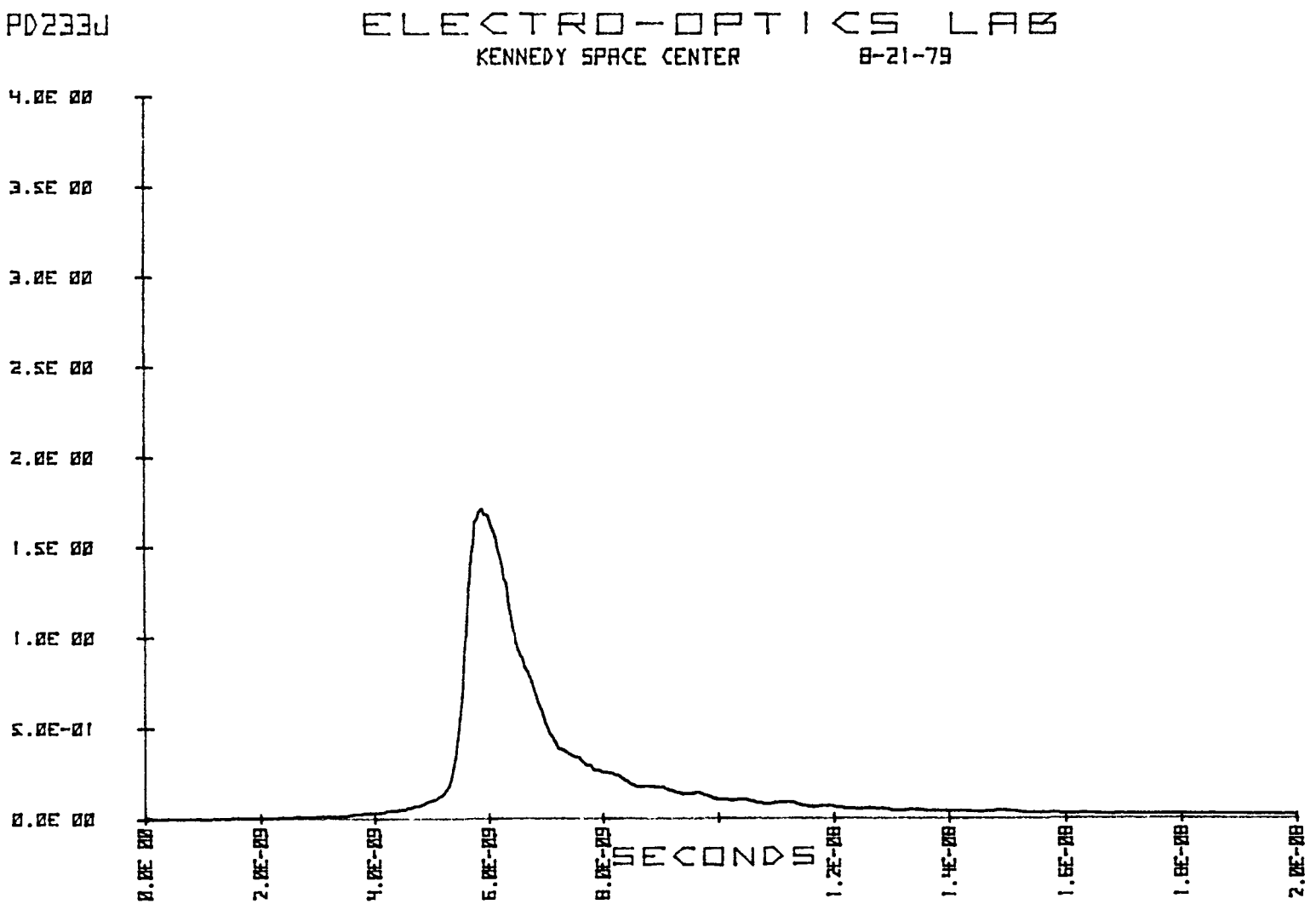

FIGURE 29a: RESPONSE WAVEFORM OF A SINGLE OPTICAL CONNECTOR.

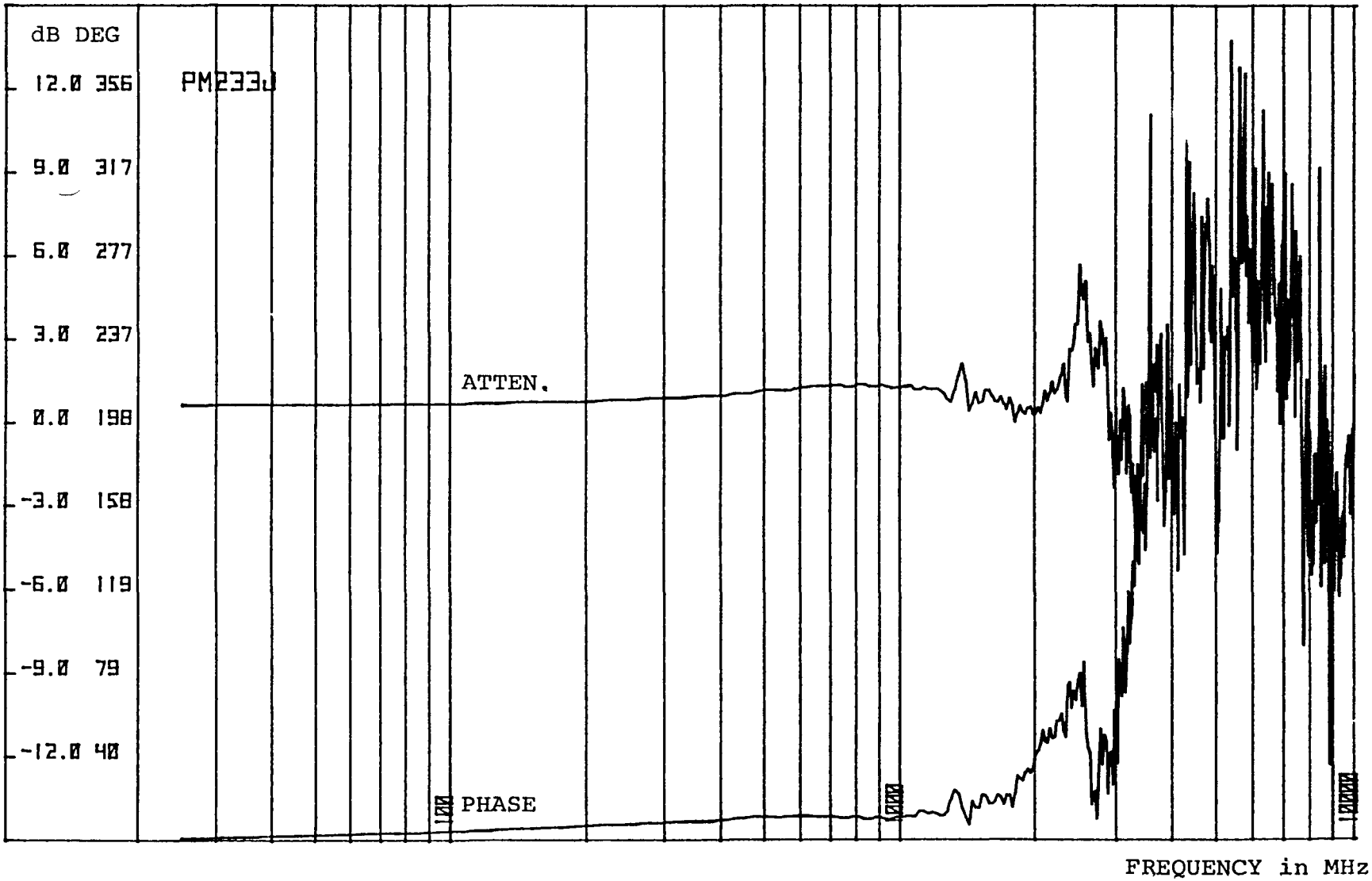

FIGURE 29b: ATTENUATION AND PHASE FUNCTIONS OF A SINGLE OPTICAL CONNECTOR

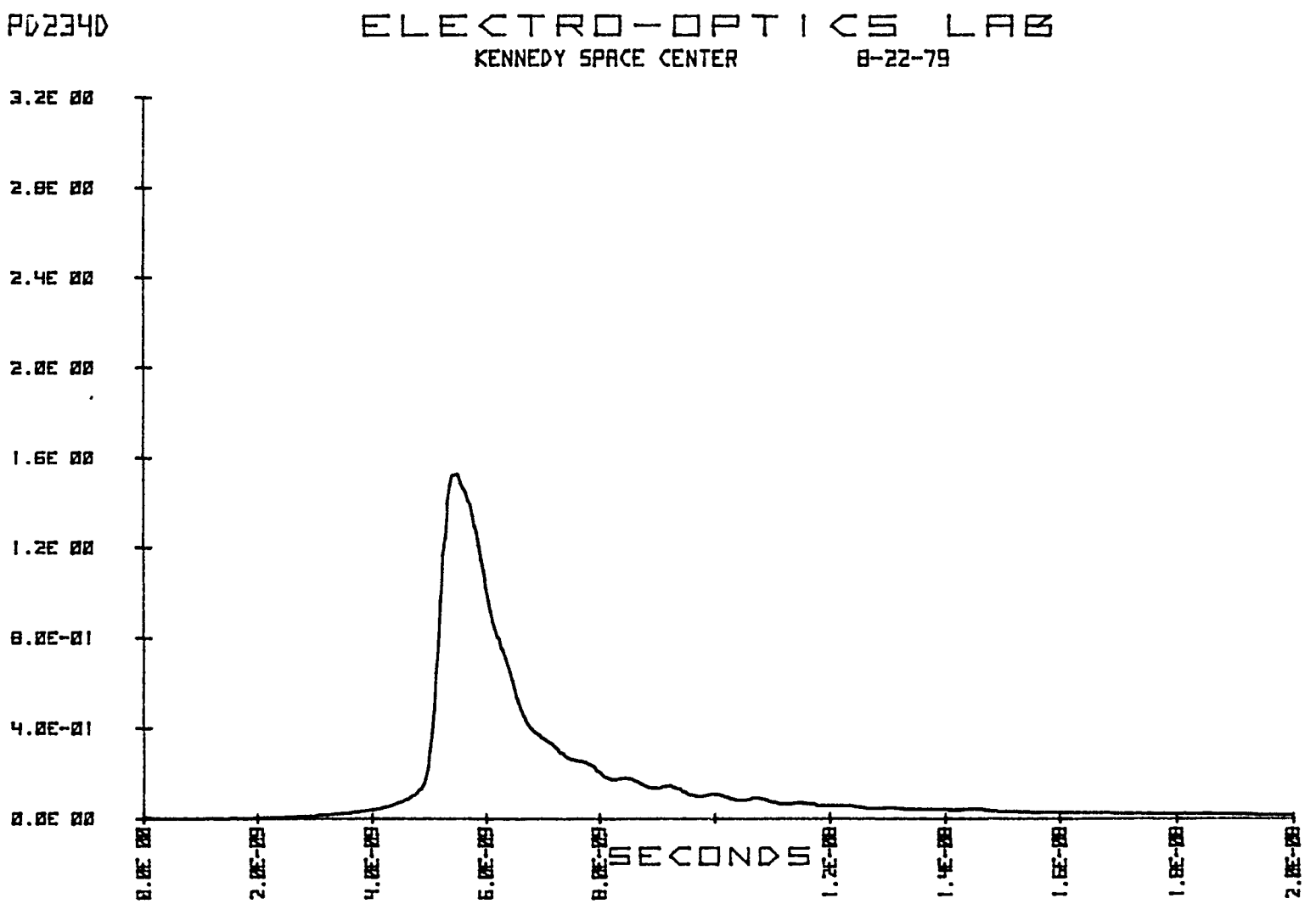

FIGURE 30a: RESPONSE WAVEFORM OF THREE CLOSELY SPACED OPTICAL CONNECTORS.

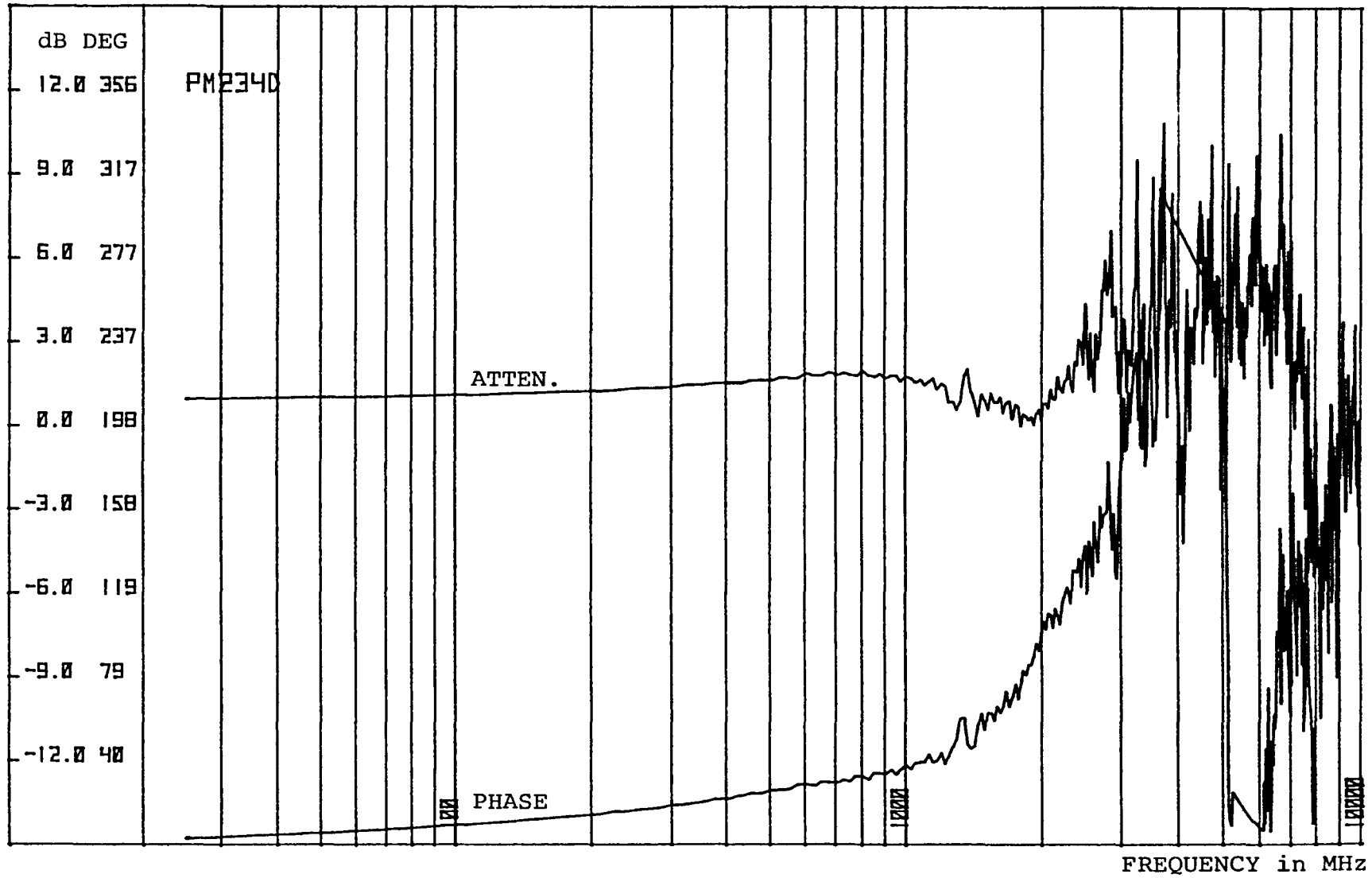

FIGURE 30b: ATTENUATION AND PHASE FUNCTIONS OF THREE CLOSELY SPACED OPTICAL CONNECTORS.

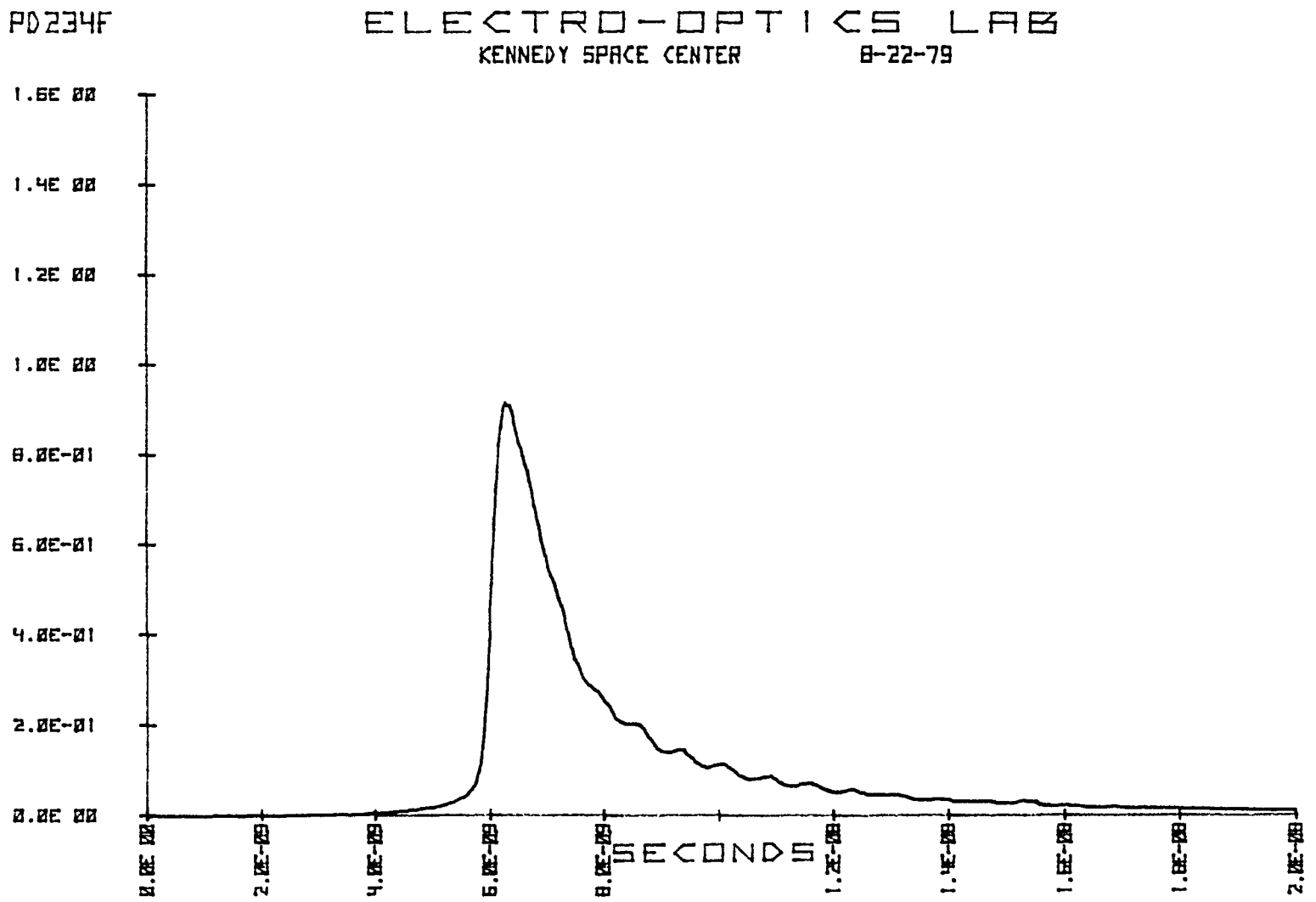

FIGURE 31a: RESPONSE WAVEFORM OF SIX CLOSELY SPACED OPTICAL CONNECTORS.

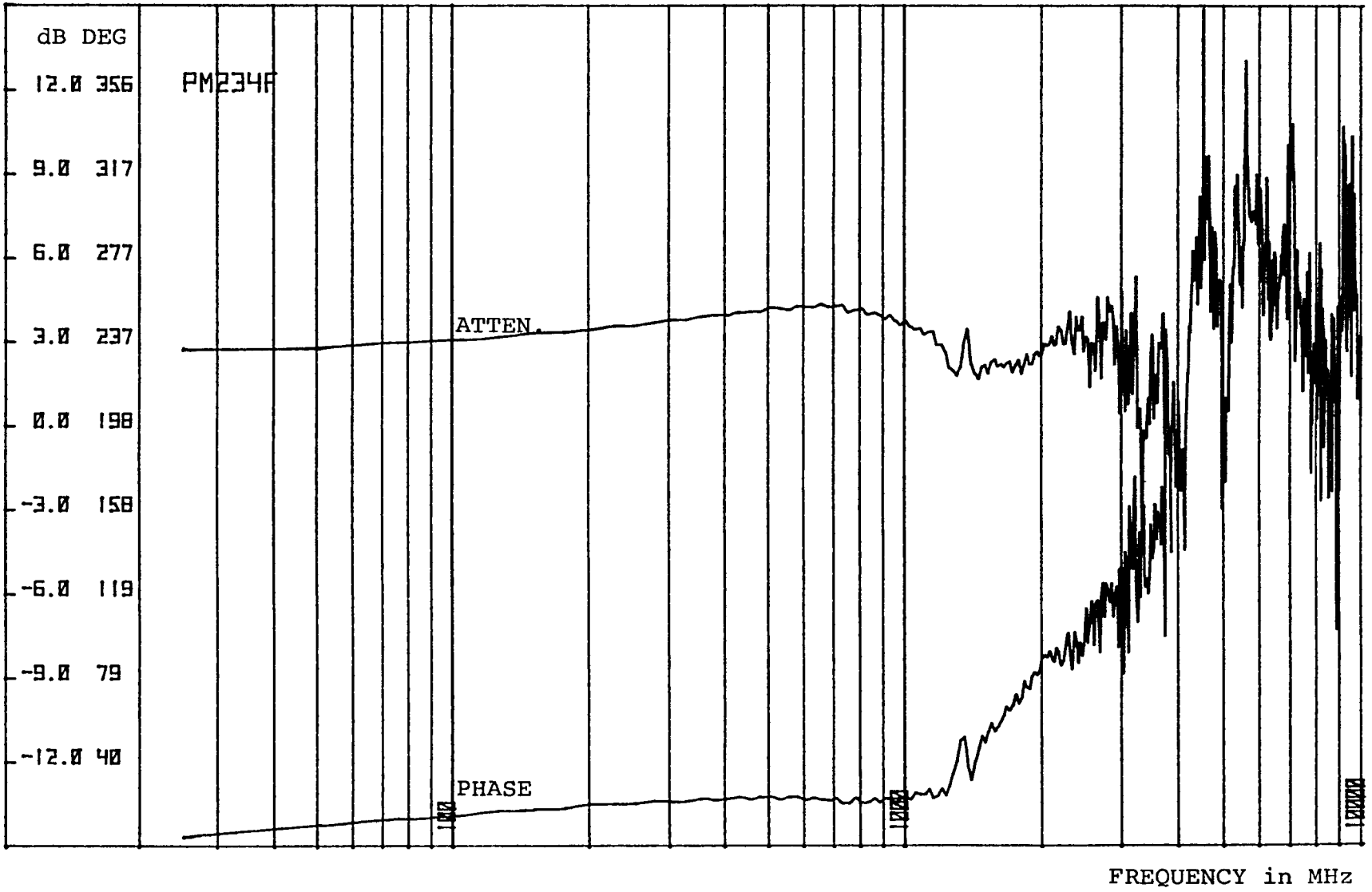

FIGURE 31b: ATTENUATION AND PHASE FUNCTIONS OF SIX CLOSELY SPACED OPTICAL CONNECTORS.

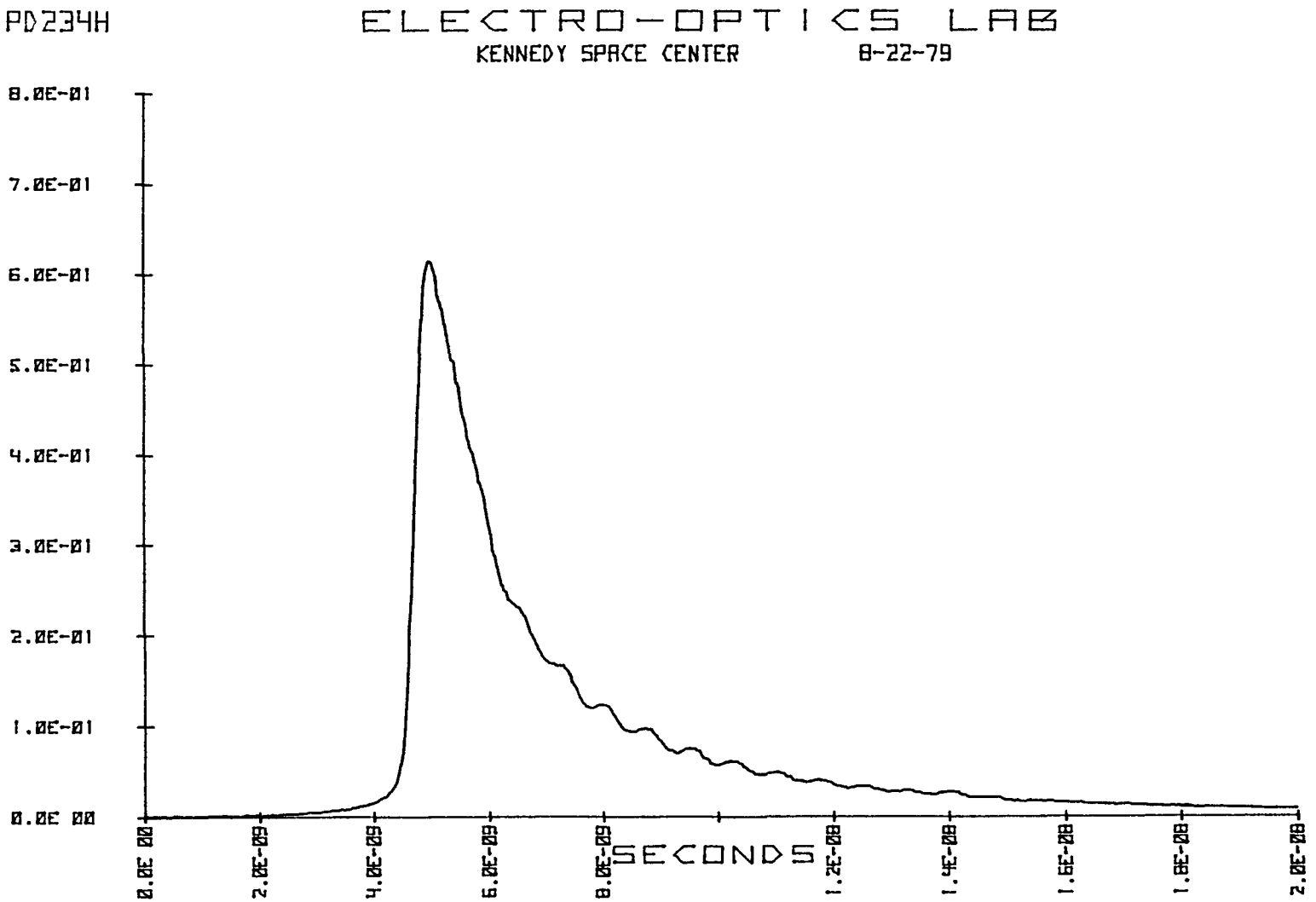

FIGURE 32a: RESPONSE WAVEFORM OF NINE CLOSELY SPACED OPTICAL CONNECTORS.

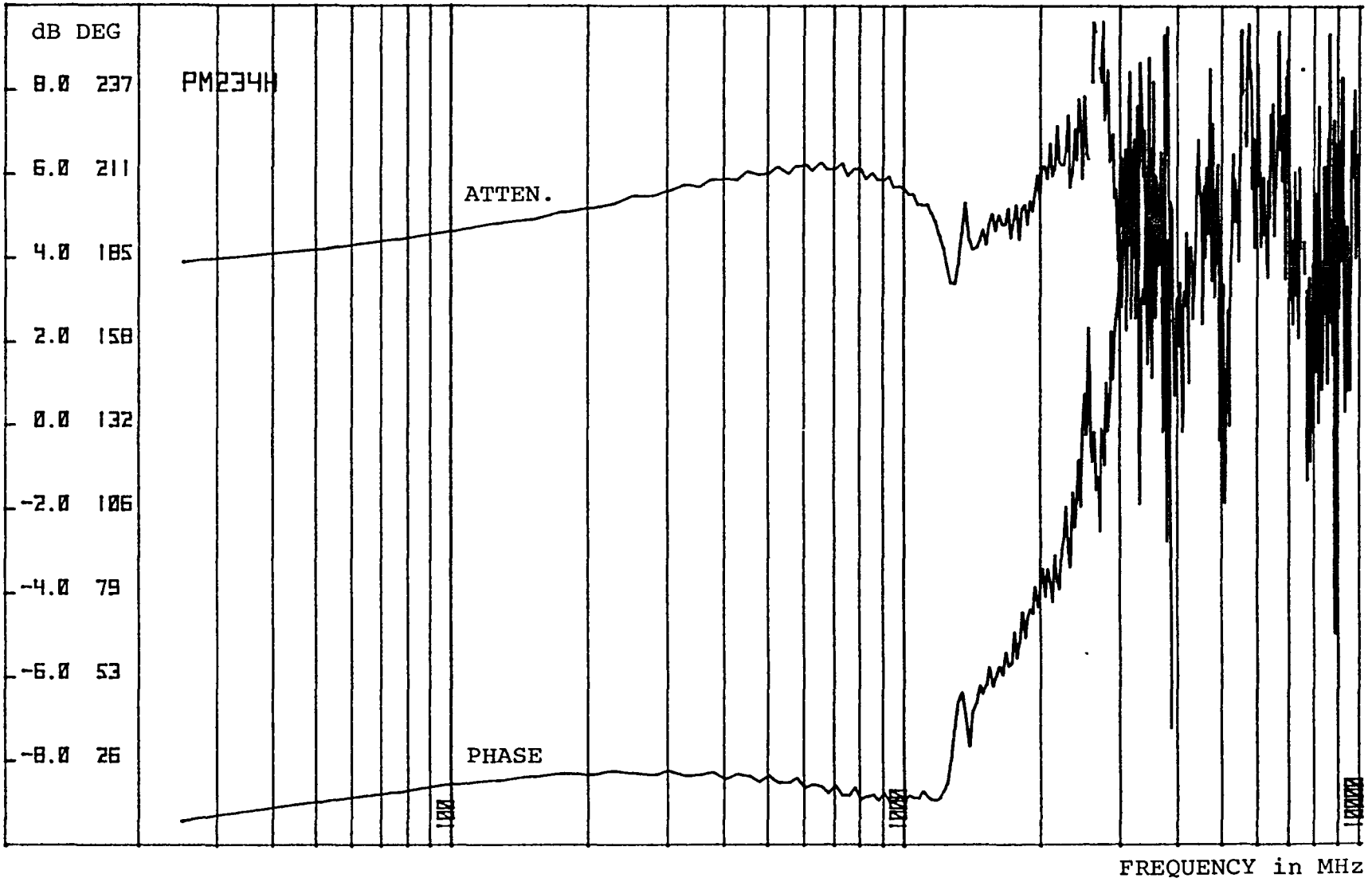

FIGURE 32b: ATTENUATION AND PHASE FUNCTIONS OF NINE CLOSELY SPACED OPTICAL CONNECTORS.

APPENDIX A
FREQUENCY DOMAIN OPTIMAL COMPENSATION DECONVOLUTION

by
Sedki M. Riad

Department of Electrical Engineering
Virginia Polytechnic Institute and State University
Blacksburg, Virginia 24061

ABSTRACT

A new approach for deconvolution in the presence of noise is presented. The approach involves a frequency domain optimization of a single variable to design an optimum frequency domain compensating function. An illustrative application on optical fiber impulse response characterization is shown with very low noise in the deconvolution results.

I. Introduction

The present paper introduces a new approach for solving the deconvolution problem in the presence of noise. The new approach involves the design of a frequency domain optimal compensating functions. This compensator is to be applied to the convolution product to yield the required deconvolution result. The design of the optimal compensator involves a frequency domain optimization of a single variable. Using the Fast Fourier Transform, FFT, the deconvolution computation time is considerably short and the programing is simple.

In the next section, the deconvolution problem will be defined and noise source will be identified. Previous approaches to deconvolution are surveyed and discussed. In section III, the development of the optimal compensator design is presented. And finally, in section IV, an illustrative application is shown to yield successful low noise deconvolution.

II. THE DECONVOLUTION PROBLEM

Deconvolution is the process of separating a convolution component from a known convolution product. In time domain representation, if x(t) and h(t) and the convolution components, y(t), the convolution product is

$$y(t) = \int_{-\infty}^{\infty} x(\tau)\, h(\tau - t)\, d\tau \tag{1}$$

or

$$y(t) = \int_{-\infty}^{\infty} h(\tau)\, x(\tau - t)\, d\tau \tag{2}$$

The symbolic representation of either of the above convolution integrals is

$$y(t) = x(t) * h(t) \tag{3}$$

where * denotes the convolution operation. Hence, deconvolution is the process of determining x(t) knowing both y(t) and h(t), or determining h(t) knowing both y(t) and x(t).

The deconvolution process is often encountered in linear system analysis and characterization. In time domain measurements of a linear system, Figure 1, y(t) represents the output signal of a system due to an exciting input signal x(t), while the system's impulse response is h(t).

In frequency domain representation, Figure 2, the convolution process converts into a product one

$$Y(e^{j\omega}) = X(e^{j\omega}) \cdot H(e^{j\omega}) \tag{4}$$

where $Y(e^{j\omega})$, $X(e^{j\omega})$ and $H(e^{j\omega})$ are the frequency domain representations (Fourier transforms) of y(t), x(t) and h(t), respectively. Based on equation (4), deconvolution takes the simple form of division, i.e.

$$X(e^{j\omega}) = Y(e^{j\omega})/H(e^{j\omega}) \tag{5}$$

or

$$H(e^{j\omega}) = Y(e^{j\omega})/X(e^{j\omega}) \tag{6}$$

From equations (4), (5), and (6) it is clear that the same deconvolution process may be used to obtain either of $X(e^{j\omega})$ or $H(e^{j\omega})$. Therefore, without loss of generality, only equation (6), the deconvolution to obtain $H(e^{j\omega})$ will be considered in the rest of this paper.

It can be concluded from equation (4) that the zeros of $X(e^{j\omega})$ are also zeros of $Y(e^{j\omega})$. The same is also true for poles. At these points, (zeros and poles), equations (6) will become indeterminate. Consequently, the result of the division operation will be erronious unless the poles and the zeros of $X(e^{j\omega})$ are exactly cancelled out by those of $Y(e^{j\omega})$. Any errors in the data representing $X(e^{j\omega})$ and $Y(e^{j\omega})$ degrade the cancellation and introduce errors (noise) in the resultant $H(e^{j\omega})$. These noise like errors in the $H(e^{j\omega})$ will be clustered around the poles and zeros of $X(e^{j\omega})$. When $H(e^{j\omega})$ is transformed to the time domain to obtain h(t), the noise like errors will cover the entire transform time window, swamping the useful information content.

Typical sources of errors in $X(e^{j\omega})$ and $Y(e^{j\omega})$ are

sampling errors and noise in signal acquisition, leakage and aliasing errors in the Fourier transformation, and rounding and computational errors in the computing machine. The latter two sources can be greatly reduced and neglected in most cases. While the first source, signal acquisition errors and noise, is the major one and cannot be overcome in most practical applications.

Various techniques were developed to reduce the noise in the deconvolution result, $H(e^{j\omega})$. In the following, four primary approaches will be briefly examined. The first approach, acquisition averaging is aimed to reduce signal acquisition errors and noise by averaging several acquisitions taken within a short period of time. This technique is known to help reduce the noise greatly, but it introduces another class of errors to the signal due to time drift.[1] A second approach is aimed at suppressing the noise in the deconvolution result by applying a filter.[2] The filter will modify the result $H(e^{j\omega})$ as it eliminates the noise, thereby introducing its own errors. The third approach in this survey is the iterative technique,[3] in which successive approximations to an estimated $H(e^{j\omega})$, (or h(t)), are made in order to minimize the error between the computed output (based on the estimate) and the actual output $Y(e^{j\omega})$, (or y(t)). The main difficulties in this technique lie in having a close estimate for $H(e^{j\omega})$ to start with, and also in formulating a correction function for error minimization.

Moreover, repeating the iteration process for each deconvolution operation presents complications since the iteration is dependent on the form of $Y(e^{j\omega})$. The fourth and final approach is the optimal compensation technique.[4] It involves the design of a compensator (deconvolution) function that operates on a convolution output to yield one of its inputs. The design of the compensator involves an iteration process on a single variable. The iteration process need not be repeated for various deconvolution operations involving the same input signal $x(t)$, since the compensator is a function of $X(e^{j\omega})$ only as will be shown in the next section. Deconvolution using optimum compensation was developed in the time domain by previous workers. The process in the time domain is very inconvenient since it requires inversion of large size matrices.[4] Also, the previous workers' development did not include an optimization argument for the interation process other than getting 'stationary results'.

In the following section, optimal compensation in the frequency domain will be presented taking advantage of the convenience and speed of the FFT computations over matrix inversion.

III. OPTIMAL COMPENSATION DECONVOLUTION

The compensation principle in deconvolution is to design a transfer function $C(e^{j\omega})$ to be applied to $Y(e^{j\omega})$ to yield $H_e(e^{j\omega})$, an estimate to $H(e^{j\omega})$, Figure 3; i.e.,

$$H_e(e^{j\omega}) = Y(e^{j\omega}) \cdot C(e^{j\omega}) \tag{7}$$

The main design criteria is to minimize E_e, the error energy in the estimate given by

$$E_e = \int_0^{\Omega} |H_e(e^{j\omega}) - H(e^{j\omega})|^2 \, d\omega \tag{8}$$

where Ω is the frequency band of interest. This minimization condition yields

$$C(e^{j\omega}) = 1/X(e^{j\omega})$$

which results in an unbounded value for $C(e^{j\omega})$, which in turn yields a noisy form for $H_e(e^{j\omega})$. To limit the noise, another design criteria will be imposed, $C(e^{j\omega})$ will be constrained to be a bounded function. Since $H(e^{j\omega})$ is a bounded function, (a physical one), for convenience, the second design criteria will be to keep the energy E_c finite, where E_c is defined as

$$E_c = \int_0^{\Omega} |H(e^{j\omega}) \; C(e^{j\omega})|^2 \, d\omega \tag{9}$$

So, the problem is to minimize E_e while keeping E_c finite. These two requirements can be grouped into one, to minimize the energy E defined as

$$\left.\begin{aligned} E &= E_e + \lambda E_c, \\ \lambda &\geq 0 \end{aligned}\right\} \qquad (10)$$

where λ is an optimization parameter whose significance can be demonstrated by considering the two extreme cases:

a: $\lambda = 0$, which results in a minimization of E_e with no constraints on $C(e^{j\omega})$.

b: $\lambda = \infty$, which results in a minimization of $C(e^{j\omega})$; an extreme of keeping it finite.

Both extremes of λ are undesirable, and an optimum value λ_{opt} is expected to yield an optimum compensator $C_{opt}(e^{j\omega})$, for which $H_{e,opt}(e^{j\omega})$ is the best estimate for the unknown input function $H(e^{j\omega})$.

Substituting equations (8) and (9) in (10), E takes the form

$$E = \int_0^{\Omega} \{ |H_e(e^{j\omega}) - H(e^{j\omega})|^2 + \lambda |H(e^{j\omega}) C(e^{j\omega})|^2 \} d\omega \qquad (11)$$

using equations (4) and (7), $H_e(e^{j\omega})$ takes the form:

$$H_e(e^{j\omega}) = H(e^{j\omega})\ X(e^{j\omega})\ C(e^{j\omega}) \qquad (12)$$

which when substituted in (11) yields

$$\begin{aligned} E &= \int_0^{\Omega} \{ |H(e^{j\omega})\ X(e^{j\omega})\ C(e^{j\omega}) - H(e^{j\omega})|^2 \\ &\qquad + \lambda |H(e^{j\omega})\ C(e^{j\omega})|^2 \} d\omega \\ &= \int_0^{\Omega} |H(e^{j\omega})|^2 \{ |X(e^{j\omega})\ C(e^{j\omega}) - 1|^2 \\ &\qquad + \lambda |C(e^{j\omega})|^2 \} d\omega \end{aligned}$$

$$= \int_0^{\Omega} |H(e^{j\omega})|^2 \, Q(e^{j\omega}) \, d\omega \tag{13}$$

where

$$Q(e^{j\omega}) = \{|X(e^{j\omega}) \, C(e^{j\omega}) - 1|^2 + \lambda |C(e^{j\omega})|^2\} \tag{14}$$

To make the compensator design a general one, the error energy E should be minimized for all possible forms of $H(e^{j\omega})$, which implies the minimization of $Q(e^{j\omega})$, as can be seen from equation (13). Using the complex forms

$$\left.\begin{aligned} X(e^{j\omega}) &= X_R(e^{j\omega}) + jX_I(e^{j\omega}), \\ C(e^{j\omega}) &= C_R(e^{j\omega}) + jC_I(e^{j\omega}), \end{aligned}\right\} \tag{15}$$

where the subscripts R and I indicate real and imaginary parts, respectively, equation (14) yields

$$\begin{aligned} Q(e^{j\omega}) = {} & \left[X_R(e^{j\omega}) \, C_R(e^{j\omega}) - X_I(e^{j\omega}) \, C_I(e^{j\omega}) - 1 \right]^2 \\ & + \left[X_R(e^{j\omega}) \, C_I(e^{j\omega}) + X_I(e^{j\omega}) \, C_R(e^{j\omega}) \right]^2 \\ & + \lambda \left[C_R^2(e^{j\omega}) + C_I^2(e^{j\omega}) \right] . \end{aligned}$$

To minimize Q, the partial derivatives are set to zero;

$$0 = \frac{\partial Q(e^{j\omega})}{\partial C_R(e^{j\omega})} = C_R(e^{j\omega}) \left[|X(e^{j\omega})|^2 + \lambda \right] - X_R(e^{j\omega}) \tag{16}$$

and

$$0 = \frac{\partial Q(e^{j\omega})}{\partial C_I(e^{j\omega})} = C_I(e^{j\omega}) \left[|X(e^{j\omega})|^2 + \lambda \right] + X_I(e^{j\omega}) \tag{17}$$

Using equations (15, (16) and (17), it can be shown that

$$C(e^{j\omega}) = X^*(e^{j\omega}) / [\,|X(e^{j\omega})|^2 + \lambda\,] \qquad (18)$$

where the superscript (*) denotes the complex conjugate. Equation (18) above, shows the form for the compensating transfer function $C(e^{j\omega})$ for a given input $X(e^{j\omega})$. Combining equations (7) and (18), the compensation deconvolution process yields:

$$H_e(e^{j\omega}) = Y(e^{j\omega}) \cdot X^*(e^{j\omega}) / [\,|X(e^{j\omega})|^2 + \lambda\,] \qquad (19)$$

The value of λ in this relation has to be optimized as discussed earlier. An iterative process is required to find λ_{opt}, the optimum λ, for which an optimization criteria has to be decided. In the next section, an example is given where visual inspection of the noise in $|H_e(e^{j\omega})|$ was used to select λ_{opt}, which yielded good results for $H_{e,opt}(e^{j\omega})$ and its corresponding time form $h_{e,opt}(t)$.

IV. AN ILLUSTRATIVE APPLICATION

In this section, the impulse response characterization of a 4-km optical fiber link will be considered as an illustrative application of the optimal compensation deconvolution technique. The reference waveform (input), x(t),and response waveform (output), y(t), are shown in Figures 4 and 5, respectively. The fiber's complex transfer function $H(e^{j\omega})$, as computed using equation (6), (or equation (19) with $\lambda = 0$), is given in Figures 6 and 7 in the form of magnitude and phase functions. The corresponding impulse response h(t) is given in Figure 8; while its integration, the step response, is given in Figure 9. In Figures 6 and 7, the frequency domain division resulted in noise in the high frequency range above 1400 MHz due to the small values (zeros) of $X(e^{j\omega})$ in that range. This noise resulted in the noise observed in Figure 8 obscuring the impulse response information.

In order to find λ_{opt} in the optimal compensation deconvolution technique, equation (19) was used with various values for λ, for which the resulting $|H(e^{j\omega})|$ are shown in Figure 10. From the figure, it is noticed that in the variation of λ between 0 and 100 did not introduce any significant changes in the low noise portion of the response. While a $\lambda = 1000$ value introduced a noticable change. Based on the above discussion, $\lambda_{opt} = 100$ was chosen for optimal compensation. The corresponding $H_{e,opt}(e^{j\omega})$ as resulting from equation (19) is given in Figures 11 and 12. The corresponding optimum impulse

response $h_{e,opt}(t)$ is given in Figure 13, while its integration, the step response is given in Figure 14.

Comparing Figures 8 and 13, also 9 and 14, it can be concluded that optimal compensation eliminated the noise in the deconvolution operation without any noticeable distortion of the information content.

V. CONCLUSION

The frequency domain optimal compensation deconvolution presented here was successful in eliminating deconvolution noise. Although visual inspection of the deconvolution result was used to select the optimum valve for λ in the example presented here, other selection criteria can be developed to suit various application. For example, one good criterion is to minimize the rms error between the step responses of the cases $\lambda = 0$ and $\lambda = \lambda_{opt}$, e.g., to minimize the rms error between Figures 9 and 14.

It is important to mention in the conclusion that the iteration in the frequency domain optimal compensation to find the optimum deconvolution involved only one variable λ and was performed in the frequency domain, thus greatly reducing the computation time as well as the simple formulation (programming) required by equation (19).

VI. ACKNOWLEDGEMENT

This work was done as a part of the NASA contract, NAS 10-9455, "Optical Fiber Dispersion Characterization Study", for Kennedy Space Center.

VII. REFERENCES

1. W. L. Gans and J. R. Andrews, "Time Domain Automatic Network Analyzer for Measurement of RF and Microwave Components," NBS Tech. Note 672, Ch. 9, September 1975.

2. S. M. Riad, "Optical Fiber Dispension Characterization Study," Progress Report III, NAS 10-9455, NASA, Kennedy Space Center, Florida, April 1979.

3. See as an example H.F. Silverman and A. E. Pearson, "On Deconvolution Using the Discrete Fourier Transform," IEEE Trans. Audio Electroacoust., vol. AU-21, pp. 112-118, April 1973.

4. M. P. Ekstrom, "An Iterative, Time Domain Method of System REsponse Correction," WESCON Technical Papers, Part 14, August 19-22, 1969.

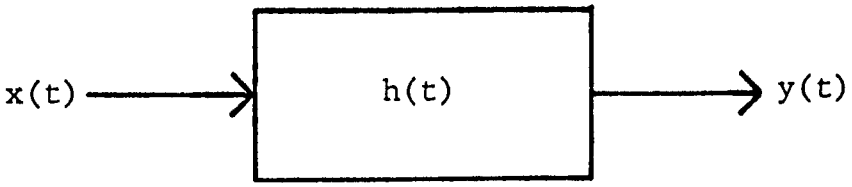

Figure 1. Time Domain Representation of a Linear System.

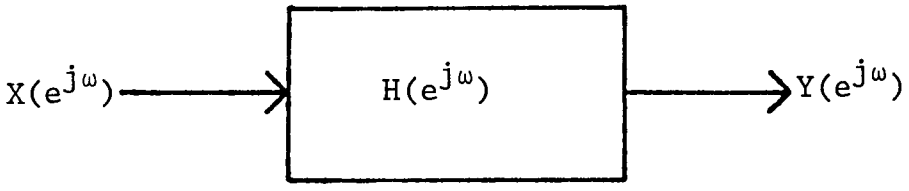

Figure 2. Frequency Domain Representation of Figure 1.

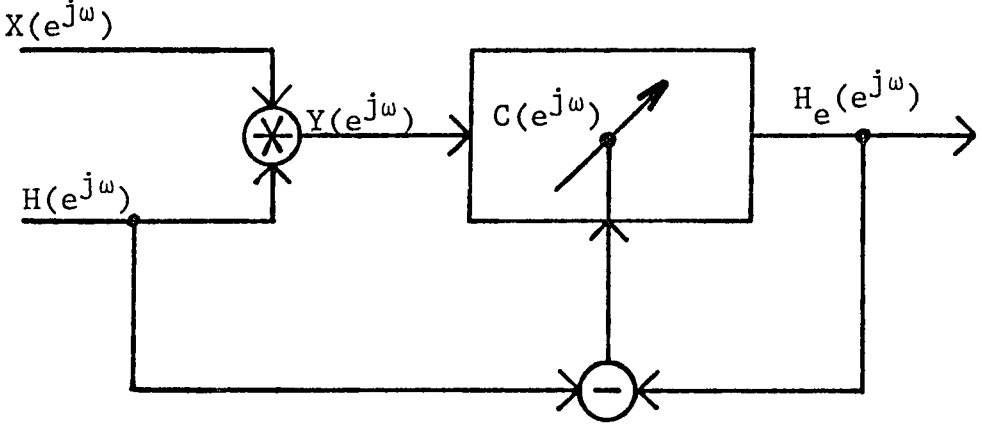

Figure 3. Frequency Domain Optimal Compensator Design.

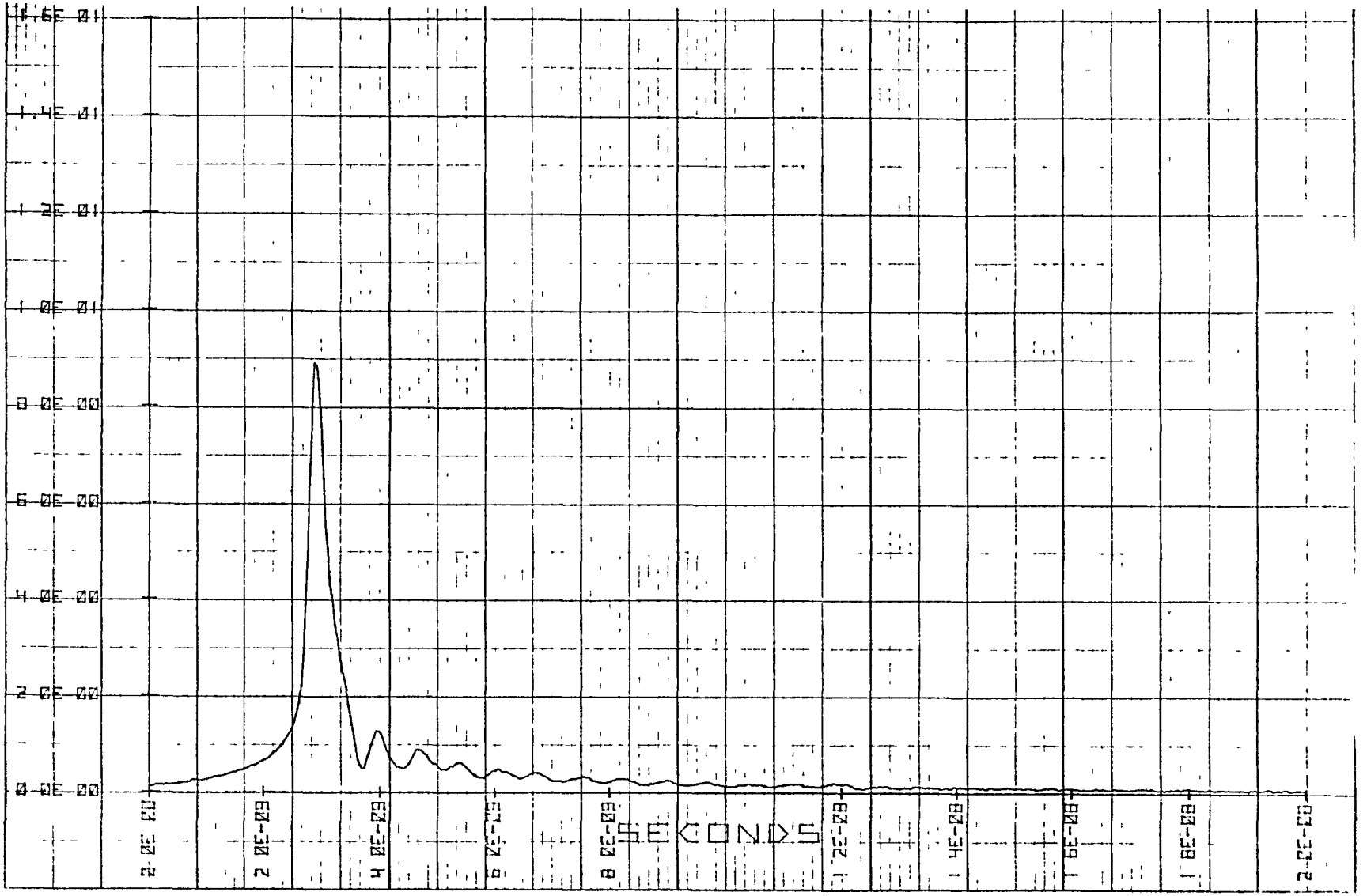

Figure 4. x(t); Reference Waveform for Fiber Impulse Response Characterization

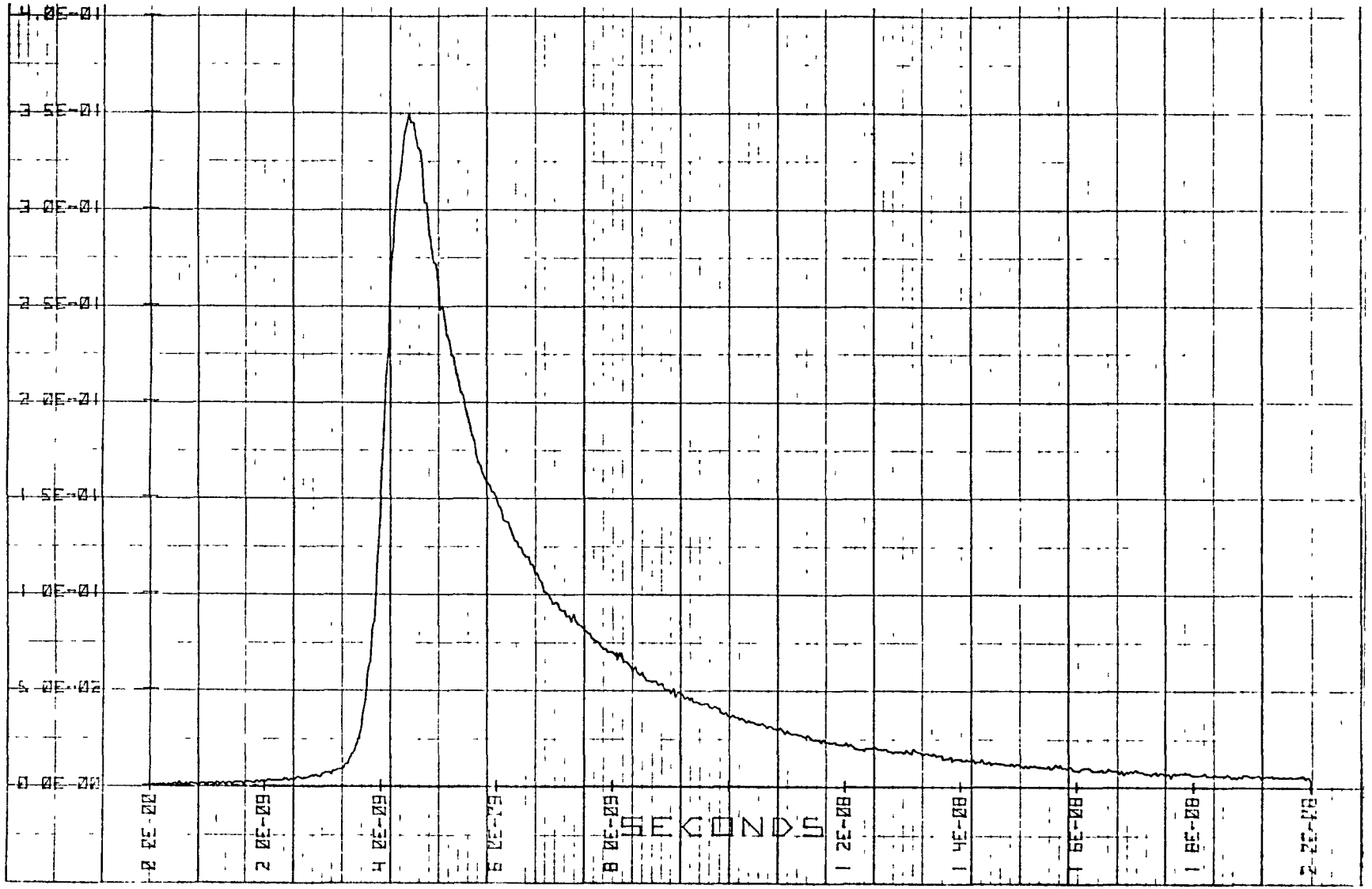

Figure 5. y(t), Response Waveform of a 4-km Fiber.

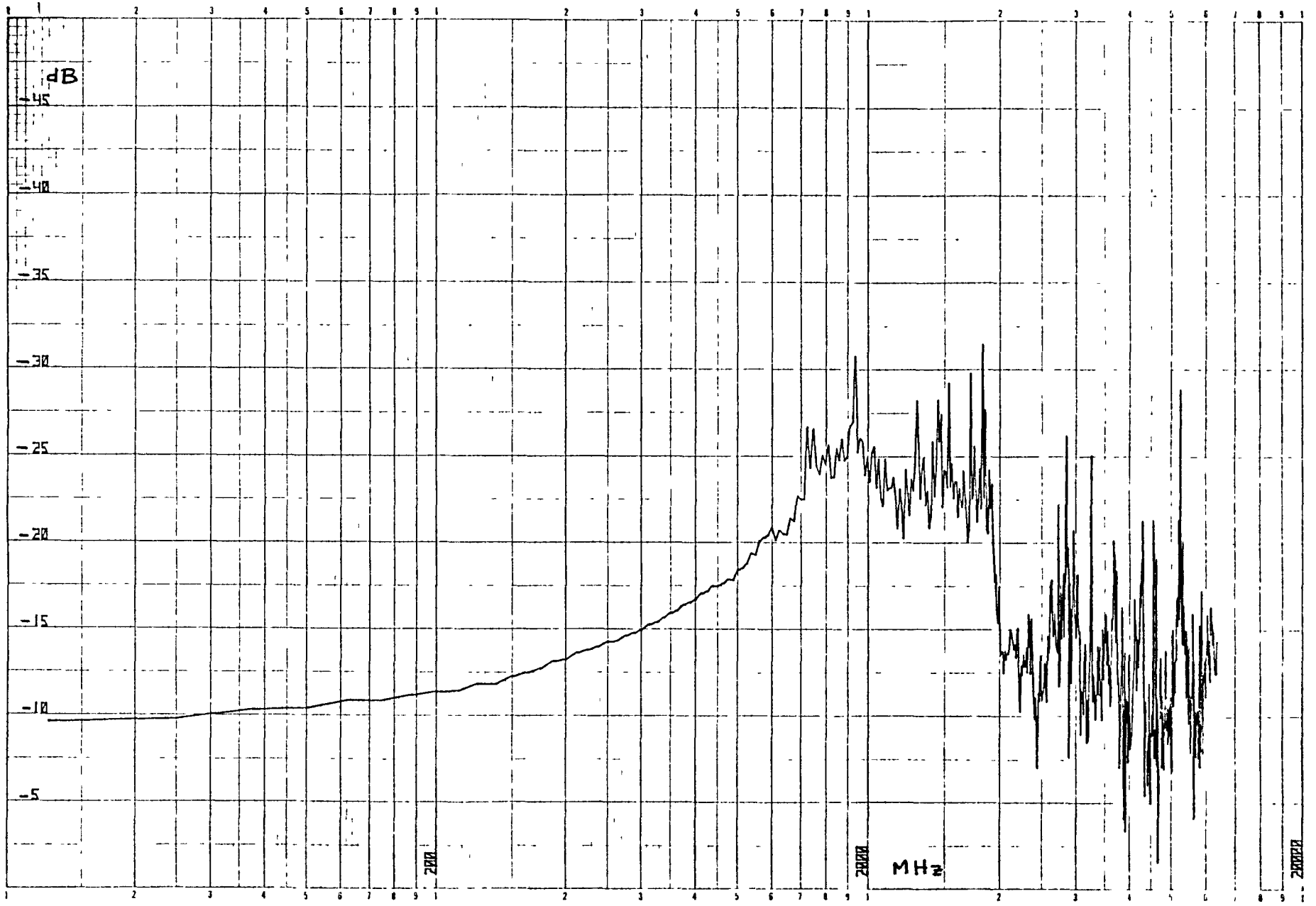

Figure 6. $|H(e^{j\omega})|$; Magnitude of Fiber Transfer Function in dB vs. Frequency, as computed using Equation (6) (direct frequency domain division)

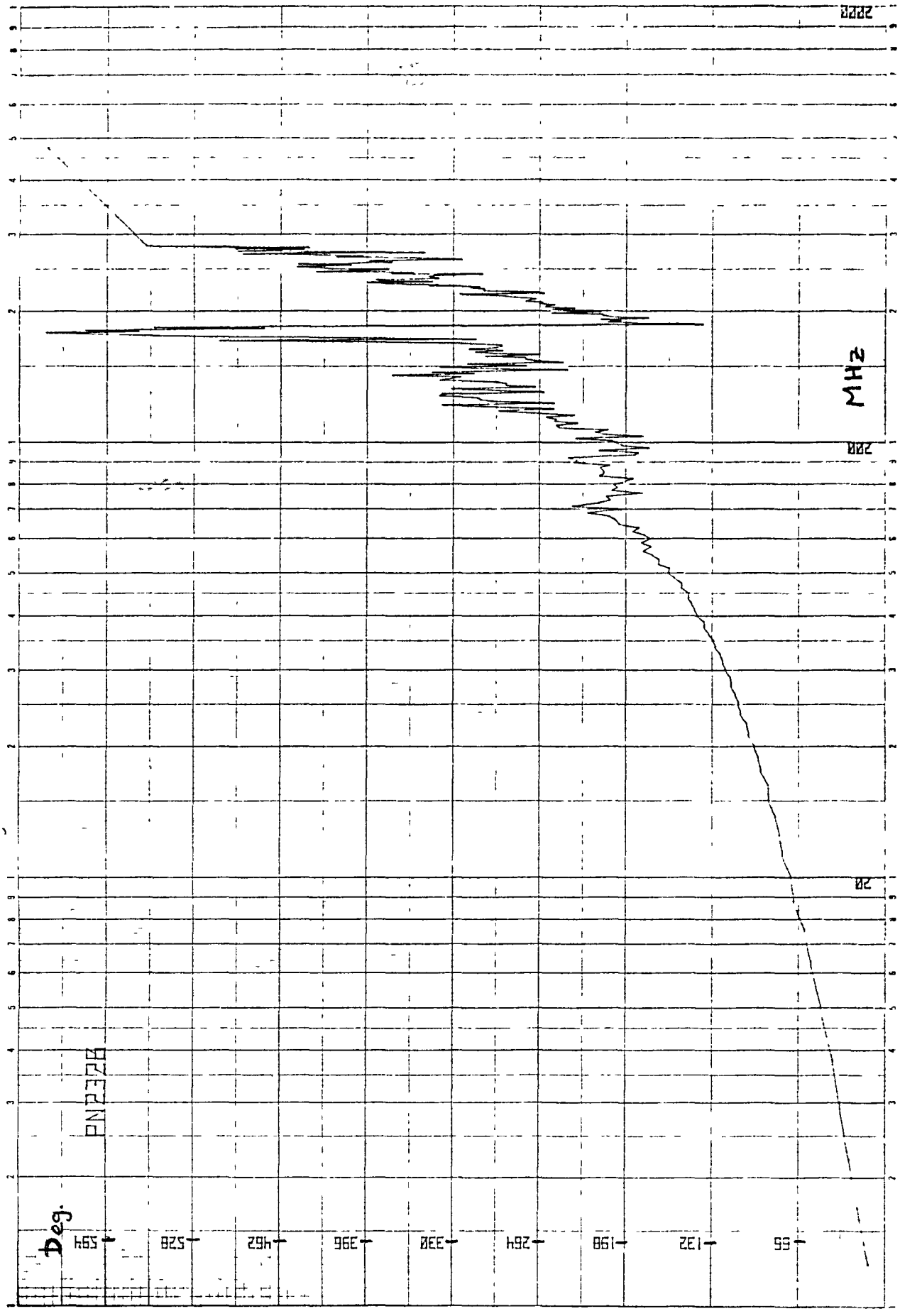

Figure 7. Phase of $H(e^{j\omega})$ of Figure 6.

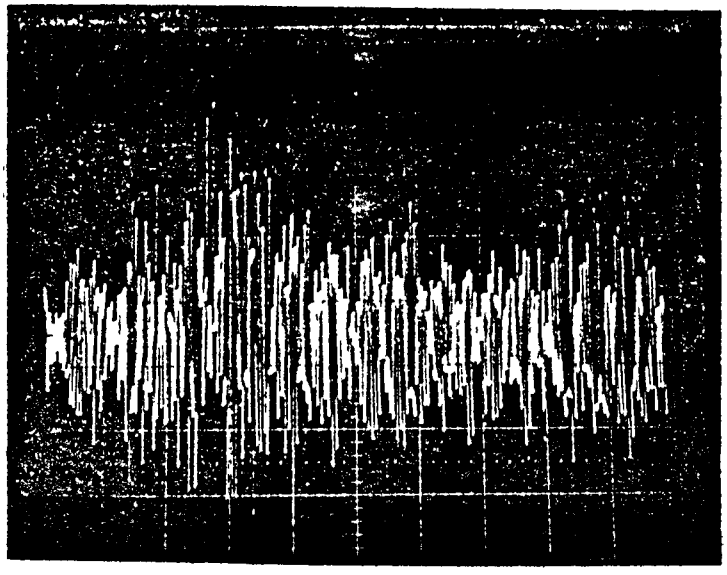

Figure 8. Fiber Impulse Response h(t); The Inverse Fourier Transform of $H(e^{j\omega})$ of Figures 6 and 7. (2ns per horiz. div.)

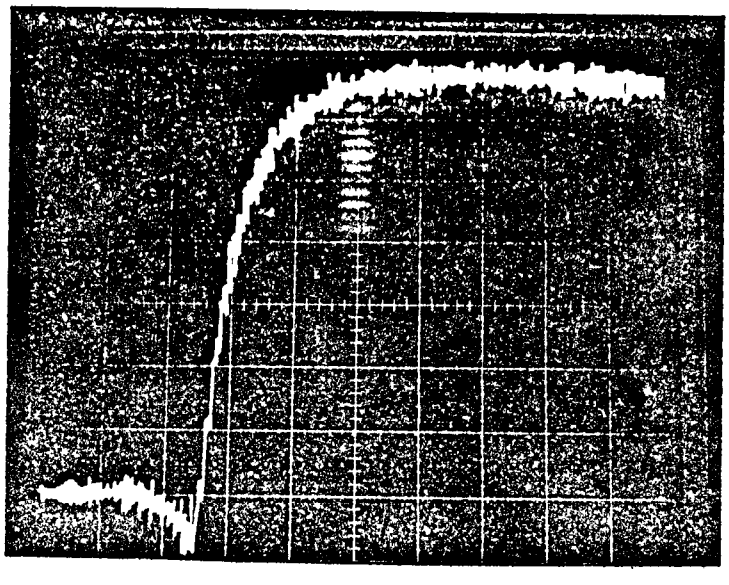

Figure 9. Fiber Step Response; The Integral of h(t) of Figure 8. (2ns per horiz. div.)

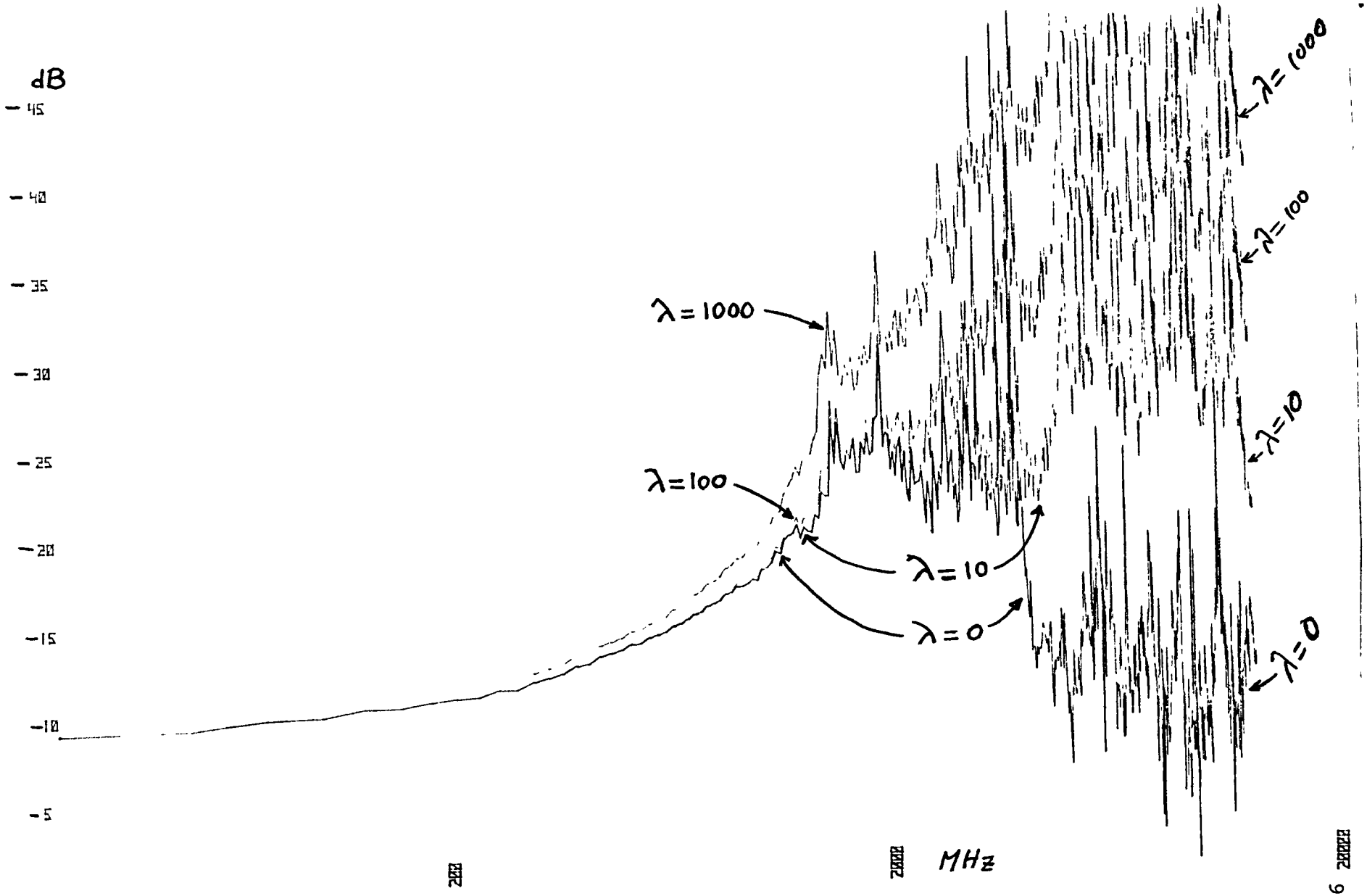

Figure 10. Choosing λ_{opt}, $|H(e^{j\omega})|$ vs. Frequency for various values of λ.

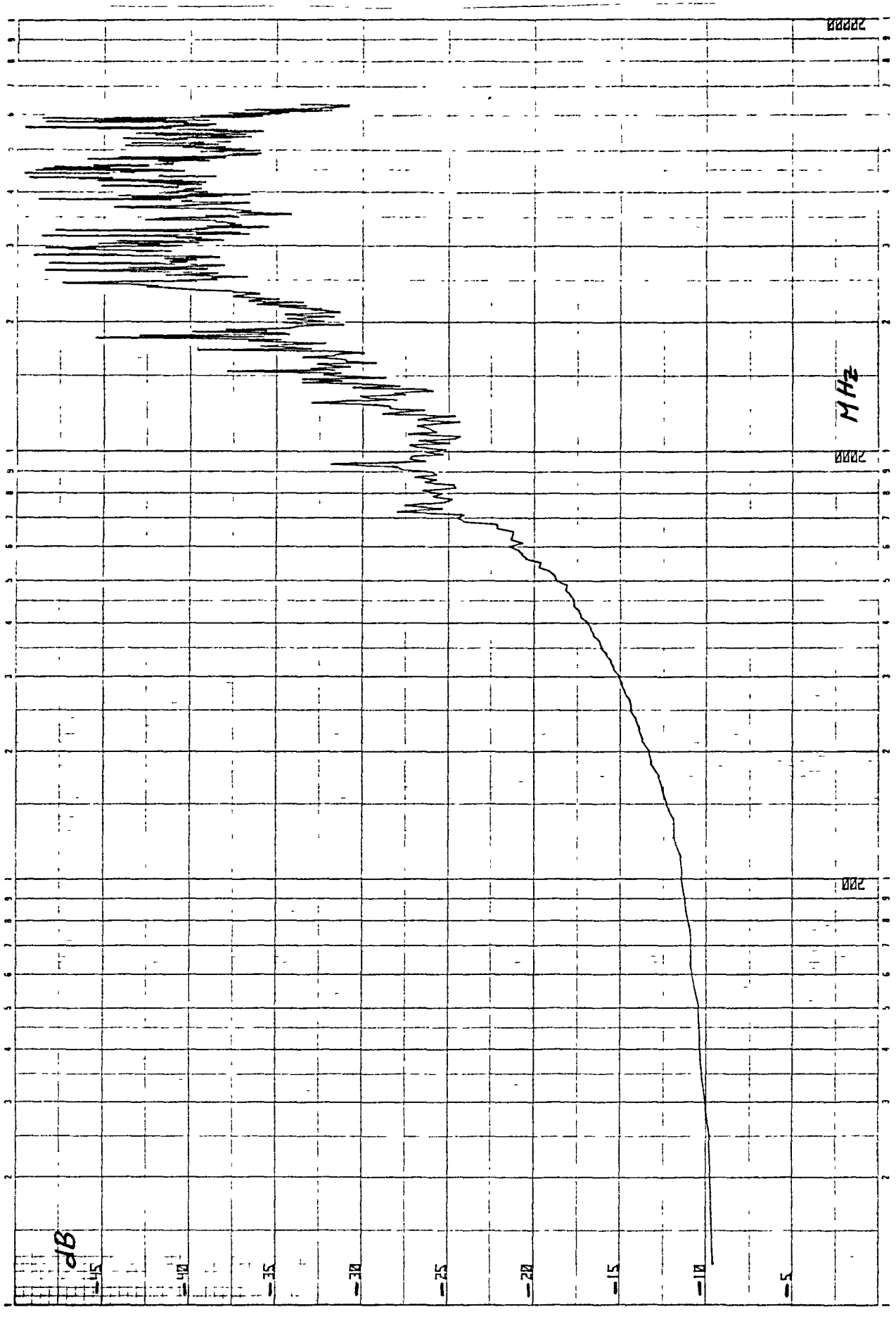

Figure 11. Magnitude of $H_{e,opt}(e^{j\omega})$ vs. Frequency.

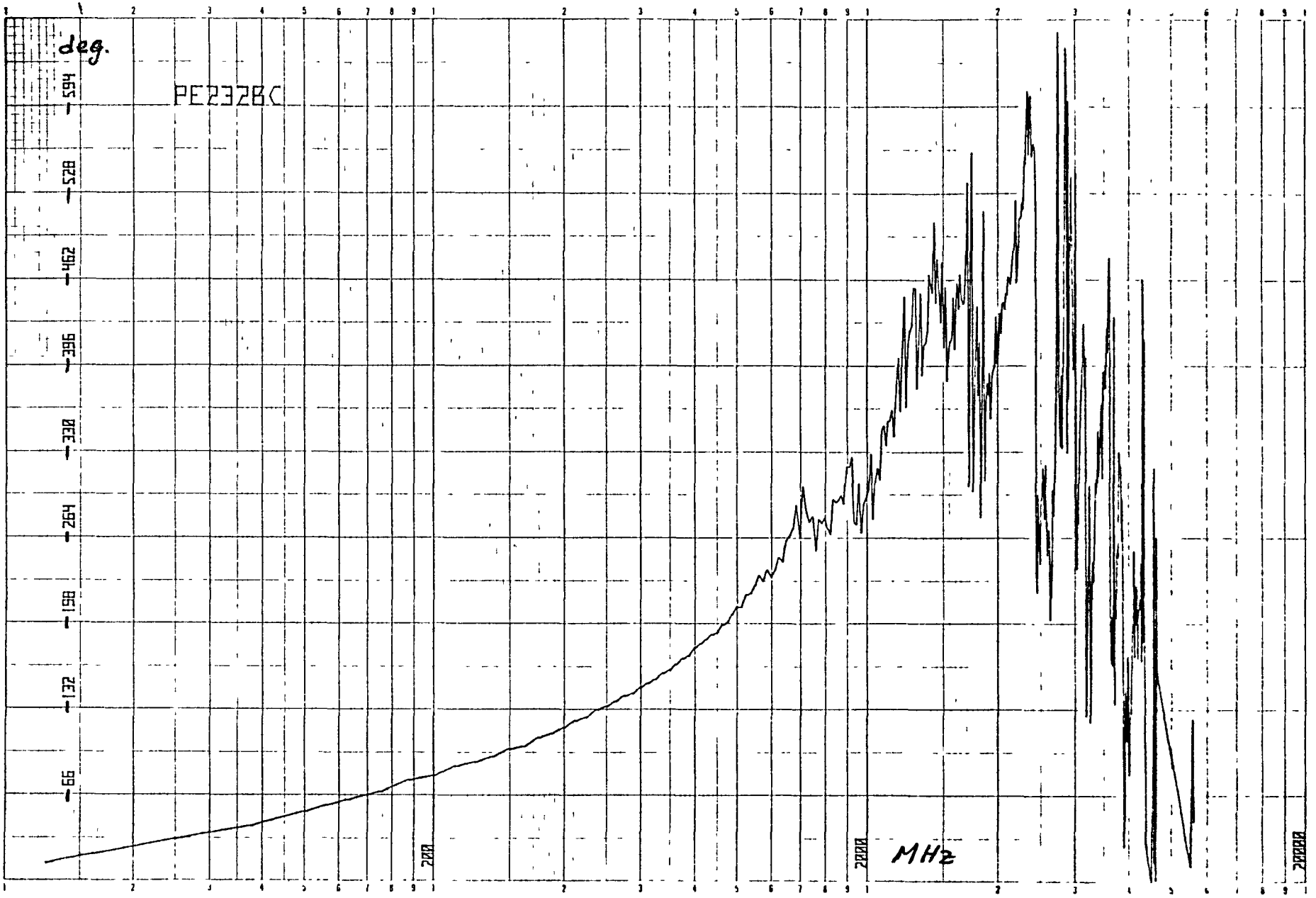

Figure 12. Phase part of $H_{e,opt}(e^{j\omega})$ vs. Frequency.

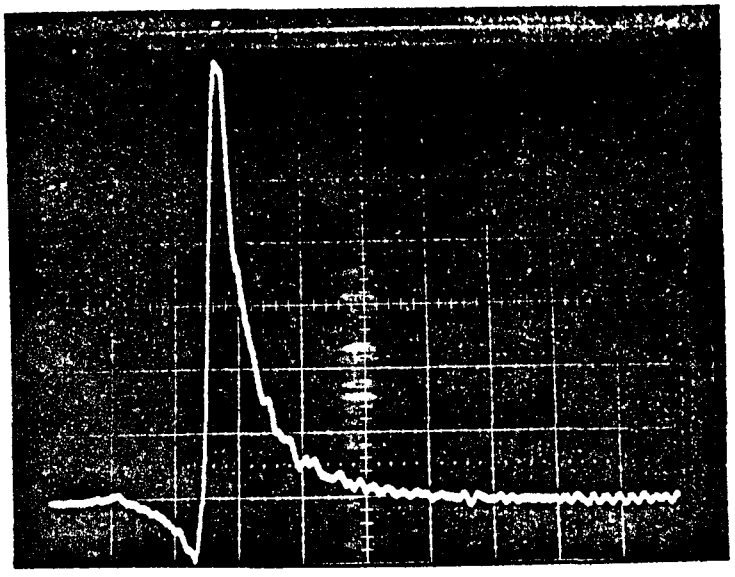

Figure 13. Fiber's Optimum Impulse Response $h_{e,opt}(t)$.
(2ns per horiz. div.)

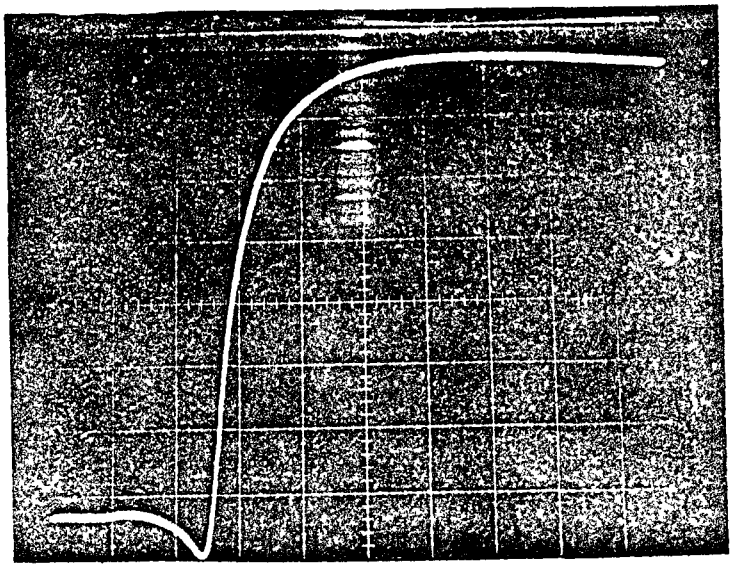

Figure 14. Fiber's Optimum Step Response, the Integration of $h_{e,opt}(t)$.
(2ns per horiz. div.)

APPENDIX B

COMPUTER SOFTWARE

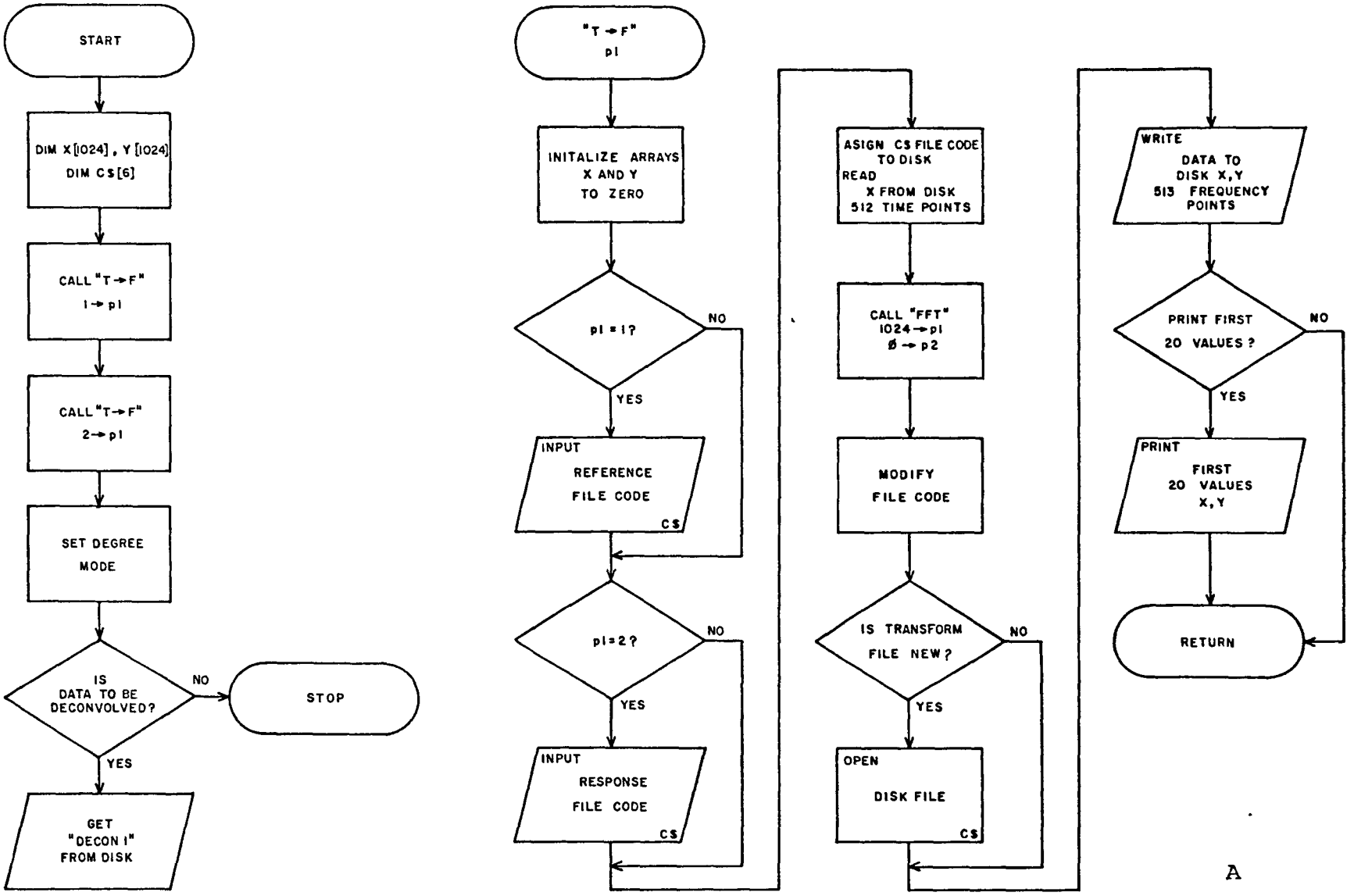

A

PULSE DISPERSION TEST

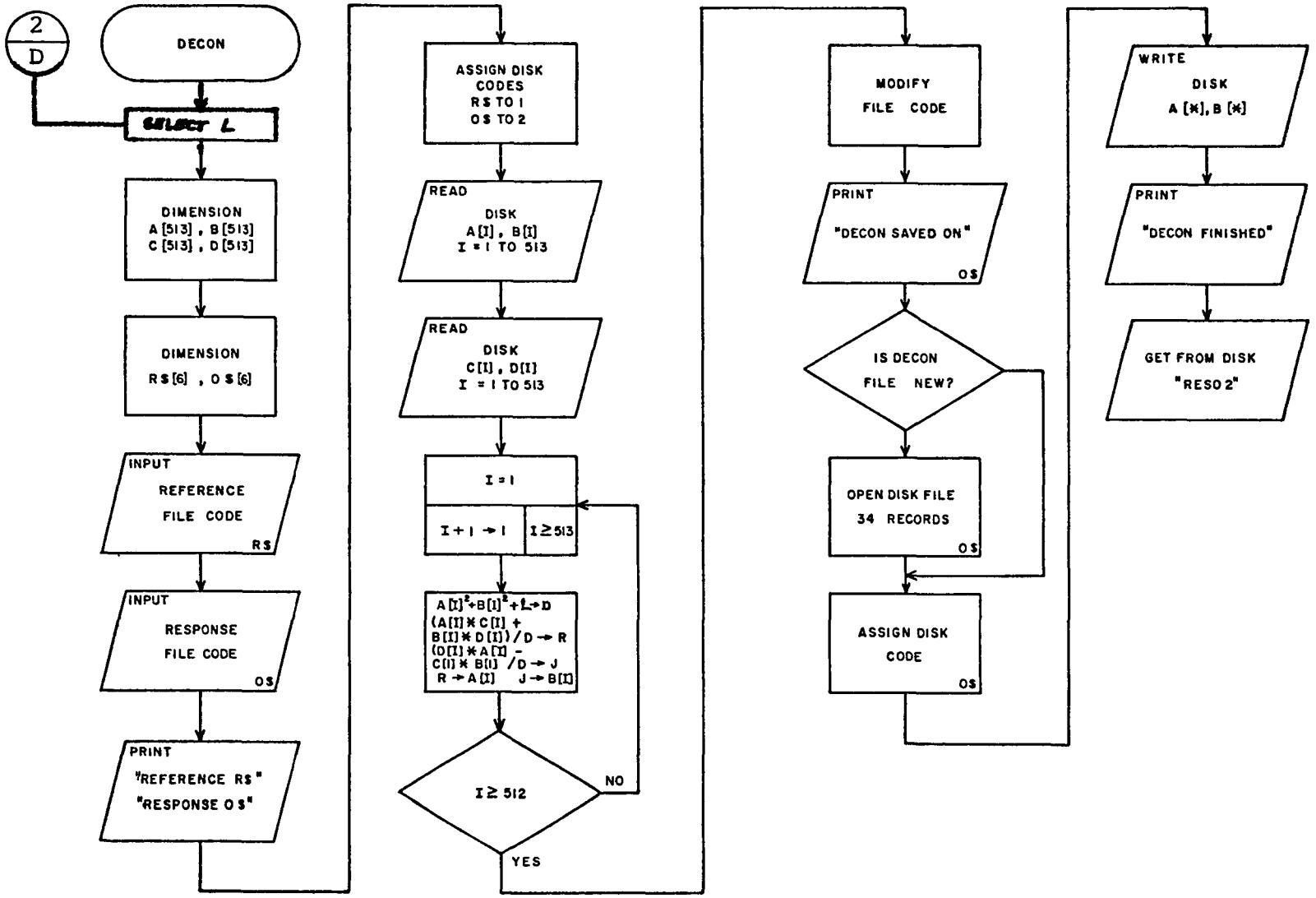

B

DECONVOLUTION PROGRAM

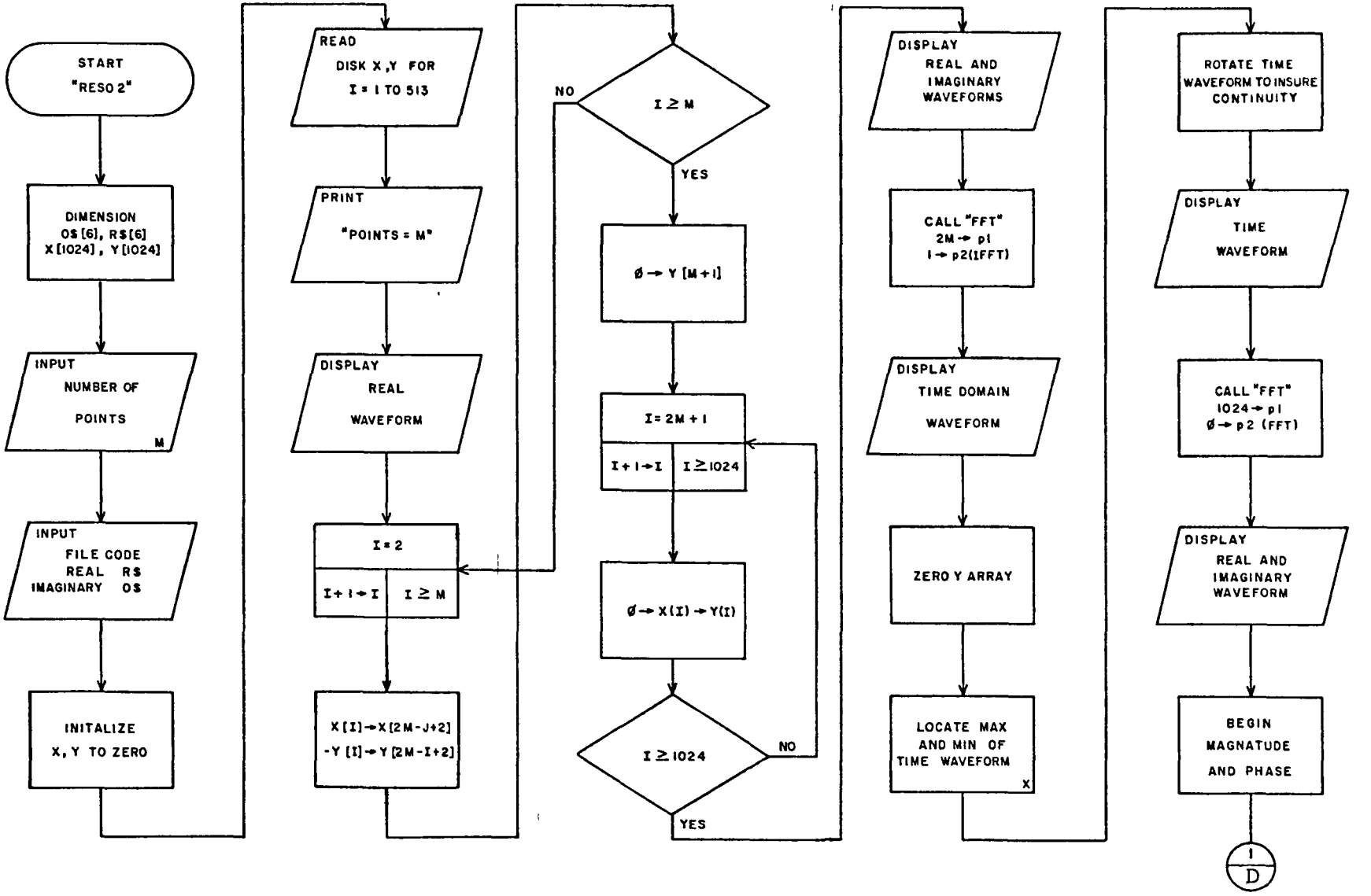

C

RESOLUTION

ENHANCEMENT PROGRAM

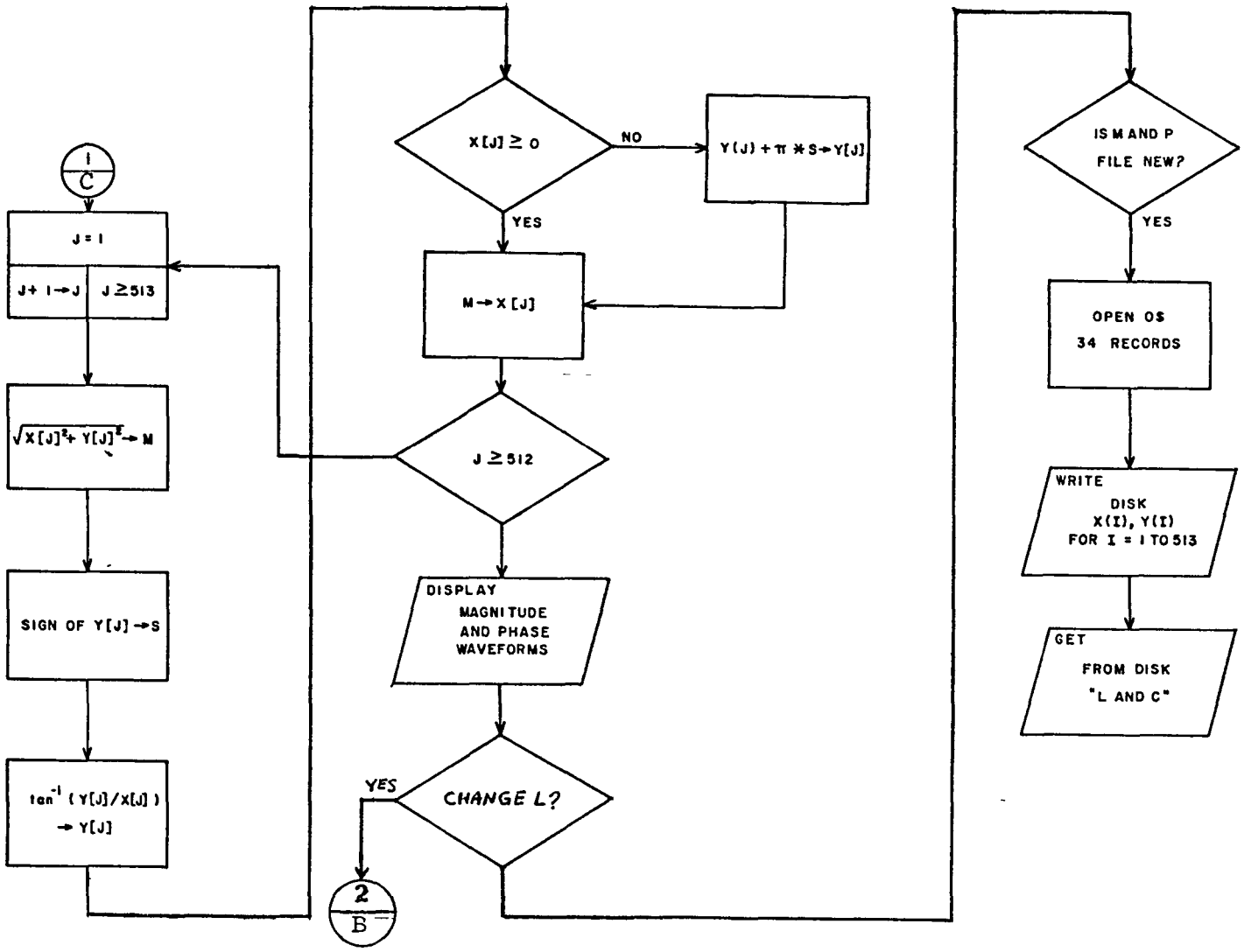

D

RESOLUTION
ENHANCEMENT PROGRAM

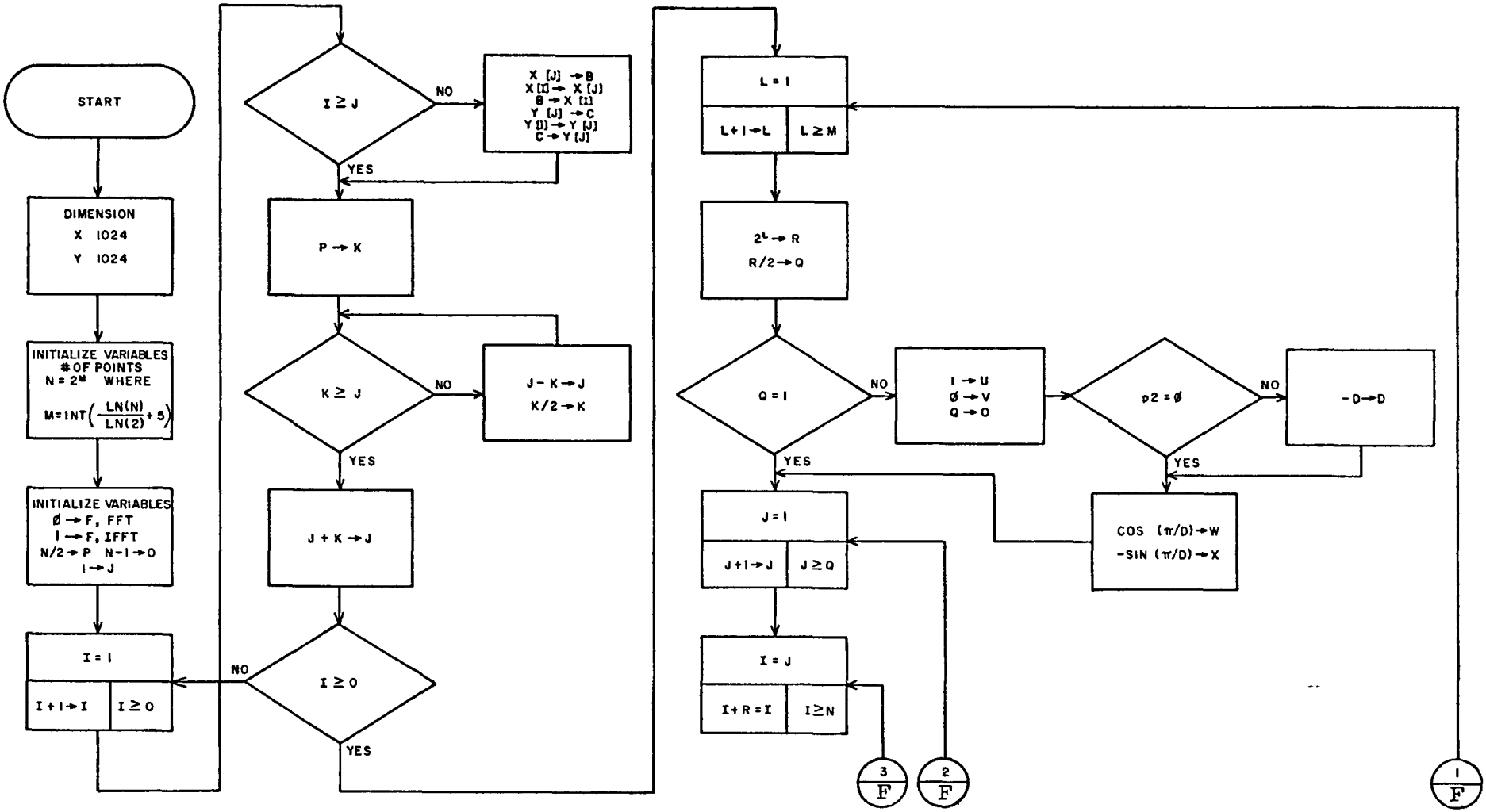

E

FFT AND INVERSE FFT (IFFT)

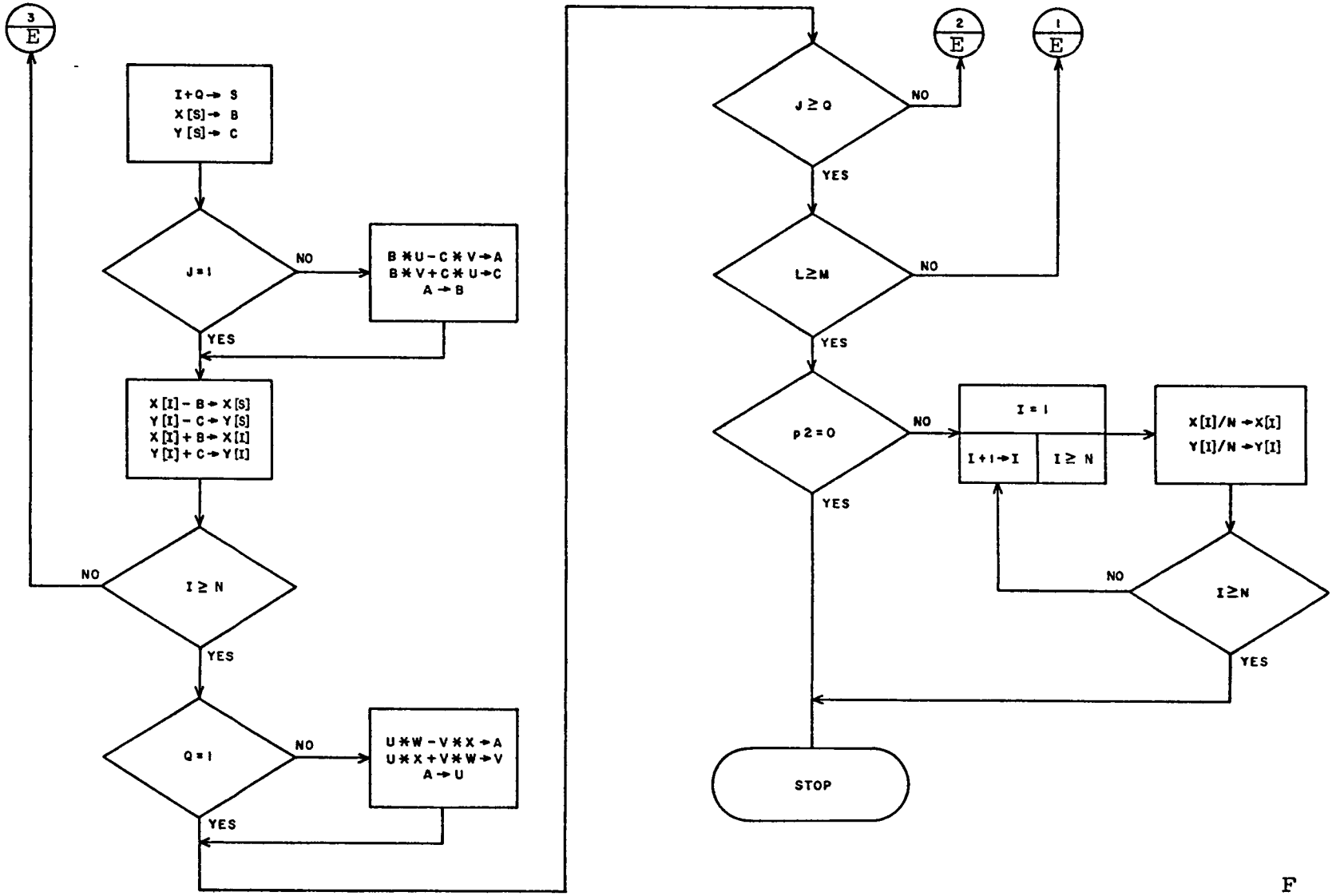

F

FFT AND INVERSE FFT (IFFT)

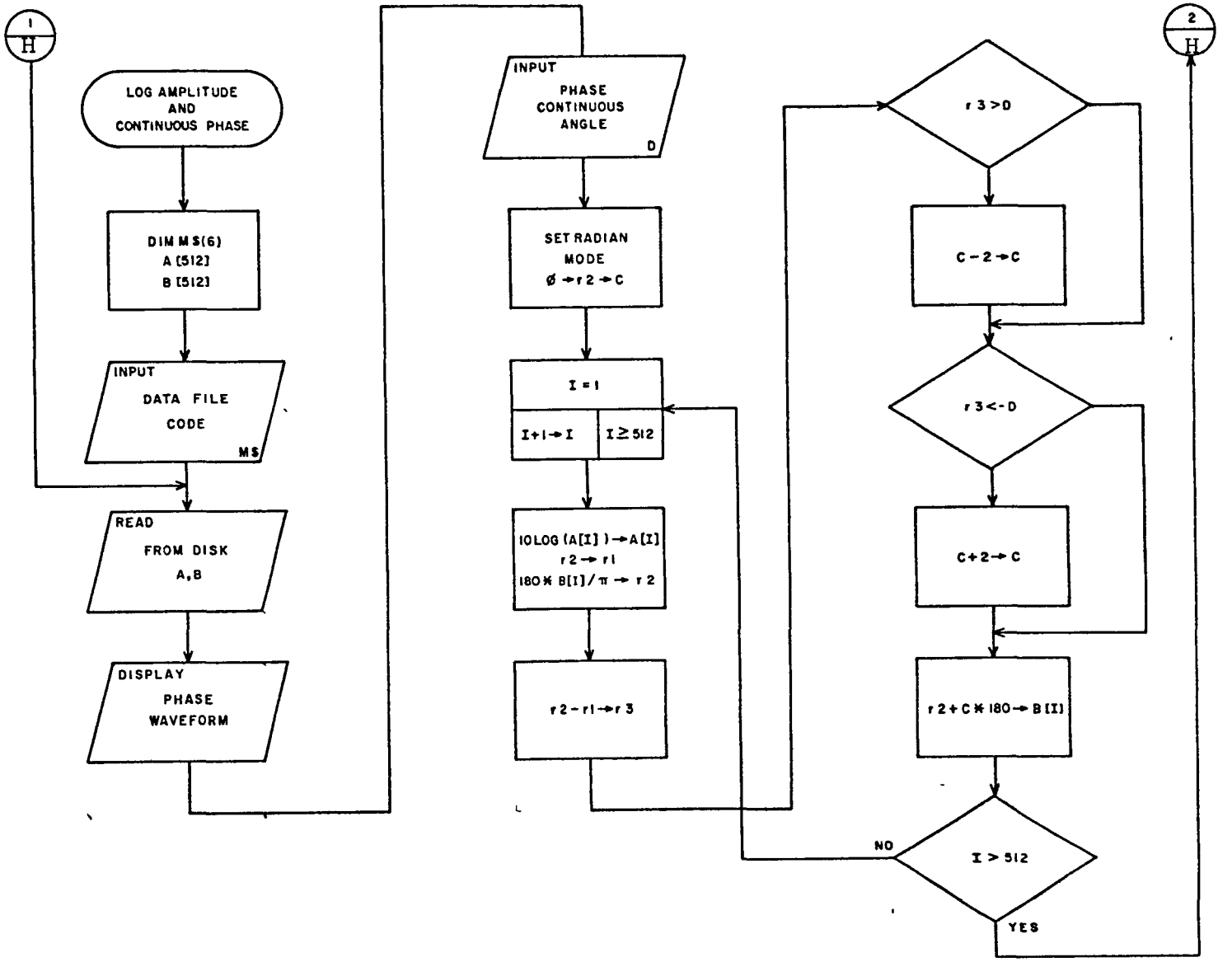

G

LOG AMPLITUDE AND CONTINUOUS PHASE

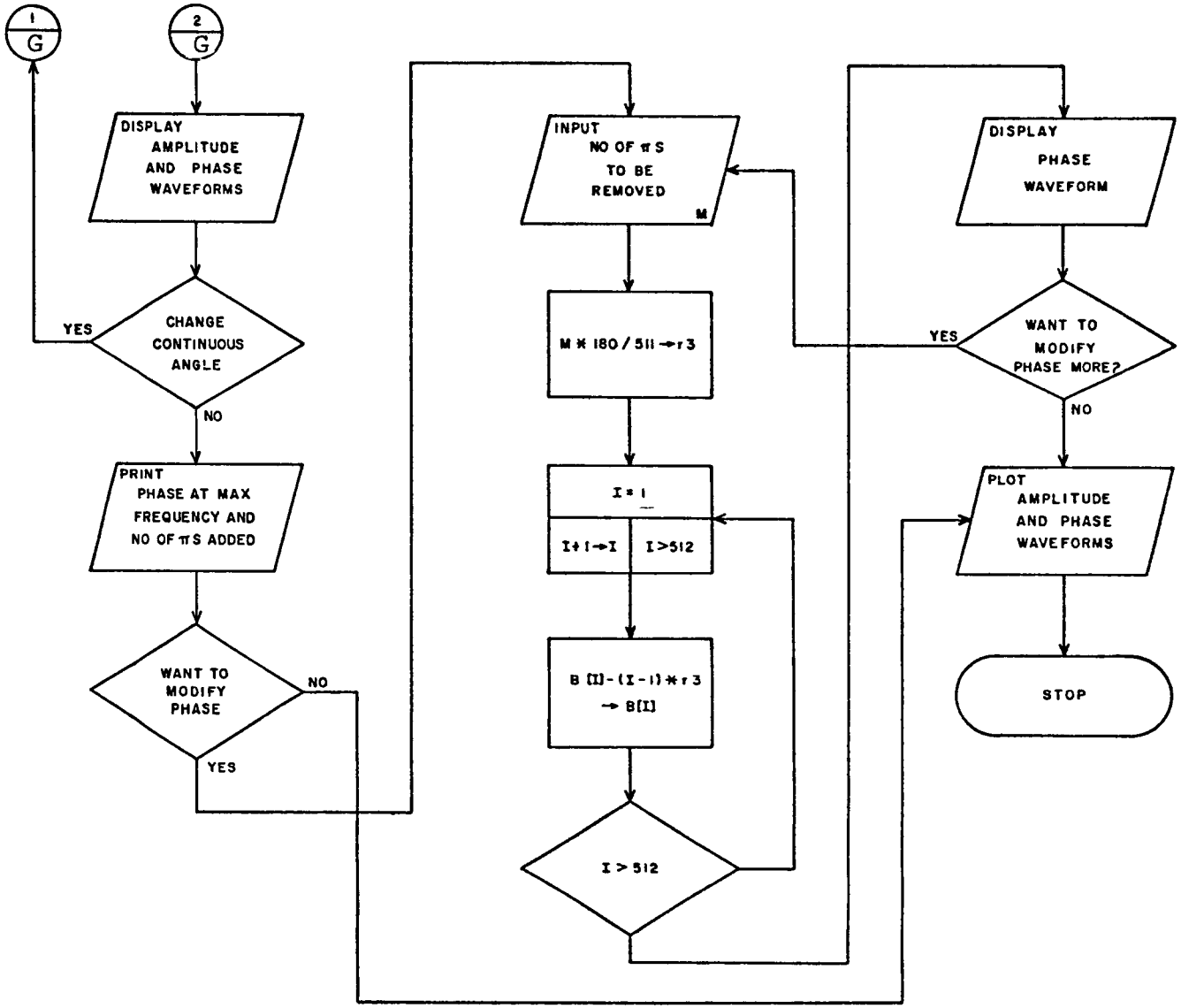

H

LOG AMPLITUDE
AND CONTINUOUS PHASE

PULSE DISPERSION TEST 4-16-79

```
0: "PULSE DISPERSION TEST":
1: dim X[1024],Y[1024]
2: dim C$[6]
3: cll 'T→F'(1)
4: cll 'T→F'(2)
5: deg
6: ent "IS THIS DATA TO BE DECONVOLVED?",L;if L=0;stp
7: get "DLCON1"
8: "T→F":
9: ina X,Y
10: if p1=1;ent "ENTER REFERENCE FILE CODE",C$
11: if p1=2;ent "ENTER OUTPUT FILE CODE",C$
12: asgn C$,1
13: rread 1,1
14: for I=1 to 512
15: sread 1,X[I]
16: next 1
17: cll 'FFT'(1024,0)
18: "PF"&C$[3,6]→C$
19: ent "IS TRANSFORM FILE NEW?",r1;if r1;open C$,34
20: asgn C$,2
21: rread 2,1
22: for I=1 to 513
23: sprt 2,X[I],Y[I]
24: next 1
25: ent "WANT THE FIRST 20 VALUES??",r2;if r2=0;jmp 4
26: for I=1 to 20
27: prt 1,X[I],Y[I];spc 2
28: next 1
29: ret
30: "FFT":
31: "WRITTEN BY MIKE PADGETT 10-21-78":
32: "p1=NO. OF POINTS IN FFT":
33: "p2=0→FFT, p2=1→IFFT":
34: if p2=0;dsp "FFT NOW BEING PERFORMED"
35: if p2=1;dsp "IFFT IS NOW BEING PERFORMED"
36: "init":
37: rad
38: csv
39: 0→F
40: p1→N
41: int(ln(N)/ln(2)+.5)→M
42: N/2→P;N-1→O;1→J
43: "proc":beep
44: for I=1 to O
45: if I>=J;jmp 3
46: X[J]→B;X[I]→X[J];B→X[I]
47: Y[J]→C;Y[I]→Y[J];C→Y[I]
48: P→K
49: if K>=J;jmp 2
50: J-K→J;K/2→K;jmp -1
51: J+K→J
52: next I
```

```
53: for L=1 to M
54: 2^L→K
55: K/2→Q
56: if Q=1;jmp 4
57: 1→U;0→V;Q→D
58: if F#0;-L→D
59: cos(π/D)→W;-sin(π/D)→X
60: for J=1 to Q
61: for I=J to N by R
62: I+Q→S;X[S]→B;Y[S]→C
63: if J=1;jmp 4
64: B*U-C*V→A
65: B*V+C*U→C
66: A→B
67: X[I]-B→X[S];Y[I]-C→Y[S]
68: X[I]+B→X[I];Y[I]+C→Y[I]
69: next I
70: if Q=1;jmp 3
71: U*W-V*X→A;U*X+V*W→V
72: A→U
73: next J
74: next L
75: if P2=0;prt "FFT COMPLETED";beep;ret
76: for I=1 to N
77: X[I]/N→X[I]
78: Y[I]/N→Y[I]
79: next I
80: prt "IFFT COMPLETED";ret
```

DECONVOLUTION

```
0: "DECON1":
1: "THIS PROGRAM PERFORMS DECONVOLUTION OF O/R":
2: dim A[513],B[513],C[513],D[513]
3: dim R$[6],O$[6]
4: ent "LAMPDA EQUALS",L
5: ent "ENTER REFERENCE FILE CODE",R$
6: ent "ENTER OUTPUT FILE CODE",O$
7: prt "REFERENCE",R$,"OUTPUT",O$
8: asgn R$,1;asgn O$,2
9: rread 1,1
10: for I=1 to 513
11: sread 1,A[I],B[I]
12: next I
13: rread 2,1
14: for I=1 to 513
15: sread 2,C[I],D[I]
16: next I
17: for I=1 to 513
18: A[I]^2+B[I]^2+L→D
19: (A[I]C[I]+B[I]D[I])/D→R
20: (D[I]A[I]-C[I]B[I])/D→J
21: R→A[I];J→B[I]
22: next I
23: "PR"&R$[3,6]→R$;"PI"&O$[3,6]→O$
24: prt "DECON SAVED ON",R$,O$
25: ent "IS DECON FILE NEW??",r3;if r3;open R$,17;open O$,17
26: asgn R$,3;asgn O$,4
27: rread 3,1
28: sprt 3,A[*]
29: rread 4,1
30: sprt 4,B[*]
31: prt "DECON FINISHED"
32: get "RESO2"
```

RESOLUTION ENHANCEMENT

```
0: "RESOLUTION ENHANCEMENT PROGRAM":
1: dim O$[6],R$[6]
2: dim X[1024],Y[1024],T[100]
3: ent "WANT TO WATCH PROCESS??",r13
4: ent "ENTER NO. of POINTS",M
5: ent "ENTER FILE CODE FOR REAL",R$,"IMAGINARY",O$
6: "start":
7: ina X,Y
8: asgn R$,1;rread 1,1
9: for I=1 to 513
10: sread 1,X[I]
11: next I
12: asgn O$,2;rread 2,1
13: for I=1 to 513
14: sread 2,Y[I]
15: next I
16: spc 3
17: prt "======","********","======";spc 2
18: prt "POINTS=",M
19: cll 'look'(0)
20: cll 'look'(1)
21: for I=2 to M
22: X[I]→X[2M-I+2]
23: -Y[I]→Y[2M-I+2]
24: next I
25: 0→Y[M+1]
26: for I=2M+1 to 1024
27: 0→X[I]→Y[I]
28: next I
29: cll 'look'(1)
30: dsp "READY TO SHOW Y";stp
31: cll 'look'(0)
32: cll 'FFT'(2M,1)
33: cll 'look'(1)
34: dsp "ready";stp
35: cll 'look'(0)
36: ina Y
37: ent "ENTER ROTATION VALUE",T;cll 'rotate'(T)
38: cll 'tau'
39: ina Y
40: cll 'look'(1)
41: cll 'FFT'(1024,0)
42: cll 'look'(1)
43: cll 'look'(0)
44: stp
45: "MandP":
46: dsp "MandP"
47: for J=1 to 513
48: √(X[J]^2+Y[J]^2)→M
49: sgn(Y[J])→S
50: atn(Y[J]/X[J])→Y[J]
51: if X[J]<0;Y[J]+π*S→Y[J]
52: M→X[J]
53: next J
```

```
54: cll 'look'(1);prt "MAGNITUDE"
55: cll 'lcok'(0);prt "PHASE"
56: ent "WANT TO SAVE MandP RESO?",r10;if r10=0;gto "more"
57: "save":
58: "PM"&O$[3,6]→O$;prt "MandP RESO on",O$
59: ent "IS MandP FILE NEW?",r1;if r1;open O$,34
60: asgn O$,5
61: rread 5,1
62: for I=1 to 513
63: sprt 5,X[1],Y[1]
64: next 1
65: get "LandC1"
66: "more":ent "ENTER NO. OF POINTS DESIRED",M;gto "start"
67: "FFT":
68: "WRITTEN BY MIKE PADGETT 10-21-78":
69: "p1=NO. OF POINTS IN FFT":
70: "p2=0→FFT, p2=1→IFFT":
71: if p2=0;dsp "FFT NOW BEING PERFORMED"
72: if p2=1;dsp "IFFT IS NOW BEING PERFORMED"
73: "init":
74: rad
75: p1→N
76: int(ln(N)/ln(2)+.5)→H
77: N/2→P;N-1→O;1→J
78: "proc":beep
79: for I=1 to O
80: if I>=J;jmp 3
81: X[J]→B;X[I]→X[J];B→X[I]
82: Y[J]→C;Y[I]→Y[J];C→Y[I]
83: P→K
84: if K>=J;jmp 2
85: J-K→J;K/2→K;jmp -1
86: J+K→J
87: next I
88: for L=1 to H
89: 2^L→R
90: R/2→Q
91: if Q=1;jmp 4
92: 1→U;0→V;Q→D
93: if p2#0;-D→D
94: cos(π/D)→W;-sin(π/D)→X
95: for J=1 to Q
96: for I=J to N by R
97: I+Q→S;X[S]→B;Y[S]→C
98: if J=1;jmp 4
99: B*U-C*V→A
100: B*V+C*U→C
101: A→B
102: X[I]-B→X[S];Y[I]-C→Y[S]
103: X[I]+B→X[I];Y[I]+C→Y[I]
104: next I
105: if Q=1;jmp 3
106: U*W-V*X→A;U*X+V*W→V
107: A→U
108: next J
109: next L
```

```
110: if p2=0;prt "FFT COMPLETED";beep;ret
111: for I=1 to N
112: X[I]/N→X[I]
113: Y[I]/N→Y[I]
114: next I
115: prt "IFFT COMPLETED";ret
116: "look":
117: if r13=0;ret
118: flt 3
119: "p1=0 SENDS ARRAY B,p1=1 SENDS ARRAY A":
120: fmt 8,x,f.0,z
121: dsp "SELECT W/F ""B"" ON DPO";stp
122: max(X[*])-min(X[*])→A
123: if max(Y[*])#min(Y[*]);max(Y[*])-min(Y[*])→B;jmp 2
124: 1→B
125: 802/A→F;71-min(X[*])*F→G;802/B→E;71-min(Y[*])*E→S
126: wtb 701,"DPB "
127: for I=1 to 512
128: if p1=1;wrt 701.8,X[I]*F+G
129: if p1=0;wrt 701.8,Y[I]*E+S
130: next I
131: wtb 701,13,10
132: if p1;prt "MAX AMP",max(X[*]),"MIN",min(X[*]),"STEP",A/8;spc 2
133: if p1=0;prt "MAX PHASE",max(Y[*]),"MIN",min(Y[*]),"STEP",B/8;spc 2
134: fxd 2
135: ret
136: "rotate":
137: for I=1 to M
138: X[I]→Y[I+M]
139: next I
140: for I=M+1 to 2M
141: X[I]→Y[I-M]
142: next I
143: ara Y→X
144: ret
145: "tau":
146: 0→T
147: for I=1 to 2M
148: T+X[I]→T→Y[I]
149: next I
150: cll 'look'(0)
151: 0→r15
152: for I=1 to 20
153: Y[I]+r15→r15
154: next I;r15/20→r16
155: 0→r15
156: for I=2M-20 to 2M
157: Y[I]+r15→r15
158: next I;r15/20→r17
159: (r17-r16)/200→T
160: r16-T→r18;r16+T→r19
161: cll 'hist'(r18,r19,1,M/2,r21,r22)
162: r17-T→r18;r17+T→r19
163: cll 'hist'(r18,r19,3M/2,2M,r25,r26)
164: r24+(r26-r24)/10→T;r26-(r26-r24)/10→Z
```

```
165: 10→r18→r19
166: for 1=1 to 2M
167: if Y[1]-T<r18;Y[1]-T→r18;I→r16
168: if Y[1]-Z<r19;Y[1]-Z→r19;1→r17
169: next I
170: r17-r16→T
171: prt "POINTS =",T;ret
172: "hist":
173: ina T
174: for I=p3 to p4
175: int(Y[1]99/(r19-r18)+1-99r18/(r19-r18))→r20
176: if K<1 or K>100;jmp 2
177: T[K]+1→T[K]
178: next I
179: for 1=1 to 100
180: if T[1]=max(T[*]);1→p5
181: next 1
182: (p5-(1-99p1/(p2-p1)))/99/(p2-p1)→p6
183: ret
```

LOG AMPLITUDE AND CONTINOUS PHASE

```
0: "LOG AMPLITUDE AND CONTINOUS PHASE":
1: dim M$[6],A[512],B[512]
2: ent "ENTER MandP FILE CODE",M$
3: asgn M$,1
4: "start":
5: rread 1,1
6: for I=1 to 512
7: sread 1,A[I],B[I]
8: next I
9: cll 'look'(0)
10: ent "ENTER cont. ANGLE in DEG.",D
11: rad
12: 0→C
13: 0→r2
14: for I=1 to 512
15: 10log(A[I])→A[I]
16: r2→r1
17: 180*B[I]/π→r2
18: r2-r1→r3
19: if r3>D;C-2→C
20: if r3<-D;C+2→C
21: r2+C*180→B[I]
22: next I
23: cll 'look'(1)
24: dsp "READY TO SHOW PHASE";stp
25: cll 'look'(0)
26: ent "WANT TO CHANGE THE cont. ANGLE?",Q;if Q;gto "start"
27: prt "PHASE=",B[512],"at point#",512,"# of π's added",C
28: ent "WANT TO MODIFY THE PHASE?",L;if L=0;jmp 8
29: ent "ENTER π's to be removed",M;prt "π's",M
30: M*180/511→r3
31: for I=1 to 512
32: B[I]-(I-1)*r3→B[I]
33: next I
34: cll 'look'(0)
35: ent "WANT TO MODIFY PHASE MORE?",r7;if r7=1;jmp -6
36: "plotFFT":
37: prt "MAX AMP",max(A[*]),"MIN AMP",min(A[*]),"MAX PHASE",max(B[*])
38: prt "MIN PHASE",min(B[*])
39: deg
40: dsp "READY TO PLOT MAGNITUDE";stp
41: ent "Enter ""DELTA F""",H
42: "axes":
43: ent "Want AXIS Drawn?",X;if X=0;gto "scalein"
44: scl 0,150,0,100
45: for I=1 to 3
46: for J=10^(I-1) to 10^1 by 10^(I-1)
47: plt 15+120/3*log(J),10
48: iplt 0,80,-1
49: next J;next I;iplt 0,80;pen
```

```
50: for I=1 to 4
51: for J=10^(I-1) to 10^I by 10^I
52: 15.5+120/3*log(J)→K;if K>65;if K<84;gto +2
53: plt K,.7,1;csiz 1.1,2,11/15,90;fxd 0;lbl 2*J
54: next J;next I
55: plt 15,10;iplt 120,0,-1;plt 15,10
56: for I=1 to 8
57: iplt 0,10
58: iplt .5,0;iplt -1,0;iplt .5,0
59: next I;iplt 120,0,-1;pen
60: "scalein":ent "ENTER NO. OF VERT DIVISIONS",V
61: ent "ENTER VERT SCL PER DIVISION",S
62: if X=0;gto "scale"
63: csiz 1.1,2,11/15,0
64: for I=1 to V
65: plt 6,10+10I,1
66: lbl SI
67: next I
68: "scale":
69: ent "Want INVERT Data?",Y;if Y=1;smpy -1A→A;smpy -1B→B
70: scl -1.5*3/12+log(2e6),13.5*3/12+log(2e6),-VS/8,9*VS/8
71: for I=2 to 512
72: if log((I-1)*H)>log(2e9);plt log(2e9),A[I-1];512→I;jmp 2
73: plt log((I-1)*H),A[I]
74: next I;pen
75: stp
76: "phase":
77: ent "ENTER NO. PHASE VERT. DIVISIONS",V
78: ent "ENTER VERT. PHASE PER DIV",S
79: scl -1.5*3/12+log(2e6),13.5*3/12+log(2e6),-5VS/8,5VS/8
80: for I=2 to 512
81: if log((I-1)*H)>log(2e9);plt log(2e9),B[I-1];512→I;jmp 2
82: if B[I]>4VS/8;4VS/8→B[I];512→I;jmp 2
83: plt log((I-1)*H),B[I]
84: next I
85: pen
86: stp
87: "look":
88: "pl=0 SENDS ARRAY B,pl=1 SENDS ARRAY A":
89: fmt 8,x,f.0,z
90: dsp "SELECT W/F ""B"" ON DPO";stp
91: max(A[*])-min(A[*])→A;max(B[*])-min(B[*])→B
92: 802/A→F;71-min(A[*])*F→G;802/B→L;71-min(B[*])*L→S
93: wtb 701,"DPB "
94: for I=1 to 512
95: if pl=1;wrt 701.8,A[I]*F+G
96: if pl=0;wrt 701.8,B[I]*L+S
97: next I
98: wtb 701,13,10
99: if pl;prt "MAX AMP",max(A[*]),"MIN",min(A[*]),"STEP",A/8;spc 2
100: if pl=0;prt "MAX PHASE",max(B[*]),"MIN",min(B[*]),"STEP",B/8;spc 2
101: ret
```

APPENDIX C

DISPERSION TEST RESULTS ON CONCATENATED FIBERS

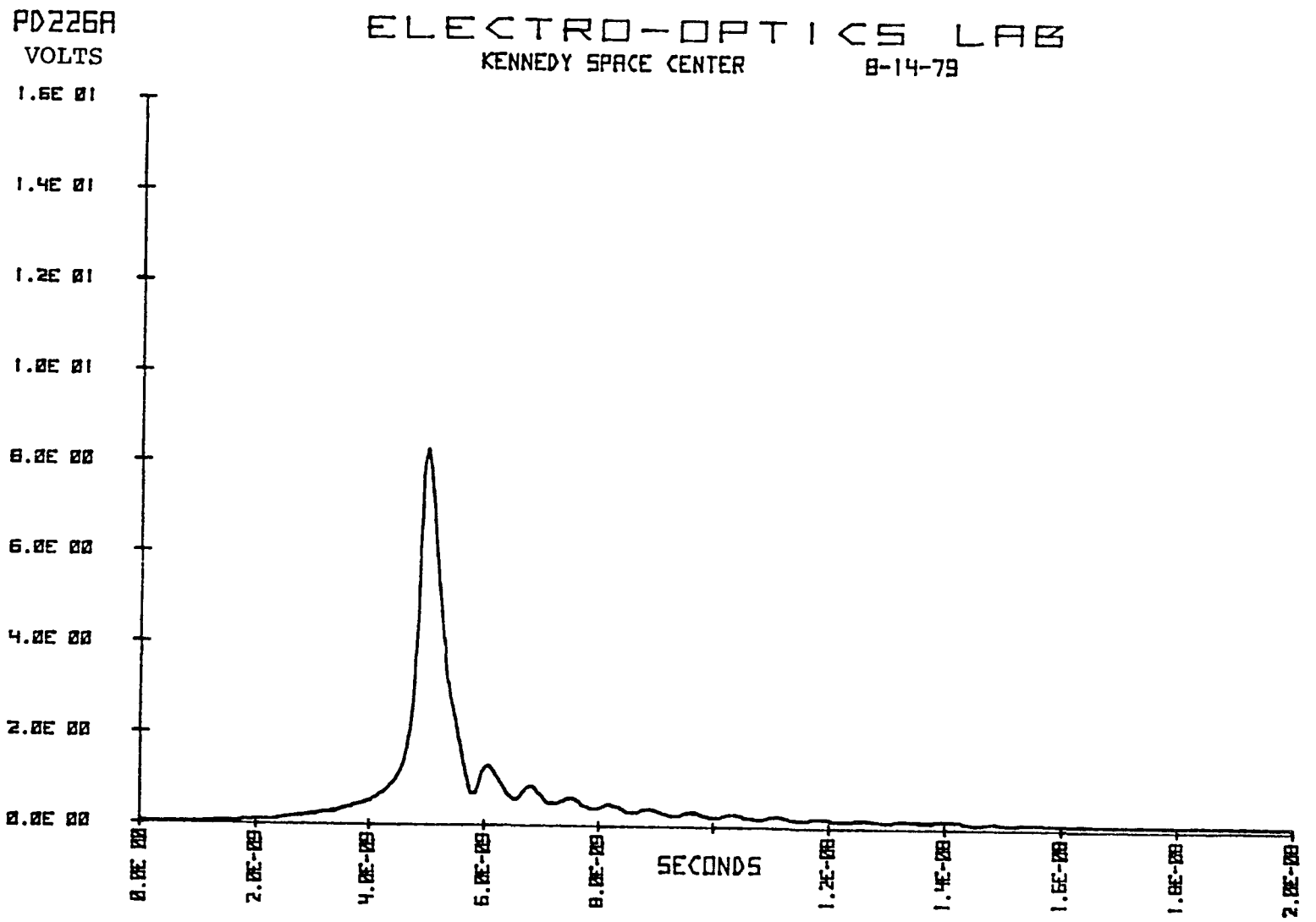

FIGURE D1: REFERENCE WAVEFORM FOR TESTING 600 m FIBER LOOPS.

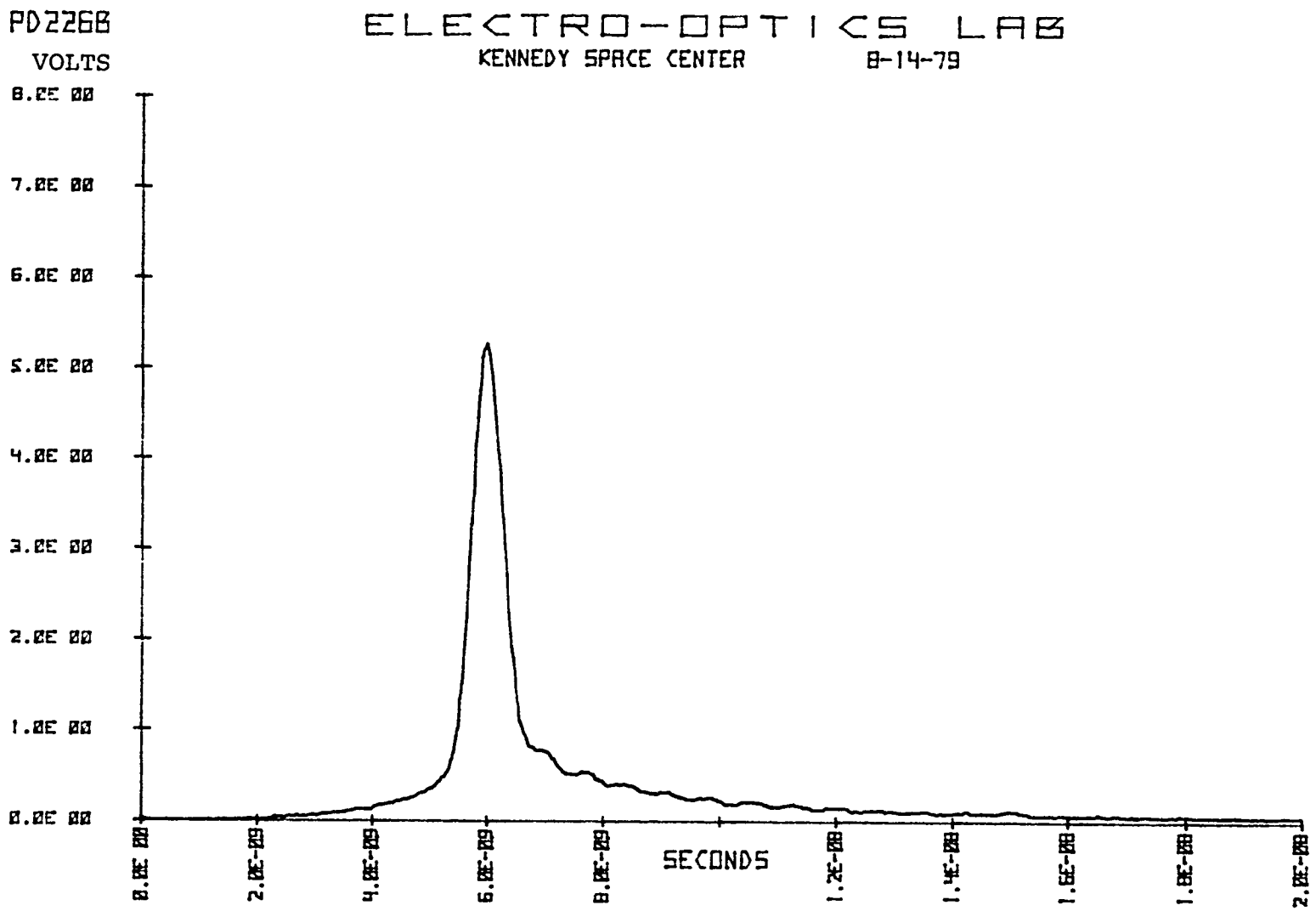

FIGURE D2a: RESPONSE WAVEFORM OF LOOP #1 600 m FIBER.

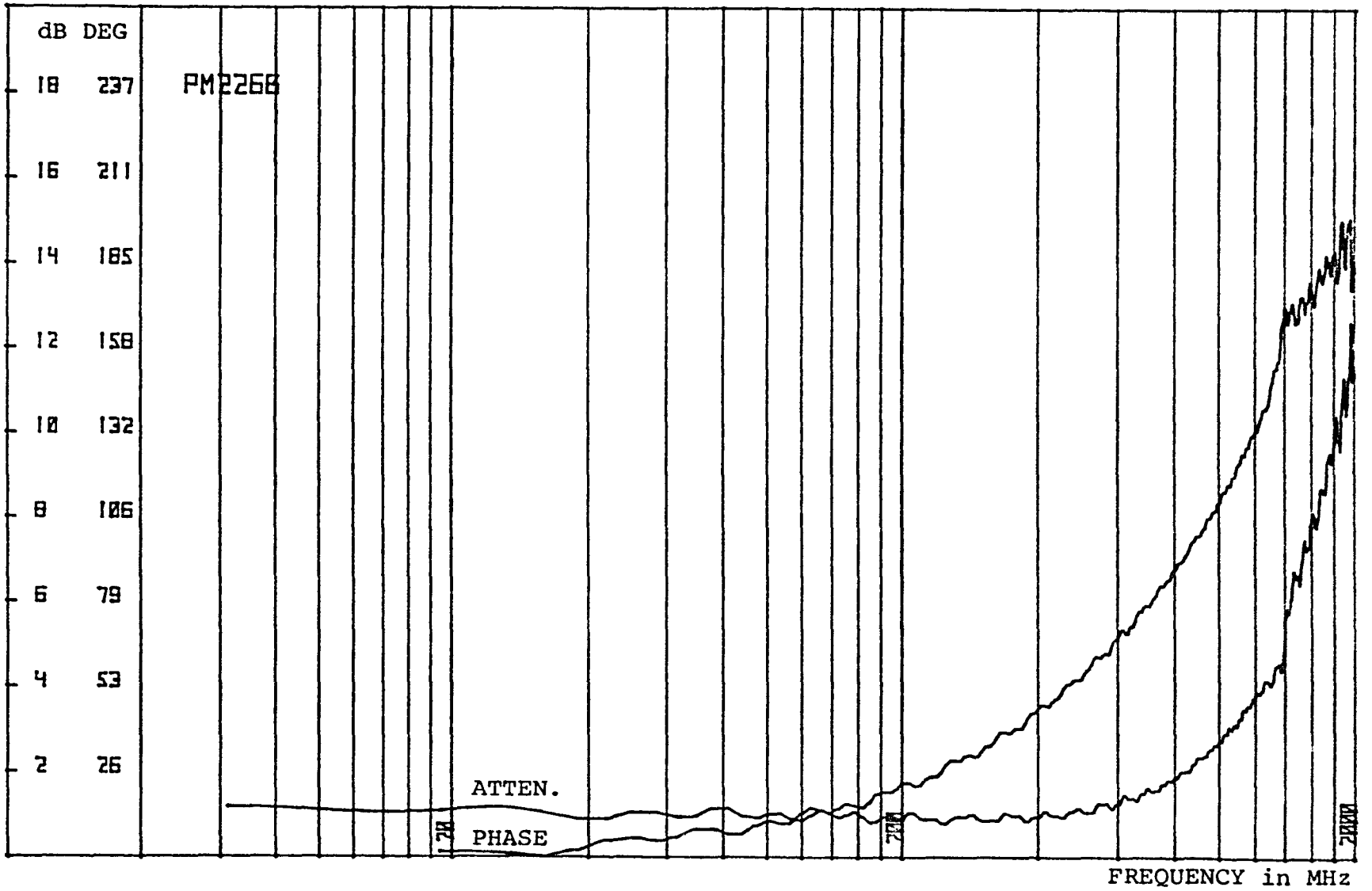

FIGURE D2b: ATTENUATION AND PHASE FUNCTIONS OF LOOP #1 600m FIBER.

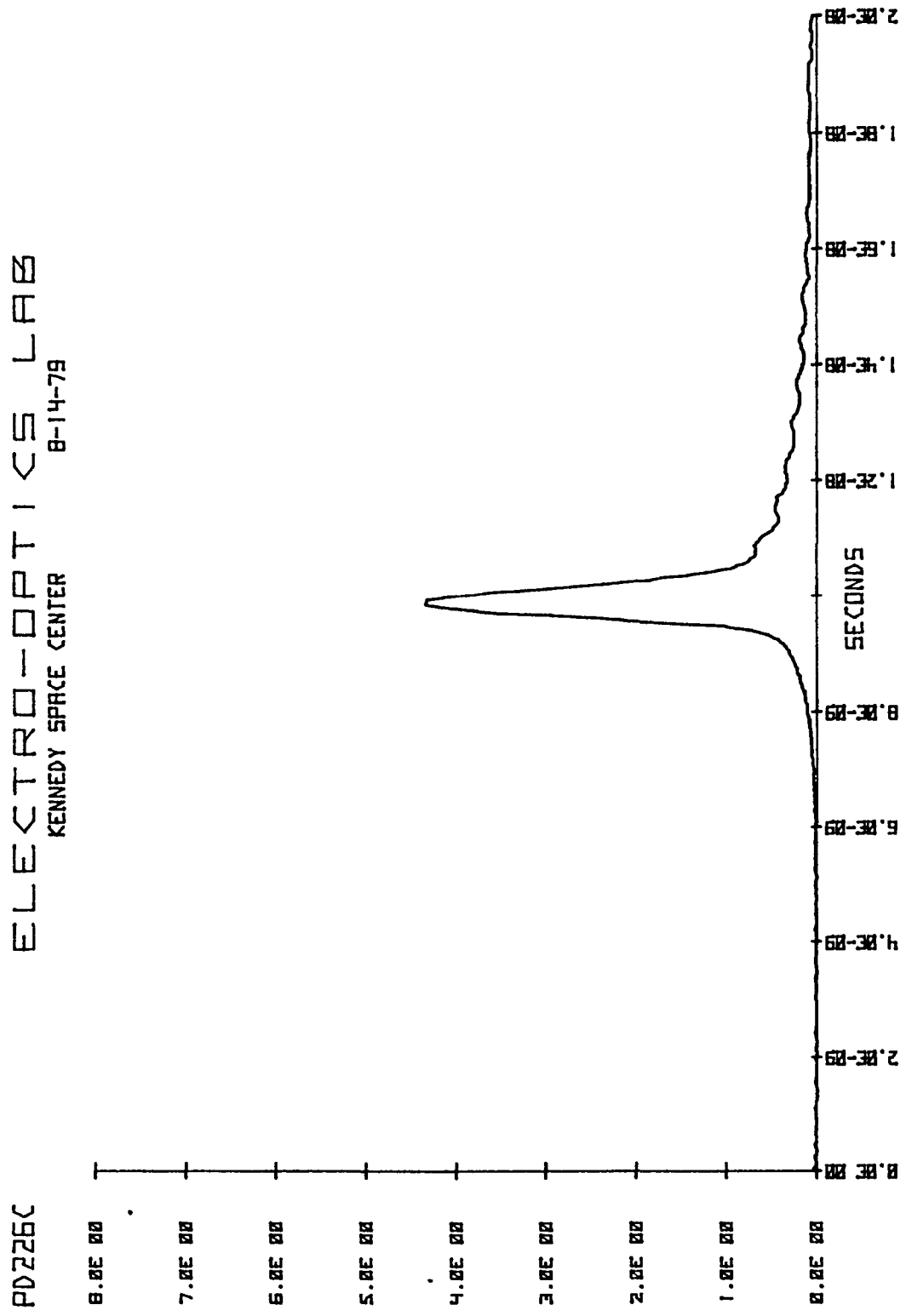

FIGURE D3a: RESPONSE WAVEFORM OF LOOP #2 600m FIBER.

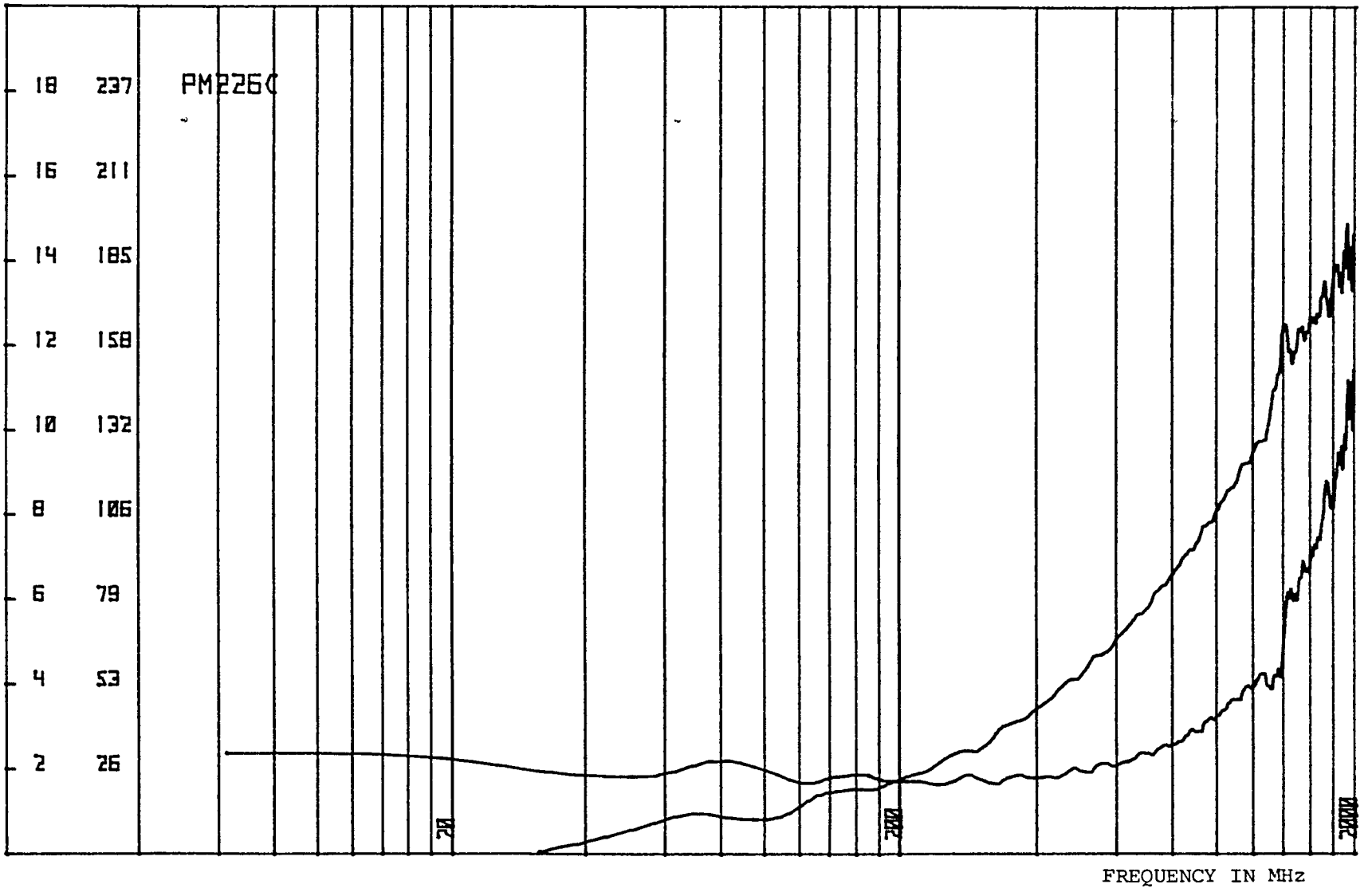

FIGURE D3b: ATTENUATION AND PHASE FUNCTIONS OF LOOP #2 600m FIBER.

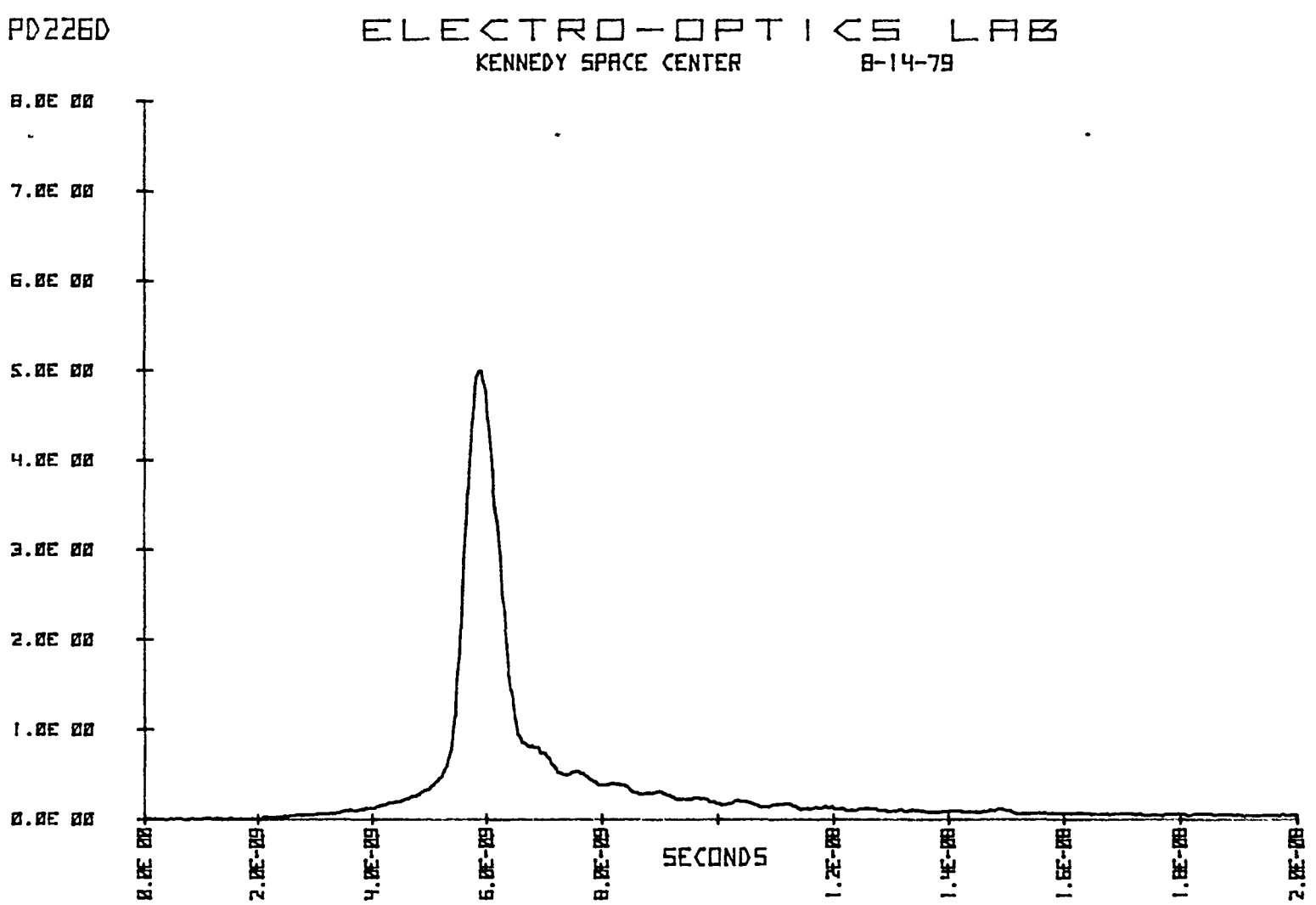

FIGURE D4a: RESPONSE WAVEFORM OF LOOP #3 600m FIBER.

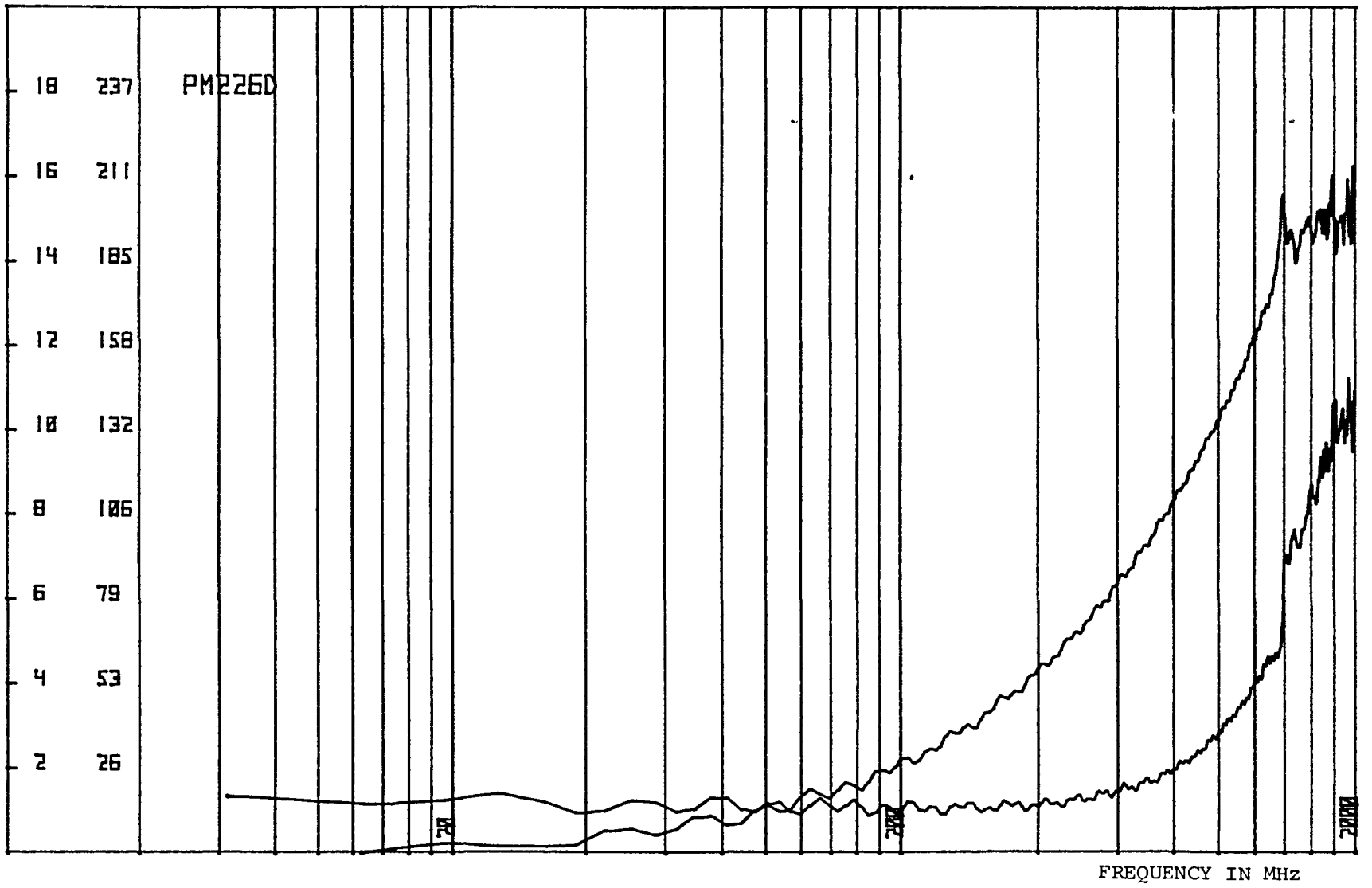

FIGURE D4b: ATTENUATION AND PHASE FUNCTIONS OF LOOP #3 600m FIBER.

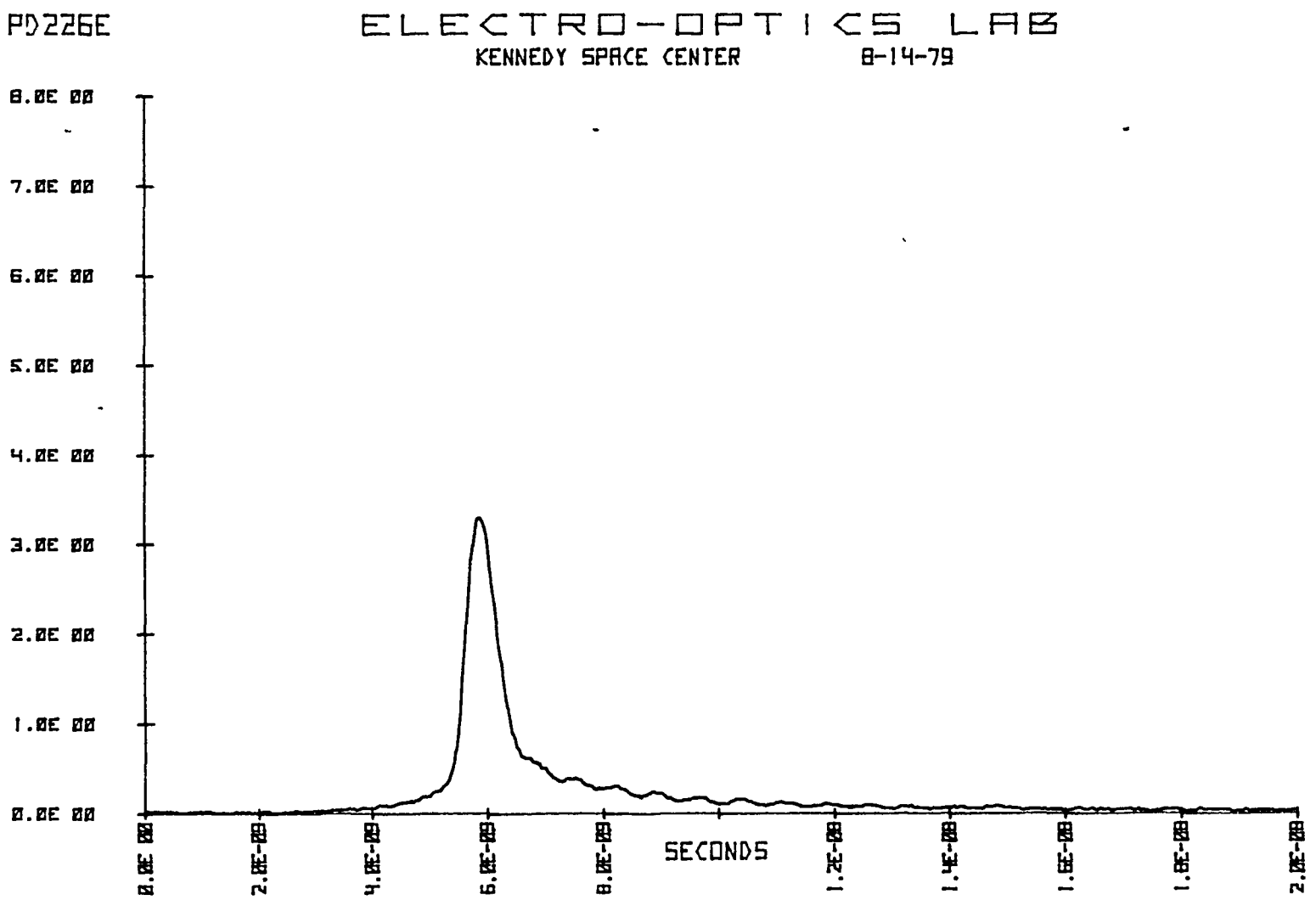

FIGURE D5a: RESPONSE WAVEFORM OF LOOP #4 600m FIBER.

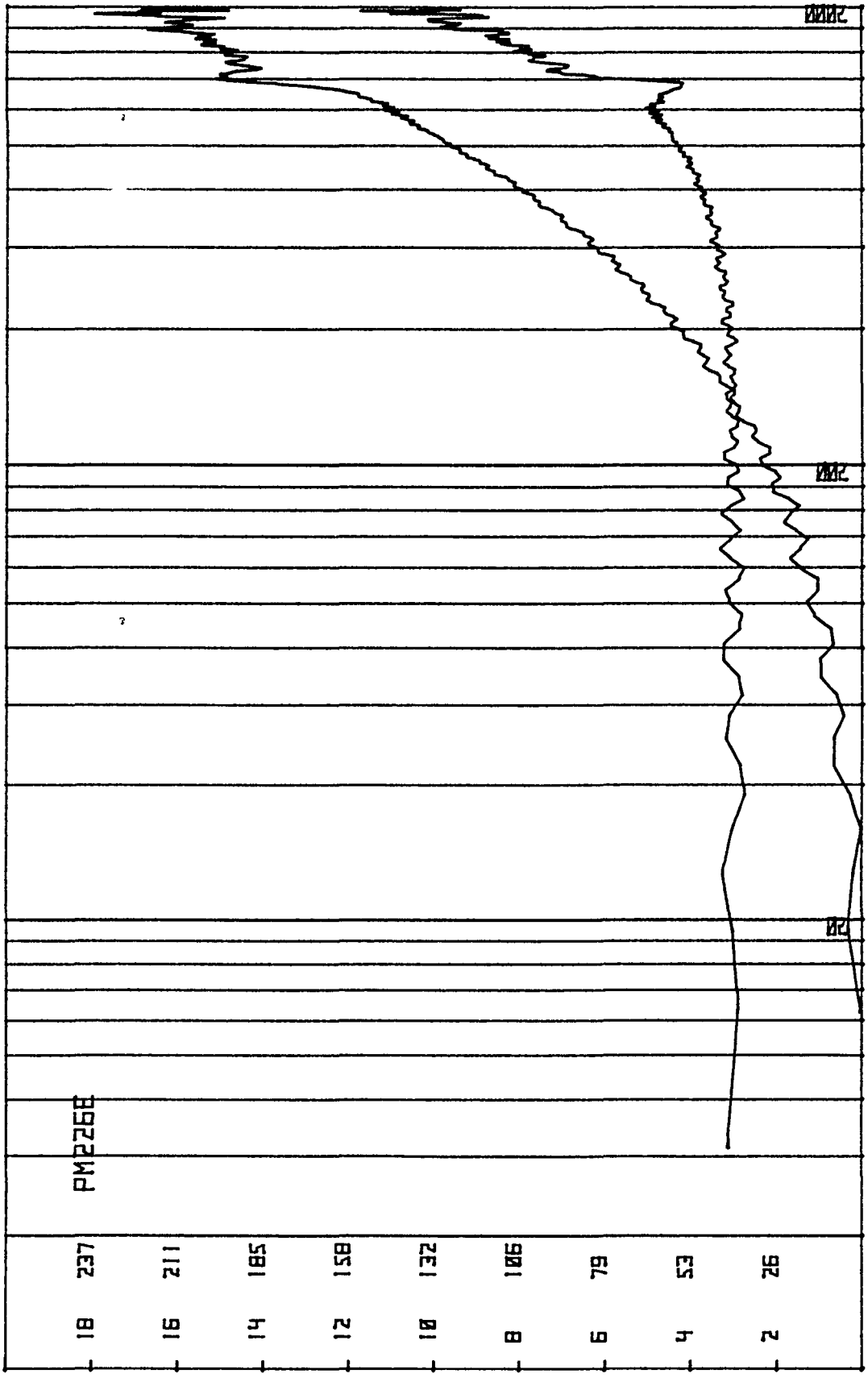

FIGURE D5b: ATTENUATION AND PHASE FUNCTIONS OF LOOP #4 600m FIBER.

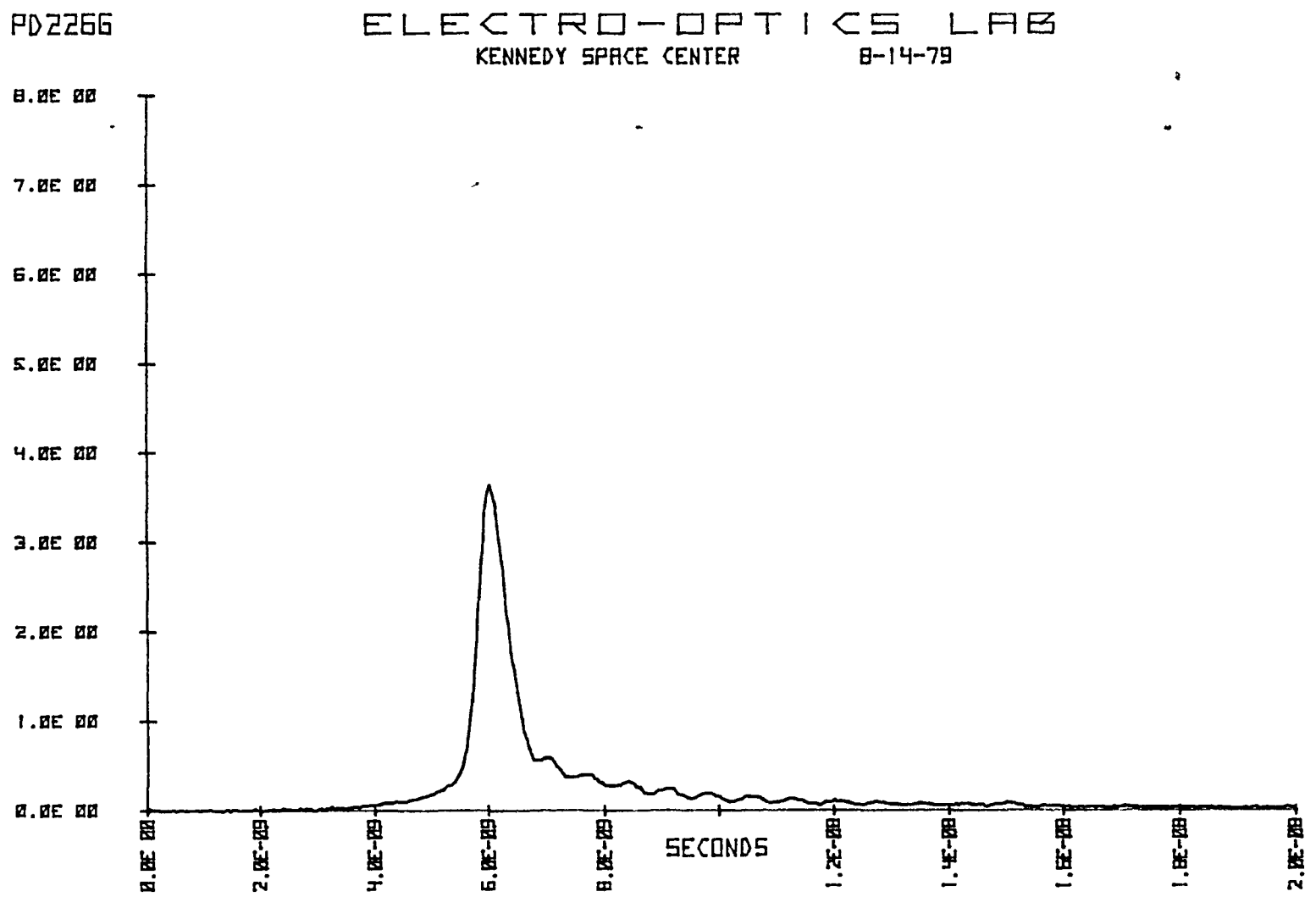

FIGURE D6a: RESPONSE WAVEFORM OF LOOP #5 600m FIBER.

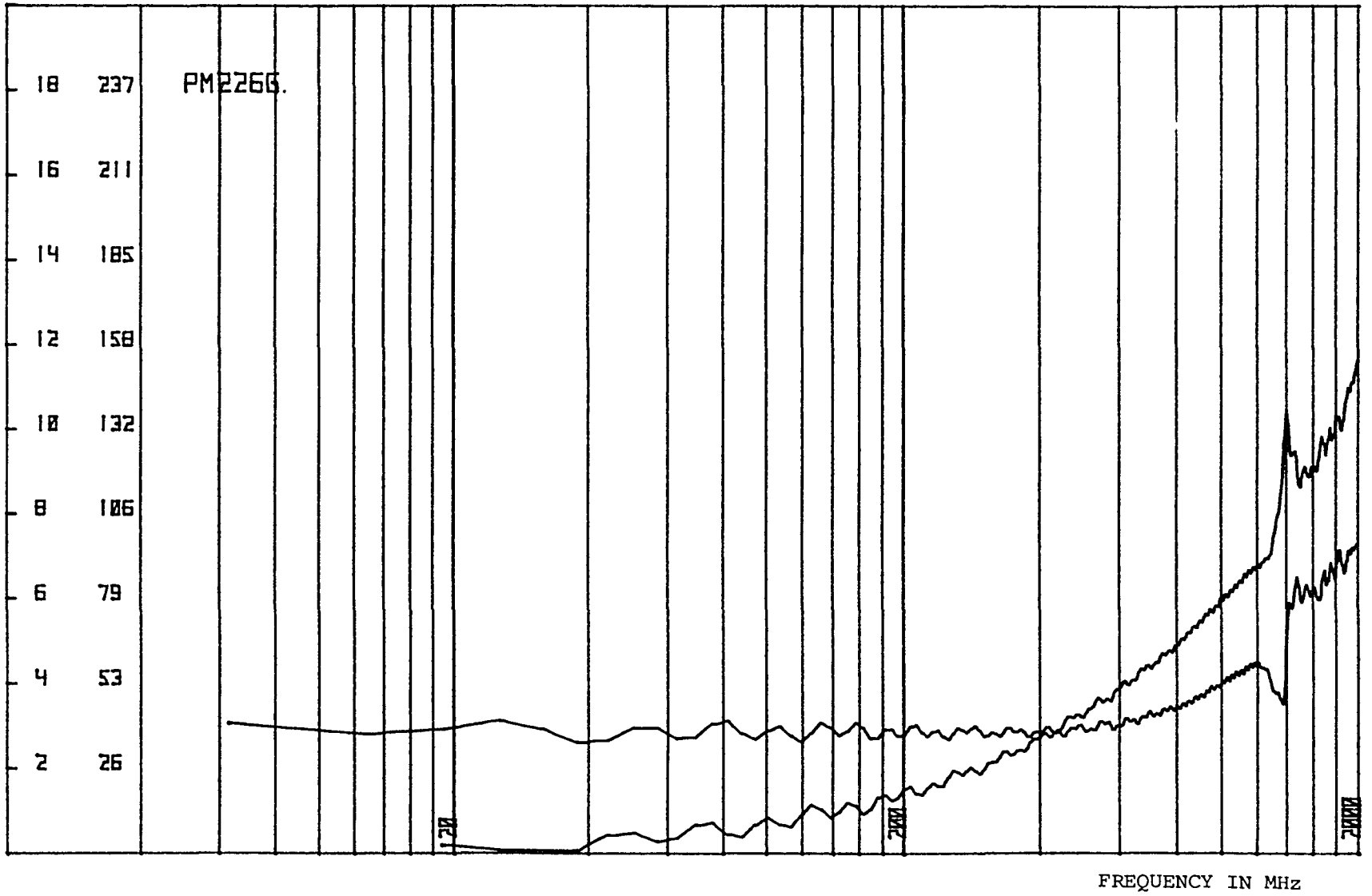

FIGURE D6b: ATTENUATION AND PHASE FUNCTIONS OF LOOP #5 600m FIBER.

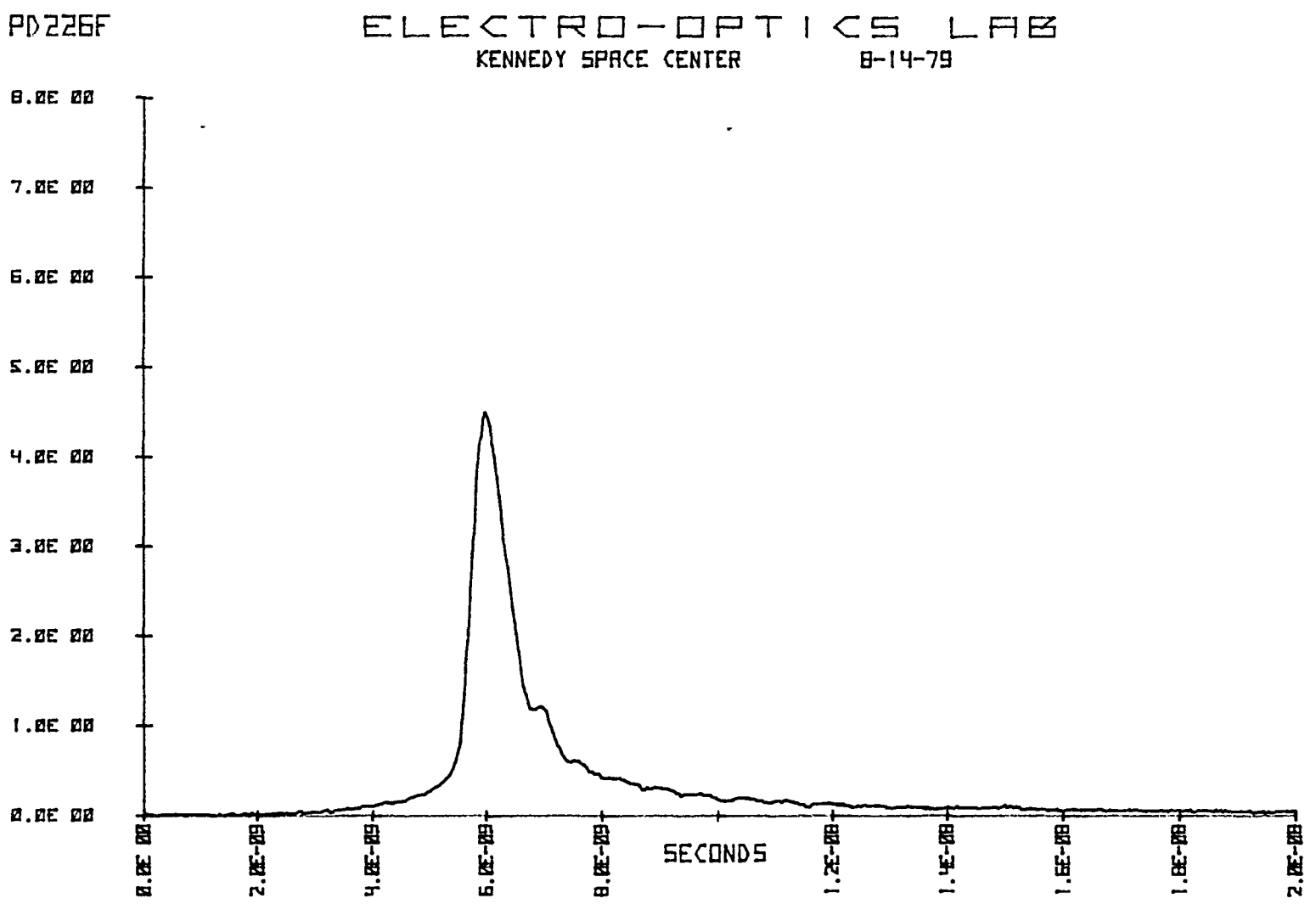

FIGURE D7a: RESPONSE WAVEFORM OF LOOP #6 600m FIBER.

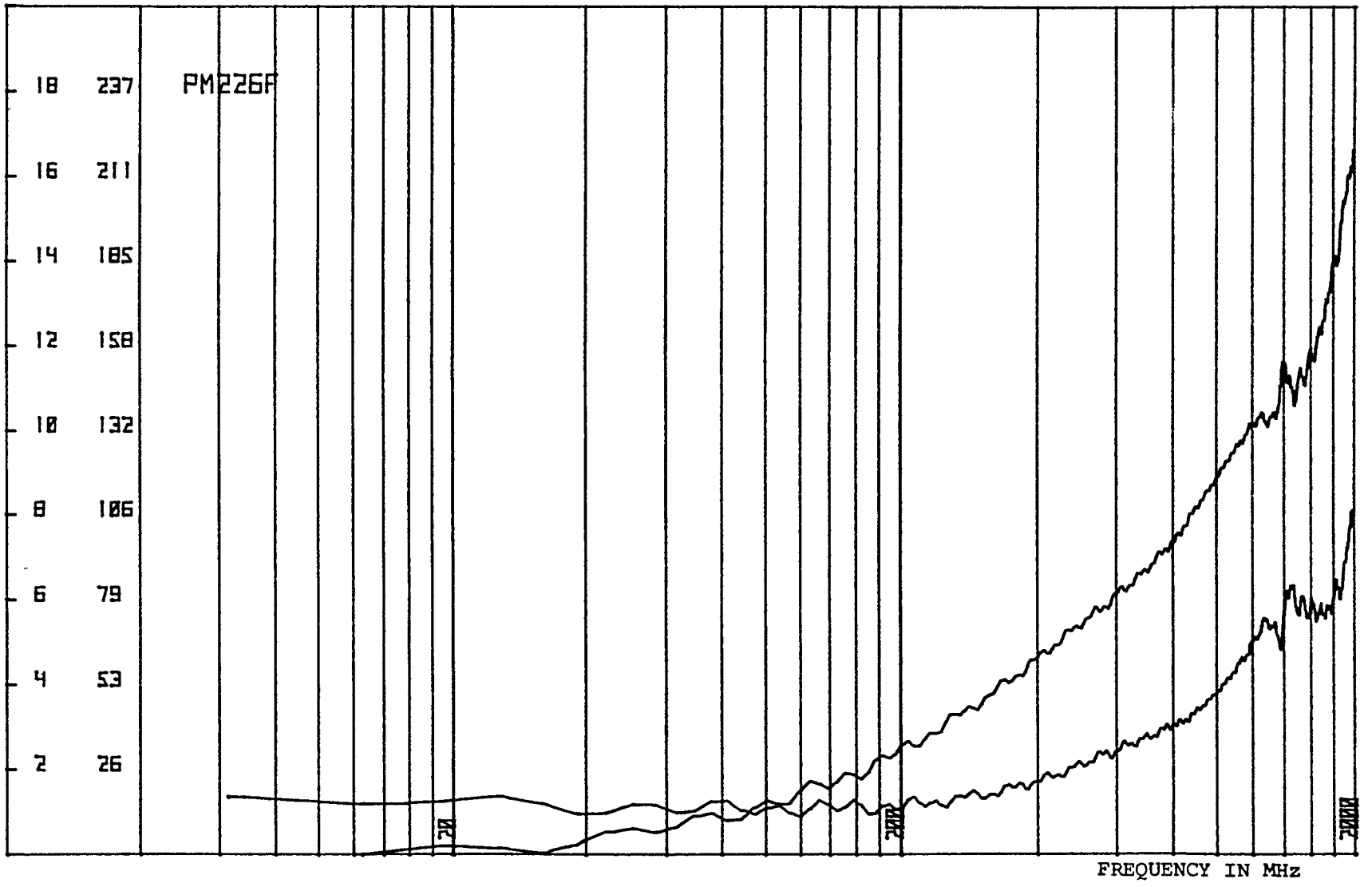

FIGURE D7b: ATTENUATION AND PHASE FUNCTIONS OF LOOP #6 600m FIBER.

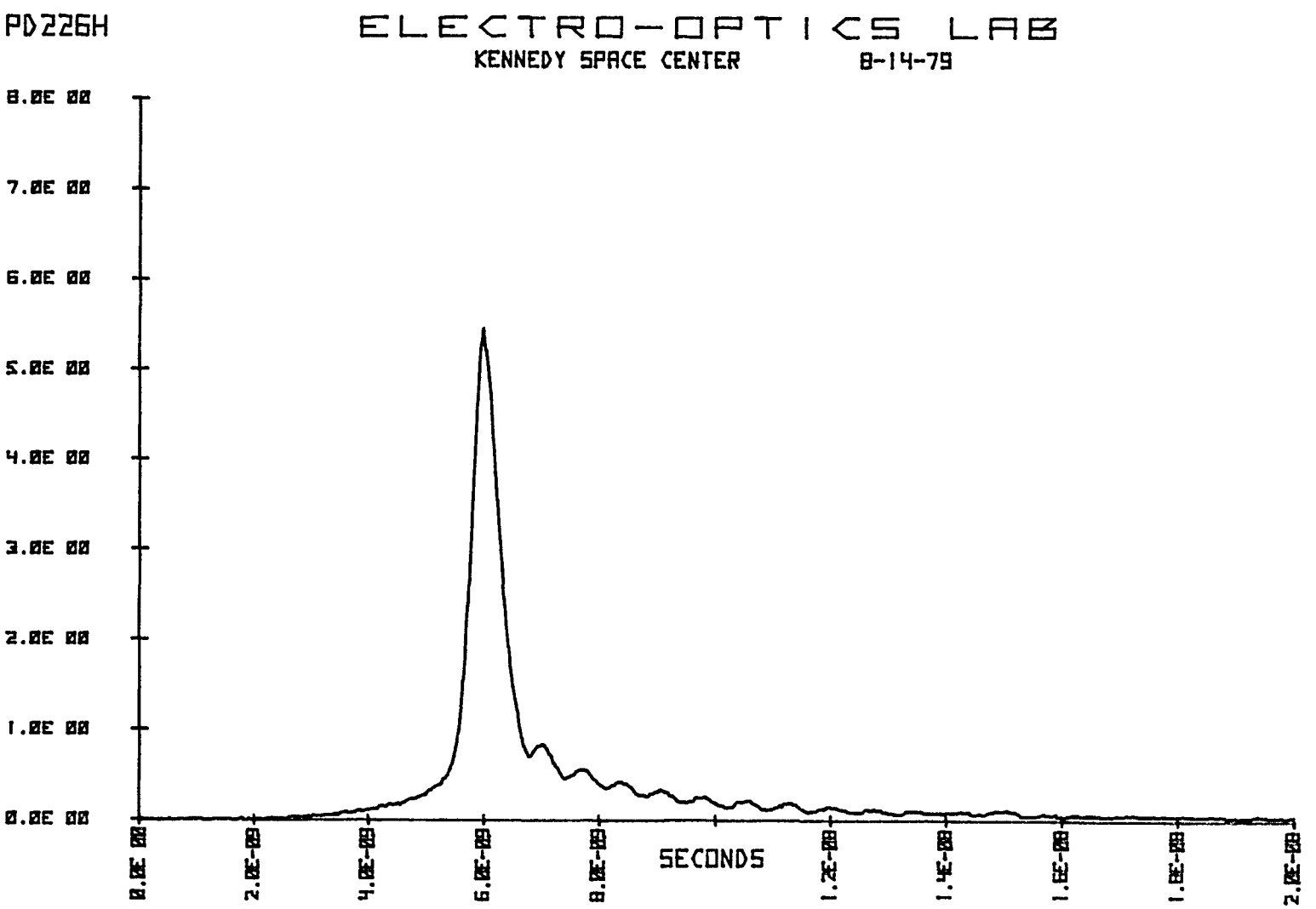

FIGURE D8a: RESPONSE WAVEFORM OF LOOP #7 600m FIBER.

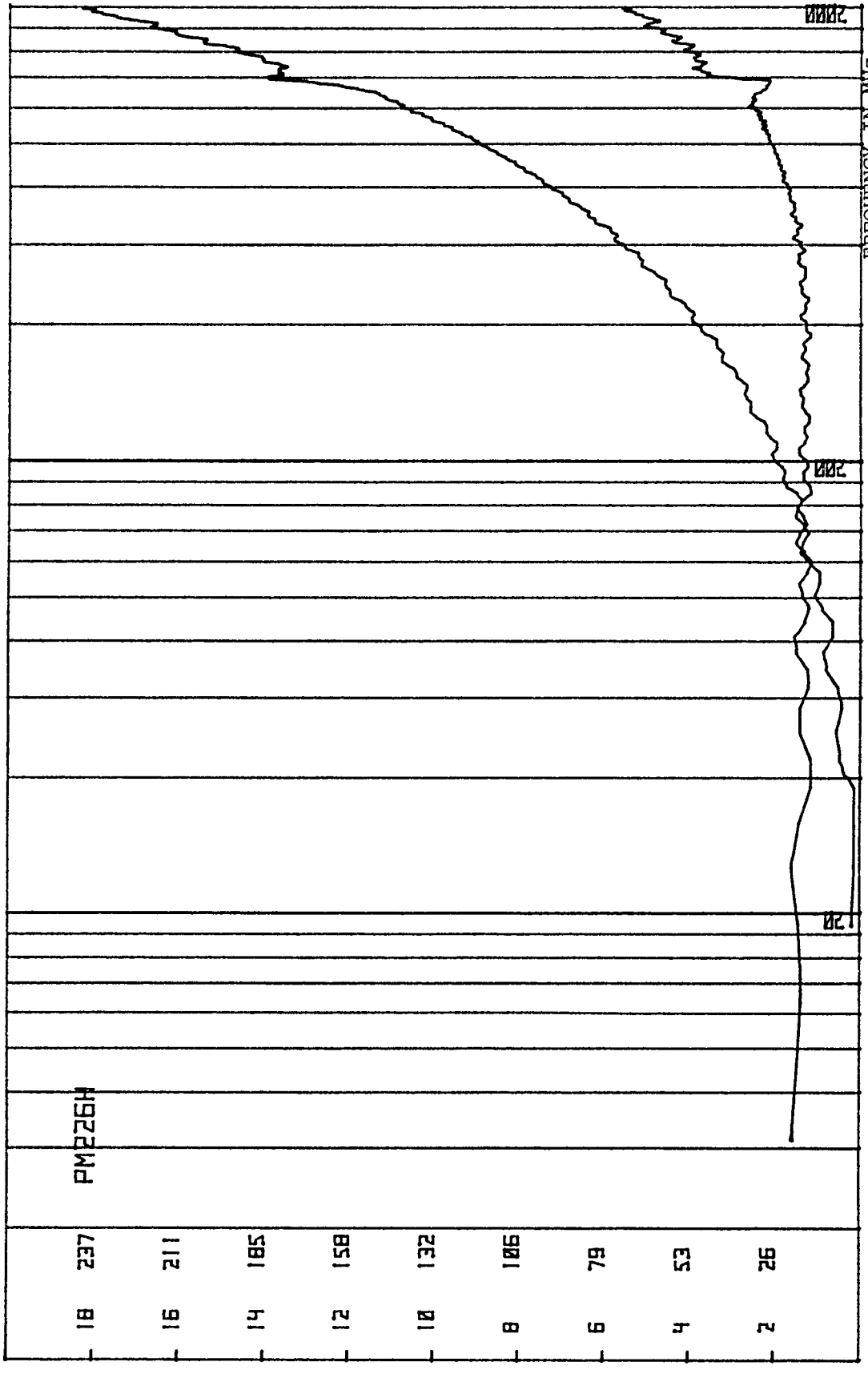

FIGURE D8b: ATTENUATION AND PHASE FUNCTIONS OF LOOP #7 600m FIBER.

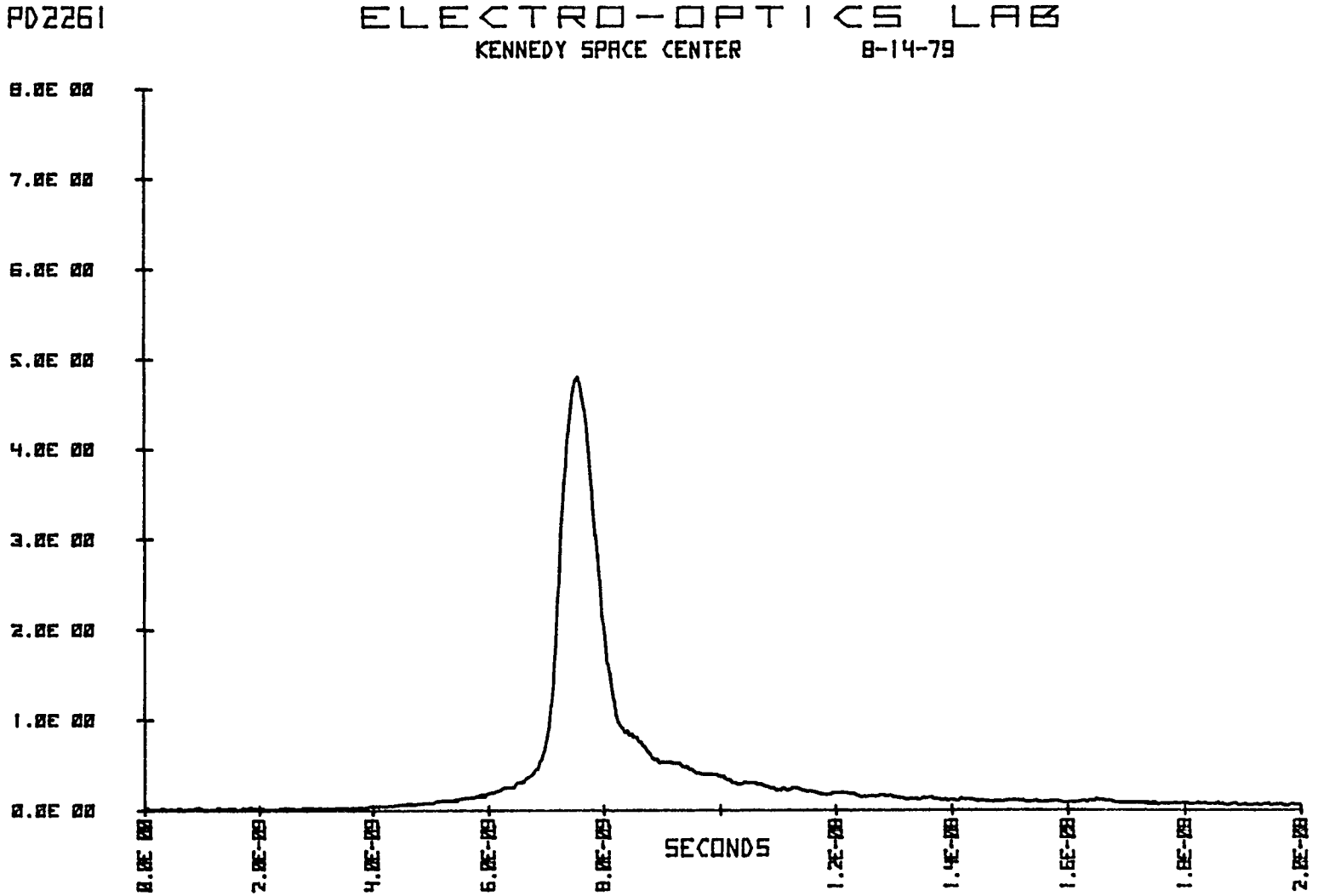

FIGURE D9a: RESPONSE WAVEFORM OF LOOP #8 600m FIBER.

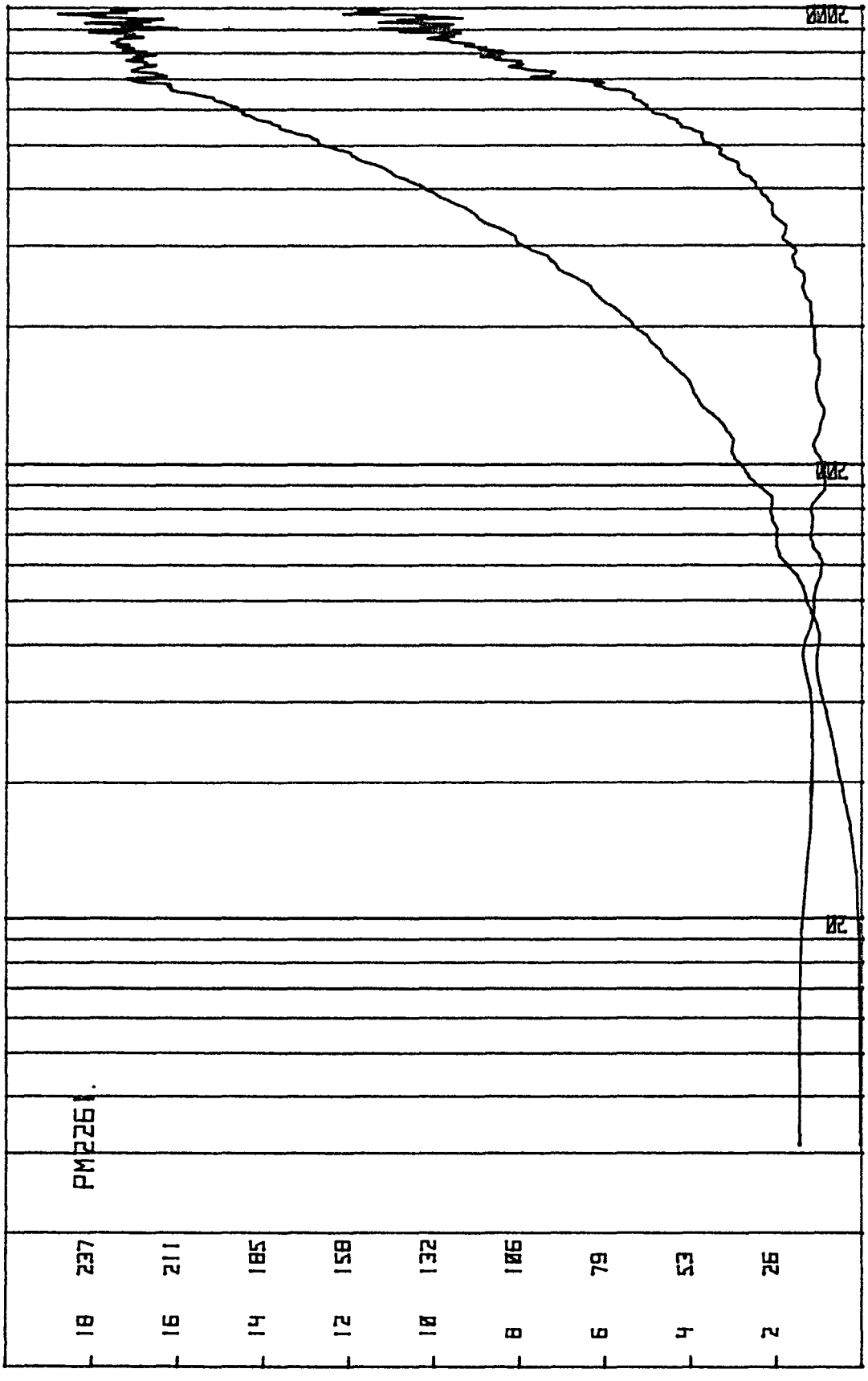

FIGURE D9b: ATTENUATION AND PHASE FUNCTIONS OF LOOP #8 600m FIBER.

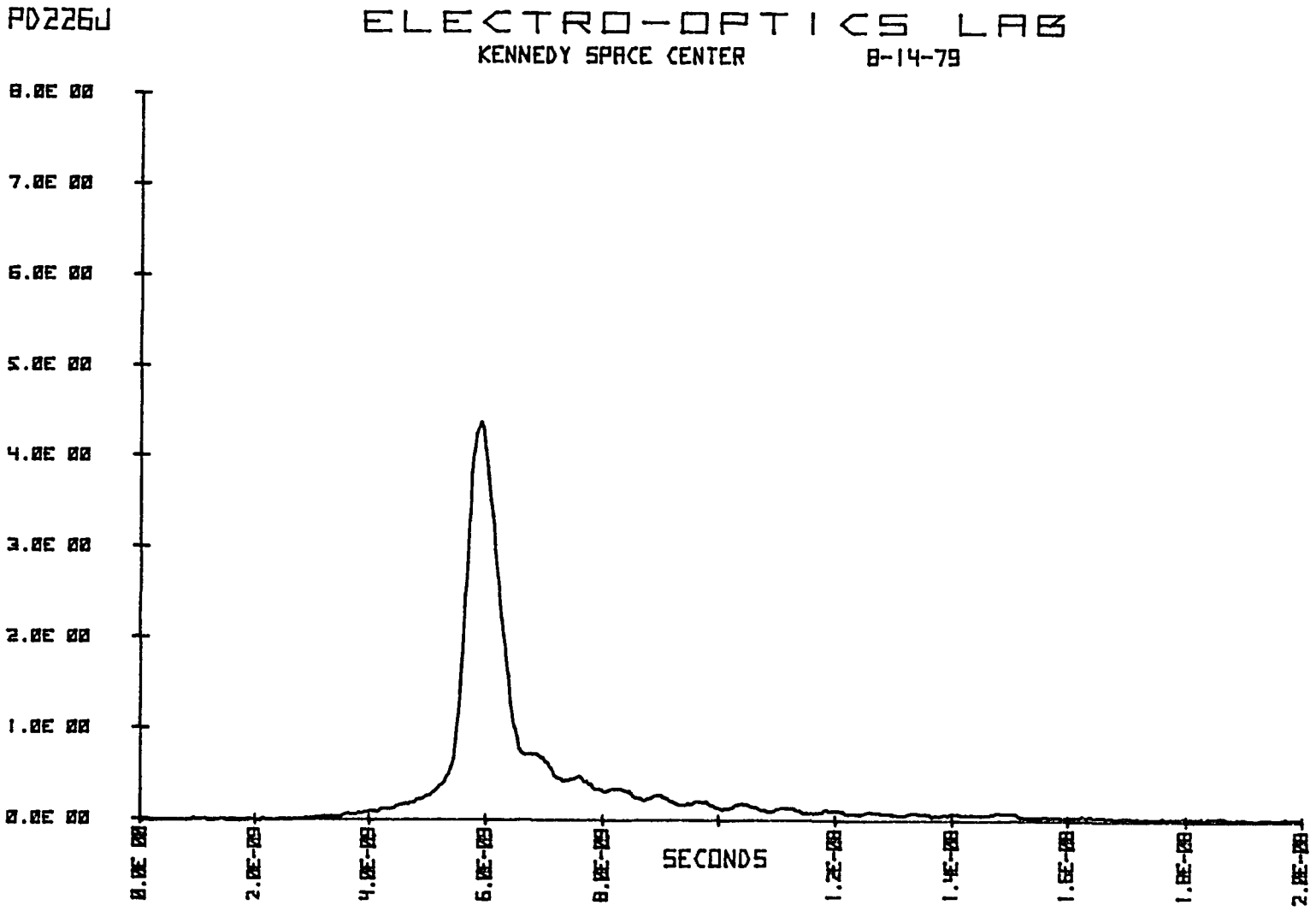

FIGURE D10a: RESPONSE WAVEFORM OF LOOP #9 600m FIBER.

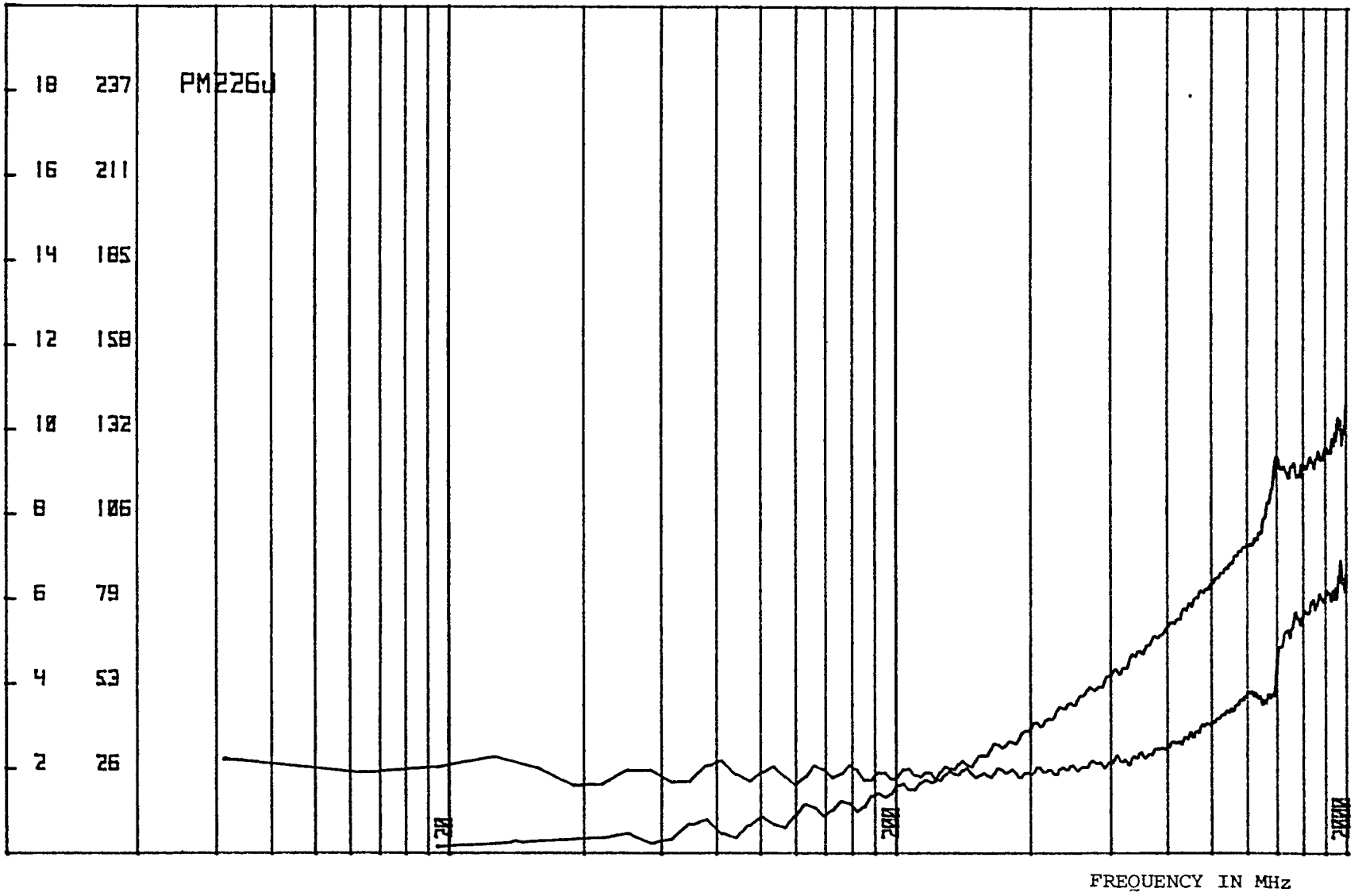

FIGURE D10b: ATTENUATION AND PHASE FUNCTIONS OF LOOP #9 600m FIBER.

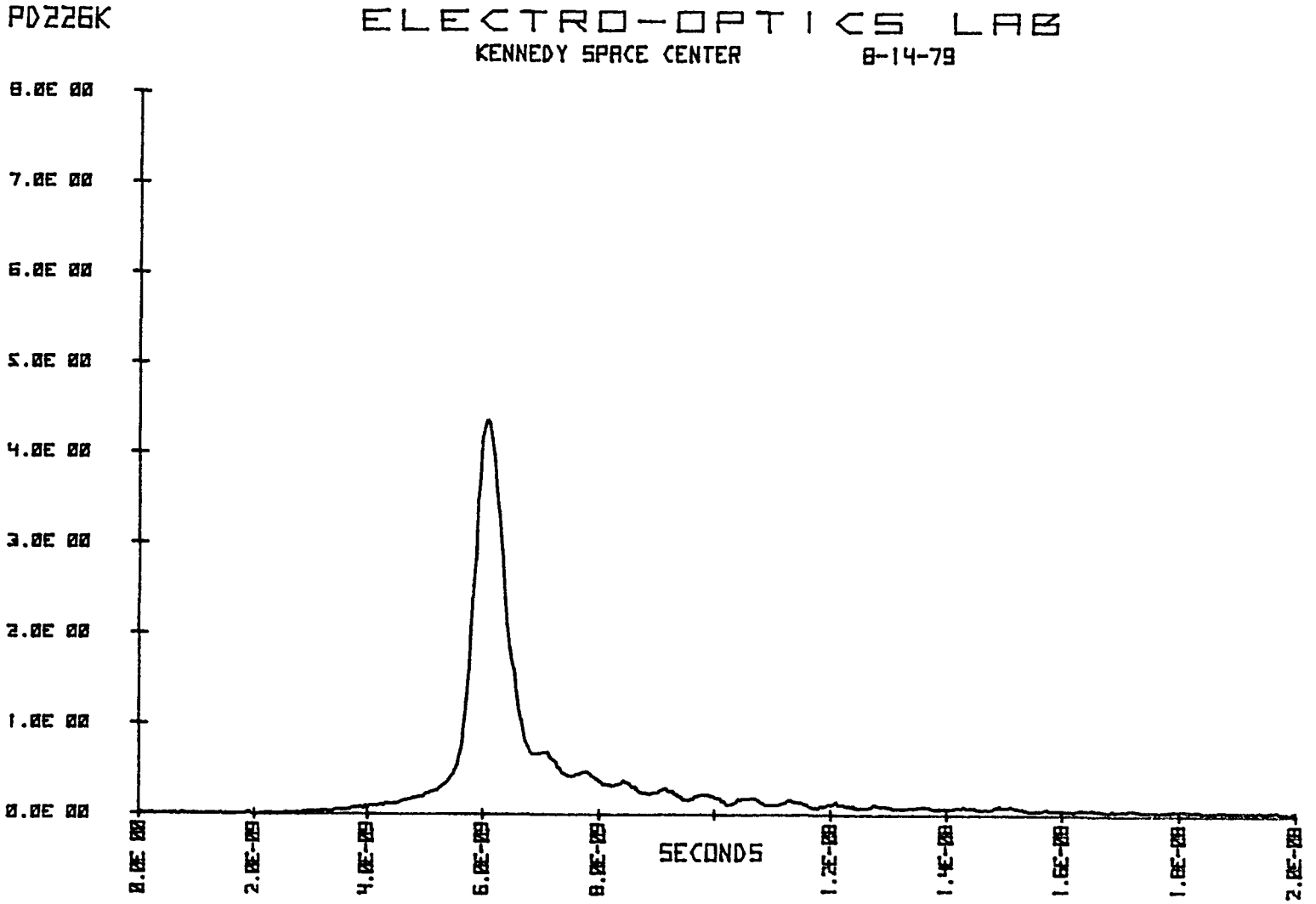

FIGURE D11a: RESPONSE WAVEFORM OF LOOP #10 600m FIBER.

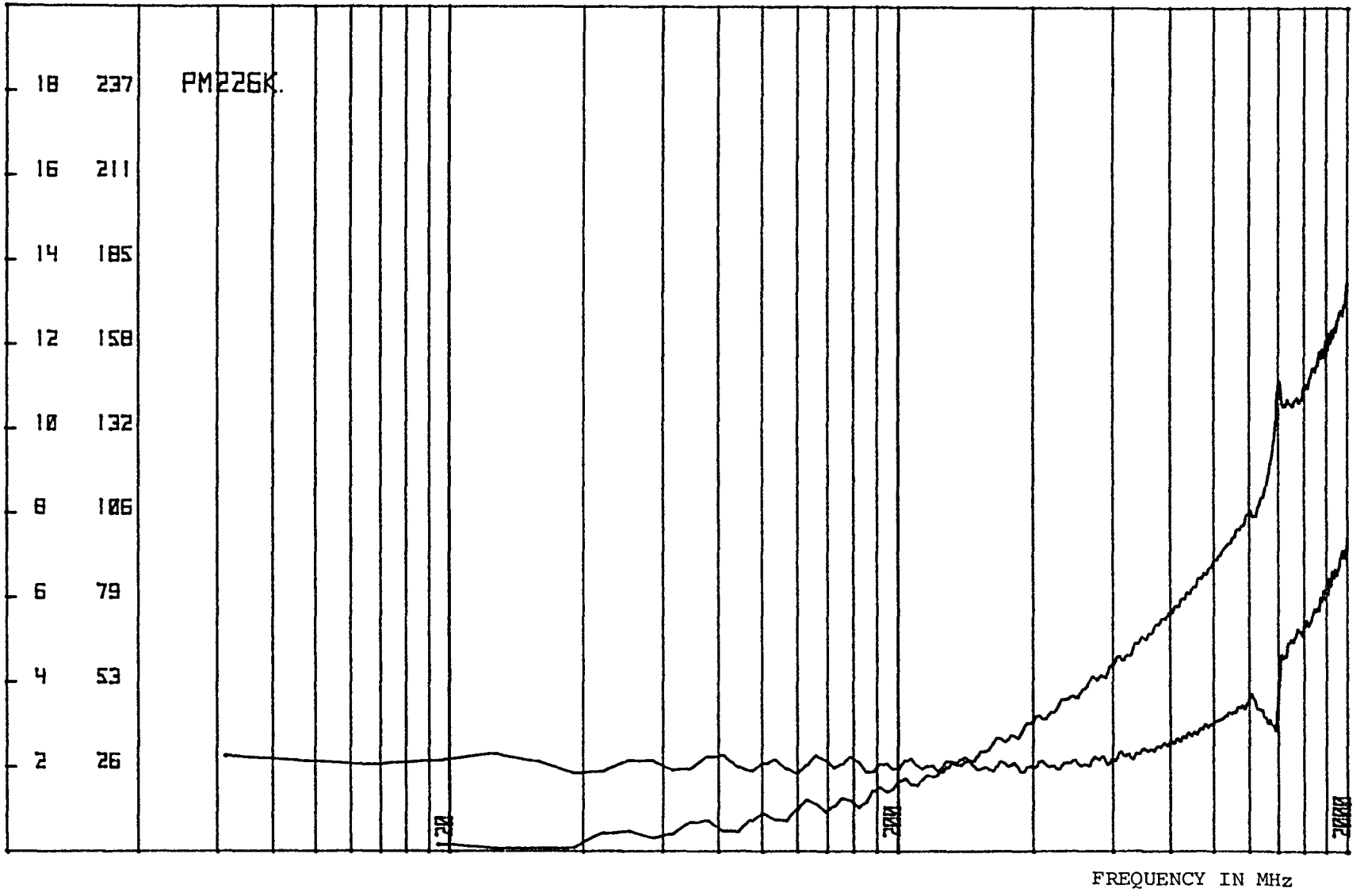

FIGURE D11b: ATTENUATION AND PHASE FUNCTIONS OF LOOP #10 600m FIBER.

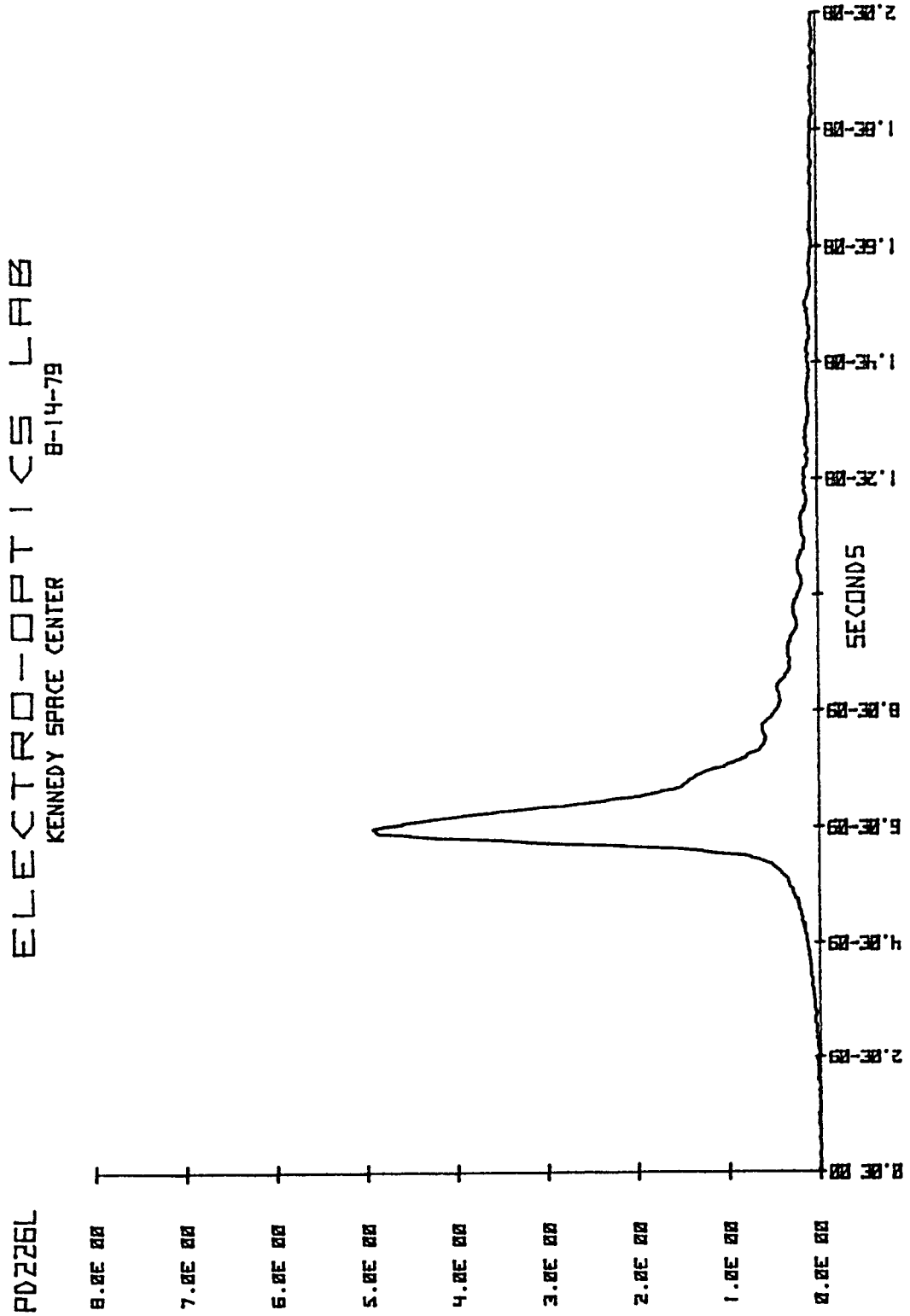

FIGURE D12a: RESPONSE WAVEFORM OF LOOP #11 600m FIBER.

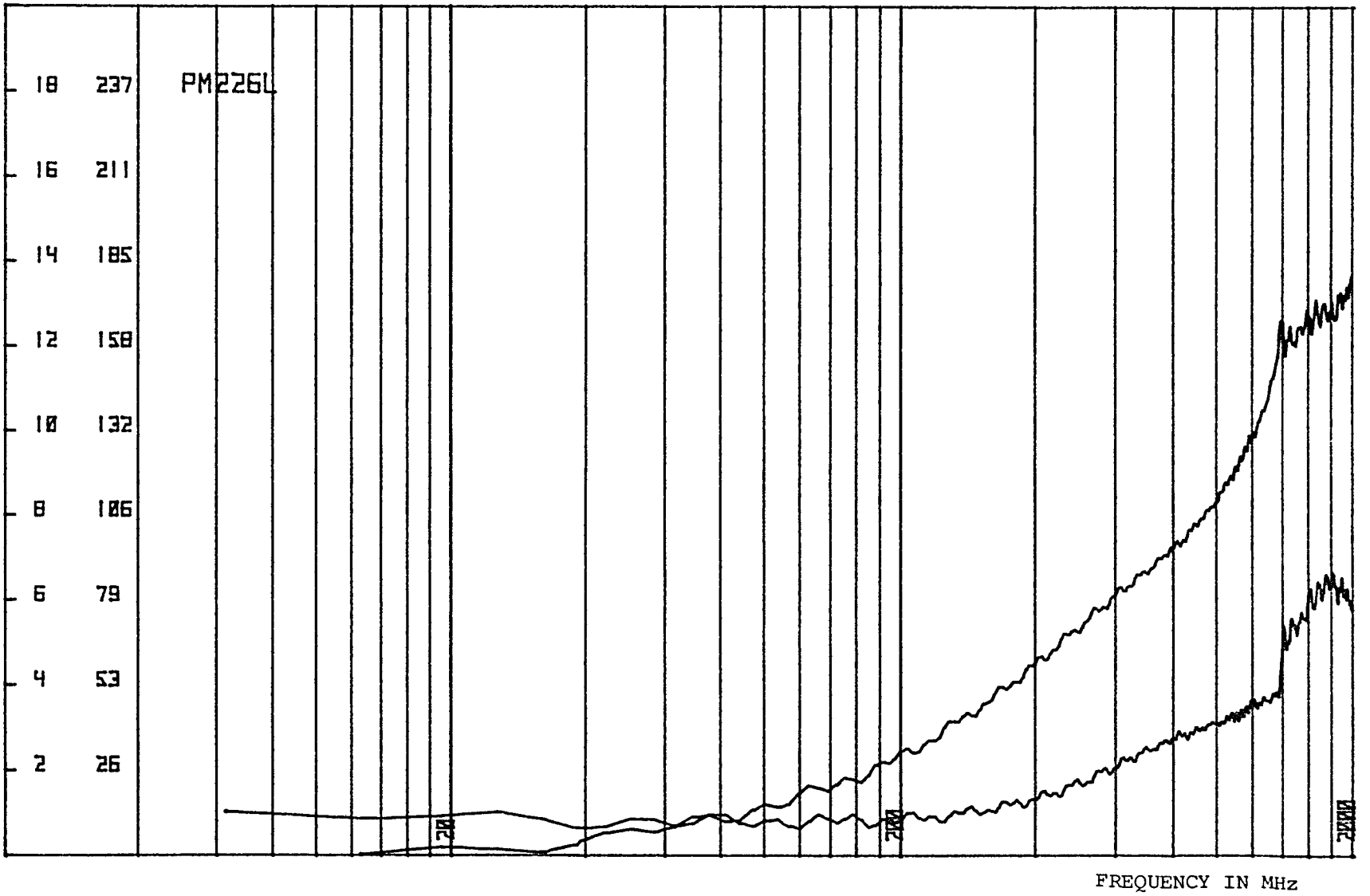

FIGURE D12b: ATTENUATION AND PHASE FUNCTIONS OF LOOP #11 600m FIBER.

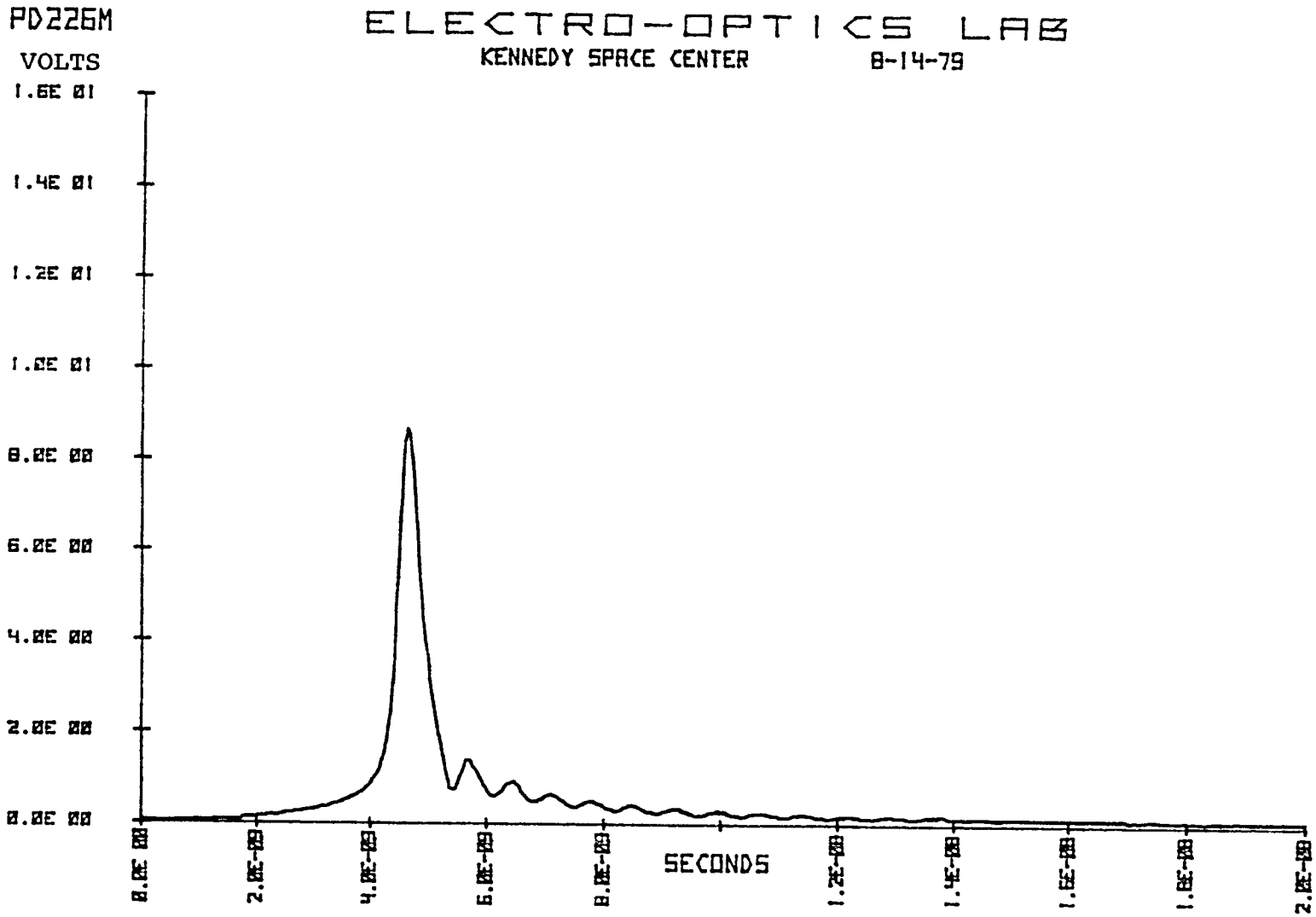

FIGURE D13: REFERENCE WAVEFORM FOR TESTING 1.2 km and 2.4 km LENGTHS.

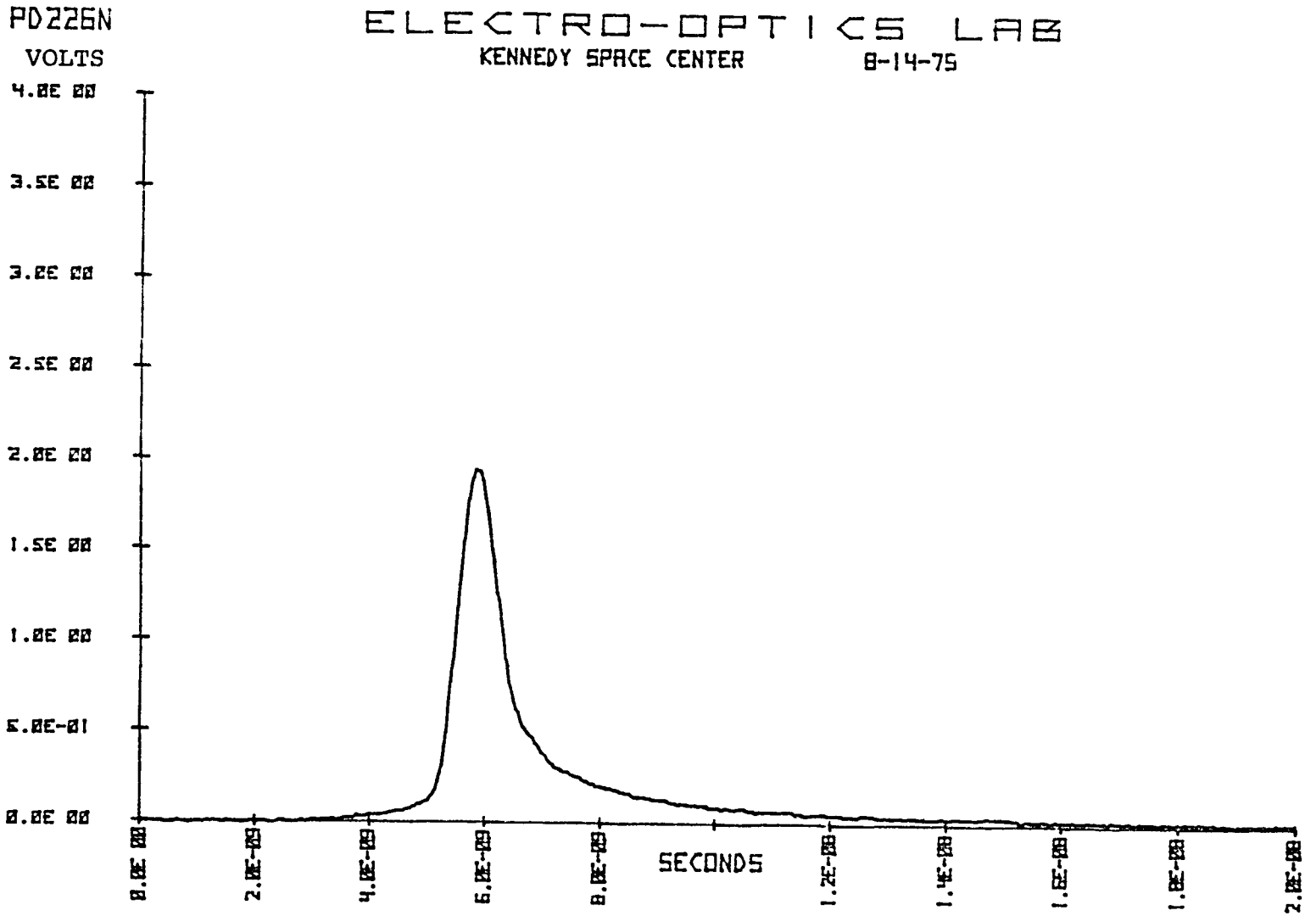

FIGURE D14a: RESPONSE WAVEFORM OF 1.2 km FIBER (LOOPS 2 & 3).

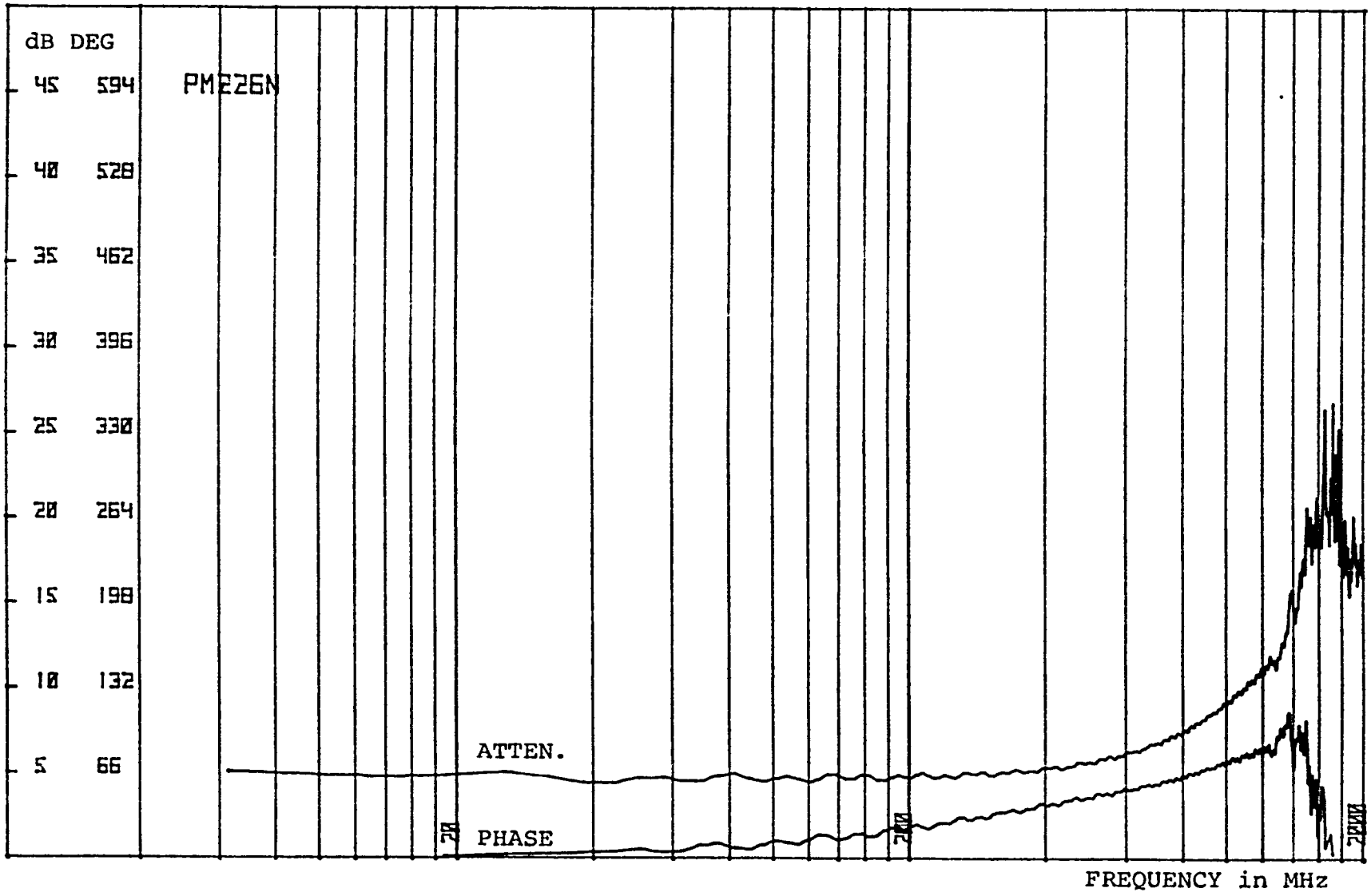

FIGURE D14b: ATTENUATION AND PHASE FUNCTIONS OF 1.2 km FIBER (LOOPS 2 & 3).

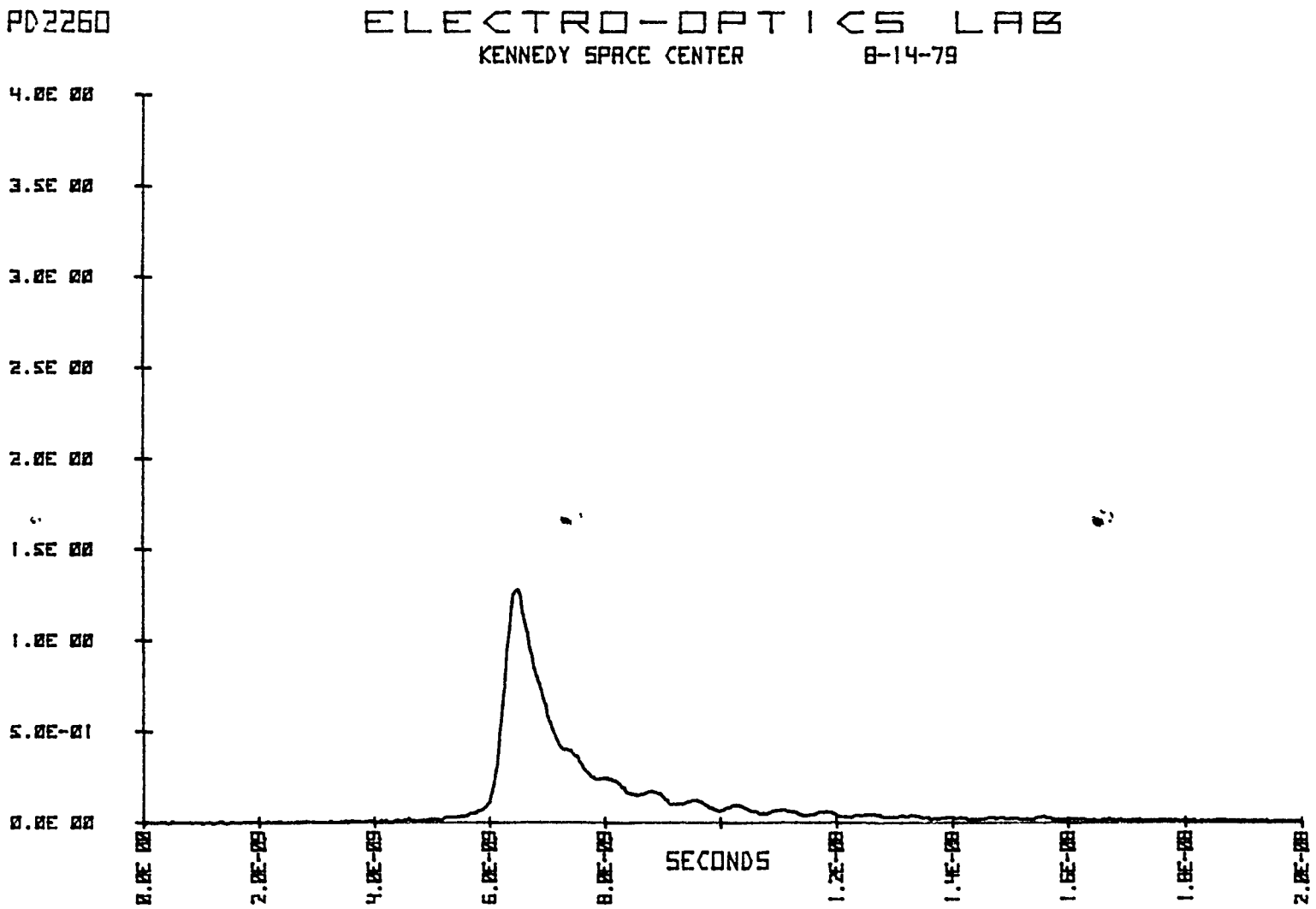

FIGURE D15a: RESPONSE WAVEFORM OF 1.2 km FIBER (LOOPS 4 & 5).

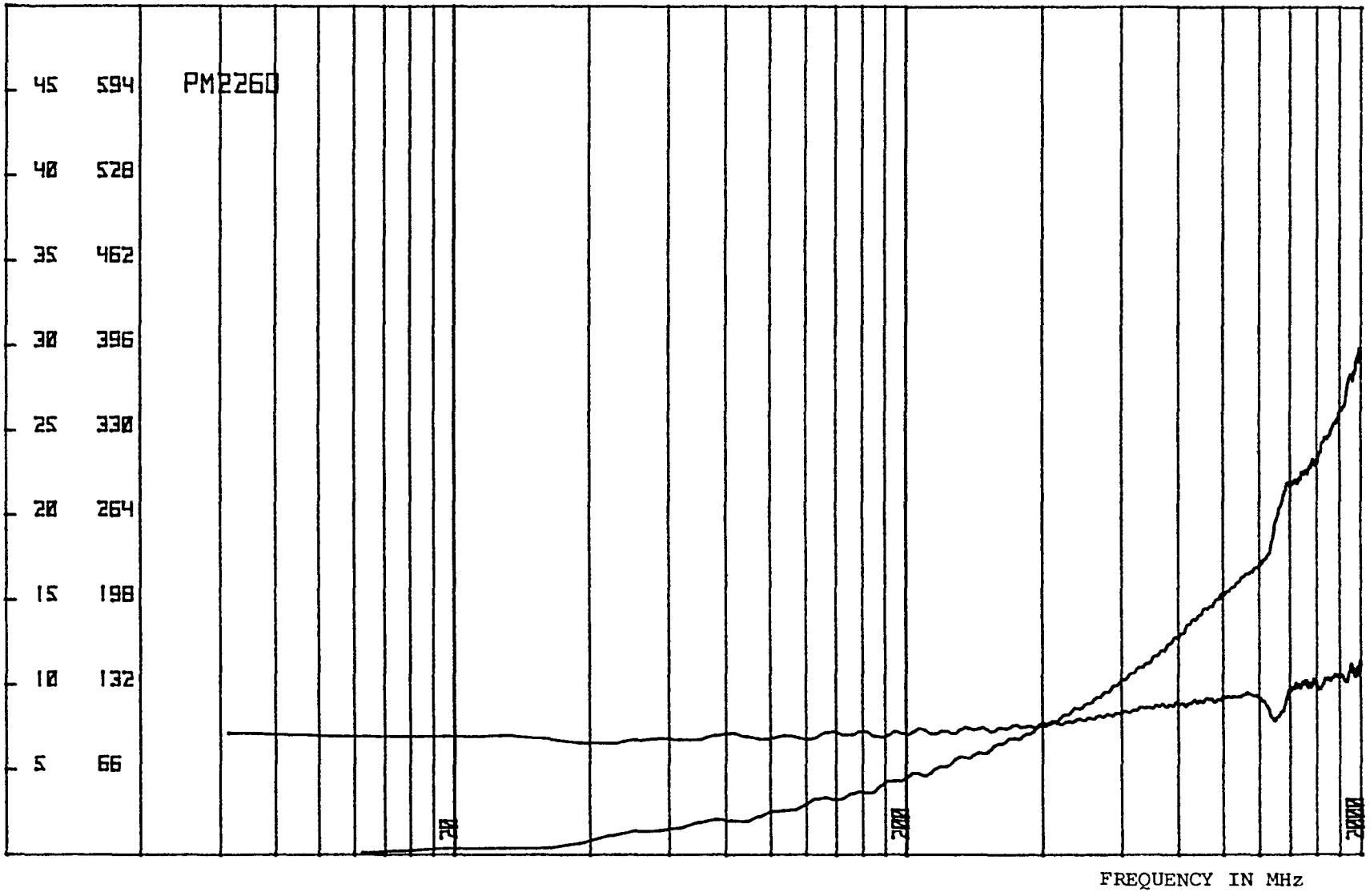

FIGURE D15b: ATTENUATION AND PHASE FUNCTIONS OF 1.2 km FIBER (LOOPS 4 & 5).

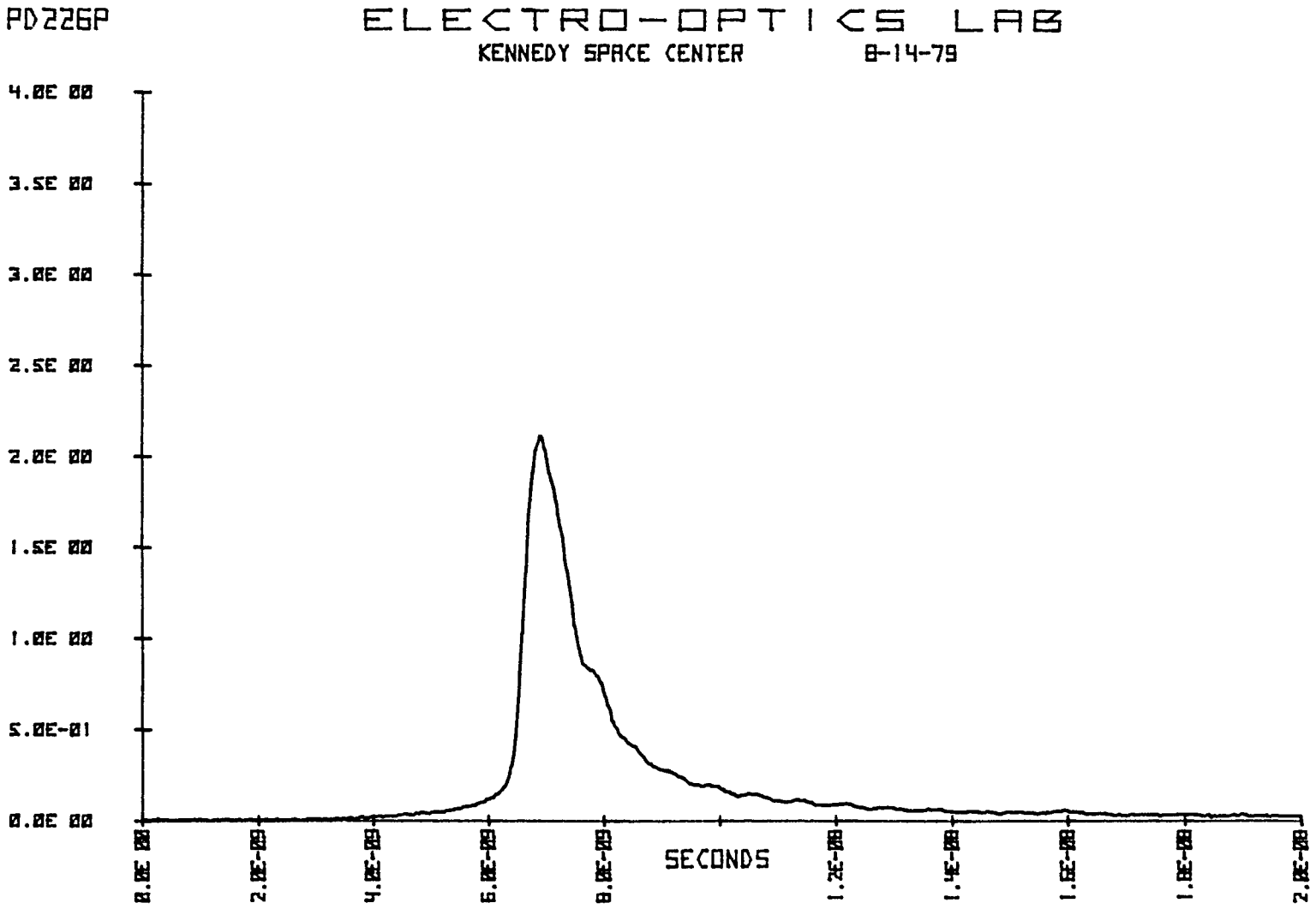

FIGURE D16a: RESPONSE WAVEFORM OF 1.2 km FIBER (LOOPS 6 & 7).

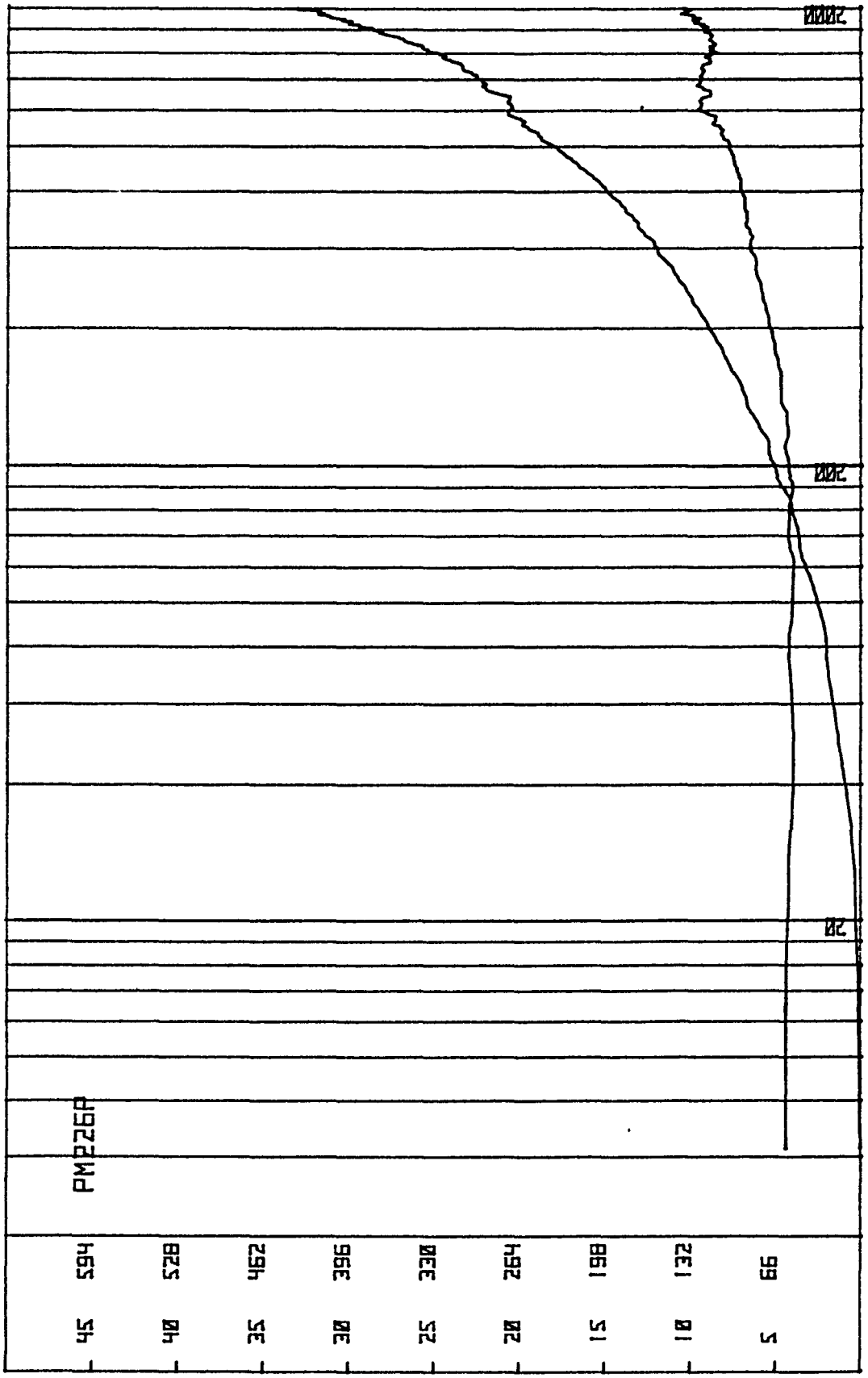

FIGURE D16b: ATTENUATION AND PHASE FUNCTIONS OF 1.2 km FIBER (LOOPS 6 & 7).

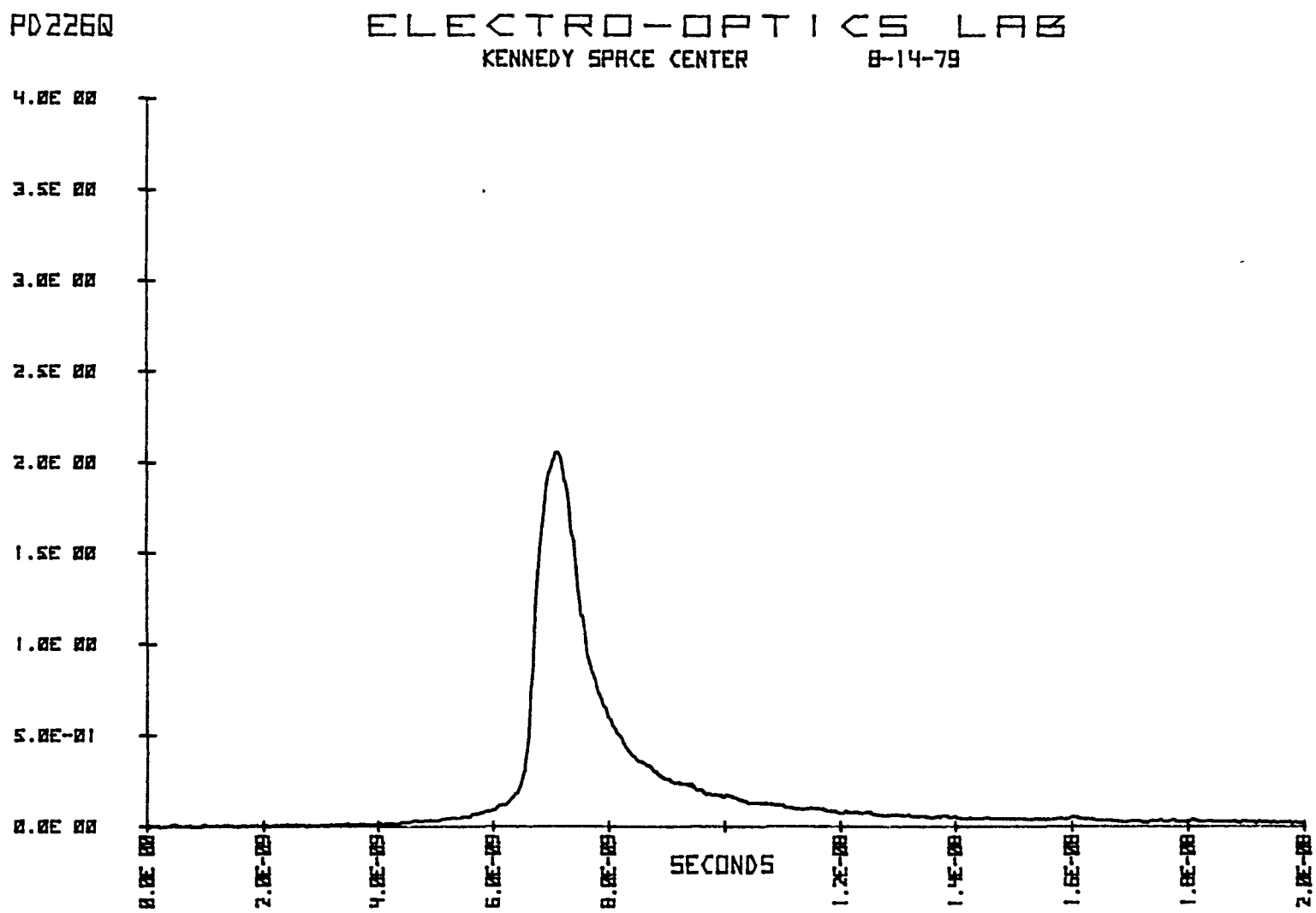

FIGURE D17a: RESPONSE WAVEFORM OF 1.2 km FIBER (LOOPS 8 & 9).

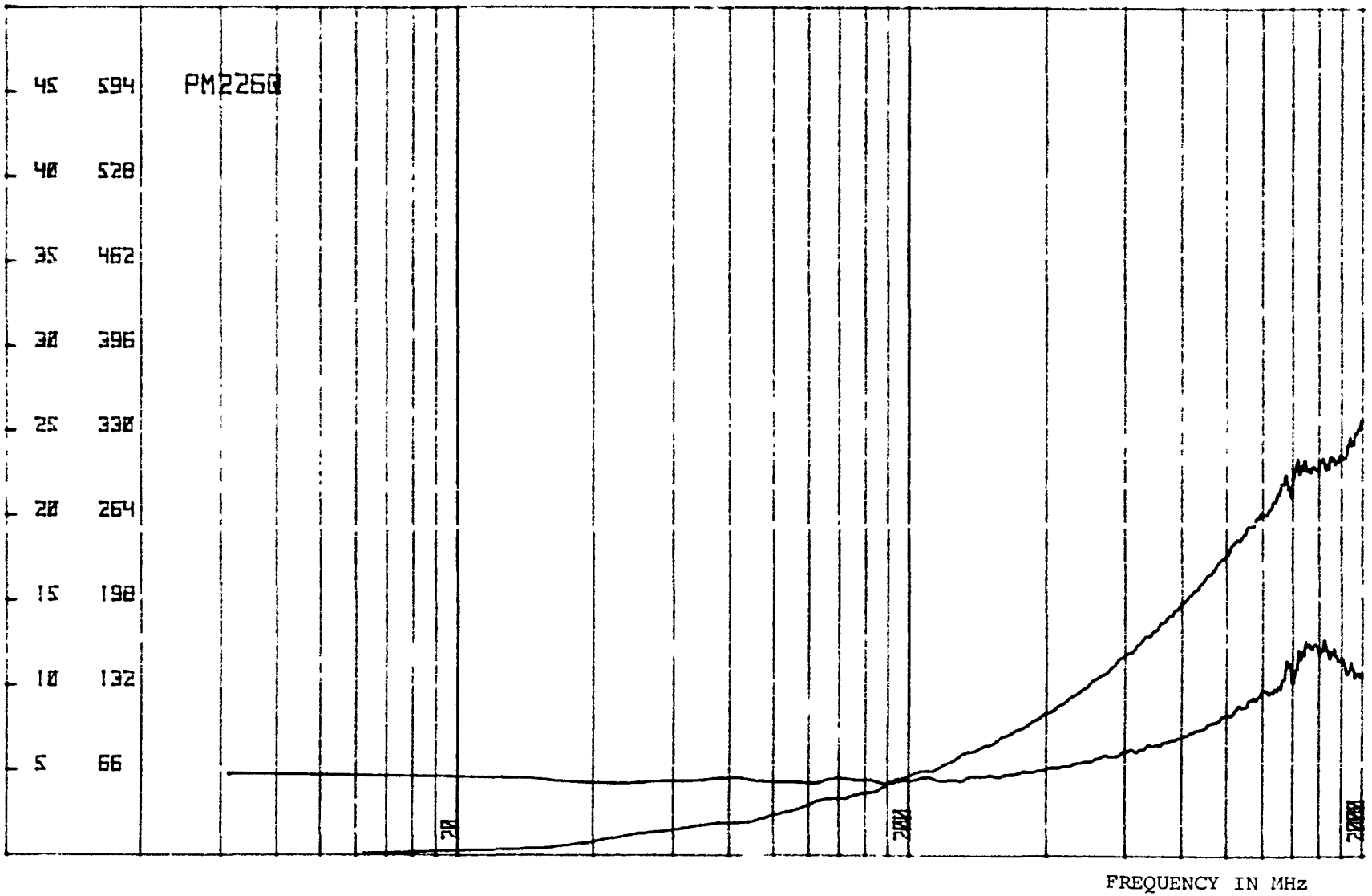

FIGURE D17b: ATTENUATION AND PHASE FUNCTIONS OF 1.2 km FIBER (LOOPS 8 & 9).

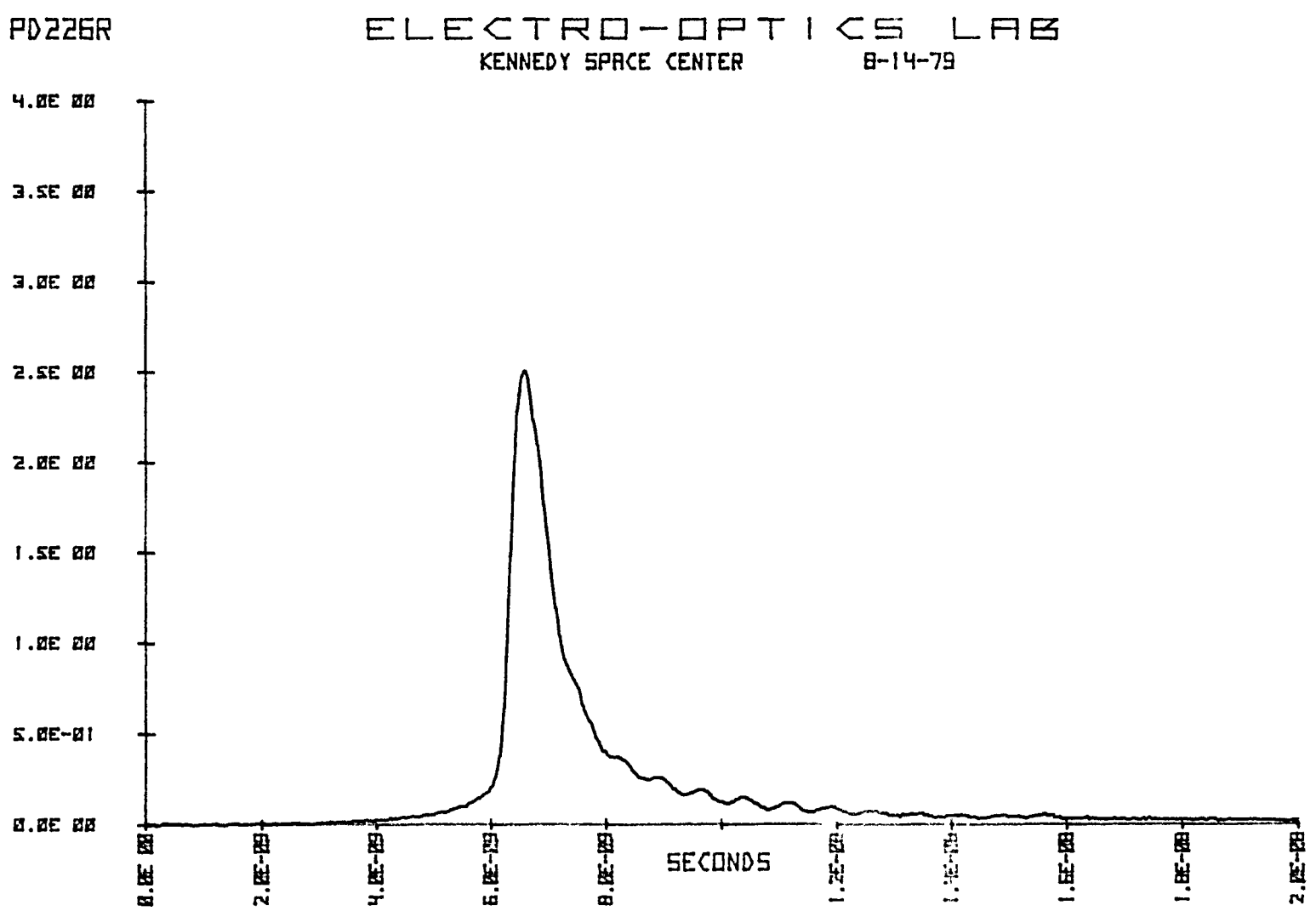

FIGURE D18a: RESPONSE WAVEFORM OF 1.2 km FIBER (LOOPS 10 & 11).

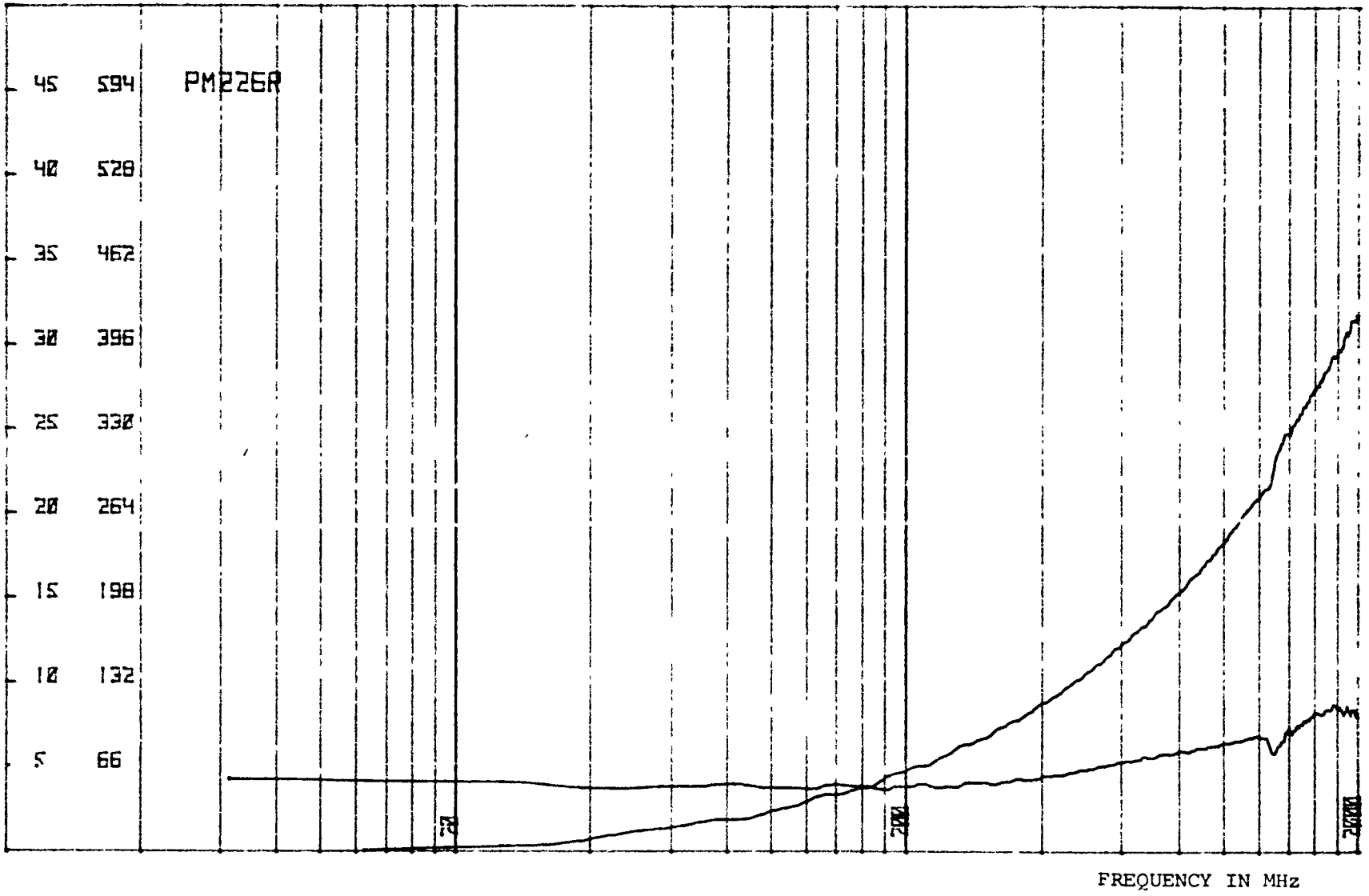

FIGURE D18b: ATTENUATION AND PHASE FUNCTIONS OF 1.2 km FIBER (LOOPS 11 & 12).

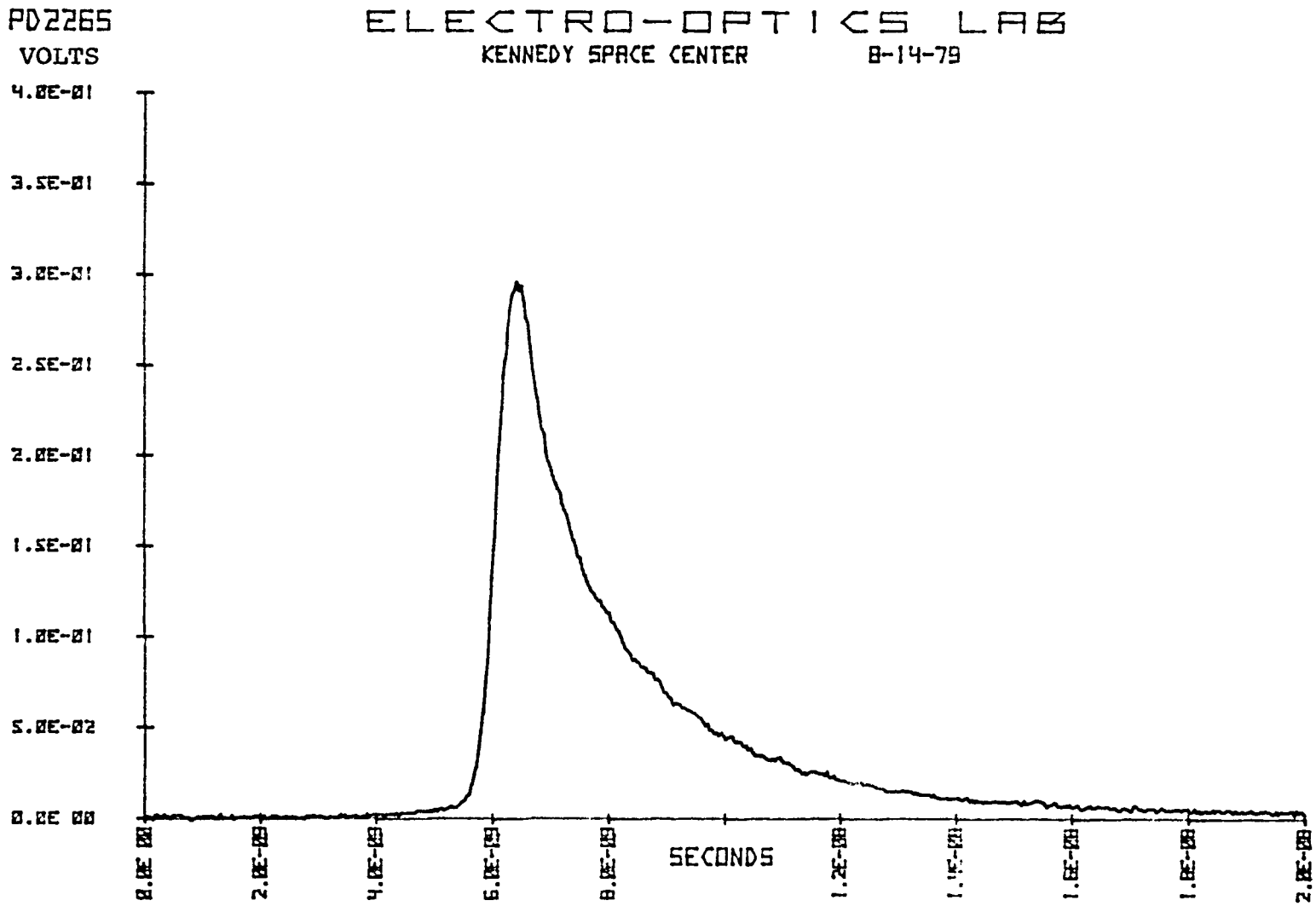

FIGURE D19a: RESPONSE WAVEFORM OF 2.4 km FIBER (LOOPS 2 - 5).

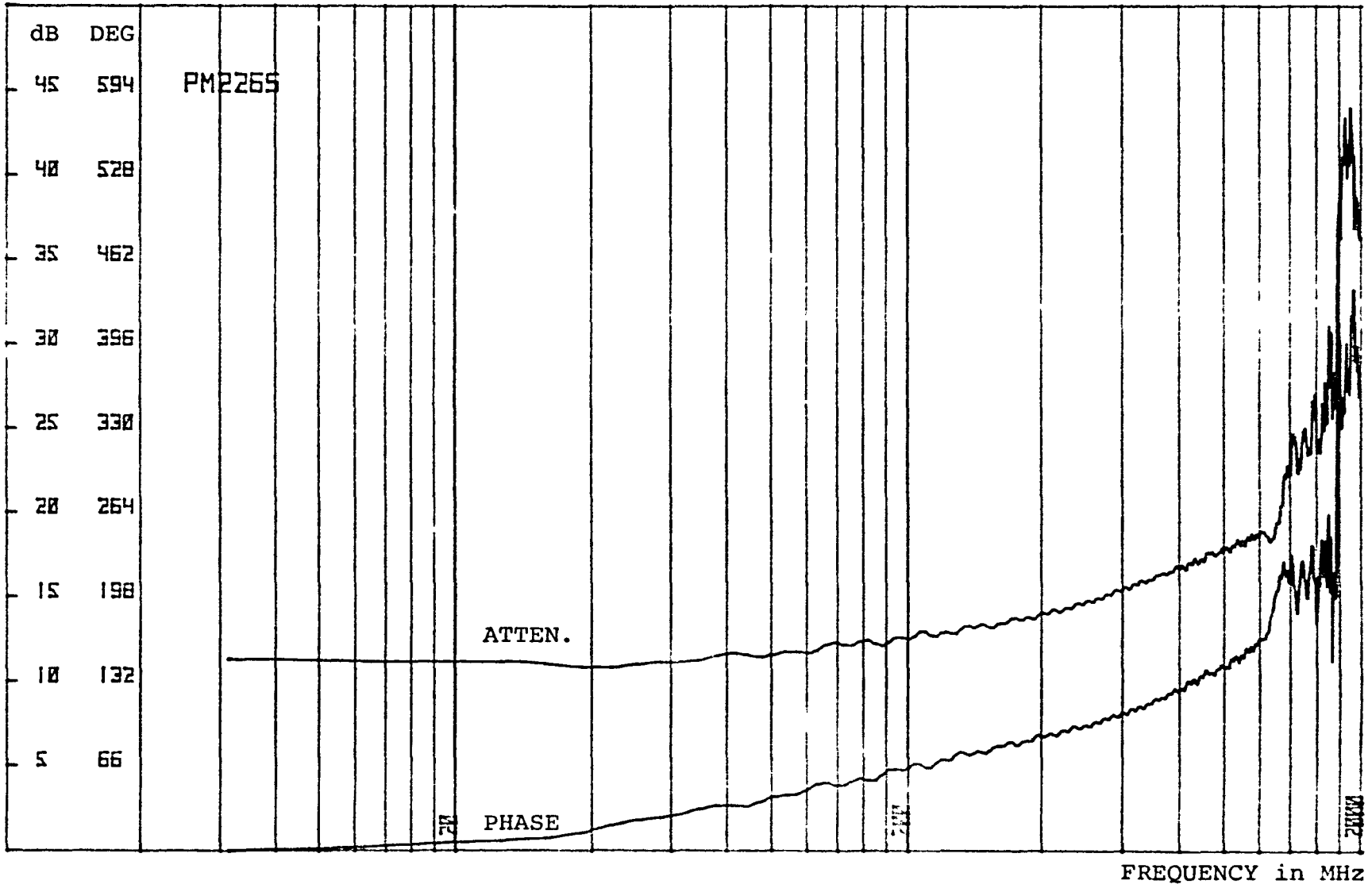

FIGURE D19b: ATTENUATION AND PHASE FUNCTIONS OF 2.4 km FIBER (LOOPS 2 - 5).

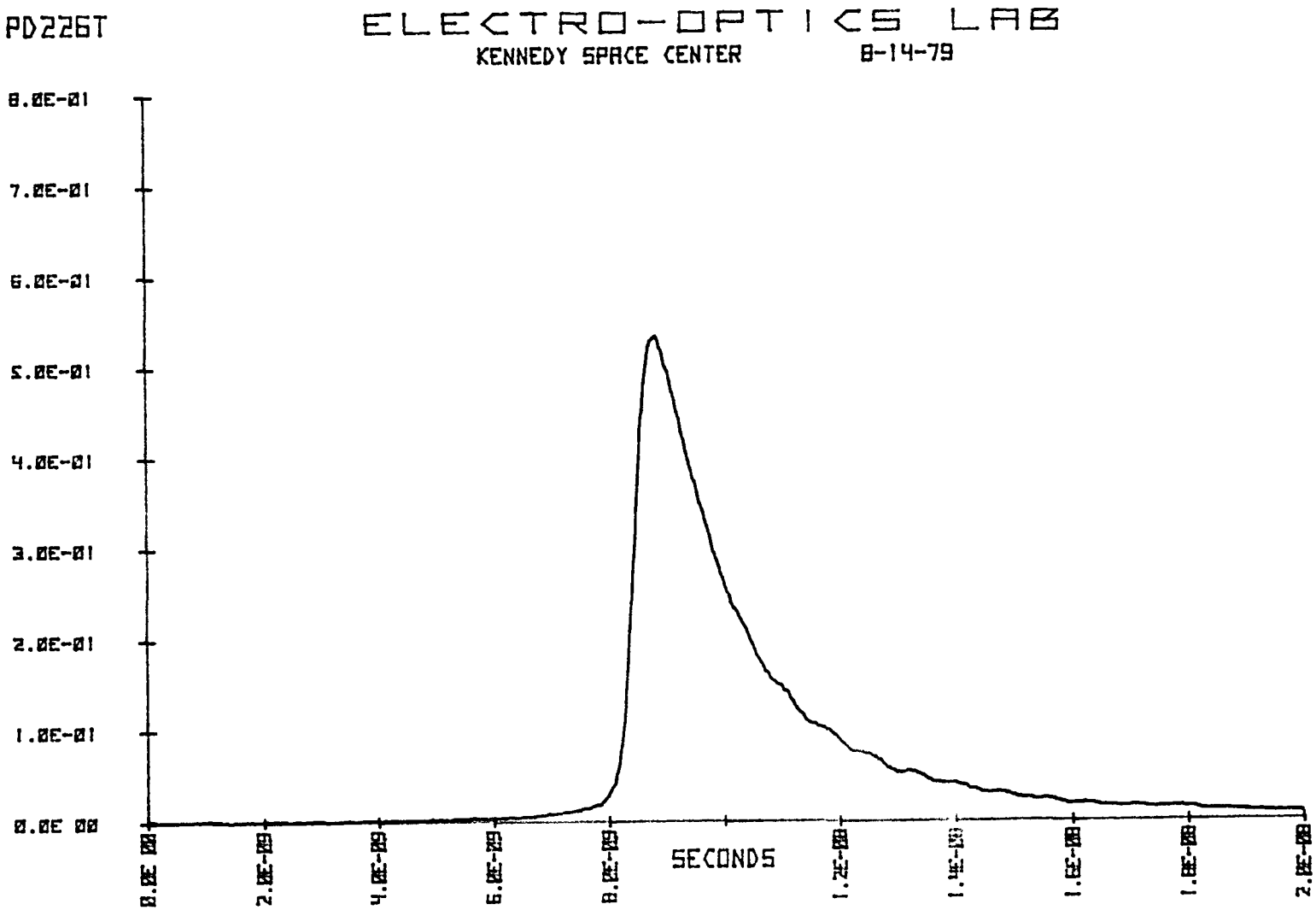

FIGURE D20a: RESPONSE WAVEFORM OF 2.4 km FIBER (LOOPS 6 - 9).

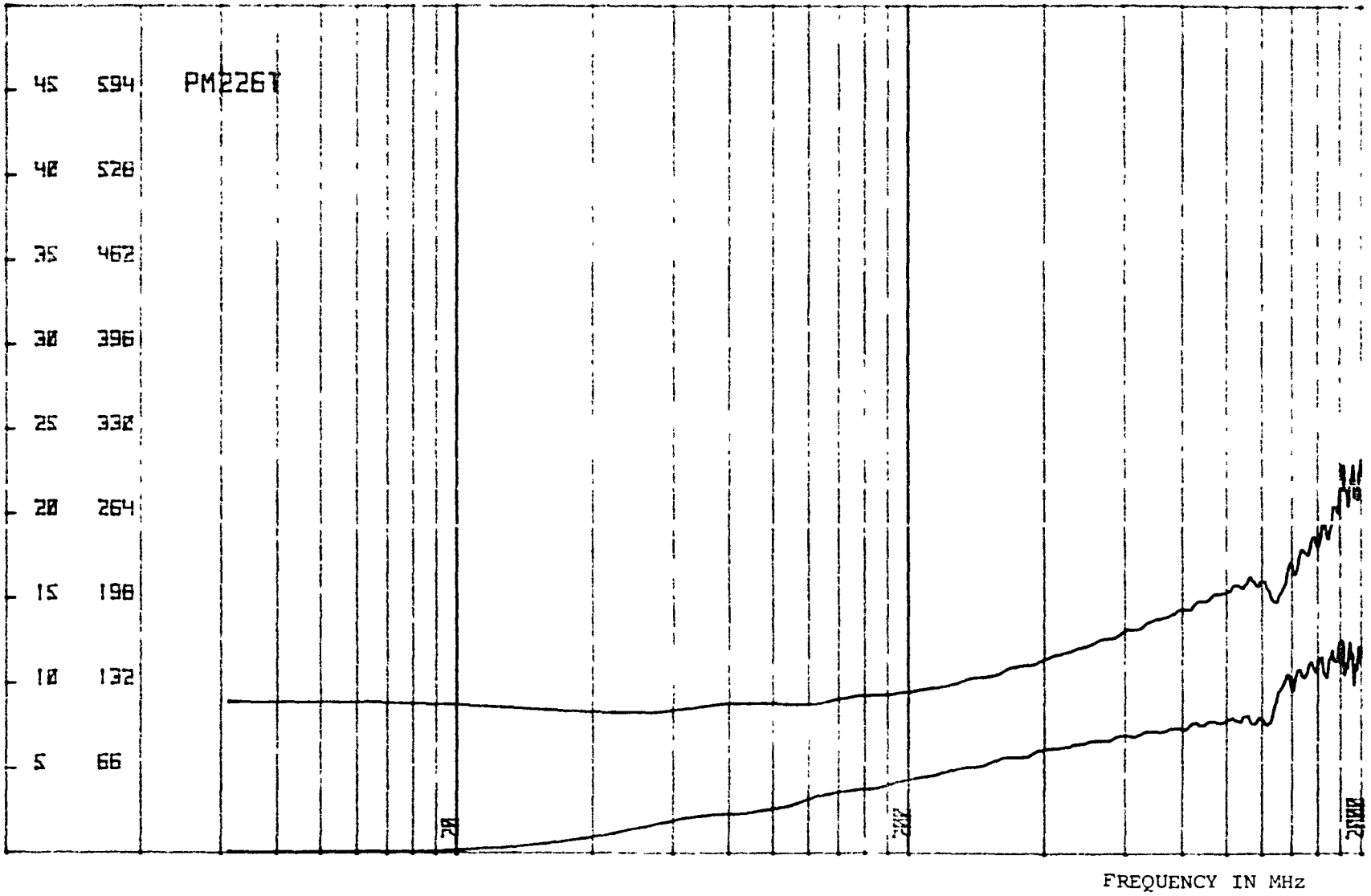

FIGURE D20b· ATTENUATION AND PHASE FUNCTIONS OF 2.4 km FIBER (LOOPS 6 - 9).

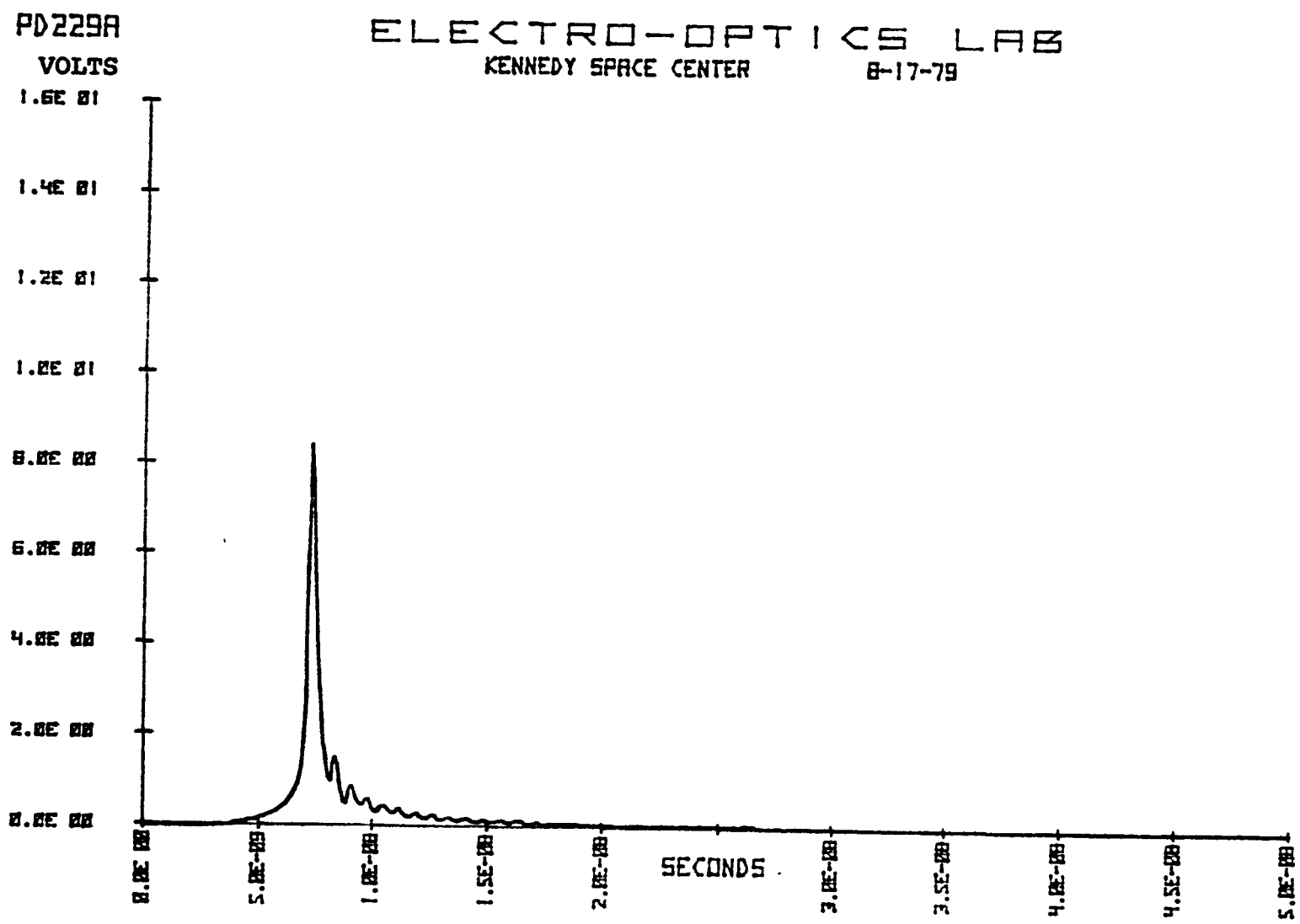

FIGURE D21: REFERENCE WAVEFORM FOR TESTING 4.8 km FIBER.

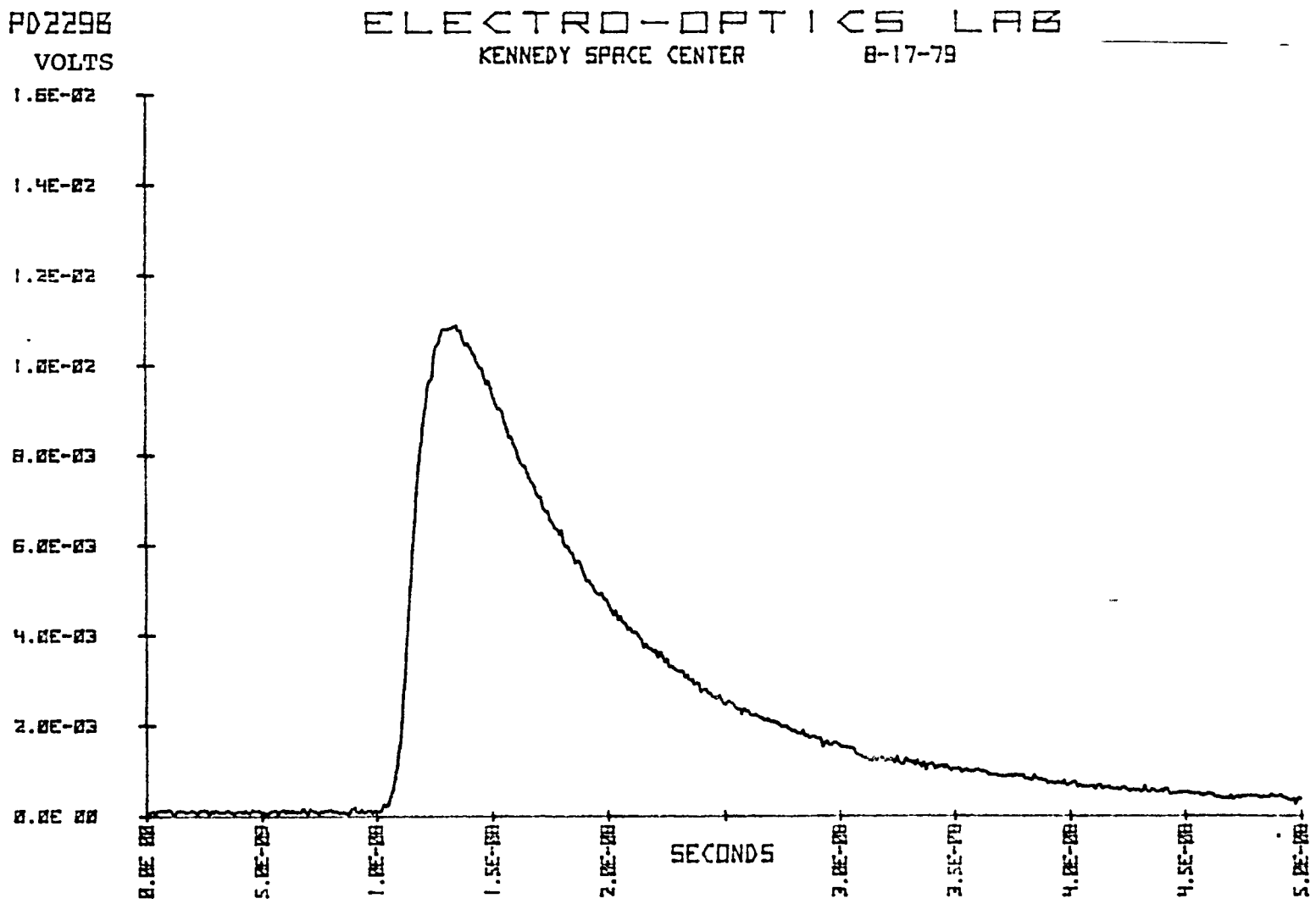

FIGURE D22a: RESPONSE WAVEFORM OF 4.8 km FIBER (LOOPS 2 - 9).

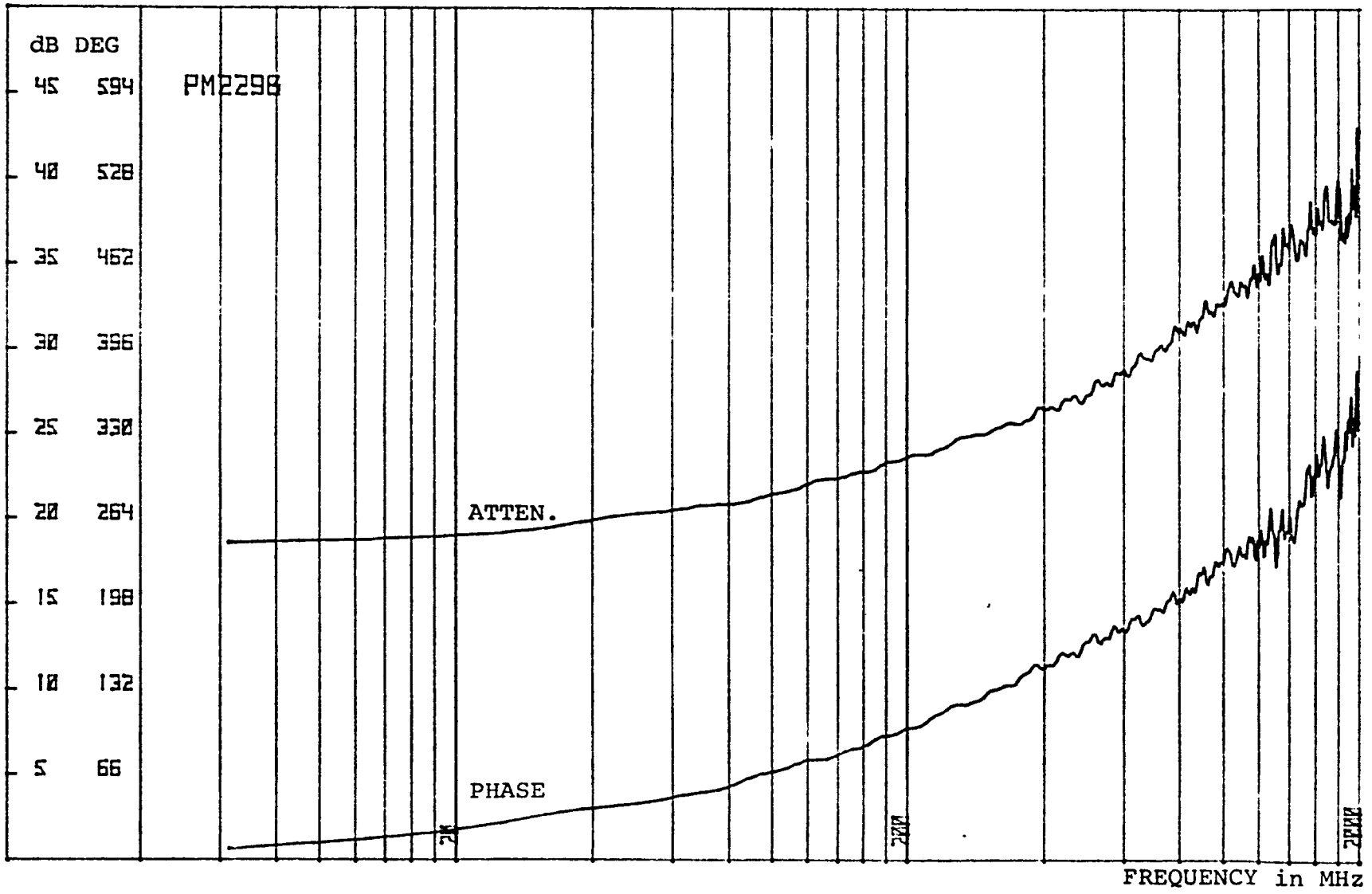

FIGURE D22b: ATTENUATION AND PHASE FUNCTIONS OF 4.8 km FIBER (LOOPS 2 - 9).

STANDARD TITLE PAGE

1. Report No	2 Government Accession No	3 Recipient's Catalog No.
CR-165624		

4. Title and Subtitle	5 Report Date
Optical Fiber Dispersion Characterization Study, Final Report	6. Performing Organization Code

7. Author(s)	8 Performing Organization Report No
Alan Geeslin, Achia AR Riad, Sedki M. Riad, Michael E. Padgett	TR 32-3

9. Performing Organization Name and Address	10. Work Unit No
Kennedy Space Center, Florida - 32899 and University of Central Florida P.O. Box 25000, Orlando, Florida	11. Contract or Grant No. NAS 10-9455
12 Sponsoring Agency Name and Address National Aeronautics and Space Administration Washington, D. C. - 20546	13. Type of Report and Period Covered Optical Fiber Dispersion Dec. 78 - Dec. 79
	14 Sponsoring Agency Code DL-DED-32

15 Abstract

This report presents the theory, design, and results of optical fiber pulse dispersion measurements. Detailed descriptions of both the hardware and software required to perform this type of measurement are presented. Hardware includes a thermoelectrically cooled ILD (Injection Laser Diode) source, an 800 GHz gain-bandwidth produce APD (Avalanche Photo Diode) and an input mode scrambler. Software for a HP 9825 computer includes fast fouirer transform, inverse fouirer transform, and optimal compensation deconvolution. Test set construction details are also included.

Test results include data collected on a 1 Km fiber, a 4 Km fiber, a fused spliced, eight 600-meter length fibers concatenated to form 4.8 Km, and up to nine optical connectors.

This work was performed at Kennedy Space Center with the Aid of the University of Central Florida, Orlando Florida under contract NAS 10-9455.

16. Key Words

Optical fiber, fiber dispersion, pulse dispersion, fiber bandwidth, optical connectors and splicers.

17. Bibliographic Control	18 Distribution
STAR Category 51	Unlimited

19 Security Classif (of this report)	20 Security Classif (of this page)	21 No of Pages	22 Price
Unclassified	None		

End of Document